Bracing Requirements for Multi-column Systems with Nonuniform Stiffness and Semi-rigid Connections

by

Linbo Zhang

A thesis
presented to the University of Waterloo
in fulfillment of the
thesis requirement for the degree of
Doctor of Philosophy
in
Civil Engineering

Waterloo, Ontario, Canada, 2023

Examining Committee Membership

The following served on the Examining Committee for this thesis. The decision of the Examining Committee is by majority vote.

External Examiner: Dr. Ronald D. Ziemian
Professor, Department of Civil and Environmental Engineering
Bucknell University

Supervisor: Dr. Lei Xu
Professor, Department of Civil and Environmental Engineering
University of Waterloo

Internal Member: Dr. Wei-Chau Xie
Professor, Department of Civil and Environmental Engineering
University of Waterloo

Internal Member: Dr. Adil Al-Mayah
Associate Professor, Department of Civil and Environmental Engineering
University of Waterloo

Internal-External Member: Dr. Elizabeth Weckman
Professor, Department of Mechanical and Mechatronics Engineering
University of Waterloo

Author's Declaration

This thesis consists of material all of which I authored or co-authored: see Statement of Contributions included in the thesis. This is a true copy of the thesis, including any required final revisions, as accepted by my examiners.

I understand that my thesis may be made electronically available to the public.

Statement of Contributions

The works presented herein, unless otherwise noted, have been accomplished solely by the author, with guidance from the supervising professor, Lei Xu. The research covered in Chapter 4 is published in [1] and [2]. Note that a part of the derivation in Section 4.2 was completed in collaboration with a former Ph.D. student in the same research group, Terence Ma [3]. The research conducted in Chapter 7 has been accepted as [4].

Abstract

For a structural system consisting of multiple columns, horizontal discrete braces are often used to increase the system's load-carrying capacity by reducing the columns' effective length. Over the past several decades, Winter's model has been extensively adopted to investigate the stiffness and strength requirements of bracing for multi-column systems. However, as Winter's model simulates the column as two perfectly-straight rigid members pin-connected at ends, it neglects the column's flexibility and initial curvature as well as the stiffness of end connections. As a consequence, the pertinent research and standards are limited to multiple columns with pin ends and may yield unconservative results due to neglecting the column initial curvature. In addition, the specifications in current standards are based on the cases in which the column sizes, applied loads, and braces are the same (referred to as uniform stiffness), which restrains its practical application scenarios. Therefore, the effect of nonuniform stiffness, i.e., different column sizes, applied loads, or brace stiffness, on the bracing requirements for multi-column systems has not been investigated.

A new analytical model (half-length column model) is proposed in this thesis to consider the aforementioned factors neglected in Winter's model. The bracing requirements for a single semi-rigidly connected column with a lateral brace at the mid-height obtained by employing the proposed model are investigated and compared with those obtained by following current standards. It is found that considering the column initial curvature will magnify the additional lateral displacement induced by the applied load and subsequently increase the brace force, as expected. Hence, the bracing requirements for a single column specified in current standards may be underestimated in some cases.

By extending the proposed half-length column model to multiple columns, an analytical method is proposed to evaluate the ideal brace stiffness and brace forces for multi-column systems with nonuniform stiffness by formulating the stiffness interaction among columns and braces. Explicit solutions and empirical equations are attained to evaluate the ideal brace stiffness and maximum brace force for systems with uniform column stiffness. The results of the presented numerical examples indicate that the design equations in current standards are not applicable to cases with nonuniform column stiffness.

Due to the interactive relationship between the brace stiffness and brace force in multi-column systems, the design process of evaluating the maximum brace force and column

lateral displacement with presupposed brace stiffness may require cumbersome iterations and overestimate the bracing requirements. Therefore, instead of presupposing the brace stiffness to calculate the brace forces and column lateral displacements, the bracing requirements are converted to preconditions and incorporated into the formulations established in the proposed method to assess the minimum brace area for a single column and multi-column systems, thus circumventing the iteration process.

Instead of assuming all the brace stiffness to be uniform, the effect of nonuniform brace stiffness on bracing requirements is also investigated. The effect of solid blocking on bracing requirements for cold-formed steel bearing walls is assessed, indicating that considering solid blocking will always reduce the bracing requirements, which is not considered in the current standards. An optimization problem is proposed to investigate alternative bracing patterns that are more economical than the uniform bracing pattern.

As building fires are responsible for momentous losses of property and life, fire safety has become an inseparable part of structural design, especially for steel structures. Also, it has reached a consensus in the structural fire research community that the creep effect should be considered when evaluating the fire resistance of steel members because it will decrease the material stiffness, thus leading to larger deformations and premature failure. A numerical method is established in this thesis to assess the column's mid-height deflection at elevated temperatures induced by the creep effect. The method is validated against the creep buckling tests on steel columns at elevated temperatures. In particular, it has been found that the creep-induced deflection of the steel column is led by the nonuniform strain and stress distributions on the cross-section, which is triggered by the initial imperfection.

As the assumptions adopted in the proposed numerical method are experimentally verified to be reasonable, a simplified formulation is proposed to evaluate the creep effect on the column lateral stiffness at elevated temperatures. Analytical expressions are proposed to attain the additional column lateral displacements and internal forces induced by the thermal expansions of braces. The modified plastic-hinge method is adopted to account for the adverse effect of partial yielding on the lateral stiffness of steel columns at elevated temperatures. Finally, a numerical method is established incorporating the effects of thermal expansions of braces, and partial yielding and creep of columns, to evaluate the critical temperature of multi-column systems.

As necessary, finite element modelling is used to validate the theoretical accuracy of the proposed methods. Overall, the proposed model and analytical methods in this study are comprehensively applicable to assessing the bracing requirements for multi-column systems, providing certain reference significance for researchers and engineers.

Acknowledgements

Melissa Febos, in *Abandon Me*, writes: "*Making darkness visible is a lonely process, but I have never done it alone*", a fitting description for my four-year PhD study experience. Coming up with a new idea and then completing this thesis was unquestionably the most depressing and arduous task I have ever undertaken. It would not have been possible to get through the hard time and finish this thesis without the help of many cordial people around me. So, I would like to thank those who contributed to this thesis and supported me during my PhD study.

First and foremost, I would like to express my deepest gratitude to my supervisor, **Prof. Lei Xu**, for his invaluable advice and continuous support during my PhD study. He told me the most important thing for conducting theoretical research is to keep calm and carry on. The first time I knew this was when I visited Oxford University as an exchange student. Although I knew that, I did not comprehend it at that time. The memories are still fresh that you have helped me revise the paper sentence by sentence with sufficient patience, sometimes even until late at night. I can always learn a lot from the discussion with you because of your profound knowledge and your meticulous attitude toward academic research. Thank you, Professor Xu, for guiding me in the right direction and making me realize the essence of academic research. You made me more determined to become a professor like you one day.

I must also thank the former supervisor of my M.Sc. program at Chongqing University, **Prof. Weiyong Wang**. I really appreciate that you offered me an opportunity to become your postgraduate student. I still remember the day you messaged me at almost 11:00 pm asking me if I was in the office and wanting to have a talk with me. I was so afraid of being lectured by you. However, it turned out that you found I had been very stressed and just wanted to have a drink with me. By sharing your experiences, you gave me a big relief and confidence. Whenever I felt lost, I would seek guidance from you, and you always enlightened me with patience. You told me, "*don't worry about something that you cannot control; once you figure out what you want, just do your best for it without making plan B.*" Thank you, Mentor Wang, for giving me my confidence back. I wish I could be the student that you are proud of.

Special thanks to the examining committee, **Prof. Elizabeth Weckman, Prof. Wei-Chau Xie, and Dr. Adil Al-Mayah**, for their valuable suggestions to improve this thesis at the Comprehensive Exam stage.

I would like to extend my sincere thanks to my external examiner, **Prof. Ziemian**, who revised my thesis quite thoroughly and made lots of constructive comments. In fact, this thesis would not have been possible without Prof. Ziemian because the research with regard to the bracing requirements was inspired by his work [5].

Many thanks to **Prof. Schuster**, who gives me emotional support and confidence from time to time.

I am glad I could have very nice colleagues in this research group. Thanks to **Terence, Daniel, and Ghaith**. Terence is so self-disciplined and intelligent, so he only used two years and five months to finish his master's and PhD studies. Also, he is very humble and always willing to help me. Thank you, Terence, for being the one I have been trying to emulate during the last four years. Daniel, thanks for your suggestions and dedicated time to polishing my papers. You really helped me a lot in improving my English writing. I still remember the first day we met when you kept teaching me much English slang, although I have forgotten most of them now. Ghaith, thanks for saying hi to me almost every day in the last year, providing suggestions for my thesis, and lending your tie to me for my defence. In particular, it surprised me that we did have a lot in common.

Special thanks to **China Scholarship Council** for the scholarship for my PhD study, which gave me the opportunity to study aboard and have a wonderful journey.

Thanks to Williams Fresh Cafe. You offered me countless coffee during the last year and only charged me 25 dollars per month.

To my family, particularly my parents, **Zhimin Zhang** and **Feixue Zhou**, thank you for your love and unswerving belief in me. Without you, I would not be the one I am today.

Table of Contents

List of Figures

List of Tables

Nomenclature

A_b	cross-sectional area of the beam (tie-bracing)
A_c	cross-sectional area of the column
$A_{b,\text{AISC}}$	required cross-sectional area of bracing according to AISC 360-16
$A_{b,\text{op}}$	optimum cross-sectional area of bracing
A_{bl}	cross-sectional area of the solid blocking
A_{br}	cross-sectional area of diagonal bracing
E	elastic modulus of steel at ambient temperature
E_T	elastic modulus at elevated temperature
E_b	elatic modulus of the beam (tie-bracing) at ambient temperature
E_c	elatic modulus of the column at ambient temperature
E_{cp}	modified secant modulus at elevated temperature considering creep effects
E_{tan}	tangent modulus of the steel
E_{br}	elatic modulus of diagonal bracing at ambient temperature
I_b	moment of inertia of the beam (tie-bracing)
I_c	moment of inertia of the column
K	effective length factor of the column
K_p	effective length factor of the column in the inelastic analysis

K_{app}	approximate value of the effective length factor
L	half-length of column in Winter's model and proposed model
L_b	full length of the beam (tie-brace)
L_c	full length of the column
L_{br}	length of diagonal bracing
L_{cb}	braced length of the column
M_m	internal bending moment at mid-height of the full-length column
M_p	plastic bending moment resistance
M_y	elastic bending moment resistance
N_c	compressive load in column
P	axial applied load on column
P_{max}	maximum gravity load among all the applied loads on a multi-column system
P_e	Euler non-sway buckling load of a column with pin ends
P_y	yield strength of the column
P_{th}	thermal-induced additional force in column
P_{cr}	non-sway (rotational) buckling load of the column
Q_0	equivalent lateral force induced by the column initial imperfection and applied axial load
Q_b	brace force
Q_n	internal force in the brace adjoining to the anchor in the multi-column system, which is typically the maximum brace force when the system consists of identical columns and braces
Q_{th}	additional compressive force in braces induced by thermal restraints

R	rotational stiffness of the beam-to-column connection or column base connection
R'_{ule}	restraint stiffnesses provided by the left beam and connecting beam-to-column connection at column upper end
R'_{uri}	restraint stiffnesses provided by the right beam and connecting beam-to-column connection at column upper end
R_e	rotational restraint stiffness at the lower end of the proposed half-length column model
R_m	rotational restraint stiffness at the upper end of the proposed half-length column model
R_{ule}	rotational stiffness of the connection at column upper end connecting the adjacent left beam
R_{uri}	rotational stiffness of the connection at column upper end connecting the adjacent right beam
S_L	lateral stiffness provided by the external brace that can provide reaction force
S_b	axial stiffness of the beam (or tie-bracing)
S_c	column lateral stiffness
S_x	elastic section modulus about the major axis
S_{DEN}	denominator of the equivalent lateral stiffness
S_{NUM}	numerator of the equivalent lateral stiffness, which is the same for all the columns in the multi-column system
S_{ef}	effective lateral stiffness of the column in the multi-column system
$S_{b,\text{ids}}$	ideal brace stiffness for a single column
$S_{b,\text{idt}}$	ideal brace stiffness of a multi-column system

$S_{b,\mathrm{op}}$	optimum brace stiffness
S_{bl}	axial stiffness of the solid blocking
$S_{br,\mathrm{t}}$	total lateral stiffness of diagonal bracing
$S_{c,T}$	column lateral stiffness at the elevated temperature, T
$S_{c,\mathrm{cp}}$	column lateral stiffness considering the creep effect
$S_{c,\mathrm{cr}}$	column lateral stiffness when the applied load is the non-sway buckling load
$S_{c,\mathrm{mod}}$	column lateral stiffness considering the partial yielding effect
T	temperature
Z	distance from the centroid of a strip to the bottom of the cross-section
Z_x	plastic section modulus about the major axis
$\Delta_{\max}$	the maximum column lateral displacement in the multi-column system
$\Delta_{\min}$	the minimum column lateral displacement in the multi-column system
α_p	the ratio of the applied load P to the critical load P_{cr}
$\alpha_{b,\mathrm{op}}$	optimum brace stiffness scale factor satisfying both strength and stiffness requirements, i.e., the maximum value of $\alpha_{b,\mathrm{disp}}$ and $\alpha_{b,\mathrm{force}}$
$\alpha_{b,\mathrm{pre}}$	presupposed scaled factor, the ratio of the selected brace stiffness to the ideal brace stiffness
$\bar{Q}_1$	brace force for a single column
$\bar{R}_l$	effective value of restraint stiffness at column lower end
$\bar{R}_u$	effective value of restraint stiffness at column upper end

β	modification factor accounting for the effect of the axial force on the column lateral stiffness
β_u	modification factor accounting for the effect of the critical buckling load on the column lateral stiffness
β_{br}	coefficient varying with the number of brace points along column length stipulated in CSA S16-19
η	reduction factor considering the initial imperfection randomness for multiple columns
λ	slenderness ratio of the column
ϕ	axial load coefficient
ϕ_u	axial load coefficient associated with non-sway buckling load P_{cr}
$\phi_{u,0}$	initial guess of ϕ_u
ψ	column initial curvature coefficient representing the effect of column initial curvature on the additional displacement induced by the applied load
ψ_u	column initial curvature coefficient associated with $P = P_{cr}$
σ	stress
$\sigma_{ec,T}$	maximum exterior stress in compression on the cross-section at elevated temperature T
$\sigma_{et,T}$	minimum exterior stress on the cross-section at elevated temperature T
τ_b	inelastic stiffness reduction factor
θ	angle of diagonal bracing with repect to the horizontal direction
θ_F	joint ration of the far end
θ_N	joint ration of the near end

ε	strain
$\varepsilon_{y,T}$	yield strain at elevated temperature T
ε_{cp}	creep strain
ε_{st}	instantaneous mechanical strain induced by the stress
ε_{th}	thermal strain induced by the thermal expansion
$\varepsilon_{p,T}$	strain associated with the proportional limit at elevated temperature T
$\varepsilon_{t,T}$	limiting strain for yield strength at elevated temperature T
$\varepsilon_{u,T}$	ultimate strain at elevated temperature T
a_1, a_2, and a_3	coefficients in evaluating the lateral stiffness of a semi-rigidly connected column
a_{max}	ratio of ideal brace stiffness for multiple columns to ideal brace stiffness of a single column
c	ratio of the stiffness of tie-bracing to the stiffness of the adjoining anchor bracing
f_p	proportional limit at ambient temperature
f_y	yield strength of the steel
$f_{0.5}$, $f_{1.0}$, $f_{1.5}$, and $f_{2.0}$	stresses associated with the strain being 0.5%, 1.0%, 1.5%, and 2.0%, respectively
$f_{0.2\text{offset}}$	stress of the intersection of the stress-strain curve and the proportional line offset by 0.2% strain
$f_{p,T}$	proportional limit at elevated temperature
$f_{y,T}$	yield strength at elevated temperature
$f_{yb,T}$	yield strength for the hot-rolled class 4 sections at elevated temperature

f_{yb}	yield strength for the hot-rolled class 4 sections at ambient temperature
k_E	retention factor of elastic modulus at elevated temperature
k_p	retention factor of proportional limit at elevated temperature
k_y	retention factor of yield strength at elevated temperature
k_{yb}	retention factor of yield strength for hot-rolled class 4 sections at elevated temperature
r	column end-fixity factor
r_l	end-fixity factor of the column lower end
r_u	end-fixity factor of the column upper end
v	ratio of joint ration of the far end to the joint rotaion of near end
z_{le}	end-fixity factor of beam left end
z_{ri}	end-fixity factor of beam right end
$S_{\text{eq},1}$	equivalent lateral stiffness of the leftmost column in the multi-column system
Δ_0	column initial imperfection
Δ	additional column lateral displacement induced by the applied load
Δ_{ep}	total length change of brace induced by free thermal expansion
Δ_{th}	column lateral displacement induced by the thermal expansion of braces and restraints
α_{th}	thermal expansion coefficient of steel
$\alpha_{b,\text{disp}}$	the value of the brace stiffness scale factor satisfying the stiffness requirement, i.e., $\Delta = \Delta_0$
$\alpha_{b,\text{force}}$	the value of the brace stiffness scale factor satisfying the strength requirement, i.e., $Q_b / f_y = S_b L_b / E_b$

Chapter 1

Introduction

1.1 Background

For multi-column systems such as industrial buildings and cold-formed steel bearing walls, horizontal bracing is an efficient and common way to improve the stability and strength of columns by reducing the columns' effective length. Such bracing needs to fulfill both strength and stiffness requirements to ensure the stability of the multi-column system [6]. For simplicity, Winter [7] proposed a model in which the column is divided into two perfectly straight and rigid members pin-connected at ends to investigate the bracing requirement for a single column. Subsequently, Winter's model has been widely adopted and extended to assess the bracing requirements for multi-column systems [5, 8, 9]. The universally accepted philosophy of determining the required brace stiffness is to compute the ideal brace stiffness first, which refers to the minimum stiffness required for braces to ensure that the full buckling strength of the braced system can be achieved [5]. The analysis regarding ideal brace stiffness can be carried out by investigating perfect systems without considering possible column initial imperfections. However, the presence of initial imperfections would theoretically result in infinite brace forces when the columns are subjected to their buckling loads and the braces possess the ideal brace stiffness. For that reason, the brace stiffness must be magnified from the ideal brace stiffness to a certain value to reduce the brace forces from infinity to an acceptable magnitude. It is stipulated in AISC 360-16 [10] and AISI S100-16 [11] that the brace stiffness shall be at least twice the ideal brace stiffness (stiffness requirement) to reduce the strength demand for bracing members. Then, the maximum

brace force, i.e., strength requirement for bracing members, in a multi-column system is attained with the brace stiffness being twice the ideal brace stiffness. Finally, the stiffness of the bracing member is determined according to the stiffness and strength requirements. Although the research regarding determining the ideal brace stiffness [5, 8, 9] and brace forces [12–16] for multi-column systems has been well conducted, there are still several important issues that need to be addressed:

1. Due to adopting Winter's model, the previous studies assume that the column ends are pin-connected. However, realistic connections at column ends possess a certain degree of rotational restraint; thus, the column ends should be considered semi-rigid to accurately predict the stability of the system.

2. As Winter's model simulates the column as two perfectly straight rigid members, it neglects the column's flexibility and initial curvature, which will magnify the additional displacement induced by the applied load and consequently increase the brace force [10, 17]. Therefore, the effect of column initial curvature on brace forces in multiple columns needs to be investigated.

3. Considering the previous studies were limited to the system in which all the columns and braces are identical, there is a lack of research on the system with nonuniform column stiffness and brace stiffness.

1.2 Scope and Objectives

The purpose of this study is to develop a comprehensive, analytical design methodology for evaluating the bracing requirements of multi-column systems. On account of the aforementioned issues, the methodology should consider the effects of stiffness of column end connections, column flexibility, and column initial curvature. Also, this methodology should be applicable to systems in which the column sizes, brace sizes, end connections, or applied loads are not limited to being identical. The objectives of this research are outlined below:

- To investigate the effects of the column's flexibility and initial curvature as well as the end connection stiffness on bracing requirements. Given that these factors are not

considered in Winter's model [7], it is therefore necessary to establish a new analytical model.

- To propose an analytical method of assessing the ideal brace stiffness and brace forces for multi-column systems by accounting for the stiffness interaction among columns and braces.
- To propose simple-to-use expressions for the ideal brace stiffness and maximum brace force for systems with uniform stiffness.
- To propose an analytical method for evaluating the minimum required brace stiffness satisfying the bracing requirements.
- To compare the results obtained from the proposed methods against those obtained from the current standards.
- To investigate the effect of nonuniform bracing on bracing requirements, which has not been considered in the previous research and current standards.
- To propose a numerical method of assessing the creep effect on the column stability at elevated temperatures.
- To extend the proposed methods towards fire scenarios, including determining the critical temperature of braced multi-column systems.

The scope of research work presented in this study regarding bracing requirements for multi-column systems is completely analytical and involves a number of theoretical derivations. Examples and parametric studies are presented in each chapter to illustrate the application of the proposed method and illustrate how design parameters influence the ideal brace stiffness, brace forces, and bracing requirements. Where necessary, finite element analyses (FEA) were carried out to verify the accuracy of the proposed methods. Overall, compared to alternative methods such as finite element modelling and second-order analysis that may suffer from the disadvantage of complexity, the proposed methods are relatively easy to use and understand given the simplicity of the derived, closed-form equations.

1.3 Thesis Organization

The contents of each section in this thesis are outlined as follows:

- Chapter 2 reviews the current research and standards pertaining to all concepts incorporated in the proposed methods.
- Chapter 3 illustrates the development of the proposed analytical model for a single semi-rigidly connected column. The relationship among the column's mid-height deflection, applied axial load, and lateral force is derived. The bracing requirements for a single semi-rigidly connected column are investigated to demonstrate the differences between the results obtained from the proposed model and Winter's model.
- Chapter 4 proposes the analytical methods for determining the ideal brace stiffness and brace forces for multi-column systems by formulating the stiffness interaction among columns and braces. In particular, the effect of nonuniform column lateral stiffness on ideal brace stiffness and brace forces is investigated.
- Chapter 5 presents an analytical method to determine the minimum required stiffness of bracing members for a single column and multi-column systems. By employing the methods proposed in Chapter 4 and Chapter 5, the results of the required stiffness of bracing members following two different design philosophies are compared.
- Chapter 6 investigates the effect of solid blocking on bracing requirements for multi-column systems. In addition, an optimization problem is proposed to explore the minimum total bracing stiffness with nonuniform bracing stiffness.
- Chapter 7 proposes a numerical method of assessing the creep buckling behaviour, i.e., the creep-induced deflection of steel columns at elevated temperatures. The numerical method is verified against the experimental results, and the failure mechanism of creep buckling is investigated.
- Chapter 8 extends the proposed methods to evaluate the critical temperature of multi-column systems with the considerations of effects of thermal expansion of braces, partial yielding and thermal creep.

- Chapter 9 summarizes the main conclusions drawn from this thesis and provides some recommendations for future research.

Chapter 2

Literature Review

2.1 Bracing Requirements for Multi-column Systems

For multi-column systems, intermediate bracing is an efficient approach to increase the column strength by reducing the column effective length; thereby, it has been widely adopted in engineering practice. By adopting a single column-brace model proposed by Winter [7], the stiffness and strength requirements of the bracing for a single column have been well investigated by researchers [18–20] and documented in standards [10, 11, 21]. However, when it comes to multiple columns, the corresponding bracing requirements are not clearly specified in current standards except for the revisions recently adopted in AISI S100-16 [11].

In this section, Winter's model is briefly introduced first. Next, the bracing requirements for multi-column systems in existing research and current standards are reviewed. Finally, some overlooked aspects of current research and standards are discussed.

2.1.1 Winter's model

A simplified model was proposed by Winter [7] to assess the stiffness and strength requirements for the brace at mid-height of a column with pin ends, as shown in Fig. 2.1. Winter's model divides the column into two rigid segments at the brace point and introduces a fictitious hinge to connect the two rigid segments and brace, as illustrated in Fig. 2.1a. If the column's initial imperfection Δ_0 is to be considered (Fig. 2.1b), the relationship between

the total deflection and the brace stiffness can be obtained via the equilibrium expressed in Eq. (2.1a). Then, the mid-height deflection Δ can be written as Eq. (2.1b).

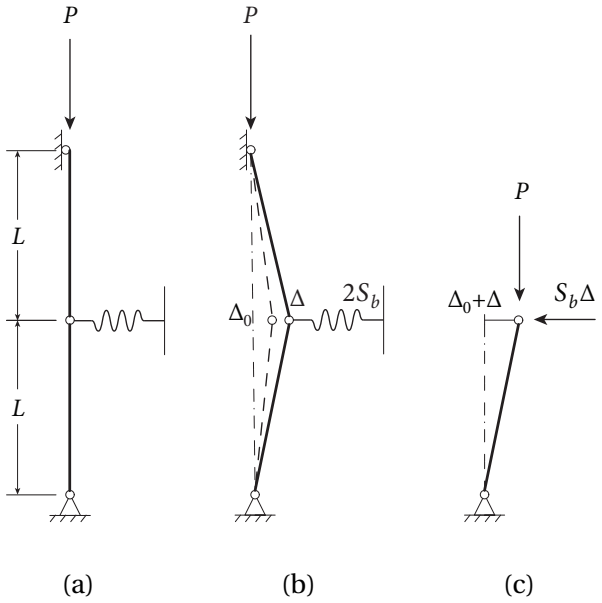

Figure 2.1: Force diagram of Winter's model

$$P(\Delta_0 + \Delta) = S_b \Delta L \tag{2.1a}$$

$$\Delta = \frac{P\Delta_0}{S_b L - P} \tag{2.1b}$$

where S_b is the brace stiffness and Δ is the additional displacement induced by the applied load, P.

Although it has been extensively used in research and practice regarding bracing requirements, Winter's model adopts certain assumptions which may hinder its applications. First, Winter's model neglects the column flexural stiffness by adopting rigid segments and a fictitious hinge. As such, the column stability solely relies on the support of the brace. In a multi-column system, columns possessing a greater lateral stiffness can be referred to as "strong" columns. In resisting system instability, "strong" columns can provide certain degrees of lateral support to "weak" columns in addition to that of the brace. Such column stiffness interaction is neglected when Winter's model is adopted. Second, although the out-of-plumbness of the half-length column is introduced in the model, the initial curvature (the lateral deflection of a member relative to its cord [17]) is not considered, which will result in additional lateral displacement of the column. Furthermore, Winter's model is not applicable to columns with semi-rigid connections.

2.1.2 Ideal brace stiffness of Winter's model

For multiple compressive members, Tong and Chen [8, 22] established the theoretical bases for the stiffness and strength requirements of bracing that can reduce the column effective length by half. In the assessment of brace stiffness requirement, the ideal brace stiffness $S_{b,\mathrm{id}}$ is a crucial indicator, which is determined such that the half-column's non-sway buckling load equals its sway buckling load, and an increase in brace stiffness beyond the ideal value will not increase the buckling strength of the multi-column system.

For a single column, the ideal brace stiffness $S_{b,\mathrm{ids}}$ is obtained by the equilibrium at the hinge of Winter's model (Fig. 2.1c) as:

$$S_{b,\mathrm{ids}} = \frac{2P_{cr}}{L} \tag{2.2}$$

where P_{cr} is the critical buckling load of the half-length column. For a system consisting of multiple identical compressive members, Ziemian and Ziemian [5] indicated that its ideal brace stiffness $S_{b,\mathrm{idt}}$ can be expressed using the product of a scale factor $a_{\max}$ and the ideal brace stiffness for a single column $S_{b,\mathrm{ids}}$, as below:

$$S_{b,\mathrm{idt}} = a_{\max} S_{b,\mathrm{ids}} \tag{2.3}$$

By fitting the analytical results, Ziemian and Ziemian [5] proposed an easy-to-use formula to calculate the value of $a_{\max}$, as expressed in :

$$a_{\max} = 0.4N^2 + (0.4 + c)N + 0.2 \tag{2.4}$$

where $N = n/j$ in which n is the number of columns in the system, and j is the number of ends anchored; $j = 1$ or 2. c is the ratio between the stiffness of tie bracing and anchor bracing. If the system is braced with one or two rigid anchors, $c = 0$. Eq. (2.4) was demonstrated to be useful for dealing with systems of multiple columns with discrete bracing between columns, such as that presented in Fig. 2.2.

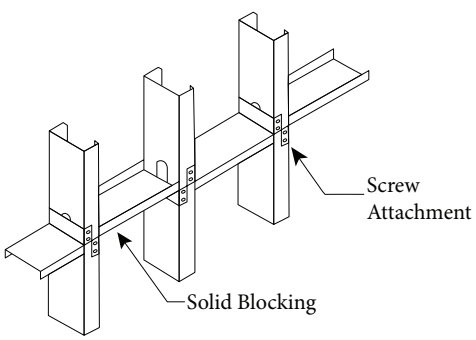

(a) Diagram [9]

(b) Example [23]

Figure 2.2: Discrete blocking between columns

Subsequently, to investigate the effect of shear connectors on the ideal brace stiffness of tie-bracing for multi-column systems depicted in Fig. 2.3, Ziemian and Ziemian [9] propose a more general single column-brace model in which the shear connector is connected in series with the adjacent tie-bracing. It was found that a decrease in the shear connector stiffness leads to higher ideal brace stiffness of the tie-bracing. Taking the shear connector and the tie-bracing as the discrete bracing as per Fig. 2.2, the shear connector stiffness shall be larger than the ideal brace stiffness of the discrete bracing; otherwise, the stiffness resulting from the shear connector and tie bracing is less than the ideal brace stiffness, even if the tie-bracing stiffness is theoretically infinite. Based on the thorough analytical results, Ziemian and Ziemian [9] proposed empirical expressions to evaluate the ideal brace stiffness for multi-column systems considering the effect of shear connectors.

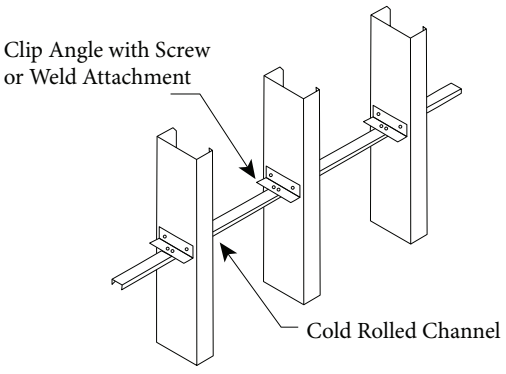

(a) Diagram [9]

(b) Example

Figure 2.3: Continuous cold-rolled channel attached to studs with shear connectors

Despite the successful achievements being made in the previous studies, further research

advancements can certainly be made in the following aspects. First, due to the adoption of Winter's model, the research is based on the assumption that the column is pin-connected. The effect of column end connection stiffness on ideal brace stiffness is yet to be investigated. Second, since all the multi-column systems investigated in the foregoing research are comprised of identical columns and the axial loads applied on columns are assumed to be identical; thereby, the bracing requirements for systems with nonidentical columns or with identical columns but different applied loads need to be investigated.

2.1.3 Brace force of Winter's model

As the analysis regarding ideal brace stiffness is based on bifurcation theory, it can be carried out by investigating perfect systems without considering possible column initial imperfections. However, the presence of initial imperfections would theoretically result in brace forces becoming infinite when the columns are subjected to their non-sway buckling loads and the braces possess the ideal brace stiffness, as illustrated by the solid line associated with $S_b = S_{b,\text{ids}}$ in Fig. 2.4. This is unacceptable as the strength requirement for bracing members cannot be fulfilled.

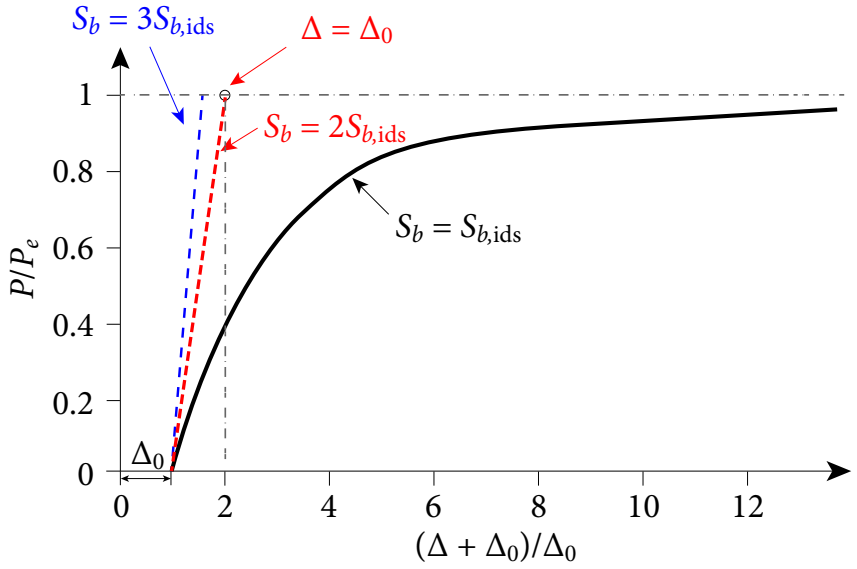

Figure 2.4: Effect of brace stiffness on additional displacement [10]

$P_e = \pi^2 E_c I_c / L^2$ is the elastic non-sway buckling load of a column with pin ends. Theoretically, increasing the brace stiffness can reduce the brace forces induced by applied axial loads on columns. To that end, standards such as AISC 360-16 [10] and AISI S100-16 [11]

stipulate that the brace stiffness is taken as two times the ideal brace stiffness to ensure that the additional displacement equals the initial imperfection, $\Delta = \Delta_0$, when the column is subjected to its non-sway buckling load, as per Fig. 2.4. Based on the equilibrium of Winter's model (Fig. 2.1c), the brace force Q_b with $P = P_e$ is:

$$Q_b = 2S_b\Delta = \frac{4P_e\Delta_0}{L} \tag{2.5}$$

By doing so, with the required brace stiffness being two times the ideal brace stiffness, the corresponding brace force can be attained from Eq. (2.5) in terms of P_e if Δ_0 is given. For most current standards [10, 11, 24], the initial imperfection tolerance is taken as $L/500$, and thus the brace force is $0.8\%P_e$ with $S_b = 2S_{b,\text{ids}}$ and $\Delta_0 = L/500$, as shown in Fig. 2.5 . Blum et al. [13] indicated that a lower brace stiffness of 1.33 times the ideal brace stiffness could also significantly reduce the brace forces to an acceptable level of $1.6\%P_e$, providing greater leeway for designers.

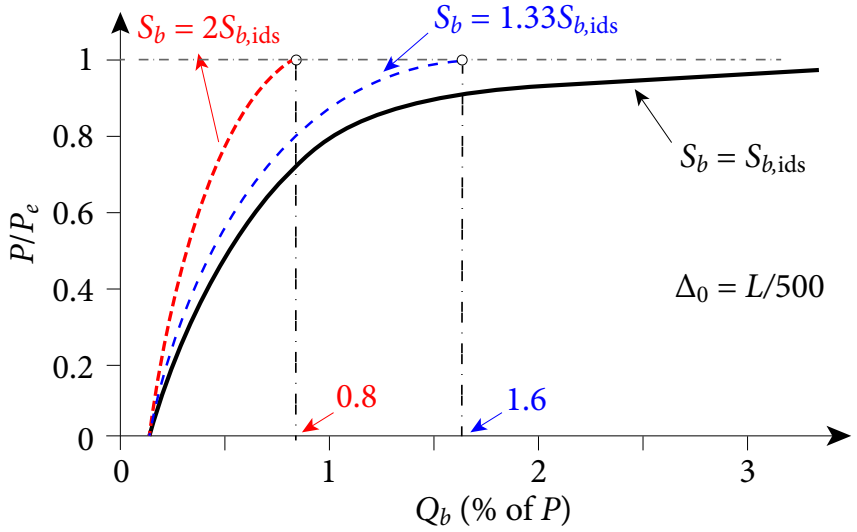

Figure 2.5: Effect of brace stiffness on brace force

However, Winter's model neglects the fact that the initial curvature associated with the half-column's initial out-of-straightness results in additional lateral displacement of the column, which consequently will increase the brace force. For that reason, several standards [10, 11, 24] increase the theoretical value of $0.8\%P_e$ to $1\%P_e$ in an attempt to compensate for neglecting the column curvature and continuity [10]. Nevertheless, whether the amplification of brace force by 25% (from 0.8% to $1\%P_e$) is still adequate for columns with semi-rigid end connections is yet to be answered. Therefore, the effect of column initial

curvature on the brace force of a semi-rigidly connected column is to be investigated in Chapter 3.

2.1.4 Bracing requirements in current standards

The simplified analysis in CSA S16-19 [21] requires that the brace strength shall be at least 0.02 times the factored compressive force at the braced member. Alternatively, the direct method in CSA S16-19 [21] can be used to calculate the required brace force for a single column:

$$\bar{Q}_1 = \frac{\beta_{br}(\Delta_0 + \Delta_b)P}{L_{cb}} \tag{2.6}$$

where β_{br} is a coefficient varying with the number of brace points along the column height, e.g., $\beta_{br} = 2$ for columns with a brace at the mid-height. L_{cb} is the length between braces, Δ_0 is the initial misalignment of the member at a brace point, and Δ_b is the sum of the brace deformation, the brace connection deformation, and the brace support displacement. For multiple columns, the reduction factor η in Eq. (2.7) can be applied to decrease Δ_0 with the consideration of the initial imperfection randomness [21].

$$\eta = (0.2 + 0.8\sqrt{n}) \tag{2.7}$$

where n is the number of members being braced. For multiple compressive members braced at the mid-height, with $\beta_{br} = 2$, $\Delta_b = \Delta_0 = L_{cb}/500$, the maximum brace force is:

$$Q_n = 0.8\%\Sigma P(0.2 + 0.8\sqrt{n}) \tag{2.8}$$

where $\sum P$ is the summation of gravity loads applied on the columns. However, if the simple analysis is adopted, $Q_n = 2\%\Sigma P(0.2 + 0.8\sqrt{n})$, which is considerably greater than that obtained from the direct method.

The Eurocode EN 1993-1-1 [24] specifies that the brace force for multiple columns is:

$$Q_n = 1\%\Sigma P\sqrt{0.5((1 + 1/n))} \tag{2.9}$$

While stipulating that the brace force shall be at least 1% of the axial compressive load for a single column, AISC 360-16 [10] does not clearly specify the brace strength requirement for multiple columns. For multiple members, as per AISC 360-16, if the use of an average initial displacement recommended by Chen and Tong [25] is adopted, the brace force is:

$$Q_n = 1\%\Sigma P/\sqrt{n} \tag{2.10}$$

The Chinese standard GB 50017-2017 [26] stipulates that the bracing force Q_n is determined by:

$$Q_n = \sum P(0.6 + \frac{0.4}{n})/60 \tag{2.11}$$

The Australian standard AS4100-2020 [27] specifies that the brace force Q_n should be calculated by:

$$Q_n = 0.025P_{\max} + 0.0125(\sum P - P_{\max}) \tag{2.12}$$

where $P_{\max}$ is the maximum gravity load.

AISI S100-16 [11] requires the following brace strength for multiple parallel members.

$$\overline{P}_{rb} = \frac{0.5}{j}\left(1 + \frac{1}{\sqrt{n}}\right)\sum \overline{P}_{rb,i} \tag{2.13a}$$

$$\overline{P}_{rb,i} = 0.01\overline{P}_{ra,i} \tag{2.13b}$$

where $\overline{P}_{rb}$ is the required brace strength to brace multiple parallel members; $\overline{P}_{ra,i}$ is the required compressive axial strength of the ith member; $\overline{P}_{rb,i}$ is the required brace strength of the ith member; j is the number of brace anchor ends (j = 1 or 2). For a system with tension-only braces, two anchor ends shall be provided with j taken as 1.

Apparently, there are pronounced discrepancies among the bracing requirements stipulated in standards in different countries. For a single column, 1% of the applied axial load is adopted as the brace strength requirement in EN 1993-1-1 [24], AISC 360-16 [10], and AISI S100-16 [11], but 0.8%, 2%, 1.67%(1/60), and 2.5% in CSA S16-19 simplified analysis, CSA S16-19 direct method, GB 50017-2017 [26], and AS4100-2020 [27], respectively. The comparison of the brace forces for a single column between the analytical result obtained from the newly proposed model and the predictions obtained from AISC 360-16 [10] and CSA S16-19 [21] is discussed in Chapter 3. Except for AS4100-2020 [27], the brace strength requirements for multiple columns in these standards are specified in the form of scaling the sum of applied axial loads on all columns with considering the initial imperfection reduction. Only AS4100-2020 [27] considers the effect of a nonuniform load pattern on the brace force by applying a larger scaling factor to the maximum axial load. However, AS4100-2020 does not account for the favourable effect of the initial imperfection randomness on the brace force, which tends to be overly conservative in this regard. Only AISI S100 [11] specifies that the brace strength requirement can be reduced by half if the multi-column system is anchored on both sides and the braces are not tension-only. In a nutshell, the effects of

semi-rigid connections and load patterns on the brace force for multiple columns are not introduced in current standards, which are to be investigated in Chapter 4.

2.2 Storey-Based Stability of Semi-rigidly Connected Frames

Since 1960's, the alignment chart method has been commonly used in practice to evaluate the capacity of columns in continuous frames by assessing the column effective length factor, K [28]. Because of its simpleness, the alignment chart method is still adopted in current standards [10, 21] in lieu of an actual stability analysis to evaluate the capacity of a frame. However, as might be expected, the overall loading capacity of a frame is usually higher than the prediction based on its individual members due to the capacity of redistribution of loads in frames. The concept of storey-based stability was primarily developed by Higgins [29], Salem [30], and Yura [28], under the notion that the overloaded columns in a frame can be laterally supported by other columns as long as the capacity of the whole frame is not exceeded, so that the sidesway buckling of the frame must occur with all columns in a storey buckling simultaneously.

Subsequently, Yura [28] and LeMessurier [31, 32] proposed the storey buckling approach and storey stiffness approach, respectively, to evaluate the stability of storey frames. Nevertheless, the approaches by Yura [28] and LeMessurier [31, 32] are still based on the assessment of column effective length, which can be tedious and confusing when designing structures containing leaning columns [10].

Besides neglecting the interaction among columns, another important assumption in the development of the alignment charts is that all columns are rigidly connected to beams, which is not realistic and as such may produce overestimated results. Following the storey-based concept, Xu and Liu [33] derived an analytical method to evaluate the stability of a planar frame with semi-rigid connections. The generalized visualization of the semi-braced and semi-rigidly connected storey frame analyzed by Xu and Liu [33] is presented in Fig. 2.6.

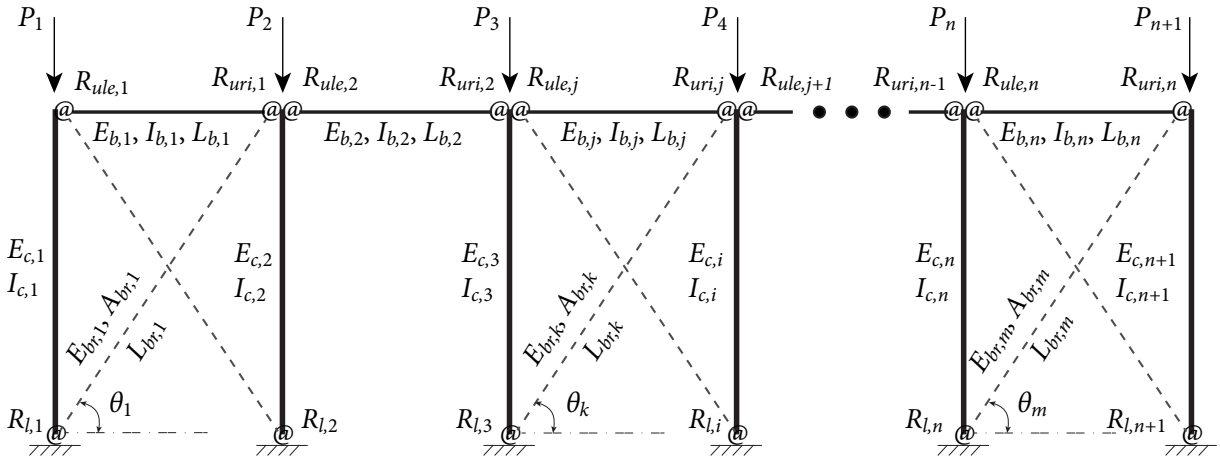

Figure 2.6: Generalized semi-rigidly connected semi-braced storey frame analyzed by Xu and Liu [33]

The n-bay frame illustrated in Fig. 2.6 consists of n beams and $n+1$ columns. E, I, L, and A are the elastic modulus, in-plane moment of inertia, length, and cross-sectional area of the members. R is the rotational stiffness of the beam-to-column connection or the column base connection. P is the applied gravity load. For the symbols of section properties, the subscripts c, b, and br correspond to columns, beams, and diagonal braces, respectively. Accordingly, let the subscript i, j, and k stand for the numbering, from left to right, of the columns (connections), beams, and diagonal braces, respectively. $R_{l,i}$, $R_{ule,j}$, $R_{uri,j}$ are the rotational stiffness of the connections at the lower end of column i, the left end of beam j, and the right end of beam j, respectively. The total bracing stiffnesses provided by the diagonal braces in the frame can be calculated by:

$$S_{br,\mathrm{t}} = \sum_{k=1}^{m} \left[\frac{E_{br,k} A_{br,k}}{L_{br,k}} \left(\frac{1}{1 + \left(A_{br,k}/A_{c,k}\right) \sin^3\theta_k} \right) \cos^2\theta_k \right] \tag{2.14}$$

where θ_k is the angle of the brace with respect to the horizontal direction, as per Fig. 2.6. $A_{c,k}$ is the cross-sectional area of the column connecting the top end of brace k. If $A_c \gg A_{br}$ then the sine term in Eq. (2.14) can be ignored, and thus Eq. (2.14) can be simplified as:

$$S_{br,\mathrm{t}} = \sum_{k=1}^{m} \left[\frac{E_{br,k} A_{br,k}}{L_{br,k}} \cos^2\theta_k \right] \tag{2.15}$$

It should be noted that the presented expressions of $S_{br,\mathrm{t}}$ only apply to tension-only bracing. Xu and Liu [33] adopted the end-fixity factor proposed by Monforton and Wu [34]

to represent the rotational restraint at the ends of columns, as below:

$$r_{u,i} = \frac{1}{1 + \frac{3E_{c,i}I_{c,i}}{\bar{R}_{u,i}L_{c,i}}} \tag{2.16a}$$

$$r_{l,i} = \frac{1}{1 + \frac{3E_{c,i}I_{c,i}}{\bar{R}_{l,i}L_{c,i}}} \tag{2.16b}$$

where $\bar{R}_{u,i}$ and $\bar{R}_{l,i}$ are the effective value of restraint stiffness at the upper and lower end of the column, respectively. For the storey frame shown in Fig. 2.6, $\bar{R}_l$ equals the rotational stiffness of the base connection, R_l, and $\bar{R}_u$ is evaluated based on the beam-to-column connection stiffness and flexural stiffness of beams [35], as expressed in

$$\bar{R}_{u,i} = R'_{ule,i} + R'_{uri,i-1} \tag{2.17a}$$

$$R'_{ule,i} = \frac{6z_{le,i}}{4 - z_{le,i}z_{ri,i}} \frac{E_{b,i}I_{b,i}}{L_{b,i}} (2 + \upsilon z_{ri,i}) \tag{2.17b}$$

$$R'_{uri,i-1} = \frac{6z_{ri,i-1}}{4 - z_{ri,i-1}z_{le,i-1}} \frac{E_{b,i-1}I_{b,i-1}}{L_{b,i-1}} (2 + \upsilon z_{le,i-1}) \tag{2.17c}$$

where $R'_{ule,i}$ and $R'_{uri,i-1}$ are the values of restraint stiffnesses provided by the corresponding beam and connecting beam-to-column connection. $z_{le,i}$ and $z_{ri,i}$ are the end-fixity factors of the left and right end of beam i, respectively, calculated via:

$$z_{le,i} = \frac{1}{1 + \frac{3E_{b,i}I_{b,i}}{R_{ule,i}L_{b,i}}}; \quad z_{ri,i} = \frac{1}{1 + \frac{3E_{b,i}I_{b,i}}{R_{uri,i}L_{b,i}}} \tag{2.18}$$

where υ is the ratio of joint rotation of the far end θ_F to the joint rotation of near end θ_N. Xu [35] indicated that adopting $\upsilon = 1$ associated with the asymmetric buckling mode can yield sufficiently accurate results. Alternatively, the value of υ can be obtained using numerical analysis for better accuracy [36]. Theoretically, the magnitude of an end fixity factor r ranges from zero to unity, which corresponds to an idealized pinned and an idealized fixed connection, respectively. The advantages of adopting r are that it avoids the possible mathematical issues arising from assuming connection stiffness as infinity, i.e., $R = \infty$, and it is more intuitive for engineers to assess the level of restraints on members.

By compiling the stiffnesses of diagonal bracing into $S_{br,\mathrm{t}}$ and using end-fixity factor r to describe the restraints from the connections and adjacent beams on columns, the generalized semi-rigid frame in Fig. 2.6 can be further simplified as the system illustrated in Fig. 2.7.

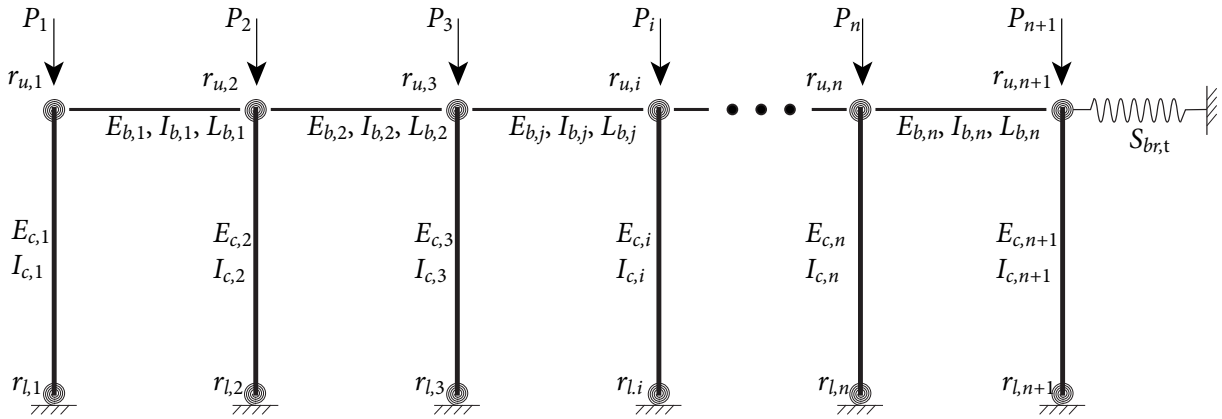

Figure 2.7: Generalized diagram of the storey frame with end-fixity factor

As a consequence, the total lateral stiffness of the system shown in Fig. 2.7 can be expressed as Eq. (2.19) [33].

$$\Sigma S = \left(\sum_{i=1}^{n+1} S_{c,i}\right) + S_{br,\mathrm{t}} = \sum_{i=1}^{n+1} \frac{12 E_{c,i} I_{c,i}}{L_{c,i}^3} \beta_i + S_{br,\mathrm{t}} \tag{2.19}$$

where ΣS is the lateral stiffness of the storey frame, taken as the summation of the lateral stiffnesses of individual columns, $S_{c,i}$ and the total diagonal bracing stiffness, $S_{br,\mathrm{t}}$.

It is worth noting that the premise of using Eq. (2.19) is that beams in the frame can be assumed to be axially rigid, and thus all the columns have the identical lateral displacement induced by possible lateral force or the $P-\Delta$ effect. In this way, the column lateral stiffnesses are additive. β is a modification factor accounting for the effect of axial force on the stiffness and can be calculated from Eq. (2.20) [35].

$$\beta = f(\phi, r_l, r_u) = \frac{\phi^3}{12} \frac{a_1 \phi \cos\phi + a_2 \sin\phi}{18 r_l r_u - a_3 \cos\phi + (a_1 - a_2)\phi \sin\phi}, \quad \phi > 0 \tag{2.20a}$$

$$a_1 = 3[r_l(1 - r_u) + r_u(1 - r_l)] \tag{2.20b}$$

$$a_2 = 9 r_l r_u - (1 - r_l)(1 - r_u)\phi^2 \tag{2.20c}$$

$$a_3 = 18 r_l r_u + a_1 \phi^2 \tag{2.20d}$$

$$\phi = L\sqrt{N_c / E_c I_c} \tag{2.20e}$$

where ϕ is the axial load coefficient, and N_c is the compressive axial force in the column. The derivation of Eqs. (2.20) is based on Euler-Bernoulli theory, and only flexural deformations are considered, neglecting the shear and axial deformations of members.

If $\beta > 0$, i.e., $S_c > 0$, then the column has sufficient retention capacity to bear the axial load by itself and can provide lateral support to other columns in the frame. While a

column with $\beta \leq 0$ requires the support from other columns to maintain its sidesway stability. Consequently, ΣS is an indicator of the frame's lateral instability: the frame is stable only if $\Sigma S > 0$ and unstable when $\Sigma S = 0$. Note that β decreases non-linearly and monotonically with the increase of axial load N_c until rotational buckling occurs. When the axial load in the column is zero ($\phi = 0$), Eq. 2.20a converges to

$$\lim_{\phi \to 0} \beta = \beta_0 = \frac{r_l + r_u + r_l r_u}{4 - r_l r_u} \tag{2.21}$$

Additionally, for leaning columns where $r_u = r_l = 0$, the lateral stiffness S_c converges to the column geometric stiffness, $-N_c/L_c$:

$$\lim_{r_l \to 0, r_u \to 0} S_c = -\frac{N_c}{L_c} \tag{2.22}$$

2.2.1 Non-sway buckling of columns

The previous section shows that the lateral stiffness of a semi-rigidly connected column is a product of $12E_cI_c/L_c^3$ and β, and β is a non-linear function of ϕ, r_l, and r_u. It should be pointed out that Eq. (2.20) is only applicable when the column is in compression ($N_c > 0$) and does not experience yielding failure and flexural rotational buckling:

$$0 \leq N_{c,i} < P_{cr,i} = \frac{\pi^2 E_{c,i} I_{c,i}}{\left(K_i L_{c,i}\right)^2} \tag{2.23a}$$

$$N_{c,i} < P_{y,i} = f_y A_{c,i} \tag{2.23b}$$

where $P_{cr,i}$ and K_i are the rotational (non-sway) buckling load and the effective length factor of column i, respectively. $P_{y,i}$ is the yielding strength of column i, and f_y is the yield stress of steel. The column non-sway buckling load P_{cr} can be obtained by setting the denominator of β in Eq. (2.20a) to zero, as expressed in

$$18 r_l r_u - a_3 \cos\phi_u + (a_1 - a_2)\,\phi_u \sin\phi_u = 0 \ \left(\phi_u > 0\right) \Longrightarrow P_{cr} = \frac{\phi_u^2 E_c I_c}{L_c^2} \tag{2.24}$$

Due to the transcendental function in Eq. (2.24), root-finding algorithms are required to obtain the value of ϕ_u. Ma [37] indicated that the Newton-Raphson method [38] converges well when an initial value $\phi_{u,0} = \pi/K_{\text{app}}$ is adopted. The approximate value of the effective length factor K_{app} can be obtained from the equation proposed by Newmark, as below:

$$K_{\text{app}} = \frac{\left[\pi^2 + r_u(6 - \pi^2)\right] \times \left[\pi^2 + r_l(6 - \pi^2)\right]}{\left[\pi^2 + r_u(12 - \pi^2)\right]\left[\pi^2 + r_l(12 - \pi^2)\right]} \tag{2.25}$$

Although multiple roots exist in Eq. (2.24), corresponding to different buckling modes, they will not typically be encountered when taking $\phi_{u,0} = \pi / K_{\text{app}}$ as the initial value because this value is very close to the exact solution of ϕ_u.

2.2.2 Inelastic buckling of columns

All the aforementioned formulae are limited to the elastic stability analysis of steel frames, assuming that the columns in a frame will be adequately slender; thus, no inelastic buckling or yielding failures will occur prior to lateral instability. However, columns with slenderness ratios corresponding to inelastic buckling are commonly adopted in engineering practice. In the case that columns behave inelastically, the inelastic stiffness reduction factor τ_b specified in AISC 360-16 [10] can be adopted to account for the inelastic buckling of the columns [5], as below:

$$P_{cr} = \frac{\pi^2 E_{\tan} I}{(K_p L)^2}, \quad \text{with} \quad E_t = \tau_b E \tag{2.26a}$$

$$\tau_b = \begin{cases} 1 & \frac{P_{cr}}{P_y} \le 0.5 \\ 4\frac{P_{cr}}{P_y}\left(1 - \frac{P_{cr}}{P_y}\right) & \frac{P_{cr}}{P_y} > 0.5 \end{cases} \quad \text{with} \quad P_y = A_c f_y \tag{2.26b}$$

where K_p is the column effective length factor for inelastic analysis. If the values of end-fixity factors are predetermined, the effective length factor for inelastic analysis equals that for elastic analysis. Accordingly, Eq. (2.26) can be directly used to calculate τ_b with $K_p = K$. But if the connection stiffness R is given, the reduced elastic modulus E_t will affect the end-fixity factor defined in Eq. (2.16) and subsequently affect the effective length factor K_p. In that case, substituting the expression of P_{cr} in Eq. (2.26a) into Eq. (2.26b) and replacing the elastic modulus E in Eq. (2.24) by $E_t = \tau_b E$ give the expressions involving τ_b and K_p, as shown in Eqs. (2.27). As such, the values of τ_b and K_p can be obtained by solving Eqs. (2.27) [1].

$$\frac{\pi^2 \tau_b E_c I_c}{\left(K_p L_c\right)^2} - \left[1 - \frac{A_c f_y \left(K_p L_c\right)^2}{4\pi^2 E_c I_c}\right] A f_y = 0 \tag{2.27a}$$

$$18 r_l r_u - a_3 \cos\phi_u + (a_1 - a_2)\,\phi_u \sin\phi_u = 0 \tag{2.27b}$$

where

$$\phi_u = \pi / K_p \tag{2.28a}$$

$$r_i = \frac{1}{1 + 3E_c \tau_b I / (R_i L_c)} \tag{2.28b}$$

2.2.3 Effects of axial deformations

As mentioned in Section 2.2, the storey-based stability approach by Xu [35] was developed based on assuming all the beams are axially rigid, which is feasible for structures with rigid floors or rigid roof diaphragms. However, due to neglecting the axial deformations of beams, applying Eq. (2.19) to evaluate the instability of structures without rigid floors or with flexible diaphragms, such as industrial workshops and storage racks, may yield unconservative results. The research reported in [3] proposed a method to incorporate the effect of beam axial deformations into evaluating the storey-based stability of steel frames using the concept of equivalent spring stiffness. It was found that the effect of beam axial deformations should not always be neglected in structural analysis as it will reduce the lateral stiffness and critical load of a frame.

In contrast to beam axial deformations, the axial deformations in columns due to the compressive loads will shorten the columns, thus increasing the lateral stiffness and capacity by marginal amounts [37]. Therefore, the effects of column axial deformations are typically neglected in structural design and analysis for the reason of conservation and convenience. Likewise, the effects of column axial deformations on the stability of structures are not considered in this study.

2.3 Fire-Structural Analysis

Admittedly, fire safety has become an inseparable part of structural design, especially for steel structures that are vulnerable to fire hazards due to steel's high thermal conductivity and dramatic deterioration of mechanical properties at elevated temperatures.

Presented in Fig. 2.8 is a typical structural fire engineering (SFE) design process [39]. First, the design fuel load is established according to the combustible material in a given space. Once the design fuel load is attained, the fire development can be simulated with enclosure and ventilation conditions. Then, the analysis regarding thermal response is carried out based on the well-established theory of heat transfer to determine the temperature histories of structural members. The structural response associated with temperature (time) can be analyzed by modelling the structural system and incorporating the mechanical properties. Compared to structural analysis at ambient temperature, the fire-structural analysis should

account for the material nonlinearity, possible thermally induced stresses, and geometrical imperfections, which play crucial roles in structural analysis at elevated temperatures.

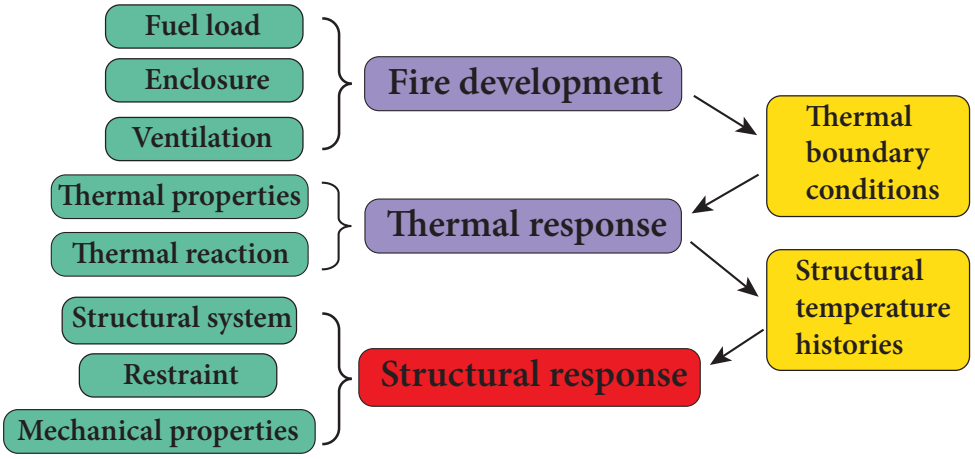

Figure 2.8: Typical SFE design process [39]

As fire development is more within the fire engineering scope, structural fire engineering typically only adopts design fires which prescriptively describe the gas temperature variations with time [39]. Accordingly, as this study mainly focuses on the structural response of the multi-column systems, the research pertinent to steel mechanical properties, stress-strain relationships, and the stability of steel frames at elevated temperatures is reviewed in this section.

2.3.1 Mechanical properties of steel at elevated temperatures

The mechanical properties of steel, i.e., strength and modulus, deteriorate at elevated temperatures, which subsequently reduces the strength and stiffness of structural steel members in a fire. As a result, the mechanical properties of steel at elevated temperatures are essential to achieve an appropriate fire analysis on steel structures. As the tensile tests on steel at elevated temperatures are expensive and laborious, researchers establish the mechanical properties of steel using the retention factors (a ratio of the mechanical properties at elevated temperature to that at ambient temperature) obtained from the existing experimental research or current fire design standards, together the measured mechanical properties at the ambient temperature.

For a typical stress-strain relationship of steel at the elevated temperature, the definitions of elastic modulus E_T, proportional limit $f_{p,T}$, and yield strengths are illustrated in Fig. 2.9.

Conventionally, different yield strengths are introduced to characterize the stress-strain relationships of steel at elevated temperatures due to the lack of an obvious yield plateau. As shown in Fig. 2.9, the 0.2% offset yield strength ($f_{0.2\text{offset}}$) is the stress of the intersection of the stress-strain curve and the proportional line offset by 0.2% strain [40]. The yield strengths, $f_{0.5}$, $f_{1.0}$, $f_{1.5}$, and $f_{2.0}$ correspond to the stresses associated with the strains being 0.5%, 1.0%, 1.5%, and 2.0%, respectively. Generally, $f_{0.2\text{offset}}$ and $f_{2.0}$ are more widely adopted by researchers to portray the stress-strain curves of steel at elevated temperatures.

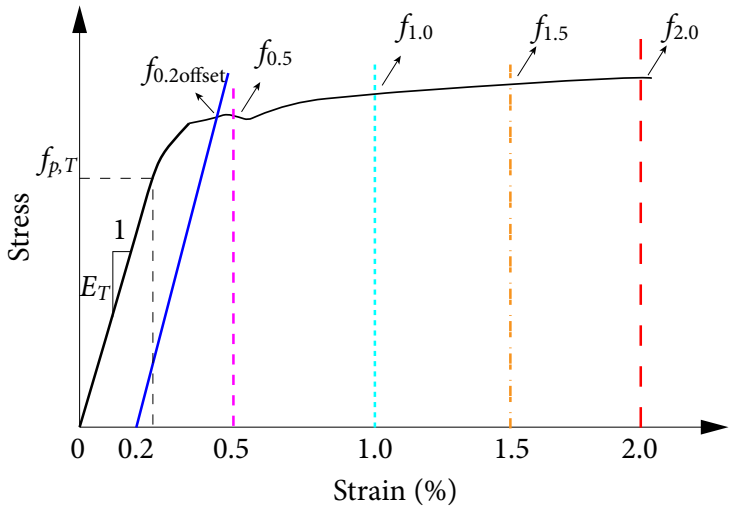

Figure 2.9: Definitions of elastic modulus, proportional limit, and yield strengths at elevated temperatures

The European Code EN 1993-1-2 [41] provides the retention factors for structural steel at elevated temperatures, which are also adopted by AISC 360-16 [10], as presented in Table 2.1, in which the yield strength $f_{y,T}$ corresponds to the stress associated with the strain being 2.0%, $f_{2.0}$. Note that EC3 [41] specifies alternative retention factors of yield strength for the hot-rolled class 4 sections, represented as k_{yb} in Table 2.1. allows that the linear interpolation can be used for intermediate values of the steel temperature. With the consensus of the international fire engineering and research community, the values in Table 2.1 have been widely used in fire design.

Studies [42–46] show that high-strength steels have different retention factors from mild steels as they possess distinctive chemical compositions. There, since values in Table 2.1 are mainly based on experimental results of steel with normal strength, AISC 360-16 stipulates that Table 2.1 does not apply for steels with yield strengths in excess of 65 ksi (450 MPa).

Moreover, the mechanical properties of cold-formed steels may vary from those of hot-rolled steels due to the cold-forming procedure. The experimental research by Craveiro et al. [47] indicates that the yield strengths predicted in current design standards [27, 41, 48] are unconservative for low-strength (up to 350 MPa) cold-formed steels. For cold-formed steels, large variations were found among the existing experimental results of different cold-formed steel sections [47, 49–52], or even different elements in the same section [53], due to the different levels of cold-forming experienced in manufacturing.

Table 2.1: Temperature-dependent retention factors for steel specified in EN 1993-1-2 [41]

T(°C)	$k_y = f_{y,T}/f_y$	$k_p = f_{p,T}/f_p$	$k_E = E_T/E$	$k_{yb} = f_{yb,T}/f_{yb}$
20	1.000	1.000	1.000	1.00
100	1.000	1.000	1.000	1.00
200	1.000	0.807	0.900	0.89
300	1.000	0.613	0.800	0.78
400	1.000	0.420	0.700	0.65
500	0.780	0.360	0.600	0.53
600	0.470	0.180	0.310	0.30
700	0.230	0.075	0.130	0.13
800	0.110	0.050	0.090	0.07
900	0.060	0.0375	0.0675	0.05
1000	0.040	0.0250	0.0450	0.03
1100	0.020	0.0125	0.0225	0.02
1200	0.000	0.0000	0.0000	0.00

Given that there are no universally accepted retention factors for high-strength hot-rolled and cold-formed steels at elevated temperatures, fire analyses on steel structures should adopt the available experimental results of the used steel or adopt those of the steel with equivalent grade and same type for better accuracy.

2.3.2 Stress-strain models

Besides the deterioration of elastic modulus and yield strength discussed in the previous section, another major characteristic of steel at elevated temperatures is that the yield plateau almost disappears when the temperature exceeds 300 °C [49, 54, 55]. In the past decades, various models were proposed to describe the stress-strain relationships of steel at elevated temperatures, mainly consisting of multilinear approximations [56, 57], smooth curves [58, 59] and the combination of linear and smooth curves [41, 60, 61]. Compared to the multilinear models, the stress-strain relationship models with smooth curves are more consistent with the inelastic material behaviour of steel at elevated temperatures, and consequently can fit the experimental results more accurately. Two stress-strain models that are mostly adopted in the current fire structural research community are introduced in this subsection.

EC3 Model

The stress-strain curve specified in EN 1993-1-2 [41] (referred to as the EC3 model) is subdivided into four portions and can be expressed in Eq. (2.29).

$$\sigma = \begin{cases} \varepsilon E_T, & \varepsilon \le \varepsilon_{p,T} \\ f_{p,T} - c + \frac{b}{a}\left[a^2 - \left(\varepsilon_{y,T} - \varepsilon\right)^2\right]^{0.5}, & \varepsilon_{p,T} < \varepsilon < \varepsilon_{y,T} \\ f_{y,T}, & \varepsilon_{y,T} \le \varepsilon \le \varepsilon_{t,T} \\ f_{y,T}(1 - (\varepsilon - \varepsilon_{t,T}))/(\varepsilon_{u,T} - \varepsilon_{t,T}), & \varepsilon_{t,T} < \varepsilon \le \varepsilon_{u,T} \end{cases} \tag{2.29}$$

where $\varepsilon_{p,T}$ is the strain at the proportional limit; $\varepsilon_{y,T}$ is yield strain, taken as 0.02; $\varepsilon_{t,T}$ is limiting strain for yield strength, taken as 0.15; $\varepsilon_{u,T}$ is ultimate strain, taken as 0.2; a, b and c are coefficients related to the above parameters to depict the elliptical curve and are given in:

$$a^2 = \left(\varepsilon_{y,T} - \varepsilon_{p,T}\right)\left(\varepsilon_{y,T} - \varepsilon_{p,T} + c/E_T\right) \tag{2.30a}$$

$$b^2 = c\left(\varepsilon_{y,T} - \varepsilon_{p,T}\right)E_T + c^2 \tag{2.30b}$$

$$c = \frac{\left(f_{y,T} - f_{p,T}\right)^2}{\left(\varepsilon_{y,T} - \varepsilon_{p,T}\right)E_T - 2\left(f_{y,T} - f_{p,T}\right)} \tag{2.30c}$$

Ramberg-Osgood Model

In 1943, Ramberg and Osgood proposed [58] a formula, as given in Eq. (2.31), to describe the stress-strain relationship of steel at ambient temperature.

$$\varepsilon = \frac{\sigma}{E} + \alpha_r \left(\frac{\sigma}{E}\right)^{\eta_r} \tag{2.31}$$

where α_r and η_r are coefficients determined according to the experimental data. When the stress is relatively small, as the value of the exponential term in Eq. (2.31) is insignificant, the strain is governed by the term σ/E, and consequently the material exhibit almost linear. Conversely, the material becomes more nonlinear as the stress increases. Such a characteristic, plus its simple format, makes Ramberg-Osgood formula suitable to describe the stress-strain curves of steel at elevated temperatures with appropriate modifications [59], especially for cold-form steels [47, 52, 53, 62].

2.3.3 Creep effects on steel structures

The phenomenon of creep refers to the permanent deformation a material will undergo over time, even under constant loading. Typically, the creep strain variation over time consists of three stages: primary, secondary, and tertiary stages, as shown in Fig. 2.10. In the primary stage, the creep strain rate is relatively high but decreases with time; in the secondary stage, the creep strain rate remains stable; and in the tertiary stage, the creep strain accelerates with time until rupture [63].

Experimental research [45, 64, 65] indicates that the creep strain path highly depends on the temperature and stress levels; more importantly, it varies greatly among different types of steel. Thereby, researchers [66–70] developed various mathematical expressions, referred to as creep models, to describe the creep strain variations of steel at elevated temperatures. As shown in the previous studies [4, 45, 65], Fields and Fields creep model [67] exhibits good agreements with creep test results of different steel types. In addition to its simple format, as expressed in Eq. (2.32), Fields and Fields creep model has been widely used in fire structural analyses [70–72].

$$\varepsilon_{\text{cp}} = a t^b \sigma^c \tag{2.32}$$

where ε_{cp} is the creep strain; t is time; a, b and c are coefficients determined by fitting the creep test results.

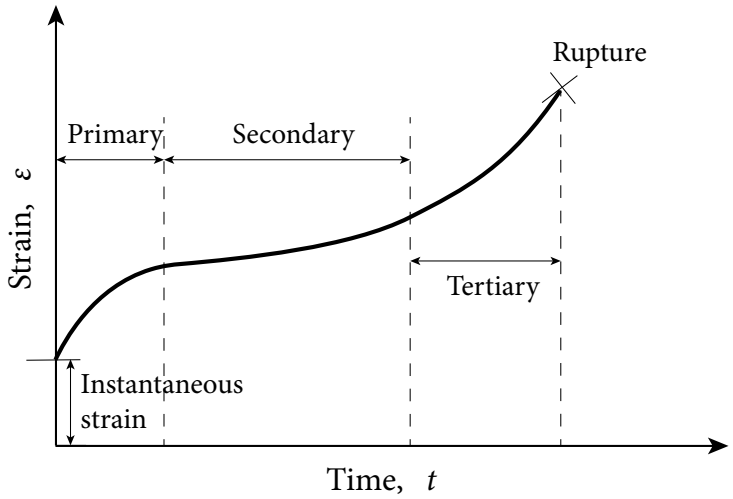

Figure 2.10: Typical creep strain curve

For steel structures, the creep effect is usually neglected in design at ambient temperature due to the extremely low creep strain rate. However, research [73] indicates that the creep strain rate becomes dominant when the temperature reaches 30% of the melting point of metals, corresponding to around 400°C for steel. Accordingly, when it comes to the fire design of steel structures, the creep strain increases rapidly at elevated temperatures, which reduces stiffness and consequently increases deformations of steel members. In the past several decades, it has reached a consensus in the research community of fire-structural analysis [74–77] that the creep effect should not be neglected for steel structures to avoid unconservative predictions of structural behaviour at elevated temperatures.

Huang et al. [75] used the finite element software FEMFAN2D to analyze the structural behaviour of restrained steel columns subjected to fire. The study shows that creep should be considered in fire analysis even for cases in which steel columns are heated at rapid paces, and the creep effect can be significant over 350°C for some extreme cases. Li and Zhang [76] investigated the creep effect on the buckling temperature of restrained steel columns. Different from their adverse effects on unrestrained steel columns, the creep strains in the axially restrained steel columns can partially release the thermal-induced compressive force, which may result in a higher buckling temperature. A finite element model for simulating the fire behaviour of a high-strength steel column was established in ABAQUS by Wang et al. [77] with considering the creep effect, and the model was validated with experimental results. The subsequent parametric studies indicate that the reduction of the critical temperature of the steel column due to the creep effect is primarily affected

by the heating rate. Overall, the aforementioned research emphasizes the necessity of considering the creep effect in the fire design of steel structures.

When subjected to the constant applied load and elevated temperature, structural steel columns may buckle after a certain duration due to the increasing creep-induced lateral deflection. This phenomenon is referred to as creep buckling. The creep buckling of steel columns was initially investigated by Marin [78], who assumed that the creep deflection curve of an axially loaded column could be obtained by amplifying the elastic deflection curve, and the mid-height deflection induced by creep was assumed to be linear with time. Subsequent research regarding creep buckling of columns [79–83] showed that even if the applied load was less than the Euler buckling load of the column, the column deflection could be significant as time increases, and the deflection increased rapidly with time when the applied load approached the Euler buckling load.

Although the previous research [72, 79–81, 84] provides plausible methods to evaluate the creep buckling behaviour of steel columns at elevated temperatures, there are some discrepancies among the assumptions adopted in those methods. As the validity of the assumptions is still unknown, the accuracy of the corresponding failure mechanism of creep buckling is yet to be answered. In Chapter 7, these issues are to be discussed.

2.3.4 Steel frame stability at elevated temperatures

Due to the difficulty and complexity of investigating the instability of steel frames at elevated temperatures, the majority of past experimental [85–88] and theoretical research [75, 89–93] focused on the structural behaviour of individual steel columns at elevated temperatures. The following can be concluded from the prior research:

1. The load ratio is the most crucial factor for determining the critical temperature of a steel column.

2. For a restrained steel column, axial restraint generally reduces the critical temperature as the restraint on thermal expansion at elevated temperature will induce additional axial force, while the presence of rotational restraints increases the critical temperature by decreasing the effective length of the column.

3. The nonlinear stress-strain relationships of steel at elevated temperatures and initial imperfections of steel columns should be incorporated into the fire-structural analysis.

4. As the creep of steel becomes pronounced at certain elevated temperatures, lowering the heating rate will decrease the critical temperatures of steel columns.

Xu and Zhuang [94] indicated that the buckling strength of a steel frame at elevated temperatures could be underestimated if the evaluation is solely based on the fire behaviour of individual columns, as unheated columns in the same storey still have the capacity to laterally support the columns exposed to fire. Thus, this subsection highlights some representative research to signify the significant factors that need to be concerned in the fire-structural analysis of steel frames.

Rubert and Schaumann [60] conducted a series of fire tests on steel frame assemblies, in which the structural responses and critical temperatures were acquired at differing heating rates, load ratios and system slenderness ratios. This research indicated that the critical temperature decreases with a lower heating rate, which experimentally demonstrated that the creep effect has adverse effects on the fire behaviour of steel frame assemblies. As the experiments carried out by Rubert and Schaumann [60] focused on the lateral instability of unbraced steel frames, they were frequently utilized to verify the numerical approaches in the subsequent fire-structural research regarding steel frames [59, 71, 93, 95–97].

In practice, robust firewalls are commonly constructed between large buildings to prevent the fire from spreading to other buildings, subsequently decreasing the economic losses. At elevated temperatures, unbraced steel frames may deform laterally due to thermal expansions of beams and lower mechanical properties, and consequently contact and damage the fire walls. Ali et al. [71] found that shorter columns or columns with stronger cross-sections would provide larger resistance to lateral expansion of the girder, and thus reduce the minimum required clearance between the frame and firewall. As a matter of fact, the shorter columns or columns with stronger cross-sections mentioned by Ali et al. [71] are the columns with relatively larger lateral stiffness. Overall, their research emphasizes the effect of beams' thermal expansion on the structural behaviour of steel frames and the contribution of column lateral stiffness to restrain beam deformations in fires. Accordingly, the thermal expansion of braces should be considered when evaluating the fire resistance of braced multi-column systems. To that end, an analytical method is proposed in Chapter 8

to calculate the additional lateral displacements of columns and additional forces in braces in multi-column systems induced by the braces' thermal expansion.

When it comes to fire scenarios, the column lateral stiffness will decrease due to the deterioration of material properties at elevated temperatures. In the preliminary investigation on the storey-based stability of unbraced steel frames at elevated temperatures, Xu and Zhuang [98] assume the temperature to be uniformly distributed in steel columns and incorporate the retention factor of steel elastic modulus at elevated temperatures, k_E. In such a way, Eq. (2.20) can be extended to evaluate the lateral stiffness of a semi-rigidly connected column at elevated temperatures by replacing the elastic modulus at ambient temperature E with the elastic modulus at elevated temperatures $E_T = k_E E$.

Nevertheless, only adopting the elastic modulus of steel at elevated temperatures E_T in the storey-based stability analysis [94, 98] may not be a satisfying approach to evaluate the steel frame's capacity at elevated temperatures because the stress-strain relationships of steel at elevated temperatures are characterized by its obvious non-linearity, as discussed above. More importantly, the research by Xu and Zhuang [94, 98] ignored the reduction of steel yield strength at elevated temperatures. Subsequently, instead of using the elastic modulus, Ma and Xu [99] adopted the tangent modulus of steel at elevated temperatures $E_{\tan,T}$ specified in the EC3 [41] and proposed new criteria to assess the stability of an unbraced n-bay steel frame at elevated temperatures.

Despite adopting the tangent modulus of steel at elevated temperature, the current calculation of column lateral stiffness assumes that the stress is uniformly distributed on column cross-section: $\sigma = P/A_c$. The assumption neglects the cross-sectional stress gradient resulting from the internal bending moment in the column, which may overestimate the critical temperature of steel frames. Owing to this, the effect of partial yielding on the column lateral stiffness is to be investigated in Chapter 8. Besides the partial yielding of steel columns, the failure criterion that a steel frame loses its sidesway stability when the total lateral stiffness of the frame equals zero may not be practical for cases at elevated temperatures as it represents a bifurcation phenomenon where the lateral displacement is theoretically infinite; thereby, it is necessary to establish a new failure criterion or criteria for storey-based stability analysis.

Chapter 3

Bracing Requirements for a Single semi-rigidly connected column

3.1 Introduction

Intermediate bracing is an efficient way to increase the column strength by decreasing the column's effective length. The prevailing practice for designing the brace [10, 11] requires determining the ideal brace stiffness first, which is the minimum brace stiffness required to ensure that the full buckling strength of the braced column can be achieved [5].

Due to the existence of the column initial imperfection Δ_0, if the ideal brace stiffness is adopted, the additional displacement Δ associated with the applied load becomes considerably large as the load approaches the column's critical buckling load, which subsequently results in a large brace force and is structurally unacceptable. Thus, the additional displacement Δ shall be limited to avoid the large brace force in practice. The AISC specification [10] adopts twice the ideal brace stiffness to ensure that the additional displacement equals the initial imperfection: $\Delta = \Delta_0$. By taking the brace stiffness as twice the ideal brace stiffness and Δ as 1/500 of the braced length, the theoretical brace force is 0.8% of the required axial strength of the column, P_r [10].

So far, the research regarding the brace force is primarily based on Winter's model [7], which mimics a column as two rigid segments at the brace point and uses a fictitious hinge to connect the two segments and brace, as per Fig. 2.1. However, Winter's model neglects effects of the column stiffness and shape of the initial curvature on the lateral

displacement of the column. For that reason, the AISC specification [10] increases the theoretical value, 0.8%, to 1%P_r with an attempt to compensate for neglecting the column curvature and continuity. Besides neglecting the column the shape of the initial curvature, as Winter's model assumes the column ends to be pinned connected, the specification [10] admits that the specified bracing requirements are not sufficient for the column with the corresponding effective length factor of K less than 1.0. Although the assumption of ideally pinned connection behaviour greatly facilitates the analysis and design procedures, it may be conservative because all the connections in practice possess some degree of rotational stiffnesses. Hence, whether the amplification of brace force by 25% (from 0.8% to 1%P_r) is adequate for semi-rigidly connected columns is yet to be answered. In addition, as Winter's model neglects the column continuity across the brace, it does not realistically characterize the actual stiffness interaction between the column and the brace. To bridge the gap, a new analytical model is proposed in this chapter to investigate the effects of column initial curvature and semi-rigid end connection on the bracing requirements.

3.2 Half-length Column Model

A new half-length column model is proposed in this section to consider the effects of the column initial curvature, semi-rigid column end connections and column continuity at the bracing point on the bracing requirements, as illustrated in Fig. 3.1. The column shown in Fig. 3.1a is semi-rigidly connected at both ends with the same end-fixity factor r_e and is laterally braced at its mid-height. Considering the initial imperfection Δ_0 induces the lateral deflection Δ under the action of the applied load P, as per Fig. 3.1b. The column-brace system in Fig. 3.1b can be modelled by two identical half-column-brace systems in Fig. 3.1c due to symmetry. Furthermore, the half-column-brace system in Fig. 3.1c can be equivalently converted to the system in Fig. 3.1d by introducing an equivalent lateral load Q_0 and column lateral stiffness S_c to evaluate the lateral deflection of the half-length column. The expressions of S_c and Q_0 for the half-length semi-rigidly connected column of Q_0 are to be derived in the following section.

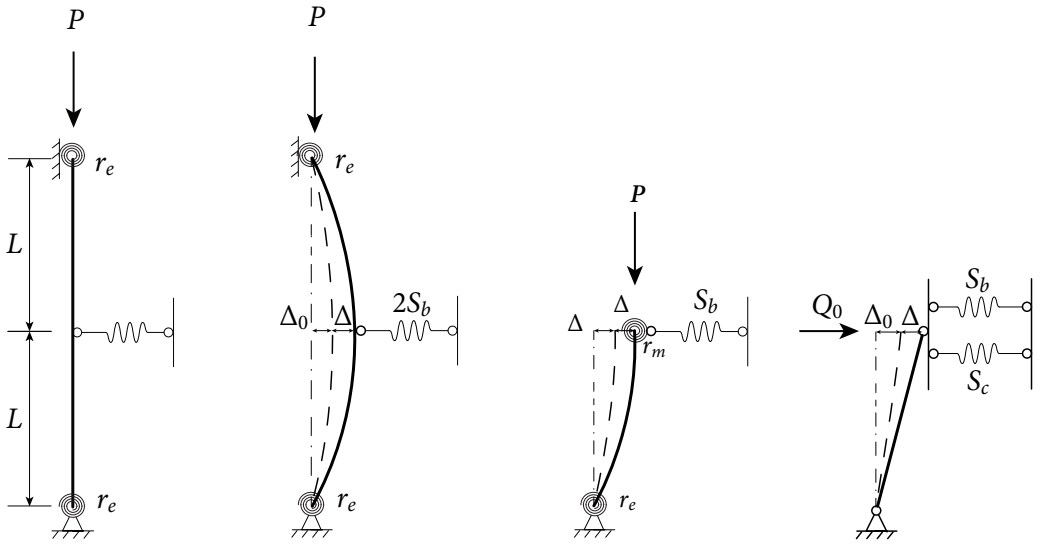

Figure 3.1: Half-length column model

The lateral stiffness of the equivalent spring system in Fig. 3.1d is the summation of the column lateral stiffness and brace stiffness. The criterion for determining the ideal brace stiffness is to let the half-length column reach its sway buckling load and non-sway buckling load (critical buckling load) simultaneously. Therefore, the ideal brace stiffness for the single column $S_{b,\text{ids}}$ is obtained when the lateral stiffness of the half-column-brace system in Fig. 3.1d becomes zero with the critical buckling load being applied on the half-length column, as below:

$$\Sigma S = S_c\,(P_{cr}, r_e) + S_{b,\text{ids}}/2 = 0 \Longrightarrow S_{b,\text{ids}} = -2S_c(P_{cr}, r_e) \tag{3.1}$$

3.3 Mid-height lateral deflection of a semi-rigidly connected column

The dashed lines in Fig. 3.2 represent the initial imperfection of the column that can be expressed using Eq. (3.2). Let y be the additional lateral deflection induced by the axial load P and lateral load Q, and $y(L) = \Delta$.

$$y_0(x) = \Delta_0 \sin\left(\frac{\pi}{2L}x\right) \tag{3.2}$$

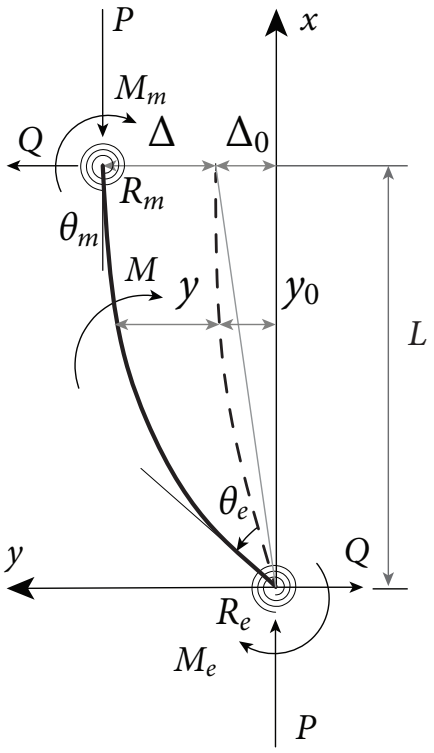

Figure 3.2: Column imperfection and equilibrium based on the deformed shape

The relationships between bending moments and rotational stiffnesses at the upper and lower ends of the half-length column are:

$$M_m = R_m \theta_m \tag{3.3a}$$

$$M_e = R_e \theta_e \tag{3.3b}$$

Thus, based on the equilibrium of the half-length column:

$$R_m \theta_m + R_e \theta_e = QL + P(\Delta + \Delta_0) \tag{3.4}$$

The governing differential equation associated with the flexural deformation of the half-length column shown in Fig. 3.2 can be written as:

$$-EI\frac{d^2y}{dx^2} = P(y + y_0) - \theta_e R_e + Qx \tag{3.5}$$

By solving the differential equation, the deformation and rotation of the column can be obtained from Eqs. (3.6).

$$y(x) = C_1 \cos\left(\frac{\phi x}{L}\right) + C_2 \sin\left(\frac{\phi x}{L}\right) + \frac{\theta_e R_e}{P} - \Delta_0 \frac{4\phi^2}{4\phi^2 - \pi^2} \frac{\sin(\pi x/2L)}{P} - \frac{Q}{P}x \tag{3.6a}$$

$$y'(x) = -C_1 \frac{\phi}{L} \sin\left(\frac{\phi x}{L}\right) + C_2 \frac{\phi}{L} \cos\left(\frac{\phi x}{L}\right) - \Delta_0 \frac{4\phi^2}{4\phi^2 - \pi^2} \frac{\pi}{2L} \frac{\cos(\pi x/2L)}{P} - \frac{Q}{P} \tag{3.6b}$$

where ϕ is the axial load coefficient expressed in Eq. (2.20e), and C_1 and C_2 are coefficients to be determined by the boundary conditions, namely:

$$y(0) = 0 \tag{3.7a}$$

$$y(L) = \Delta \tag{3.7b}$$

$$y'(0) = \theta_e \tag{3.7c}$$

$$y'(L) = \theta_m \tag{3.7d}$$

By substituting Eq. (3.4) and Eqs. (3.7) into Eqs. (3.6), the system of five equations is obtained and then solved for Δ, C_1, C_2, θ_e and θ_m. The lateral displacement of the column Δ is therefore obtained:

$$\Delta = \frac{Q + \frac{P\Delta_0}{L}\psi}{S_c} = \frac{Q + \frac{P\Delta_0}{L}\psi}{\frac{12E_cI_c}{L^3}\beta} \tag{3.8}$$

where β is the same modification factor given in Eq. (2.20a), and ψ is an amplification factor accounting for the influence of the column initial curvature on the lateral deflection and can be expressed as Eq. (3.9a) by incorporating the end-fixity factor in Eq. (2.16). The S_c in Eq. (3.8) is the same as the S_c in Eq. (2.20), which was derived without considering the column initial curvature [33].

$$\psi = \frac{\phi^2 \left[\begin{array}{l} (1-r_e)(1-r_m)\phi\sin\phi\left(4\phi^2-\pi^2\right) - 4a_1\phi^2\cos\phi - \\ 3\pi^2 r_e\left(1-\cos\phi\right)(1-r_m) + 18\pi r_e r_m\left(1-\cos\phi\right) + \\ 6\pi\phi\sin\phi r_e(1-r_m) - 36\phi r_e r_m\sin\phi \end{array} \right]}{\left(4\phi^2-\pi^2\right)\left[18r_e r_m - a_3\cos\phi + (a_1-a_2)\phi\sin\phi\right]} \tag{3.9a}$$

$$a_1 = 3[r_e(1-r_m) + r_m(1-r_e)] \tag{3.9b}$$

$$a_2 = 9r_e r_m - (1-r_e)(1-r_m)\phi^2 \tag{3.9c}$$

$$a_3 = 18r_e r_m + a_1\phi^2 \tag{3.9d}$$

For the proposed half-length column model shown in Fig. 3.1c, if the column fails in lateral sway buckling, the column deformed shape will be symmetrical about the mid-height, which indicates that there is no rotation at the column mid-height. As a consequence, the upper end-fixity factor of the half-column r_m should be taken as 1.0 when calculating the lateral stiffness of the half-length column, S_c. By doing so, Eq. (2.20) and Eq. (3.9a) can be simplified as Eq. (3.10) and Eq. (3.11a), respectively.

$$S_c = \frac{3EI}{L^3}\frac{\phi^3\left[3r_e\sin\phi + \phi\cos\phi(1-r_e)\right]}{18r_e\left(1-\cos\phi\right) - 3\phi^2\cos\phi(1-r_e) - 3\phi\sin\phi(4r_e-1)} \tag{3.10}$$

$$\psi = \frac{2\phi^2\left[2\phi^2\cos\phi(1-r_e)+6\phi r_e\sin\phi+3\pi r_e\left(\cos\phi-1\right)\right]}{\left(4\phi^2-\pi^2\right)\left[\left(6r_e+\phi^2-r_e\phi^2\right)\cos\phi-6r_e+(4r_e-1)\phi\sin\phi\right]}, \qquad \phi>0 \tag{3.11a}$$

$$\lim_{\phi\to 0}\psi = \frac{1.216-0.433r_e}{1-0.25r_e} \tag{3.11b}$$

As a result, the relationship among the axial compressive load P, lateral load Q, and mid-height lateral deflection Δ of a column with semi-rigid connections is attained, as expressed in Eq. (3.8).

3.4 Effect of End-Fixity Factor on Ideal Brace Stiffness

This section investigates the variation of the ideal brace stiffness of a single semi-rigidly connected column with the end-fixity factor. As indicated in Eq. (3.1), the requisite of determining the ideal brace stiffness is obtaining the magnitude of the half-length column's critical buckling load P_{cr}, which can be obtained via Eq. (2.24). It is worth noting that in the evaluation of P_{cr}, r_m shall be taken as 0 to mimic the anti-symmetric deformed shape of the full-length column associated with the non-sway buckling. Thus, substituting $r_u = r_m = 0$ and $r_l = r_e$ into Eq. (2.24) gives

$$3r_e\phi_u\cos\phi_u+\left[3r_e+(1-r_e)\phi_u^2\right]\sin\phi_u=0 \ \left(\phi_u>0\right) \Longrightarrow P_{cr}=\frac{\phi_u^2 EI}{L^2} \tag{3.12}$$

When the critical buckling load is applied on the single column ($P = P_{cr}$,) let β_u and ϕ_u be the corresponding values of β and ϕ defined in Eq. (2.20a) and Eq. (2.20e), respectively. With known r_e, column section properties and length, the critical buckling load P_{cr} and ideal brace stiffness $S_{b,\text{ids}}$ of the single full-length column can be obtained via Eq. (3.12) and Eq. (3.13) for elastic analysis, respectively. If necessary, the stiffness reduction factor τ_b in Eq. (2.26b) can be incorporated into evaluating P_{cr} and $S_{b,\text{ids}}$.

$$S_{b,\text{ids}} = -2S_{c,\text{cr}} = -\frac{24E_cI_c}{L^3}\beta_u \tag{3.13}$$

where $S_{c,\text{cr}}$ is the lateral stiffness of the half-length column with $P = P_{cr}$.

The variations of P_{cr} and $S_{b,\text{ids}}$ with r_e are presented in Fig. 3.3, in which the numerical results obtained from the finite element software ABAQUS are also presented for the verification purpose, indicating good agreements with the analytical results. For the sake of brevity, the general features of the finite element modelling are given in Appendix A.

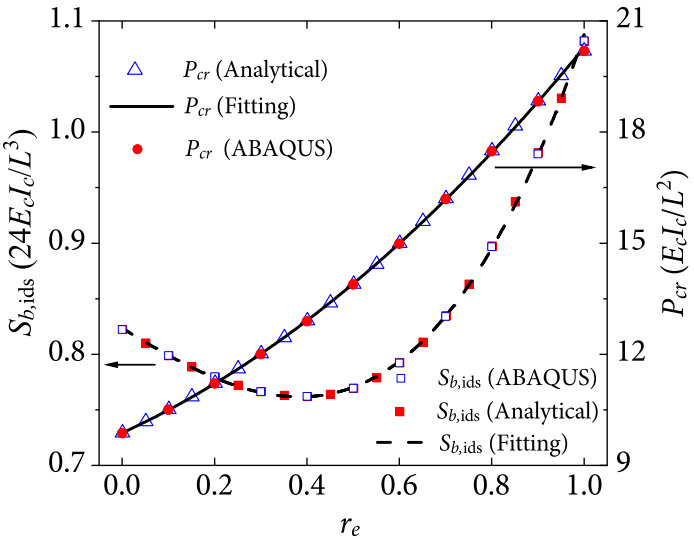

Figure 3.3: Influence of end-fixity factor on the ideal bracing requirement of a single semi-rigidly connected column

Two fitting formulas for ϕ_u^2 and β_u are presented in Eq. (3.15) with R^2 being 0.99979 and 0.99995, respectively, which agrees well with the analytical results, as shown in Fig. 3.3. By adopting Eq. (3.14) and Eq. (3.15), with known end-fixity factor r_e, the corresponding critical buckling load is $P_{cr} = \phi_u^2 E_c I_c / L^2$, and the ideal brace stiffness for a single semi-rigidly connected column $S_{b,\text{ids}}$ can be obtained without solving the implicit equation in Eq. (2.24).

$$\phi_u^2 = 9.8766 + 5.7064 r_e + 4.6981 r_e^2 \tag{3.14}$$

$$\beta_u = -0.8235 + 0.257 r_e - 0.0815 r_e^2 - 0.4397 r_e^3 \tag{3.15}$$

For inelastic analysis, E_c varies with r_e and is associated with the column's yield strength P_y. For elastic analysis, E_c is constant, and the critical buckling load of column P_{cr} increases as the end-fixity factor r_e increases, as per Fig. (3.3). It is worth noting that $S_{b,\text{ids}}$ decreases as r_e increases in the region of $0 \le r_e \le 0.392$ and then increases as r_e increases from 0.392 to 1.0. The ideal brace stiffness of a semi-rigidly connected column reaches the minimum value when the end-fixity factor is 0.392.

The reason can be explained as follows. As r_e increases, P_{cr} will increase, which is likely to require the increase of the ideal brace stiffness; however, the increase of the column end rotational restraints is likely to decrease the ideal brace stiffness. Therefore, the ideal brace stiffness $S_{b,\text{ids}}$ varies non-monotonically with the end-fixity factor r_e. Since the column

buckling load increases and ideal brace stiffness decreases with the increase of column end rotational restraints within the region of $0 \leq r_e \leq 0.392$, there are potential economical incentives for practitioners to consider the effect of semi-rigid connections in designing columns.

The normalized scales are used to quantify the influence of the end-fixity factor on P_{cr} and $S_{b,\text{ids}}$, as shown in 3.4, in which $P_{cr,0}$ and $S_{b,\text{ids},0}$ are the critical buckling load and ideal brace stiffness for a column with pinned ends ($r_e = 0$), respectively.

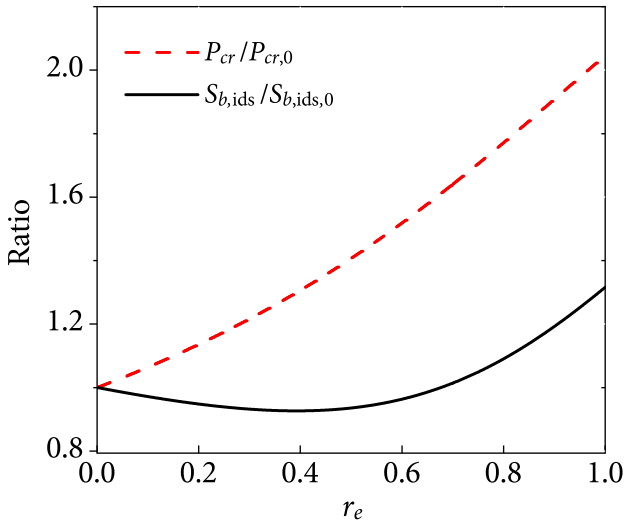

Figure 3.4: Variations of normalized critical buckling load and ideal brace stiffness of a semi-rigidly connected column with the end-fixity factor

An efficiency factor η in Eq. (3.16), is introduced to characterize the relationship between the column's critical buckling load and ideal brace stiffness corresponding to different r_e values, as presented in Fig. 3.5. It can be seen from the figure that the maximum value of η is obtained at $r_e = 0.77$.

$$\eta = \frac{P_{cr}/P_{cr,0}}{S_{b,\text{ids}}/S_{b,\text{ids},0}} \tag{3.16}$$

Fig. 3.6 illustrates the relationship between the end-fixity factor r and rotational stiffness of the connection R obtained from Eq. (2.16), indicating that the rotational stiffness of the connection increases slowly as the end-fixity factor increases from 0 to 0.6 and rapidly approaches infinity as the end-fixity factor approaches 1.0. As a consequence, the required rotational stiffness of the connection for $r = 0.392$ is only $1.93E_cI_c/L_c$, but for $r = 0.77$ is $10.34E_cI_c/L_c$. Therefore, adopting semi-rigid connections with $r_e = 0.392$ may provide a

more economical design with the minimum ideal brace stiffness and a higher buckling strength compared to those of the column with pinned ends.

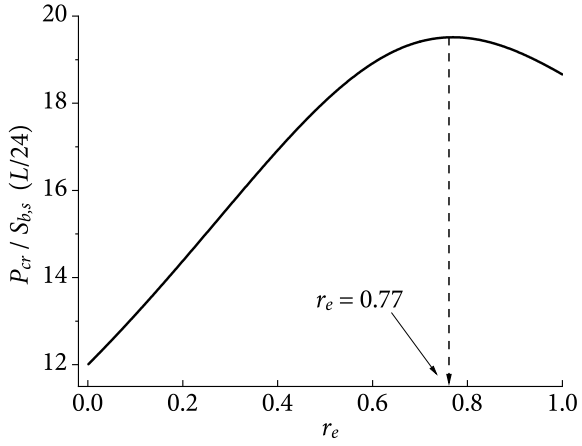

Figure 3.5: Relationship between efficiency factor and end-fixity factor

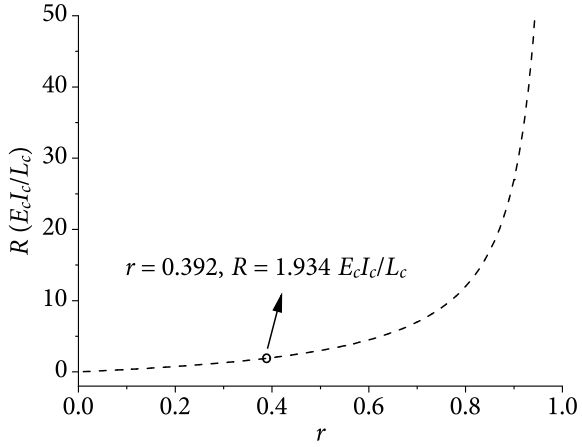

Figure 3.6: Relationship between end-fixity factor and rotational stiffness

3.5 Column Initial Curvature Coefficient ψ of a Semi-rigidly Column Braced at Mid-height

Besides the end connection stiffness (end-fixity factor), another significant factor considered in the newly proposed model is the column initial curvature. In this section, the characteristics of the column initial curvature coefficient ψ and the effects of ψ on the bracing requirements for a single semi-rigidly connected column are discussed.

3.5.1 Characteristics of column initial curvature coefficient ψ

From Eq. (3.11a), it can be seen that the initial curvature coefficient ψ is only associated with the magnitudes of load factor ϕ (i.e., the applied load level) and end-fixity factor r_e. Plotted in Fig. 3.7 are the variations of the initial curvature coefficient ψ with different end-fixity factors r_e and applied load ratios α_p, which is the ratio of the applied load to the critical buckling load, P/P_{cr}. For a semi-rigidly connected column, its critical buckling load P_{cr} can be obtained from Eq. (3.12).

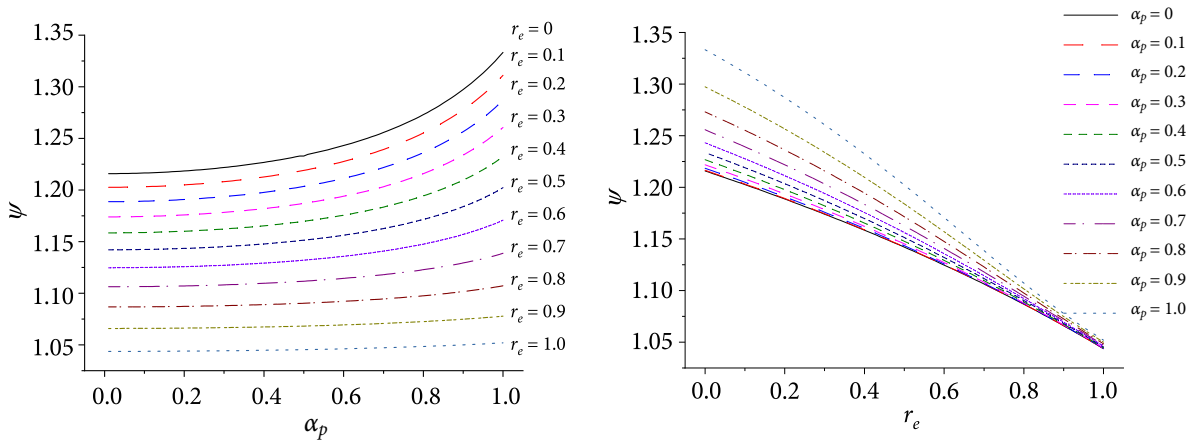

(a) (b)

Figure 3.7: Variations of ψ with different load ratios and end-fixity factors

Fig. 3.7 shows that ψ increases with the increase of α_p but decreases with the increase of r_e. This is reasonable because the larger applied load leads to a greater second-order $P-\Delta$ effect, but the larger end-fixity factor signifies a greater rotational restraint at the column ends, which reduces the column lateral displacement and consequently reduces the second-order $P-\Delta$ effect.

For a column with pinned ends ($r_e = 0$) and subjected to its critical buckling load ($P = P_{cr}$), ψ achieves the maximum value of 1.333 predicted from Eq. (3.11a) with $\phi = \pi$. Consequently, the equivalent lateral load Q_0 is increased by 33.3% with the column initial curvature being considered, which leads to the corresponding brace force to be also increased by 33.3% for the case in which no external lateral force exists, i.e., $Q = 0$. Therefore, the initial curvature coefficient ψ provides a theoretical explanation for the observation by Blum et al. [13], indicating that if a column is modelled with an initial half-sine-wave

imperfection, the predicted brace forces are approximately 33.6% greater than that based on Winter's model from MASTAN2 [100]. This is because Winter's model neglects the influence of the column initial curvature as it assumes the half-length column to be perfectly straight and rigid.

When the column ends are assumed to be fixed ($r_e = 1.0$), the increase of ψ becomes less significant as the applied load increases; as r_e decreases from unity to zero, the influence of applied load on ψ becomes more perceptible. When $\alpha_p = 0$, Eq. (3.11a) indicates that even with a very small axial load, the column initial curvature could still have a notable influence on the lateral displacement with ψ being 1.216 when the column ends are pin-connected.

Although the analytical expression of the initial curvature coefficient ψ has been derived, attaining the exact value of ψ of a semi-rigidly connected column still requires solving the implicit equation in Eq. (3.12) and employing Eq. (3.11a), which is not friendly for engineers. In analytical analysis, the magnitude of ψ associated with $P = P_{cr}$ (referred to as ψ_u hereafter) is of interest as it represents the most critical case. On that account, ψ_u can be adopted for reference in practice, which is conservative because the initial curvature coefficient decreases as the applied load decreases. For a column with semi-rigid connections subjected to P_{cr}, the relationship between ψ_u and r_e obtained from Eq. (3.11a) is presented in Fig. 3.8, wherein ψ_u ranges from 1.333 ($r_e = 0$) to 1.0520 ($r_e = 1$).

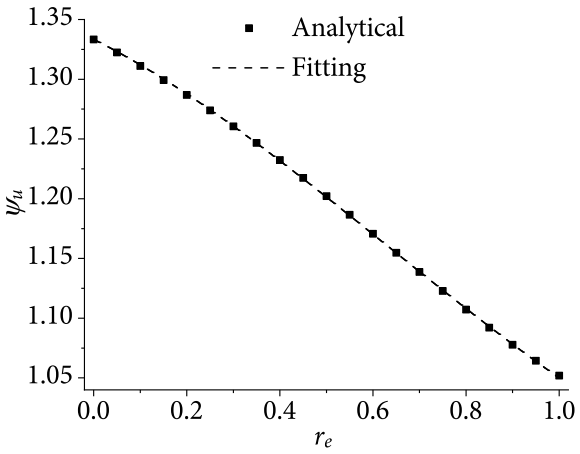

Figure 3.8: Relationship between the end-fixity factor and initial curvature coefficient of a column subjected to its critical buckling load

A simple equation for ψ_u is obtained by curve fitting, as below:

$$\psi_u = 1.3333 - 0.19448 r_e - 0.1886 r_e^2 + 0.09984 r_e^3 \tag{3.17}$$

There is a good agreement between Eq. (3.11a) and Eq. (3.17) with the corresponding adjusted coefficient of determination (R^2) being 0.99993, as demonstrated in Fig. 3.8. As such, with known end connection stiffness R, the end-fixity factor r_e can be obtained from Eq. (2.16), and Eq. (3.17) can be used to compute the value of ψ_u for convenience. Additionally, Eq. (3.17) can be incorporated into the analysis based on Winter's model to account for the influence of the column initial curvature on the brace force for semi-rigidly connected columns.

3.5.2 Effect of ψ on bracing strength requirements

For the system shown in Fig. 3.1d, adopting Eq. (3.8) yields the relationship among the brace stiffness, lateral displacement, and axial load, as below:

$$\Delta = \frac{\frac{P\Delta_0}{L}\psi}{S_c + S_b} \tag{3.18}$$

The internal force in the brace Q_b is the product of the brace stiffness and brace deformation; as the brace deformation equals the additional lateral displacement of the column Δ, the brace force is $Q_b = S_b\Delta$. Furthermore, as Eq. (3.18) is based on the half-length column, the brace force Q_b shall be doubled for the full-length column:

$$Q_b = \frac{2S_b}{S_b + S_c}\frac{P\Delta_0}{L}\psi \tag{3.19}$$

For the reason of comparison, the brace force obtained by Winter's model is briefly discussed. As illustrated in Fig. 2.1, the equilibrium in Winter's model provides the relationship between the lateral displacement and brace stiffness:

$$S_b\Delta L = P(\Delta + \Delta_0) \rightarrow \Delta = \frac{P\Delta_0/L}{S_b - P/L} \tag{3.20}$$

Because $Q_b = 2S_b\Delta$,

$$Q_b = \frac{2S_b}{S_b - P/L}\frac{P\Delta_0}{L} \tag{3.21}$$

The effect of axial load on the column lateral stiffness is introduced first to elucidate the difference between Eq. (3.19) and Eq. (3.21). Fig. 3.9 shows the relationships among column lateral stiffness, applied load, and end connection stiffness, which are normalized as $S_c/(P_e/L)$, P/P_e, and r_e, respectively. P_e is the critical buckling load of a column with pinned ends.

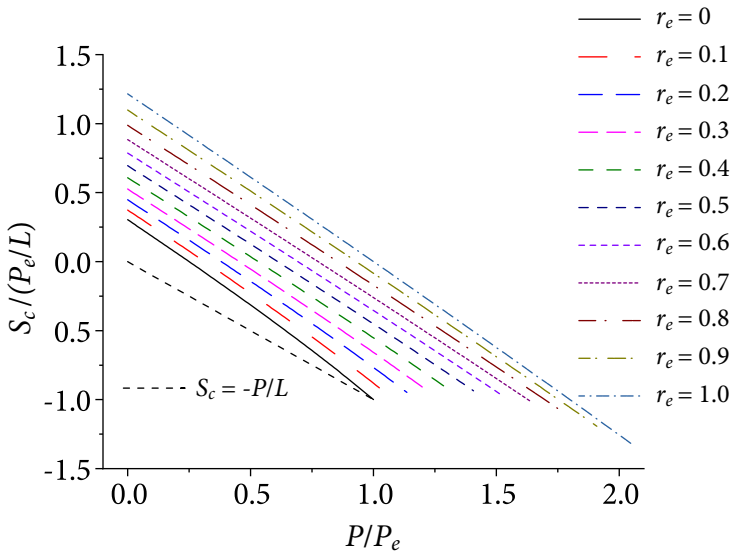

Figure 3.9: Variations of the half-length column's lateral stiffness with applied load and end-fixity factor

It can be seen that the column lateral stiffness decreases almost linearly with the increase of the applied load and becomes negative once the applied load exceeds the sway buckling load of the half-length column. For a pin-pin connected column, with $r_e = 0$, $P_{cr} = P_e = \pi^2 EI/L^2$, Eqs. (3.10) yields

$$S_c = -\frac{\pi^2 E_c I_c}{L^3} = -\frac{P_e}{L} \tag{3.22}$$

Hence, if the effect of column initial curvature is neglected ($\psi = 1$) and the column is assumed to have pinned ends ($r_e = 0$) and the column is subjected to the critical buckling load $P_{cr} = P_e$, Eq. (3.19) becomes the same as Eq. (3.21). In other words, compared to Eq. (3.21), Eq. (3.19) is a general expression that considers the effects of column initial curvature, end connection stiffness and column stiffness on the brace force. In fact, the term $-P/L$ in Eq. (3.21) can be equivalently considered as the geometrical stiffness of the half-length column with pinned ends in Winter's model. The negative magnitude of the stiffness is induced by the applied load, which signifies that the column needs an external brace to maintain its stability. However, as shown in Fig. 3.9, due to neglecting the continuity and elastic stiffness of the column in Winter's model, taking the geometrical stiffness $-P/L$ as the column stiffness S_c is conservative because the geometrical stiffness $-P/L$ increases more slowly as the applied load decreases, compared to the column lateral stiffness obtained from Eqs. (3.10).

The strength requirements for intermediate bracing and corresponding column initial imperfections stipulated in different design standards are tabulated in Table 3.1.

Table 3.1: Brace strength requirements for a single column in different standards

Standard	Single column	Δ_0
AISC 360-16 [10]	$1\%P_r$	$L/500$
EN 1993-1-1 (2005) [24]	$1\%P_r$	$L/500$
AISI S100-16 [11]	$1\%P_r$	$L/500$
CSA S16-19 Direct method [21]	$0.8\%P_r$	$L/500$
CSA S16-19 Simplified analysis [21]	$2\%P_r$	-

In Table 3.1, P_r is the applied factored load stipulated in the corresponding standard, and L is the length of the braced segment shown in Fig. 3.1. The standards AISC 360-16 [10], EN 1993-1-1 [24], and AISI S100 [11] specify the same ratio of the brace strength to the applied load and the initial imperfection Δ_0, which are 1% and $L/500$, respectively. The following is the reason for taking 1% as the brace strength requirement, as given in AISC 360-16 [10]. The theoretical value of brace force with the brace stiffness S_b being taken as the two times ideal brace stiffness, $S_b = 2S_{b,\text{id}} = 2P_e/L$, is $0.8\%P$ based on Winter's model, as below:

$$Q_b = \frac{2S_b}{S_b - P/L}\frac{P\Delta_0}{L} = \frac{2(2P_e/L)}{2P_e/L - P_e/L}\frac{P_eL/500}{L} = 0.8\%P_e \tag{3.23}$$

The AISC specification [10] points out that the theoretical value, $0.8\%P_r$, should be increased to $1\%P_r$ to consider the column curvature and continuity. If the proposed half-length column model is adopted, with the brace stiffness S_b taken as the two times ideal brace stiffness, $-2S_c$, the brace force obtained from Eq. (3.19) is

$$Q_b = \frac{2S_b}{S_b - S_c}\frac{P_e\Delta_0}{L}\psi = 4\psi P_e\Delta_0/L = 0.8\%\psi P_e \tag{3.24}$$

Hence, for a column with pinned ends, considering the effect of column initial curvature yields a 33.3% increase of brace force if $P = P_e$, and the corresponding brace force with $\Delta_0 = L/500$ is $0.8\%P_e \times 1.333 = 1.067\%P_e$. Accordingly, the augment of brace force considering column initial curvature in AISC 360-16 [10] may not be theoretically sufficient for the case with $P = P_e$. However, $\psi = 1.333$ corresponds to the elastic critical buckling load P_e. For

slender members, the AISC specification [10] stipulates that their nominal compressive strength P_n, shall not exceed $0.877P_e$. Thus, the maximum design compressive strength for slender members $\phi_c P_n$ is $0.9 \times 0.877P_e = 0.79P_e$. As discussed in Section 3.5.1, ψ is related to the applied load and end-fixity factor. With $\alpha_p = 0.79$ and $r_e = 0$, Eqs. (3.11a) yields $\psi = 1.294$. In addition, the column lateral stiffness, S_c, is greater than $-P_e/L$ if the applied load is less than the critical buckling load P_e, as illustrated in Fig. 3.9. When P equals $0.79P_e$, Eq. (2.20) yields $\beta = -0.575$ and $S_c = -0.699P_e/L$. Consequently, with the considerations of the column initial curvature and column stiffness, the brace force with $P_r = 0.79P_e$ is

$$Q_b = \frac{2S_b}{S_c + S_b}\frac{P\Delta_0}{L}\psi = \frac{2 \times 2P_e/L}{-0.699P_e/L + 2P_e/L}\frac{P_r L/500}{L}1.294 = 0.796\%P_r \tag{3.25}$$

In Eq. (3.25), since the required brace stiffness is obtained based on two times the ideal brace stiffness, the required brace stiffness is still $2P_e/L$, while the lateral stiffness of the half-length column increases from $-P_e/L$ to $-0.699P_e/L$ if the applied load decreases from P_e to $0.79P_e$. As a result, the brace force is $0.796\%P_r$ if the lateral stiffness of the half-length column is considered. Overall, if the brace stiffness is taken as two times the ideal brace stiffness, the design value of brace force specified by AISC 360-16 [10] is adequate.

CSA S16-19 [21] provides a direct method to compute the brace force for a single column, as below:

$$Q_b = \frac{2\left(\Delta_0 + \Delta\right)P_r}{L_b} \tag{3.26}$$

Like Eq. (3.21), Eq. (3.26) can be obtained from Eq. (3.19) with $S_c = -P/L$ and $\psi = 1$, indicating that Eq. (3.26) is a special case of Eq. (3.19) for the column with pinned ends and neglects the effect of column initial curvature. By setting $\Delta = \Delta_0 = L/500$ in Eq. (3.26), Q_b equals $0.8\%P_r$. Unlike AISC 360-16 [10], CSA S16-19 [21] does not require increasing Q_b from $0.8\%P_r$ to $1\%P_r$, which may underestimate the brace force in certain cases. Alternatively, CSA S16-19 [21] provides a simplified method with the requirement of brace strength not less than $2\%P_r$, which is apparently quite conservative.

For now, the brace strength requirements in current standards [10, 11, 21, 24] assume columns to be ideally pinned supported. If the standards are to be extended to consider the effects of end connection stiffness and column initial curvature on the brace force, Eq. (3.19) can be adopted for better accuracy.

3.5.3 Effect of ψ on bracing stiffness requirement

In Section 3.5.2, the induced brace force is investigated with $S_b = 2S_{b,\text{id}}$, as specified in AISC 360-16 [10]. The required brace stiffness being two times the ideal brace stiffness is derived with the criterion that the additional lateral displacement equals the initial imperfection of the column: $\Delta = \Delta_0$, as per Fig. (2.4). As such, it is not required to check the additional lateral displacement in AISC 360-16. Because the column initial curvature has no influence on the magnitude of ideal brace stiffness, it will not affect the bracing stiffness requirement in AISC 360-16. However, different from AISC 360-16, CSA S16-19 [21] specifies the bracing stiffness requirement by limiting the additional displacement Δ that Δ shall not exceed the initial imperfection Δ_0. Following this design philosophy, it is of no surprise that considering the column initial curvature increases the bracing requirement as it will magnify the additional displacement induced by the applied load.

If this criterion $\Delta = \Delta_0$ is adopted in the proposed half-length column model, the required brace stiffness for the half-length column is:

$$S_b = \frac{P}{L}\psi - S_c \tag{3.27}$$

Eq. (3.27) is obtained from Eq. (3.18) with $\Delta = \Delta_0$. It should be noted that Eq. (3.27) may yield a negative value of the brace stiffness when the applied load is considerably small. Different from Winter's model which introduces a fictitious hinge to connect two half-length columns, the proposed model considers the continuity of the full column by incorporating the column elastic stiffness into the term S_c. Hence, the value of S_c is positive, and the magnitude of the term $\psi P/L$ is insignificant with a small applied load; correspondingly, Eq. (3.27) could yield a negative brace stiffness. From the physical perspective, even without the lateral brace, the column's additional lateral displacement will not exceed the initial imperfection when the applied load is very small due to considering the continuity of the column. As a consequence, if the brace stiffness obtained from Eq. (3.27) is negative, then it means that no lateral bracing is needed to satisfy the stiffness requirement.

For a column with pinned ends and subjected to its critical buckling load, with $P = P_e$, $S_c = -P_e/L$, $\psi = 1.333$ and $S_{b,\text{id}} = P_e/L$, Eq. (3.27) becomes

$$S_b = \frac{P_e}{L}\psi - \left(-\frac{P_e}{L}\right) = (1+\psi)\frac{P_e}{L} = 2.333 S_{b,\text{id}} \tag{3.28}$$

That is to say, the required brace stiffness is 2.333 times the ideal brace stiffness based on Eq. (3.27). As expected, the bracing stiffness requirement increases if the effect of column initial curvature is considered. For a single semi-rigidly connected column, rearranging Eq. (3.27) gives:

$$S_b = \left(-\frac{P}{S_{c,\mathrm{cr}}L}\psi + 1\right) S_{b,\mathrm{id}} = \alpha_b S_{b,\mathrm{id}} \tag{3.29}$$

where α_b is a scale factor representing the ratio of the required brace stiffness to the ideal brace stiffness. For a semi-rigidly connected column subjected to its critical buckling load $P = P_{cr}$, if $\Delta = \Delta_0$ is taken as the stiffness requirement, then the variation of α_b with r_e is presented in Fig. 3.10.

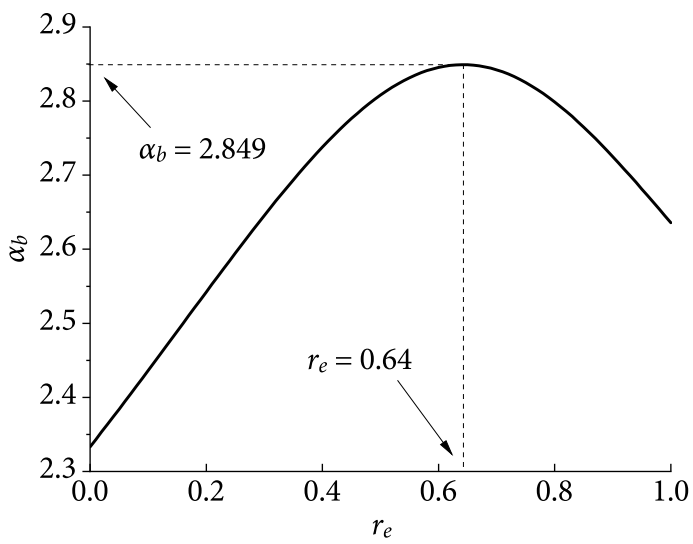

Figure 3.10: Variation of the required brace stiffness scale factor α_b with the end-fixity factor r_e for a single semi-rigidly connected column

The analytical results depicted in Fig. 3.10 indicate that for a semi-rigidly connected column subjected to P_{cr}, the required brace stiffness scale factor increases as the end-fixity factor increases from 0 to 0.65, achieving the maximum value of $\alpha_b = 2.849$ when $r_e = 0.65$, and then decreases until $r_e = 1.0$. More importantly, a semi-rigidly connected column ($r_e > 0$) requires a greater brace stiffness scale factor than a column with pinned ends. Hence, taking the scale factor as 2.0 as per the standards [10, 11] is insufficient for the displacement tolerance ($\Delta = \Delta_0$) of semi-rigidly connected columns.

If α_b in Eq. (3.29) is adopted, the corresponding brace force Q_b is:

$$Q_b = \left(\psi - \frac{S_c L}{P_{cr}}\right) \frac{2P_{cr}\Delta_0}{L}\psi \tag{3.30}$$

Based on Eq. (3.30), the effect of the end-fixity factor on the ratio of the brace force Q_b to the critical buckling P_{cr} is illustrated in Fig. 3.11. It is of no surprise that for a column with pinned ends, adopting a larger brace stiffness scale factor of $\alpha_b = 2.333$ leads to a lower brace force of $0.93\%P_{cr}$, compared to the brace force of $1.067\%P_{cr}$ with the $\alpha_b = 2.0$. In addition, the ratio Q_b/P_{cr} decreases as r_e increases.

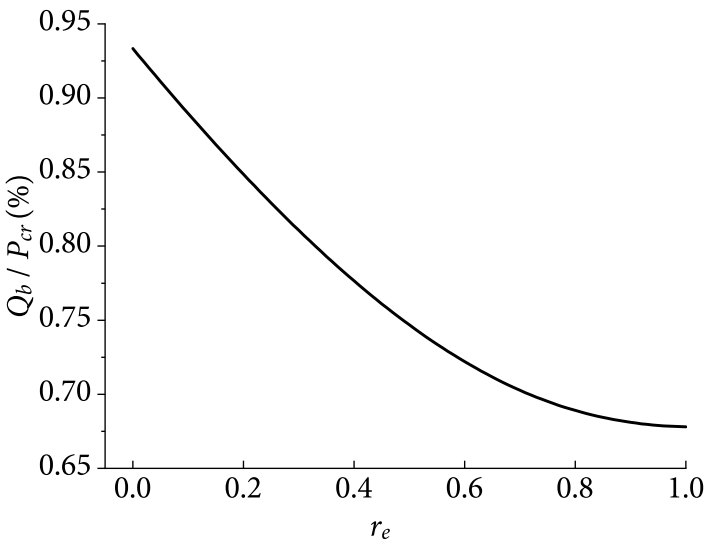

Figure 3.11: Variation of Q_b/P_{cr} with r_e

3.6 Modified Design Procedures for a Semi-rigidly Connected Column

Although the specifications in current standards regarding the bracing requirements only apply to pin-connected columns, the corresponding design philosophies provide significant guidance for assessing the bracing requirements for semi-rigidly connected columns. In this section, two different procedures are proposed to evaluate the bracing requirements for a semi-rigidly connected column by following the design philosophies of AISC 360-16 [10] and CSA S16-19 [21].

3.6.1 AISC 360-16

For a semi-rigidly connected column, following the bracing stiffness requirement in AISC 360-16, the corresponding brace stiffness shall be greater than

$$S_{b,\text{AISC}} = 2S_{b,\text{ids}} = -4S_{c,\text{cr}} \tag{3.31}$$

If the simplified equation in Eq. (3.15) is used, Eq. (3.31) becomes

$$S_{b,\text{AISC}} = \frac{E_c I_c}{L^3}(-79.06 + 24.67r_e - 7.84r_e^2 - 42.21r_e^3) \tag{3.32}$$

With the brace stiffness being two times the ideal brace stiffness in Eq. (3.19), the strength of the brace shall be greater than

$$Q_{b,\text{AISC}} = \frac{-4S_{c,\text{cr}}}{-2S_{c,\text{cr}} + S_c}\frac{P\Delta_0}{L}\psi \tag{3.33}$$

Thus, the cross-section area of the bracing satisfying the requirements in Eq. (3.31) and Eq. (3.33) can be determined.

3.6.2 CSA S16-19

As stated in CSA S16-19, the additional lateral displacement shall not exceed the initial imperfection of the column; thereby, the brace stiffness for the full-length column from Eq. (3.27) shall be greater than

$$S_{b,\text{CSA}} = 2\left(\frac{P}{L}\psi - S_c\right) \tag{3.34}$$

Once the brace stiffness is obtained from Eq. (3.34), the corresponding brace force is

$$Q_{b,\text{CSA}} = 2\left(1 - \frac{S_c L}{\psi P}\right)\frac{P\Delta_0}{L}\psi \tag{3.35}$$

which is attained by substituting Eq. (3.27) into Eq. (3.19).

If the design philosophy of CSA S16-19 [21] is followed, the cross-section area of the bracing can be determined by satisfying the requirements in Eq. (3.34) and Eq. (3.35).

3.7 Example of a Single Column

In this section, the design procedures stipulated in AISC 360-16 [10] and CSA S16-19 [21] are followed to investigate the bracing requirements of a steel column with intermediate

bracing (Fig. 3.12) by adopting the proposed half-length column model. This column has a length of 6000 mm ($2L$) and is made of a W150 × 24 section, of which the properties are $I_x = 13.4 \times 10^6\,\text{mm}^2$, $I_y = 1.83 \times 10^6\,\text{mm}^2$ (in-plane), and $A = 3600\,\text{mm}^2$. The diagonal braces in Fig. 3.12 are tension-only. The elastic modulus and yield strength of the column and brace are $E = 200\,000\,\text{MPa}$ and $f_y = 345\,\text{MPa}$, respectively. Take $\Delta_0 = L/500 = 6\,\text{mm}$ as the column initial imperfection. Two cases are considered to illustrate the effects of applied load and end-fixity factor on the bracing requirements for the single column.

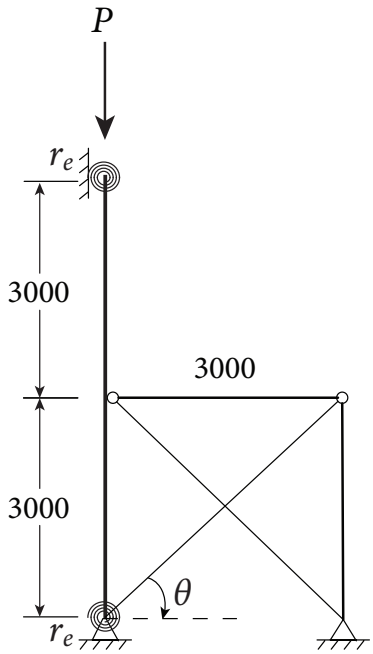

Figure 3.12: Diagram of Example 3.7

3.7.1 Effect of axial load

In this case, the column is assumed to be pin-connected at both ends ($r_e = 0$) and subjected to different applied axial loads. As such, the equations for computing the brace force specified in AISC 360-16 [10] and CSA S16-19 [21] are viable for this case, and the corresponding results are compared against those by adopting the proposed equations in this section. Because $r_e = 0$, the critical buckling load is

$$P_{cr} = \frac{\pi^2 EI}{L^2} = \frac{\pi^2 \times 2 \times 10^5\,\text{MPa} \times 1.83 \times 10^6\,\text{mm}^4}{3000^2} = 401\,364\,\text{N}$$

The ideal brace stiffness for the half-length column is

$$S_{b,\text{id}} = -S_c = P_{cr}/L = 401364/3000 = 133.8\,\text{N/mm}$$

By substituting $S_b = 2S_{b,\mathrm{id}}$ into Eq. (3.19), the brace forces subjected to different axial load ratios are obtained, as tabulated in Table 3.2. Note that all the brace forces discussed and shown in this study are in the horizontal direction.

Table 3.2: Brace force for a single column with different load ratios

α_p	$S_c/(P_e/L)$	ψ	Analytical Q_b(N)	FEM Q_b(N)	Error (%)
0.3	-0.062	1.238	615.2	615.4	-0.03
0.4	-0.187	1.247	883.2	883.6	-0.04
0.5	-0.314	1.257	1196.9	1197.3	-0.03
0.6	-0.444	1.268	1569.9	1572.1	-0.14
0.7	-0.576	1.281	2022.4	2026.5	-0.20
0.8	-0.713	1.296	2585.5	2592.7	-0.28
0.9	-0.853	1.313	3309.2	3316.8	-0.23
1	-1.000	1.333	4281.2	4309.9	-0.67

For verification purposes, the finite element analysis (FEA) software ABAQUS was used to establish the column-brace model. The results are shown in Table 3.2, indicating good agreements between the analytical and FEA results.

For comparison purposes, the brace forces associated with various applied load ratios obtained from the analytical method, FEA, AISC S360-16 [10] (1%P), and CSA S16-19 [21] direct method (0.8%P) are presented in Fig. 3.13. It can be seen that the brace force increases nonlinearly with the increase of the applied load. Theoretically, the brace force obtained from AISC 360-16 [10] is lower than the analytical result when $P > 0.95P_e$ but is higher when $\alpha_p < 0.95$; the brace force obtained from CSA S16-19 [21] is lower than the analytical result when $P > 0.8P_e$ but is higher when $P < 0.8P_e$. The factored compressive resistance of the column P_r is 313.4 kN (AISC 360-16) and 300.5 kN (CSA S16-19), respectively, corresponding to the load ratio being 0.786 and 0.749. When $P = P_r$, the brace strength requirements in both AISC 360-16 and CSA S16-19 are conservative for this case. The good agreements between the analytical and FEA results demonstrate the accuracy of the proposed analytical method.

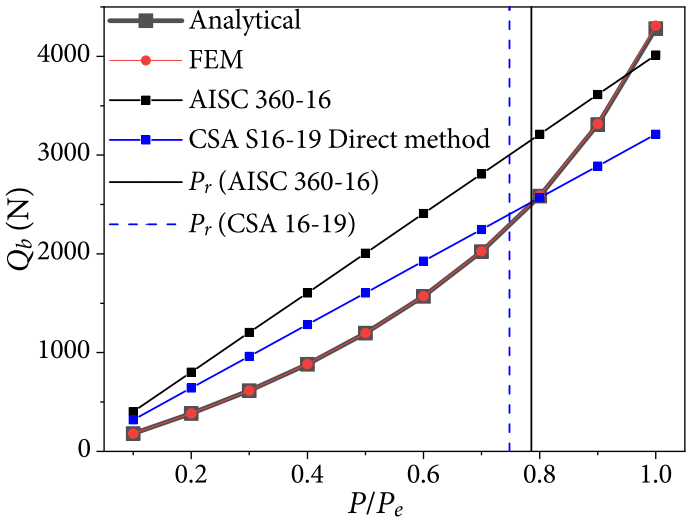

Figure 3.13: Brace forces for a pin-connected column with different load ratios

For the diagonal bracing shown in Fig. 3.12, the required cross-sectional area associated with the stiffness requirement is

$$A_b = \frac{S_b L_b}{E\cos^2\theta} \tag{3.36}$$

where S_b is obtained from either Eq. (3.31) or Eq. (3.34).

In addition, the required cross-sectional area for the diagonal bracing associated with the strength requirement is

$$A_b = \frac{Q_b}{f_y\cos\theta} \tag{3.37}$$

where Q_b is obtained from either Eq. (3.33) or Eq. (3.35).

The required cross-sectional areas of the diagonal bracing obtained from different design philosophies for the column with different applied loads are tabulated in Table 3.3, in which $A_b(Q_b)$ and $A_b(S_b)$ represent the minimum cross-sectional area satisfying the strength requirement and stiffness requirement, respectively, and A_b (Final) is the maximum value of $A_b(Q_b)$ and $A_b(S_b)$.

It can be seen that when $\alpha_p \leq 0.9$ the minimum required cross-sectional areas of the diagonal bracing obtained by following the design philosophy of AISC 360-16 are the same because they are governed by the stiffness requirement: $A_b(S_b) > A_b(Q_b)$. As the strength requirement increases with the increase of the applied load, the required cross-sectional area of the diagonal bracing is governed by $A_b(Q_b)$ when $\alpha_p = 1$. With the brace stiffness being twice the ideal brace stiffness, the additional lateral displacement Δ is less than the initial

imperfection Δ_0 when $\alpha_p \leq 0.8$. Therefore, the required cross-sectional areas associated with the stiffness requirement $A_b(S_b)$ in CSA S16-19 ($\Delta = \Delta_0$) are less than $A_b(S_b)$ in AISC 360-16 ($S_b = 2S_{b,\text{id}}$). Accordingly, the attained cross-sectional areas associated with the strength requirement $A_b(Q_b)$ in CSA S16-19 are larger than $A_b(Q_b)$ in AISC 360-16 when $\alpha_p \leq 0.9$. Conversely, when $\alpha_p \geq 0.9$, $A_b(S_b)$ in CSA S16-19 is larger than that in AISC 360-16. Overall, with different applied loads, all the required cross-sectional areas of the diagonal bracing obtained by following the design philosophy of CSA S16-19 are governed by the stiffness requirement. The predictions following the design philosophy of AISC 360-16 are greater than those following CSA S16-19 when $\alpha_p \leq 0.8$ but are smaller when $\alpha_p \geq 0.9$ in this example.

Table 3.3: Comparison of the required cross-sectional areas of the diagonal bracing obtained from different design philosophies under different applied loads

	AISC 360-16				CSA S16-19			
α_p	A_b (S_b) mm^2	A_b (Q_b) mm^2	Δ mm	A_b (Final) mm^2	A_b (S_b) mm^2	A_b (Q_b) mm^2	Δ mm	A_b (Final) mm^2
0.3	16.1	2.5	1.1	16.1	3.5	2.9	6	3.5
0.4	16.1	3.6	1.7	16.1	5.5	4.5	6	5.5
0.5	16.1	4.9	2.2	16.1	7.6	6.2	6	7.6
0.6	16.1	6.4	2.9	16.1	9.7	7.9	6	9.7
0.7	16.1	8.3	3.8	16.1	11.8	9.7	6	11.8
0.8	16.1	10.6	4.8	16.1	14.0	11.5	6	14.0
0.9	16.1	13.6	6.2	16.1	16.3	13.4	6	16.3
1	16.1	17.5	8.0	17.5	18.7	15.4	6	18.7

3.7.2 Effect of end-fixity factor

If $\alpha_p = 0.8$, the brace forces with different end-fixity factors obtained from Eq. (3.19) and FEA model, together with the parameters needed in the calculations, are tabulated in Table 3.4. It can be seen that as r_e increases, P increases, but ψ decreases. However, there is no monotonicity for the variations of S_c and S_b with r_e. The reason for that is given in Section 3.4. For semi-rigidly connected columns, a rotational spring is employed to simulate

the connection at both ends of the column in the FEM, and its rotational stiffness R is computed by Eq. (2.16).

Table 3.4: Brace forces for a single column with different end-fixity factors

r_e	P	ψ	S_c	$S_{b,\text{id}}$	Q_b (Analytical)	Q_b (FEA)	Error
	kN		N/mm	N/mm	N	N	%
0	321.1	1.296	-95.3	267.6	2585.5	2592.7	-0.28
0.1	341.7	1.276	-90.9	259.9	2681.8	2689.7	-0.29
0.2	364.8	1.255	-86.8	253.7	2784.8	2793.6	-0.31
0.3	390.6	1.233	-83.5	249.4	2895.6	2905.1	-0.33
0.4	419.5	1.209	-81.2	247.9	3015.1	3025.5	-0.34
0.5	451.8	1.183	-80.1	250.3	3144.8	3155.9	-0.35
0.6	487.5	1.156	-80.9	257.7	3285.9	3297.6	-0.35
0.7	526.7	1.129	-83.7	271.3	3439.1	3451.1	-0.35
0.8	568.7	1.101	-88.9	291.7	3603.4	3615.7	-0.34
0.9	612.7	1.075	-96.5	319.0	3776.0	3788.2	-0.32
1	656.9	1.050	-106.3	352.0	3951.5	3963.6	-0.31

The calculation results regarding the required cross-sectional areas of the diagonal bracing A_b for the column with different r_e are tabulated in Table 3.5. For this case with $\alpha_p = 0.8$, all the cross-sectional areas of the diagonal bracing A_b with different end-fixity factors are controlled by the stiffness requirement. Thus, A_b associated with the stiffness requirement of $S_b = 2S_{b,\text{id}}$ (AISC 360-16) decreases as r_e increases from 0 to 0.4 and then increases as r_e increases from 0.4 to 1.0. However, if the brace stiffness is required to satisfy the criterion of $\Delta = \Delta_0$ (CSA S16-19), the required brace stiffness and corresponding required cross-sectional area increase as r_e increases.

Table 3.5: Comparison of the required cross-sectional areas of the diagonal bracing obtained from different design philosophies with different end-fixity factors

	AISC 360-16				CSA S16-19			
r_e	A_b (S_b) mm^2	A_b (Q_b) mm^2	Δ mm	A_b (Final) mm^2	A_b (S_b) mm^2	A_b (Q_b) mm^2	Δ mm	A_b (Final) mm^2
0	16.1	10.6	4.8	16.1	14.0	11.5	6	14.0
0.1	15.6	11.0	5.2	15.6	14.2	11.6	6	14.2
0.2	15.2	11.4	5.5	15.2	14.4	11.8	6	14.4
0.3	15.0	11.9	5.8	15.0	14.6	12.0	6	14.6
0.4	14.9	12.4	6.1	14.9	15.0	12.3	6	15.0
0.5	15.0	12.9	6.3	15.0	15.5	12.7	6	15.5
0.6	15.5	13.5	6.4	15.5	16.1	13.2	6	16.1
0.7	16.3	14.1	6.3	16.3	16.9	13.9	6	16.9
0.8	17.5	14.8	6.2	17.5	17.9	14.6	6	17.9
0.9	19.1	15.5	5.9	19.1	19.0	15.5	6	19.0
1	21.1	16.2	5.6	21.1	20.2	16.5	6	20.2

3.8 Conclusions

A new half-length column model is proposed in this chapter to account for the effects of semi-rigid connections, column initial curvature, and column stiffness on the bracing requirements for a single column braced at its mid-height. The following conclusions are drawn:

1. A coefficient is introduced to assess the effect of column initial curvature on the additional lateral displacement of a semi-rigidly connected column induced by the applied axial load. It is found that if the column is assumed to be pinned supported and the applied load is the column's full critical buckling strength, considering the column initial curvature leads to a 33.3% increase of the additional lateral displacement and brace force. The column initial curvature coefficient increases as the applied load increases but decreases as the end-fixity factor increases.

2. It is discovered that the ideal brace stiffness of a single elastic column decreases with the increase of end-fixity factor in a region $r_e = [0, 0.392]$ and increases once $r_e \geq 0.392$. An efficiency factor is introduced to characterize the relationship between column critical buckling load and ideal brace stiffness corresponding to different values of r_e. The efficiency factor reaches the maximum value when $r_e = 0.77$.

3. The strength requirement of bracing specified in AISC 360-16 [10], EN 1993-1-1 [24], and AISI S100-16 [11] , $1\%P_r$, is found to be conservative if the effect of column stiffness and initial curvature is considered. However, the direct method in CSA S16-19 [21] neglects the effect of column initial curvature on the brace force, and thus may underestimate the brace force in some cases. The bracing stiffness requirements specified in current standards [10, 11] (twice the ideal brace stiffness) need to be increased to 2.33 times the ideal brace stiffness if the effect of column initial curvature is considered.

4. Theoretically, the bracing requirements in current standards only apply to columns with pinned ends. By employing the expressions derived in this chapter, the design procedures in AISC 360-16 and CSA S16-19 are extended to assess the bracing requirements for a semi-rigidly connected column considering the effect of column initial curvature.

5. Through the verification against the finite element analyses, it is demonstrated that the proposed half-length column model and corresponding derived analytical equations provide accurate evaluations of the brace forces for a semi-rigidly connected column with the considerations of column initial curvature and column lateral stiffness.

Chapter 4

Bracing Requirements for Multi-column Systems

4.1 Introduction

Chapter 3 proposed a new half-length column model to assess the bracing requirements for a single column with semi-rigid connections. In this chapter, the application of the proposed half-length column model is extended to multi-column systems. The previous research regarding the ideal brace stiffness for multi-column systems [5,8,9] was focused on cases in which all the columns were identical and reached their critical load simultaneously. Furthermore, due to their reliance on Winter's model [7], those studies assumed the column ends to be pin-connected. To investigate the effects of semi-rigid column end connections and nonidentical columns on the ideal brace stiffness of multi-column systems, an analytical method is proposed by adopting the equivalent lateral stiffness concept [3] and adapting the storey-based stability method developed by Xu [35]. The influence of column stiffness interaction associated with semi-rigid connections, column sizes, and applied loads is theoretically considered in the determination of the ideal brace stiffness for multi-column systems. The content of this part is also available on the reference [1].

Besides the ideal brace stiffness, the brace forces for multi-column systems are investigated in this chapter. Although the aforementioned research [8,14–16] and current provisions [10,11,26] regarding the brace forces for multiple columns have been well documented, there are some issues that need to be addressed.

- The previous studies [8, 10, 11, 13–16] assume that the column ends are either pinned or fixed. In practice, column ends possess a certain degree of rotational restraints; thereby, column ends should be considered semi-rigid in order to accurately predict the stability of the column [101–103].

- As Winter's model simulates the column as two perfectly straight rigid members, it neglects the column's flexibility and initial curvature, which will magnify the additional displacement induced by the applied load and consequently increase the brace force [10, 17]. Therefore, the effect of column initial curvature on brace forces in multiple columns needs to be investigated.

- Considering the previous studies were limited to the system in which the lateral stiffnesses of all columns are identical, there is a lack of research on the system with nonuniform column stiffness. The nonuniform stiffness can result from differences in column sizes, end connections, and applied loads in the system.

Hence, an analytical method is derived in this chapter to address the issues listed above by formulating the stiffness interaction among the columns and braces. The research presented in this chapter is also available in the references [1, 2].

4.2 Equivalent Lateral Stiffness of a System Considering Beam Axial Deformations

For a steel frame consisting of $n-1$ beams and n columns, the lateral stiffness of the frame ΣS is given in Eq. (2.19) [35]. The frame is stable only if the summation of the lateral stiffnesses of individual columns is greater than zero ($\Sigma S_{c,i} > 0$), and is laterally unstable when $\Sigma S_{c,i} = 0$. It should be noted that the reason the column lateral stiffnesses are additive in Eq. (2.19) is that all the beams are assumed to be axially rigid [35], which is a normal practice when accounting for the presence of concrete slabs in building structures. When the axial deformations of beams need to be considered, Ma et al. [3] derived the solution to the lateral deflection Δ_i of each column induced by a lateral load Q in a storey frame shown in Fig. 4.1, wherein S_L is the lateral stiffness provided by external braces that can provide reaction forces.

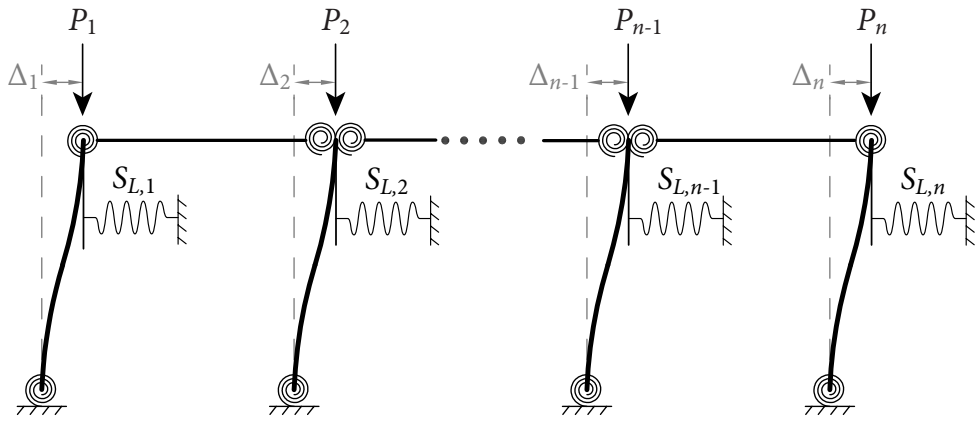

Figure 4.1: A semi-braced storey frame subjected to gravity loading

The solution varies depending on the number of columns in the frame and which column the lateral load is applied on, but it can be expressed in a general form:

$$\Delta_i = \frac{Q}{S_{\text{eq},i}} \tag{4.1a}$$

$$S_{\text{eq},i} = \frac{S_{\text{NUM}}}{S_{\text{DEN},i}} \tag{4.1b}$$

where $S_{\text{eq},i}$ is the equivalent lateral stiffness of column i.

Ma et al. [3] show that for a given number n of columns, the denominator $S_{\text{DEN},i}$ is different for each column and will vary if the lateral load is applied on a different column. Nevertheless, the numerator S_{NUM} is constant regardless of which column the lateral load is applied on. Due to this characteristic, the numerator S_{NUM} can be considered as an indicator of the stability in the frame. If S_{NUM} becomes zero, the deflections of all columns are theoretically infinite, and the frame will fail in lateral instability.

Assuming that a fictitious lateral load is applied on the left-most column, S_{NUM} can be obtained from the equivalent lateral stiffness of the left-most column, $S_{\text{eq},1}$. The equivalent spring stiffness concept [104] is adopted to attain $S_{\text{eq},1}$. By doing so, the frame shown in Fig. 4.1 is simulated as a system of springs in parallel and in series, as shown in Fig. 4.2, in which S_b is the axial stiffness of the beam. Note that the column lateral stiffness S_c has incorporated the effects of semi-rigid connections and axial load.

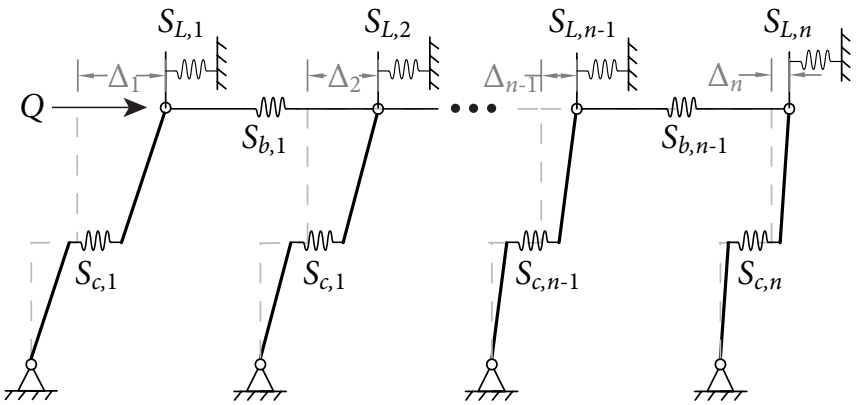

Figure 4.2: Deformed state of the equivalent spring system for a storey frame

The procedure for calculating $S_{\text{eq},1}$ is as follows. Starting from the right end of the frame in Fig. 4.2, since the n^{th} column and the n^{th} external brace have the same displacement of Δ_n, they are in parallel, and their stiffnesses are additive. Hence, this column-brace system can be represented by using an equivalent spring with spring stiffness being $S_{c,n} + S_{L,n}$, as shown in Fig. 4.3.

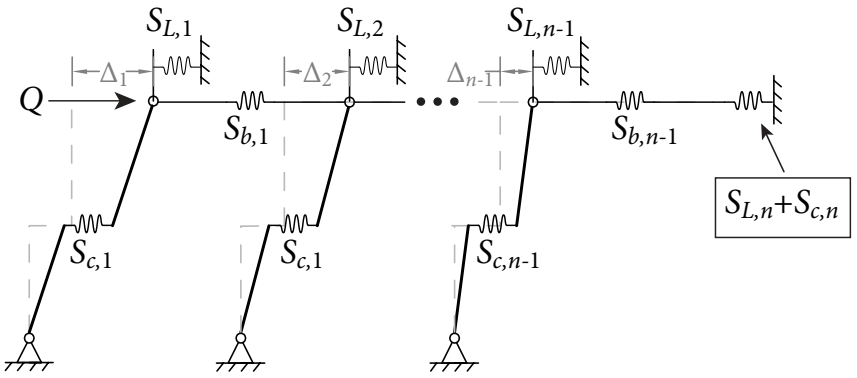

Figure 4.3: Replacing a column and its external brace in parallel with an equivalent spring

The deformation of beam $n-1$ is $\Delta_{n-1} - \Delta_n$. As such, the equivalent spring in Fig. 4.3 that represents the column-brace system is in series with the axial stiffness of beam $n-1$, since the sum of their displacements equals the displacement of the left end of beam $n-1$, $\Delta_n - 1$. For the sake of brevity, the symbol of "~" is introduced to denote the series spring stiffness operation, as below:

$$S_1 \sim S_2 = \left[\frac{1}{S_1} + \frac{1}{S_2} \right]^{-1} \tag{4.2}$$

Accordingly, if the stiffness of beam $n-1$ is incorporated into the equivalent spring stiffness, the system in Fig. 4.3 becomes the system in Fig. 4.4 with the equivalent spring stiffness

being $S_{b,n-1} \sim (S_{L,n} + S_{c,n})$.

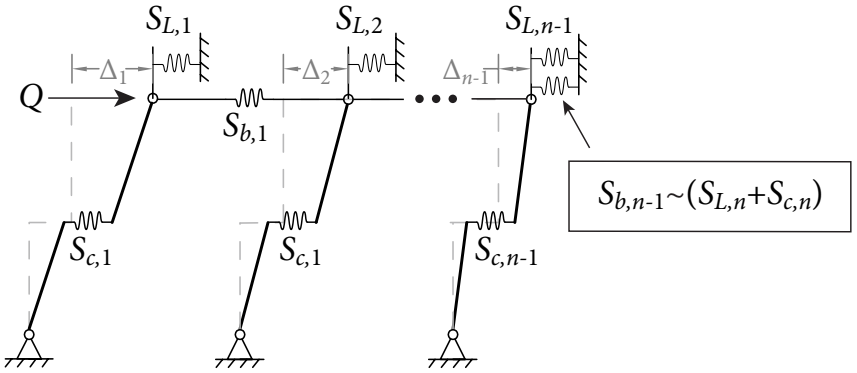

Figure 4.4: Replacing a beam and column-brace system in series with an equivalent spring

Basically, if the member to be combined with the equivalent spring can provide lateral reaction force, the spring modelling the member and the equivalent spring are in parallel and additive. Conversely, they are in series if the member cannot provide a lateral reaction force. Therefore, columns and external braces are in parallel with the equivalent spring, but the beams (internal braces) are in series with the equivalent spring. The process of replacing the springs and calculating the equivalent spring stiffness is repeated until all the members of the frame are lumped into a single equivalent spring with the spring stiffness being $S_{\text{eq},1}$, as shown in Fig. 4.5.

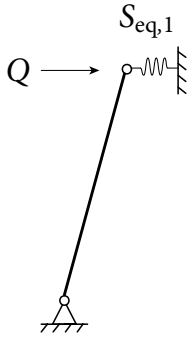

Figure 4.5: Using an equivalent spring stiffness, $S_{\text{eq},1}$, to represent the entire storey frame

Following the aforementioned procedure, the stiffness of the equivalent spring, $S_{\text{eq},1}$, can be generally expressed as Eq. (4.3).

$$\begin{aligned} S_{\text{eq},1} = \{ [(S_{c,n} + S_{L,n}) \sim S_{b,n-1} + S_{c,n-1} + S_{L,n-1}] \sim S_{b,n-2} \\ + S_{c,n-2} + S_{L,n-2} \} \sim \cdots \sim S_{b,1} + S_{c,1} + S_{L,1} \end{aligned} \tag{4.3}$$

Once $S_{\text{eq},1}$ is obtained, S_{NUM} and $S_{\text{DEN},i}$ can be obtained by simplifying $S_{\text{eq},1}$ to a single quotient $S_{\text{NUM}}/S_{\text{DEN},1}$ given in Eq. (4.1b), which is expressed algebraically in terms of $S_{c,i}$, $S_{b,i}$ and $S_{L,i}$. The frame will fail in lateral sway buckling when $S_{\text{NUM}} = 0$. Getting the expression of S_{NUM} becomes more cumbersome as the number of columns increases. For convenience, the built-in function *numden* provided by MATLAB [105] can be used to directly obtain the symbolic expression of S_{NUM} from $S_{\text{eq},1}$.

4.3 Ideal Brace Stiffness of Multiple Columns Obtained from Equivalent Lateral Stiffness

Presented in Fig. 4.6a is a system consisting of n parallel semi-rigidly connected columns anchored by both sides and subjected to gravity loads. By incorporating the proposed half-length column model, the system can be simulated by two identical half-length systems (frames) with two external rigid braces, as shown in Fig. 4.6b. The column length and brace stiffness are half of those of the original system. For the system in Fig. 4.6a, when sway buckling of the full-length columns occurs simultaneously, the mid-height lateral deflections of the columns reach infinity, which corresponds to the lateral sway buckling of the frame in Fig. 4.6b. As a consequence, for the system in Fig. 4.6a, the problem of determining the ideal brace stiffness for the non-sway buckling can be alternatively solved by determining the ideal brace stiffness to prevent the lateral sway buckling of the equivalent frame shown in Fig. 4.6b.

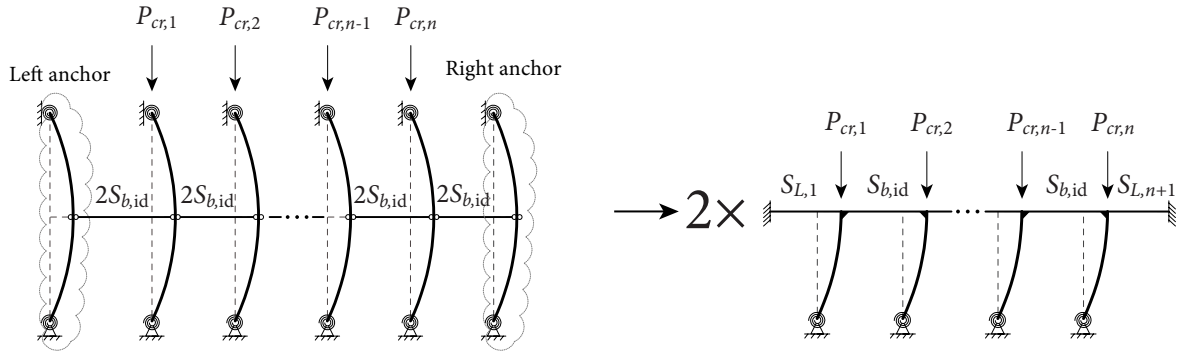

(a) Full-length column model

(b) Half-length column model

Figure 4.6: Half-length column model for a multi-column system with ideal brace stiffness

For the equivalent frame shown in Fig. (4.6b), $S_{L,1}$ and $S_{L,n+1}$ are the stiffness resulting from the anchor and adjacent tie brace [5], which is given in Eq. (4.4).

$$S_L = \frac{1}{\left(\frac{1}{S_{an}} + \frac{1}{S_b}\right)} = \frac{1}{\left(1 + \frac{S_b}{S_{an}}\right)} S_b = \frac{1}{(1+c)} S_b \tag{4.4}$$

where c is the ratio of tie bracing stiffness S_b to the anchor-bracing stiffness S_{an}.

If the tie braces possess the ideal brace stiffness $S_{b,\mathrm{id}}$, since there are no external braces provided to the interior columns in the system, Eq. (4.3) becomes

$$\begin{aligned} S_{\mathrm{eq},1} = \{ [(S_{c,n+1} + S_{L,n+1}) \sim S_{b,\mathrm{id}}] \sim S_{b,\mathrm{id}} \\ + S_{c,n-1} \} \sim \cdots \sim S_{b,\mathrm{id}} + S_{c,1} + S_{L,1} \end{aligned} \tag{4.5}$$

Equation (4.5) is also applicable for the system anchored on one side with $S_{L,1} = 0$ and the rigidly anchored system with $S_L = S_b$ ($c = 0$).

The ideal brace stiffness of the equivalent frame $S_{b,\mathrm{id}}$ can be computed by solving Eq. (4.6) with $P_i = P_{cr,i}$, which signifies that the non-sway and sway buckling loads of the frame are the same with the brace stiffness being the ideal brace stiffness. With known column dimensions and corresponding critical buckling load P_{cr}, the lateral stiffness of the half-length column $S_{c,i}$ can be computed via Eq. (3.10). By presupposing the value of c, Eq. (4.6) can be directly solved since it only has one unknown variable, $S_{b,\mathrm{id}}$. Equation (4.6) has multiple solutions of $S_{b,\mathrm{id}}$; the one with the maximum value governs.

$$S_{\mathrm{NUM}}(S_{c,i}, S_{b,i}, S_{L,i}) = 0 \tag{4.6}$$

As an example, the solution to $S_{b,\mathrm{id}}$ for a system consisting of two columns anchored only on one side is provided below.

$$S_{\mathrm{eq},1} = \left[\left(S_{c,2} + S_{L,2}\right)^{-1} + \left(S_{b,\mathrm{id}}\right)^{-1} \right]^{-1} + S_{c,1}$$

$$S_{\mathrm{eq},1} = \frac{\left(S_{c,1}\right)\left(S_{c,2} + S_{L,2}\right) + S_{b,\mathrm{id}}\left(S_{c,1}\right) + S_{b,\mathrm{id}}\left(S_{c,2} + S_{L,2}\right)}{S_{b,\mathrm{id}} + \left(S_{c,2} + S_{c,1}\right)} = \frac{S_{\mathrm{NUM}}}{S_{\mathrm{DEN},1}}$$

Then, the solution to $S_{b,\mathrm{id}}$ can be obtained by finding the maximum root of

$$S_{\mathrm{NUM}} = S_{c,1}S_{c,2} + \left(\frac{2+c}{1+c} S_{c,1} + S_{c,2}\right) S_{b,\mathrm{id}} + \frac{1}{1+c}\left(S_{b,\mathrm{id}}\right)^2 = 0$$

According to Fig. 4.6, the brace stiffness of the equivalent frame is half of the brace stiffness of the system with full-length columns. As a result, the ideal brace stiffness for the multi-column system is:

$$S_{b,\mathrm{idt}} = 2S_{b,\mathrm{id}} \tag{4.7}$$

Because Eq. (4.5) accounts for the stiffness interaction among columns and braces in the system, and Eq. (2.20) considers the effect of axial load on column lateral stiffness, the proposed method is comprehensively applicable to the systems with variable column size ($I_{c,i}$), applied loading (P_i) and semi-rigid connections ($r_{e,i}$).

4.3.1 Ideal brace stiffness of multi-column systems with uniform column lateral stiffness

If a multi-column system is composed of identical columns having the same section size (I_c) and end-fixity factor (r_e) and all columns are subjected to the critical buckling load (P_{cr}), the lateral stiffness $S_{c,\mathrm{cr}}$ for all the half-length columns would be the same. In that case, if the system is rigidly anchored on one side ($c = 0$ and $S_{L,1} = 0$), Eq. (4.6) can be simplified as Eq. (4.8) by introducing an unknown scale factor a so that $S_{b,\mathrm{id}} = -aS_{c,\mathrm{cr}}$.

$$f(a)(S_{c,\mathrm{cr}})^n = 0 \tag{4.8}$$

where $f(a)$ is an (n)th-order polynomial. Since $S_{c,\mathrm{cr}}$ is a nonzero value, the roots of $f(a) = 0$ are the solutions to the scale factor a and $S_{b,\mathrm{id}}$. Because the maximum root $a_{\max}$ governs, $(-a_{\max}S_{c,\mathrm{cr}})$ is taken as the solution of $S_{b,\mathrm{id}}$. In this study, it is found that the $f(a)$ is identical to that derived by Ziemian and Ziemian [5]. Based on the analytical results, Ziemian and Ziemian [5] proposed an easy-to-use expression given in Eq. (2.4) to predict the value of $a_{\max}$, which also applies to the systems anchored on two sides and systems with flexible anchors.

It can be seen from Eq. (4.8) that the end-fixity factor r_e only affects the value of $S_{c,\mathrm{cr}}$ and has no influence on $a_{\max}$. Due to this, Eq. (2.4) can be extended to determine the ideal brace stiffness of multiple semi-rigidly connected columns with identical column lateral stiffness, as given in Eq. (4.9); $S_{b,\mathrm{ids}}$ is the ideal brace stiffness of a single semi-rigidly connected column, computed by Eq. (3.13). In this way, the effect of semi-rigid connections on the ideal brace stiffness of multi-column systems is explicitly considered in the term $S_{b,\mathrm{ids}}$.

$$S_{b,\mathrm{idt}} = \left[0.4N^2 + (0.4 + c)N + 0.2\right] S_{b,\mathrm{ids}} \tag{4.9}$$

Note that the extension to Ziemian and Ziemian's method is only applicable to cases in which all the column dimensions, connections, and brace stiffnesses are the same. For

such cases in elastic analysis, the conclusions drawn in Chapter 3 for a single column also apply to the multi-column systems: $r_e = 0.392$ is the optimum value for design as it requires the minimum brace stiffness (Fig. 3.3), and $r_e = 0.77$ yields the maximum efficiency factor (Fig. 3.5).

4.3.2 Computational procedure

A summary of the procedure established in MATLAB that can be followed to compute the ideal brace stiffness of multiple semi-rigidly connected columns using the equivalent lateral stiffness is provided as follows.

1. Specify the brace stiffness ratio, c. Determine the basic properties of members (L_c, L_b, E_c, E_b, I_b, and I_c) and end-fixity factor (r_e) or end connection stiffness R.

2. With $K_{0,i} = 1.0$ being the initial guess, solve Eq. (3.12) using the built-in nonlinear system solver *fsolve* in MATLAB to obtain the exact effective length factor K_i and the critical buckling load $P_{cr,i}$ for each column. If the column inelastic behaviour is considered, Eq. (2.26) is to be used to calculate the tangent modulus $E_{t,i}$ with known r_e, and Eqs. (2.27) are to be solved to calculate $K_{p,i}$ and $\tau_{b,i}$.

3. If r_e was not determined, calculate the value of it for each column by Eq. (2.16) with known end connection stiffness, R. Substitute $\phi_i = \pi/K_i$ into Eq. (3.10) to attain the lateral stiffness $S_{c,i}$ for each column. The elastic modulus E_c and effective length factor K should be replaced by E_t and K_p, respectively, to account for the inelasticity of columns.

4. If the system possesses uniform column lateral stiffness, the extended Ziemian and Ziemian equation in Eq. (4.9) can be used to compute the ideal brace stiffness. If not, follow the below procedure.

5. With the obtained values of $S_{c,i}$, obtain the expression of $S_{\text{eq},1}$ by substituting $S_{b,i} = S_{b,\text{id}}$ and $S_{L,1} = S_{L,n+1} = S_{b,\text{id}}/(1+c)$ into Eq. (4.5). Then the expression of S_{NUM} can be obtained by employing the built-in function, *numden*, in MATLAB.

6. Use the numerical solver *vpasolve* in MATLAB to compute the roots of $S_{\text{NUM}} = 0$. The maximum value of the roots is taken as the value of the ideal brace stiffness of the

half-length column system, $S_{b,\mathrm{id}}$. For the whole system, the ideal brace stiffness is $S_{b,\mathrm{idt}} = 2S_{b,\mathrm{id}}$.

4.4 Examples of a 23-column System

4.4.1 Example 1

The problem studied by Sputo and Beery [12] as well as Ziemian and Ziemian [5] is adopted in this study to demonstrate the proposed method and the corresponding computational procedure. The system shown in Fig. 4.7 consists of 23 parallel cold-formed steel columns serving as the studs in a load-bearing wall. Different from the original problem in which the columns are pin-pin connected, all the columns in this example are semi-rigidly connected with $r_e = 0.3$; the corresponding rotational stiffness of connection $R = 7\,242\,532\,\mathrm{N/mm}$ is obtained from Eq. (2.16). The two exterior columns are used as lateral bracing to anchor the system. The tie bracing is modelled as the truss members between columns and located at column mid-height. The centre-to-centre spacing of the columns is 610 mm, and each column has a length of 2.4 m ($2L$).

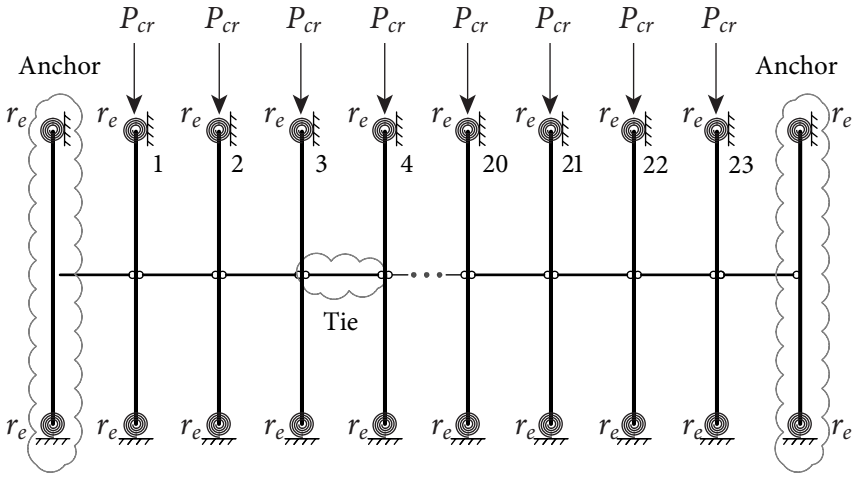

Figure 4.7: Model of a system with 23 semi-rigidly connected columns

The 250S137-54 studs are adopted as the interior column section with an in-plane moment of inertia $I = 33\,299\,\mathrm{mm}^4$ and cross-sectional area $A = 204\,\mathrm{mm}^2$. The elastic modulus E and yield stress f_y of cold-formed steel are 203 000 MPa and 345 MPa, respectively.

In this example, all the tie bracing has the same axial stiffness. This problem aims to evaluate the minimum cross-sectional area A_b of tie bracing and the minimum moment of inertia I_{an} of the anchor columns. Both A_b and I_{an} can be obtained once the ideal brace stiffness of tie bracing $S_{b,\text{idt}}$ for the system is obtained.

Analytical results

The computational procedure for evaluating the ideal brace stiffness based on the computational procedure described in subsection 4.3.2 for elastic analysis is:

1. Since design specifications generally presume the stiffness of tie bracing to be significantly greater than the stiffness of the anchor [5], assume the brace stiffness ratio $c = 100$.

2. By adopting $K_0 = 1.0$ as the initial guess, the exact value of effective length factor K is computed via Eq. (3.12) by employing a nonlinear system solver *fsolve* provided in MATLAB, $K = 0.9067$. The corresponding non-sway buckling load of the half-length column P_{cr} is

$$P_{cr} = \frac{\pi^2 EI}{(KL)^2} = \frac{\pi^2 (203000)(33299)}{(0.9067 \times 1200)^2} = 56360\,\text{N}$$

3. By substituting $K = 0.9067$, $r_e = 0.3$ into Eq. (3.10), the calculation of the lateral stiffness of each half-length column is attained as $S_c = -35.98\,\text{N/mm}$

4. Substituting $S_{c,i} = -35.98\,\text{N/mm}$, $S_{b,i} = S_{b,\text{id}}$, and $S_{L,1} = S_{L,n+1} = S_{b,\text{id}}/(1+c)$ into Eq. (4.5) yields the expression of $S_{\text{eq},1}$. The *numden* function provided in MATLAB can be used to obtain the symbolic expression of S_{NUM}. After that, the solutions of $S_{b,\text{id}}$ can be numerically solved from $S_{\text{NUM}} = 0$ via a solver *vpasolve* in MATLAB. The maximum solution of $S_{b,\text{id}}$ is taken as the ideal brace stiffness for the equivalent unbraced frame. In this example, $S_{b,\text{id}} = 43187\,\text{N/mm}$. Accordingly, the ideal brace stiffness for the system $S_{b,\text{idt}}$ is

$$S_{b,\text{idt}} = 2S_{b,\text{id}} = 2 \times 43187\,\text{N/mm} = 86374\,\text{N/mm}$$

5. Based on S_b, calculate the associated area of tie bracing A_b and the anchor's moment

of inertia I_{an}.

$$S_b = \frac{EA_b}{L_b} \geq S_{b,\text{idt}} \rightarrow A_b \geq 86374\left(\frac{610}{203000}\right) = 259.6\,\text{mm}^2$$
$$S_{an} = \frac{48EI_{an}}{L^3} \geq \frac{S_{b,\text{idt}}}{c} \rightarrow I_{an} \geq \frac{86374}{100}\left(\frac{2400^3}{48\times 203000}\right) = 1.225\times 10^6\,\text{mm}^4$$

For comparison purposes, the analysis is repeated with assuming all the columns are pin-connected. In that case, the critical buckling load P_{cr} is 46330 N; the brace area A_b and I_{an} for ideal bracing are 278.5 mm^2 and 1.315×10^6 mm^4, respectively. Thus, it is clearly demonstrated that for the case with the semi-rigid connections ($r_e = 0.3$), the system has a larger buckling load and requires a lower ideal brace stiffness.

For the inelastic analysis, the inelastic stiffness reduction factor τ_b in Eq. (2.27) needs to be incorporated in the calculation of P_{cr} and S_c. The values of τ_b and K are numerically solved from Eq. (2.27) using the *fsolve* routine with initial values of $\tau_b = 1$ and $K_p = 1$. For this example, $\tau_b = 0.8469$ and $K_p = 0.8952$. Calculate P_{cr} using Eq. (2.26):

$$P_{cr} = \frac{\pi^2 E\tau_b I}{(K_p L)^2} = \frac{\pi^2\,(203000)\,(0.8469)\,(33299)}{(0.8952\times 1200)^2} = 48958\,\text{N}$$

With $P_{cr} = 48958$ N, it is confirmed that $P_{cr}/P_y = 0.696 > 0.5$. The inelastic lateral stiffness of the half-length column is $S_c = -30.36$ N/mm.

By repeating Step 4, the ideal brace stiffness for the system in the inelastic analysis is obtained as $S_{b,\text{idt}} = 72888$ N/mm. The corresponding tie bracing's cross-sectional area and anchor's moment of inertia are $A_b = 219.0$ mm^2 and $I_{an} = 1.034\times 10^6$ mm^4, respectively. As expected, the ideal brace stiffness obtained from the inelastic analysis is less than that from the elastic analysis.

FEM results

Finite element analyses were carried out to verify the results obtained from the proposed method by following the instructions in Appendix A. The cross-sectional and material properties as well as the length of the columns and tie bracing are identical to those stated in Section 4.4.1.

Buckling analyses were performed with the *Subspace* eigensolver to obtain the first buckling mode and corresponding buckling load. Ziemian and Ziemian [5] stated that

the ideal brace stiffness could be established by varying the brace stiffness and repeating the analysis until the critical buckling mode just changed from sway buckling mode to non-sway buckling mode or the other way around. The corresponding brace stiffness at which this conversion occurs is determined as the ideal brace stiffness for the system. The sway buckling mode was obtained from FEM (Fig. 4.8a) if the area of the tie bracing and moment of inertia of the anchor column were taken as the predicted values from the elastic analysis in Section 4.4.1. By increasing I_{an} from $1.225 \times 10^6\,\text{mm}^4$ to $1.226 \times 10^6\,\text{mm}^4$, the failure changed from sway buckling to non-sway buckling mode, as shown in Fig. 4.8b.

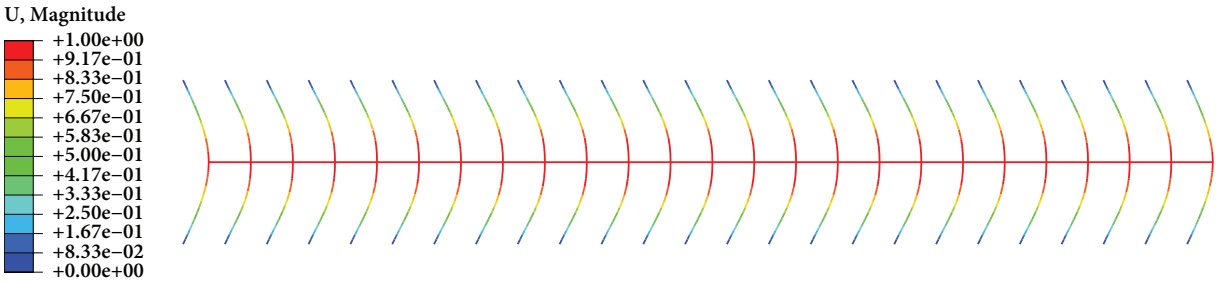

(a) Sway buckling mode: $A_b = 259.6\,\text{mm}^2$ and $I_{an} = 1.225 \times 10^6\,\text{mm}^4$

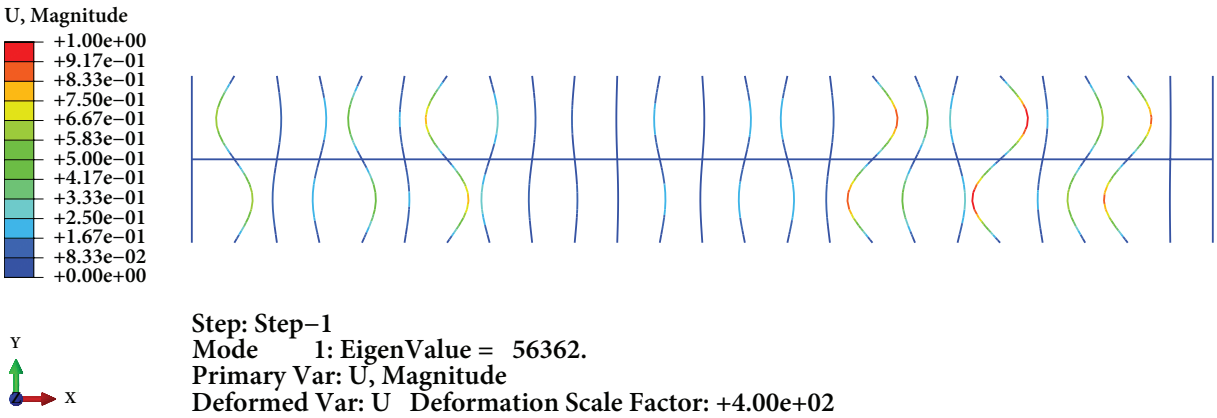

(b) Non-sway buckling mode: $A_b = 259.6\,\text{mm}^2$ and $I_{an} = 1.226 \times 10^6\,\text{mm}^4$

Figure 4.8: Deflected shapes and buckling loads of Example 1 (elastic analysis) obtained from ABAQUS

The analytical results of inelastic buckling were also verified by FEM with $E_t = \tau_b E$ for columns. With $A_b = 219.0\,\text{mm}^2$ and $I_{an} = 1.034 \times 10^6\,\text{mm}^4$ attained from the analytical method, non-sway buckling mode was obtained with $P_{cr} = 48\,960\,\text{N}$. By decreasing I_{an} from $1.034 \times 10^6\,\text{mm}^4$ to $1.033 \times 10^6\,\text{mm}^4$, the buckling mode switched to sway buckling

with $P_{cr} = 48\,852\,\text{N}$. Consequently, analytical and finite element analysis (FEA) results are consistent.

Results of the proposed simplified method

For this example, as all the columns are identical, Eq. (3.13) and Eq. (3.15) together with Eq. (2.4) can be utilized to develop a simplified procedure for evaluating the ideal brace stiffness without the iterative process of determining column effective length factor K for non-sway buckling. The simplified procedure is as follows:

1. Given the system has two anchored ends, $j = 2$, $N = n/j = 11.5$.

2. Assume $c = 100$.

3. Calculate the ideal brace stiffness needed for a single column through Eq. (3.13) and Eq. (3.15).

$$\begin{aligned}\beta_u &= -0.8235 + 0.257 r_e - 0.0815 r_e^2 - 0.4397 r_e^3 \\ &= -0.8235 + 0.257(0.3) - 0.0815(0.3)^2 - 0.4397(0.3)^3 = -0.7656\end{aligned}$$

$$S_{b,\text{ids}} = -\frac{24 E_c I_c}{L^3}\beta_u = -\frac{24(203000)(33299)}{1200^3}(-0.7656) = 71.88\,\text{N/mm}$$

4. Calculate the value of $a_{\max}$ via Eq. (2.4).

$$a_{\max} = 0.4(11.5)^2 + (0.4 + 100)(11.5) + 0.2 = 1207.7$$

5. Calculate the ideal brace stiffness for the system.

$$S_{b,\text{idt}} = a_{\max} S_{b,\text{ids}} = 1207.7 \times 71.88 = 86\,809\,\text{N/mm}$$

For the inelastic analysis, the computational procedure is the same as that of the elastic one shown above, with the elastic modulus E being replaced by the reduced modulus E_t. In that case, τ_b needs to be calculated prior to Step 3, as illustrated in Section 4.4.1. In this case, with $\tau_b = 0.8469$, $r_e = 0.336$ is obtained from Eq. (2.16). Repeating the calculation stated in Step 3 yields $\beta_u = 0.7630$ and $S_{b,\text{ids}} = 60.67\,\text{N/mm}$. As the ratio $a_{\max}$ is still 1207.7, $S_{b,\text{idt}}$ of the system in the inelastic analysis is $1207.7 \times 60.67 = 73\,269\,\text{N/mm}$. Based on the foregoing elastic and inelastic analyses, the predicted ideal brace stiffness from the simplified method is only 0.5% greater than the exact analytical value.

4.4.2 Example 2

The previous example focuses on the case in which the system is composed of the same columns. As the proposed method is also applicable to a system with nonidentical columns, this example is presented to investigate the effect of different column sizes on the ideal brace stiffness for the system. The system adopted in this example is the same as that in Example 1, except that the three centre columns are replaced by a back-to-back 250S137-54 section with $I_{c,m} = 120\,681\,\text{N/mm}^4$. Assume the rotational stiffnesses of the connections are the same for all the columns, $R = 7\,242\,532\,\text{N/mm}$. Note that the simplified method presented in Section 4.4.1 is not applicable, as different column sizes exist in this example. Two cases are considered: 1) all the columns are subjected to the same critical buckling load; 2) all the columns are subjected to their own critical buckling load. Only elastic buckling is considered.

Analytical results: Case 1

The procedure described in Section 4.3.2 is followed. Since the three centre columns have a larger moment of inertia, the associated end-fixity factor r_e is no longer 0.3. The r_e for the three centre columns is obtained as 0.1057 via Eq. (2.16). As computed in Example 1, the lateral stiffness of the original columns is $S_c = -35.98\,\text{N/mm}$. For this case, as the buckling load is governed by the critical buckling load of the original column, the lateral stiffness of the three centre half-length columns is computed as $S_{c,m} = -3.17\,\text{N/mm}$. By comparing the column lateral stiffness, it concludes that the centre columns are "stiffer" than other original columns. The maximum root of Eq. (4.6) is attained with obtained column lateral stiffnesses: $S_{b,\text{id}} = 37\,883\,\text{N/mm}$. The corresponding ideal brace stiffness for the system $S_{b,\text{idt}}$ is $2S_{b,\text{id}} = 75\,766\,\text{N/mm}$. Consequently, the minimum required area of tie bracing and moment of inertia of the anchor column are $A_b = 227.7\,\text{mm}^2$ and $I_{an} = 1.075 \times 10^6\,\text{mm}^4$, respectively. Compared to the results of Example 1 presented in Section 4.4.1, the ideal brace stiffness is reduced by 20.03% due to the presence of the "stiffer" columns.

Analytical results: Case 2

In this case, all the columns are subjected to their own critical buckling loads. The effective length factor K and critical buckling load of the three centre columns $P_{cr,m}$ are 0.9676 and 179534 N, respectively. Using Eq. (2.20) to compute the lateral stiffness of the three centre half-length columns gives $S_{c,m} = -135.72\,\text{N/mm}$, which is less than the lateral stiffness of the original columns. The ideal brace stiffness for the system is obtained as $S_{b,\text{idt}} = 118990\,\text{N/mm}$, and the corresponding A_b and I_{an} are $357.6\,\text{mm}^2$ and $1.688\times10^6\,\text{mm}^4$, respectively. It can be seen that the ideal brace stiffness for Case 2 is much greater than that of Example 1 with identical columns. This is because the three centre columns possess less lateral stiffness with their own critical buckling loads, which is more detrimental to the stability of the system, even though the three centre columns have a greater moment of inertia.

FEM results: Case 1

By modifying the FEM developed in Example 1 by accounting for the three centre columns, buckling analyses were carried out. Using the section properties predicted from Section 4.4.2, sway buckling mode was obtained from FEM with buckling load $P_{cr} = 56359\,\text{N}$. By increasing the moment of inertia of the anchor column I_{an} from $1.075\times10^6\,\text{mm}^4$ to $1.076\times10^6\,\text{mm}^4$, the buckling shape switched from sway buckling mode to non-sway buckling mode with the corresponding buckling load being $P_{cr} = 56361\,\text{N}$.

FEM results: Case 2

In this case, the applied loads on the three centre columns and the original columns were set as $P_{cr,m}/P_{cr}$ and unity, respectively. With the section properties predicted from the previous analytical analysis, sway buckling mode was obtained from FEM with buckling load $P_{cr} = 56361\,\text{N}$. By increasing I_{an} from $1.688\times10^6\,\text{mm}^4$ to $1.689\times10^6\,\text{mm}^4$, the buckling shape switched from sway buckling mode to non-sway buckling mode with $P_{cr} = 56361\,\text{N}$.

The good agreements between analytical and FEA results demonstrate that the proposed method can accurately assess stiffness interaction among columns in the determination of the ideal brace stiffness of the system.

4.5 Formulation of Stiffness Interaction in Multi-column Systems

The derivations of ideal brace stiffness and brace forces in multiple semi-rigidly connected columns are presented in this section by formulating the stiffness interaction among columns and braces. Note that the expressions presented in this section are based on the half-length column model shown in Fig. 4.6. Therefore, the obtained ideal brace stiffness and brace forces need to be doubled for the full-length multi-column system.

By adopting the proposed model, the multi-column system can be simulated as two equivalent frames. As shown in Fig. 4.9, each half-length column is subjected to a gravity load P_i, and the internal force in each brace is represented as Q_i. Two kinds of systems can be simulated using the diagram presented in Fig. 4.9: 1) the system anchored on one side with braces that can resist compressive and tensile forces; 2) the system anchored on both sides with tension-only braces.

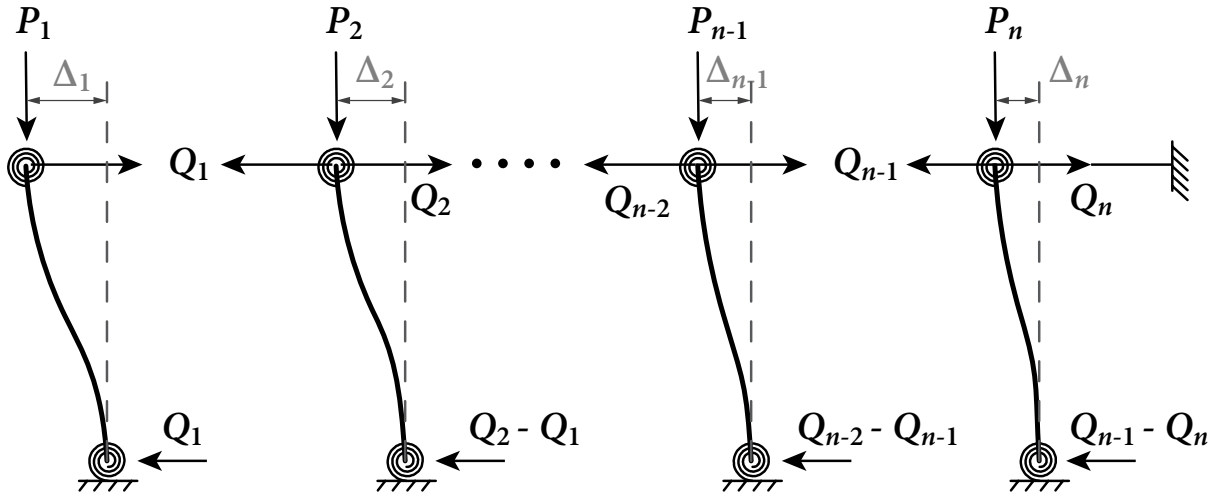

Figure 4.9: A storey frame anchored on one side subjected to gravity loading

For each column in the system shown in Fig. 4.9, the total lateral load applied on the column's upper end is the difference between adjacent brace forces, $Q_i - Q_{i-1}$, except for the left-most column, on which the lateral load equals the brace force, Q_1. An equivalent lateral force Q_0 is introduced to represent the influences of the axial load (P), column initial imperfection (Δ_0), and initial curvature (ψ) on the mid-height lateral deflection, as given in

Eq. (4.10).

$$Q_0 = P\Delta_0\psi/L \tag{4.10}$$

By doing so, Eq. (3.8) can be written as

$$\Delta = \frac{Q + Q_0}{S_c} \tag{4.11}$$

Subsequently, adopting Eq. (4.11) gives:

$$\Delta_1 = \frac{Q_{0,1} - Q_1}{S_{c,1}} \tag{4.12a}$$

$$\Delta_i = \frac{Q_{0,i} + Q_{i-1} - Q_i}{S_{c,i}} \quad i = \{2, ..., n\} \tag{4.12b}$$

For braces 1 to $n-1$, the axial deformation of the brace is the lateral displacement difference between adjacent columns $\Delta_i - \Delta_{i+1}$; for brace n, since it is the external brace, its axial deformation is the same as the lateral deflection of the adjacent column. Assuming the axial deformation of brace i is the ratio of brace force Q_i and brace stiffness $S_{b,i}$ yields

$$Q_i / S_{b,i} = \Delta_i - \Delta_{i+1} \quad i = \{1, 2..., n-1\} \tag{4.13a}$$

$$Q_n / S_{b,n} = \Delta_n \tag{4.13b}$$

If the system is anchored on both sides and the braces are designed to be able to bear compressive forces, as illustrated in Fig. 4.10, the stiffness interactions expressed in Eq. (4.12) and Eq. (4.13) become Eqs. (4.14) and (4.15), respectively.

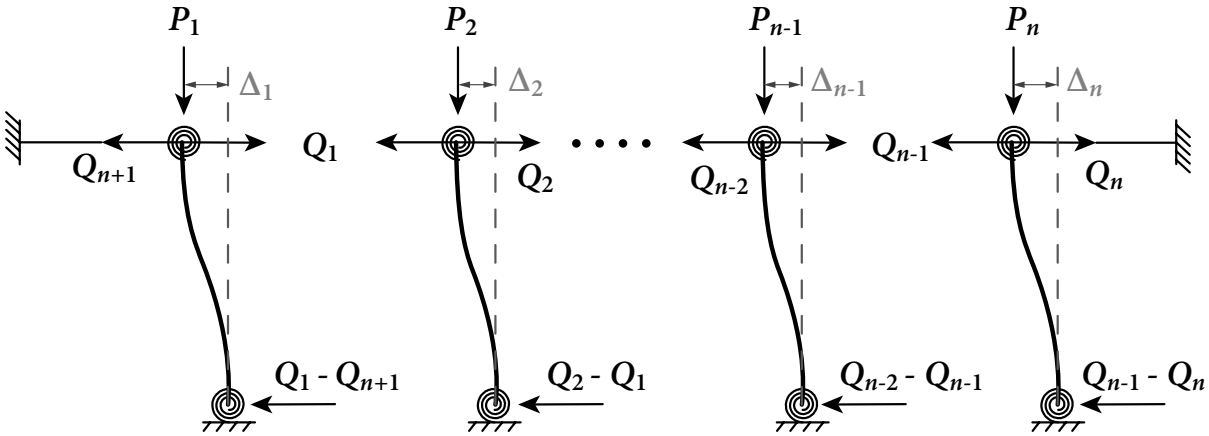

Figure 4.10: A storey frame anchored on both sides subjected to gravity loading

$$\Delta_1 = \frac{Q_{0,1} - Q_1 + Q_{n+1}}{S_{c,1}} \tag{4.14a}$$

$$\Delta_i = \frac{Q_{0,i} + Q_{i-1} - Q_i}{S_{c,i}} \quad i = \{2, ..., n\} \tag{4.14b}$$

$$Q_i / S_{b,i} = \Delta_i - \Delta_{i+1} \quad i = \{1, 2..., n-1\} \tag{4.15a}$$

$$Q_n / S_{b,n} = \Delta_n \tag{4.15b}$$

$$Q_{n+1} / S_{b,n+1} = -\Delta_1 \tag{4.15c}$$

4.5.1 Ideal brace stiffness

Section 4.3 indicates that the ideal brace stiffness for multiple columns can be obtained by finding the maximum root of $S_{\text{NUM}} = 0$. Nevertheless, S_{NUM} requires establishing the expression of the system's equivalent lateral stiffness with a sequence of series and parallel operations, which is still not straightforward enough for engineering practice. In this subsection, an alternative method for determining the ideal brace stiffness for multiple semi-rigidly connected columns is proposed.

For the system anchored on one side, substituting Eqs. (4.13) into Eqs. (4.12) to eliminate Q_i gives:

$$\Delta_1 S_{c,1} = Q_{0,1} - (\Delta_1 - \Delta_2) S_{b,1} \tag{4.16a}$$

$$\Delta_i S_{c,i} = Q_{0,i} + (\Delta_{i-1} - \Delta_i) S_{b,i-1} - (\Delta_i - \Delta_{i+1}) S_{b,i} \quad i = \{2, ..., n-1\} \tag{4.16b}$$

$$\Delta_n S_{c,n} = Q_{0,n} + (\Delta_{n-1} - \Delta_n) S_{b,n-1} - \Delta_n S_{b,n} \tag{4.16c}$$

For the system anchored on both sides, substituting Eqs. (4.15) into Eqs. (4.14) to eliminate Q_i gives:

$$\Delta_1 S_{c,1} = Q_{0,1} - (\Delta_1 - \Delta_2) S_{b,1} - \Delta_1 S_{b,n+1} \tag{4.17a}$$

$$\Delta_i S_{c,i} = Q_{0,i} + (\Delta_{i-1} - \Delta_i) S_{b,i-1} - (\Delta_i - \Delta_{i+1}) S_{b,i} \quad i = \{2, ..., n-1\} \tag{4.17b}$$

$$\Delta_n S_{c,n} = Q_{0,n} + (\Delta_{n-1} - \Delta_n) S_{b,n-1} - \Delta_n S_{b,n} \tag{4.17c}$$

The recursive relationships in Eqs. (4.16) and Eqs. (4.17) can be expressed in a general format of $[K]\{\Delta\} = \{Q_0\}$, as follows:

$$\begin{bmatrix} S_{b,1} + S_{b,n+1} + S_{c,1} & -S_{b,1} & & \\ -S_{b,1} & S_{b,1} + S_{b,2} + S_{c,2} & \ddots & \\ & \ddots & \ddots & -S_{b,n-1} \\ & & -S_{b,n-1} & S_{b,n-1} + S_{b,n} + S_{c,n} \end{bmatrix} \begin{Bmatrix} \Delta_1 \\ \Delta_2 \\ \vdots \\ \Delta_n \end{Bmatrix} = \begin{Bmatrix} Q_{0,1} \\ Q_{0,2} \\ \vdots \\ Q_{0,n} \end{Bmatrix} \tag{4.18}$$

If the system is anchored on one side, $S_{b,n+1}$ in Eq. (4.18) equals zero. Let the term "perfect system" represent the corresponding system without the initial imperfection and curvature. Thus, the equilibrium shown in Eq. (4.18) for the perfect system can be written as

$$[K]\{\Delta_i\} = 0 \tag{4.19}$$

where $[K]$ is the stiffness matrix shown in Eq. (4.18). For the homogeneous system given in Eq. (4.19), the nonlinear trivial solution exists when the determinant of $[K]$, $\det[K]$, equals zero [5]:

$$\det[K] = 0 \tag{4.20}$$

The solution to Eq. (4.18) does not exist if the determinant of the coefficient matrix $\det[K]$ equals zero, which indicates the buckling of the corresponding perfect system.

If all the braces are assumed to have the same axial stiffness S_b, then $\det[K]$ is an n-th order polynomial consisting of one unknown variable S_b with known $S_{c,i}$ and $\Delta_{0,i}$. Consequently, the maximum root of Eq. (4.20) is the ideal brace stiffness for the frame, $S_{b,\mathrm{id}}$. It is found that finding the maximum root of Eq. (4.20) yields the same results as the method proposed in Section 4.3 [1].

4.5.2 Brace forces

For the system anchored on one side, substituting Eqs. (4.12) into Eqs. (4.13) to eliminate Δ_i gives:

$$\frac{Q_1}{S_{b,1}} = \frac{Q_{0,1} - Q_1}{S_{c,1}} - \frac{Q_{0,2} + Q_1 - Q_2}{S_{c,2}} \tag{4.21a}$$

$$\frac{Q_i}{S_{b,i}} = \frac{Q_{0,i} + Q_{i-1} - Q_i}{S_{c,i}} - \frac{Q_{0,i+1} + Q_i - Q_{i+1}}{S_{c,i+1}} \quad i = \{2, \ldots, n-1\} \tag{4.21b}$$

$$\frac{Q_n}{S_{b,n}} = \frac{Q_{0,n} + Q_{n-1} - Q_n}{S_{c,n}} \tag{4.21c}$$

The system of n equations in Eqs. (4.21) can be converted to a linear system $AX = B$, as expressed in Eq. (4.22).

$$\begin{bmatrix} \frac{1}{S_{b,1}}+\frac{1}{S_{c,1}}+\frac{1}{S_{c,2}} & -\frac{1}{S_{c,2}} & & & & \\ -\frac{1}{S_{c,2}} & \frac{1}{S_{b,2}}+\frac{1}{S_{c,2}}+\frac{1}{S_{c,3}} & -\frac{1}{S_{c,3}} & & & \\ & -\frac{1}{S_{c,3}} & \ddots & \ddots & & \\ & & \ddots & \frac{1}{S_{b,n-1}}+\frac{1}{S_{c,n-1}}+\frac{1}{S_{c,n}} & -\frac{1}{S_{c,n}} & \\ & & & -\frac{1}{S_{c,n}} & \frac{1}{S_{b,n}}+\frac{1}{S_{c,n}} \end{bmatrix} \begin{Bmatrix} Q_1 \\ Q_2 \\ \vdots \\ Q_{n-1} \\ Q_n \end{Bmatrix} = \begin{Bmatrix} \frac{Q_{0,1}}{S_{c,1}}-\frac{Q_{0,2}}{S_{c,2}} \\ \frac{Q_{0,2}}{S_{c,2}}-\frac{Q_{0,3}}{S_{c,3}} \\ \vdots \\ \frac{Q_{0,n-1}}{S_{c,n-1}}-\frac{Q_{0,n}}{S_{c,n}} \\ \frac{Q_{0,n}}{S_{c,n}} \end{Bmatrix} \tag{4.22}$$

For the system anchored on both sides, the equilibrium equations and corresponding matrix format is given in Eqs. (4.23) and Eq. (4.24), respectively.

$$\frac{Q_1}{S_{b,1}} = \frac{Q_{0,1}-Q_1+Q_{n+1}}{S_{c,1}} - \frac{Q_{0,2}+Q_1-Q_2}{S_{c,2}} \tag{4.23a}$$

$$\frac{Q_i}{S_{b,i}} = \frac{Q_{0,i}+Q_{i-1}-Q_i}{S_{c,i}} - \frac{Q_{0,i+1}+Q_i-Q_{i+1}}{S_{c,i+1}} \qquad i=\{2,...,n-1\} \tag{4.23b}$$

$$\frac{Q_n}{S_{b,n}} = \frac{Q_{0,n}+Q_{n-1}-Q_n}{S_{c,n}} \tag{4.23c}$$

$$\frac{Q_{n+1}}{S_{b,n+1}} = -\frac{Q_{0,1}+Q_{n+1}-Q_1}{S_{c,1}} \tag{4.23d}$$

$$\begin{bmatrix} -\frac{1}{S_{b,n+1}}+\frac{1}{S_{c,1}} & \frac{1}{S_{c,1}} & & & & \\ -\frac{1}{S_{c,1}} & \frac{1}{S_{b,1}}+\frac{1}{S_{c,1}}+\frac{1}{S_{c,2}} & -\frac{1}{S_{c,2}} & & & \\ & -\frac{1}{S_{c,2}} & \ddots & \ddots & & \\ & & \ddots & \frac{1}{S_{b,n-1}}+\frac{1}{S_{c,n-1}}+\frac{1}{S_{c,n}} & -\frac{1}{S_{c,n}} & \\ & & & -\frac{1}{S_{c,n}} & \frac{1}{S_{b,n}}+\frac{1}{S_{c,n}} \end{bmatrix} \begin{Bmatrix} Q_{n+1} \\ Q_1 \\ \vdots \\ Q_{n-1} \\ Q_n \end{Bmatrix} = \begin{Bmatrix} \frac{Q_{0,1}}{S_{c,1}} \\ \frac{Q_{0,1}}{S_{c,1}}-\frac{Q_{0,2}}{S_{c,2}} \\ \vdots \\ \frac{Q_{0,n-1}}{S_{c,n-1}}-\frac{Q_{0,n}}{S_{c,n}} \\ \frac{Q_{0,n}}{S_{c,n}} \end{Bmatrix} \tag{4.24}$$

With known P_i, $S_{b,i}$ and $S_{c,i}$, the brace forces Q_i for systems with nonuniform column lateral stiffnesses can be attained by solving the linear system in Eq. (4.22) or Eq. (4.24). It is worth noting that the brace stiffness $S_{b,i}$ has to be greater than the ideal brace stiffness, $S_{b,\text{id}}$. Only in this way can the expressions in Eq. (4.22) and Eq. (4.24) have physical meaning.

4.6 Bracing Requirements for Systems with Uniform Column Lateral stiffness

If columns in a system have the same size and end-fixity factor, and are subjected to the same load, the column lateral stiffness in the system is uniform. In this section, the formulae

proposed in Section 4.5 are simplified for the special case in which all braces possess the same stiffness and all columns have the same lateral stiffness. In addition, all the columns are assumed to have the same initial imperfection Δ_0. The brace forces become infinity when the columns are subjected to critical buckling loads and the ideal brace stiffness is adopted, which is structurally unacceptable. Therefore, a bracing stiffness ratio α_b, the ratio of the required brace stiffness to the ideal brace stiffness, is introduced to increase the brace stiffness and reduce the braces forces accordingly. With $S_{b,i} = \alpha_b S_{b,\mathrm{id}}$, $S_{c,i} = S_c$, and $Q_{0,i} = Q_0$, Eq. (4.22) and Eq. (4.24) can be simplified as Eq. (4.25) and Eq. (4.26), respectively.

$$\begin{bmatrix} \frac{2}{S_c}+\frac{1}{\alpha_b S_{b,\mathrm{id}}} & -\frac{1}{S_c} & & & & \\ -\frac{1}{S_c} & \frac{2}{S_c}+\frac{1}{\alpha_b S_{b,\mathrm{id}}} & -\frac{1}{S_c} & & & \\ & -\frac{1}{S_c} & \ddots & \ddots & & \\ & & \ddots & \frac{2}{S_c}+\frac{1}{\alpha_b S_{b,\mathrm{id}}} & -\frac{1}{S_c} & \\ & & & -\frac{1}{S_c} & \frac{1}{S_c}+\frac{1}{\alpha_b S_{b,\mathrm{id}}} \end{bmatrix} \begin{Bmatrix} Q_1 \\ Q_2 \\ \vdots \\ Q_{n-1} \\ Q_n \end{Bmatrix} = Q_0 \begin{Bmatrix} 0 \\ 0 \\ \vdots \\ 0 \\ \frac{1}{S_c} \end{Bmatrix} \tag{4.25}$$

$$\begin{bmatrix} -\frac{1}{S_c}-\frac{1}{\alpha_b S_{b,\mathrm{id}}} & \frac{1}{S_c} & & & & & \\ -\frac{1}{S_c} & \frac{2}{S_c}+\frac{1}{\alpha_b S_{b,\mathrm{id}}} & -\frac{1}{S_c} & & & & \\ & -\frac{1}{S_c} & \frac{2}{S_c}+\frac{1}{\alpha_b S_{b,\mathrm{id}}} & -\frac{1}{S_c} & & & \\ & & -\frac{1}{S_c} & \ddots & \ddots & & \\ & & & \ddots & \frac{2}{S_c}+\frac{1}{\alpha_b S_{b,\mathrm{id}}} & -\frac{1}{S_c} & \\ & & & & -\frac{1}{S_c} & \frac{1}{S_c}+\frac{1}{\alpha_b S_{b,\mathrm{id}}} \end{bmatrix} \begin{Bmatrix} Q_{n+1} \\ Q_1 \\ Q_2 \\ \vdots \\ Q_{n-1} \\ Q_n \end{Bmatrix} = Q_0 \begin{Bmatrix} \frac{1}{S_c} \\ 0 \\ 0 \\ \vdots \\ 0 \\ \frac{1}{S_c} \end{Bmatrix} \tag{4.26}$$

When the number of columns n is even, Eq. (4.26) can be transformed to a general format shown in Eq. (4.27) using Gaussian elimination.

$$\begin{cases} AX_1 = -B \\ CX_2 = 0 \\ AX_3 = B \end{cases} \tag{4.27}$$

where

$$A = \begin{bmatrix} \frac{2}{S_c} + \frac{1}{\alpha_b S_{b,\mathrm{id}}} & \ddots & & \\ \ddots & \ddots & -\frac{1}{S_c} & \\ & -\frac{1}{S_c} & \frac{2}{S_c} + \frac{1}{\alpha_b S_{b,\mathrm{id}}} & -\frac{1}{S_c} \\ & & -\frac{1}{S_c} & \frac{1}{S_c} + \frac{1}{\alpha_b S_{b,\mathrm{id}}} \end{bmatrix} \tag{4.28a}$$

$$X_1 = \begin{Bmatrix} Q_{n/2-1} \\ \vdots \\ Q_1 \\ Q_{n+1} \end{Bmatrix} \quad X_2 = \{Q_{n/2}\} \quad X_3 = \begin{Bmatrix} Q_{n/2+1} \\ \vdots \\ Q_{n-1} \\ Q_n \end{Bmatrix} \tag{4.28b}$$

$$B = \begin{Bmatrix} 0 \\ \vdots \\ 0 \\ \frac{1}{S_c} \end{Bmatrix} \tag{4.28c}$$

The above transformation indicates that the linear system $AX_3 = B$ in Eq. (4.27) has the same solution as Eq. (4.25). In addition, $Q_{n/2}(X_2)$ equals zero. That is to say, if the number of columns n in a system anchored by both sides is even, the system can be vertically divided at the middle brace into two equivalent half-systems anchored on one side in which the number of columns is $n/2$. Subsequently, the brace forces in one half-system can be obtained from Eq. (4.25): the magnitudes of brace forces in the two half-systems have a mirror relationship; the signs of brace forces in the two half-systems are opposite; and the force of the middle brace is zero. For the system anchored on both sides with an odd number of columns, Eq. (4.26) is required to obtain the brace forces.

4.6.1 Maximum brace force for a system with uniform column lateral stiffness

In practice, the magnitude of the maximum brace force Q_n is of interest. The explicit solution of Q_n for systems with uniform column lateral stiffness and brace stiffness is explored in this section. For the linear system $AX = B$ given in Eq. (4.25), the solution of X can be obtained by:

$$X = A^{-1}B \tag{4.29}$$

Because A is a non-singular tridiagonal matrix, the inverse of it can be explicitly obtained

[106]. Let $A = [a_{ij}]$ represent the tridiagonal matrix such that $a_{ii} = a_i$, $a_{i,i-1} = b_i$, $a_{i,i+1} = c_i$, and $a_{ij} = 0$ for $|i-j| > 1$. As such, the inverse of A is given by

$$\left(A^{-1}\right)_{ij} = \begin{cases} (-1)^{i+j} b_i \cdots b_{j-1} \theta_{i-1} \tau_{j+1} / \theta_n & \text{if } i < j \\ \theta_{i-1} \tau_{j+1} / \theta_n & \text{if } i = j \\ (-1)^{i+j} c_i \cdots c_{j-1} \theta_{i-1} \tau_{j+1} / \theta_n & \text{if } i > j \end{cases} \tag{4.30}$$

where θ_i and τ_i satisfy the recurrence relations given in Eqs. (4.31) with initial conditions $\theta_0 = 1$, $\theta_1 = a_1$, $\tau_{n+1} = 1$ and $\tau_n = a_n$.

$$\theta_i = a_i \theta_{i-1} - b_{i-1} c_{i-1} \theta_{i-2} \qquad i = 2, 3, ..., n \tag{4.31a}$$

$$\tau_i = a_i \tau_{i+1} - b_i c_i \tau_{i+2} \qquad i = n-1, ..., 1 \tag{4.31b}$$

Simplify Eq. (4.25) as

$$\begin{bmatrix} M_1 & -1 & & & \\ -1 & M_2 & \ddots & & \\ & \ddots & \ddots & -1 & \\ & & -1 & M_{n-1} & -1 \\ & & & -1 & M_n \end{bmatrix} \begin{Bmatrix} Q_1 \\ Q_2 \\ \vdots \\ Q_{n-1} \\ Q_n \end{Bmatrix} = Q_0 \begin{Bmatrix} 0 \\ 0 \\ \vdots \\ 0 \\ 1 \end{Bmatrix} \tag{4.32a}$$

$$M_i = 2 - \frac{S_c}{\alpha_b a_{\max} S_{c,\mathrm{cr}}} \quad i = \{1, 2, ..., n-1\} \tag{4.32b}$$

$$M_n = 1 - \frac{S_c}{\alpha_b a_{\max} S_{c,\mathrm{cr}}} \tag{4.32c}$$

where $S_{c,\mathrm{cr}}$ is the lateral stiffness of a column with critical buckling load, and $a_{\max}$ is a scale factor, as follows:

$$a_{\max} = -S_{b,\mathrm{id}} / S_{c,\mathrm{cr}} \tag{4.33}$$

For the system consisting of identical braces and in which all the columns have the same lateral stiffness, the closed-form solution for $a_{\max}$ is given in Eq. (4.34) [9].

$$a_{\max} = \left[2 \left(1 + \cos \frac{2N\pi}{2N+1} \right) \right]^{-1} \tag{4.34}$$

where $N = n/j$; n is the number of columns, j is the number of anchors, $j = 1$ or 2.

It can be obtained from Eq. (4.29) that $Q_n = Q_0 \left(A^{-1}\right)_{nn}$. With Eq. (4.30) and Eq. (4.32), the solution of Q_n can be expressed in an explicit form:

$$Q_n = Q_0 \frac{\theta_{n-1}}{\theta_n} = Q_0 \frac{1}{M_n - \frac{\theta_{n-2}}{\theta_{n-1}}} = Q_0 \frac{1}{M_n - \frac{1}{M_{n-1} - \frac{\theta_{n-3}}{\theta_{n-2}}}} = \cdots = Q_0 \frac{1}{M_n - \frac{1}{M_{n-1} - \frac{1}{\cdots - \frac{1}{M_1}}}} \tag{4.35}$$

4.6.2 Approximation of the maximum brace force Q_n

For a system with uniform column lateral stiffness, the ratio of Q_n to Q_0 depends not only on the number of columns and anchors, but also on the magnitude of the applied load and end-fixity factor, as indicated in Eq. (4.35). This is because both the applied load and end-fixity factor affect the column lateral stiffness, which is considered in the half-length column model. As a result, Q_n obtained from Eq. (4.35) does not vary linearly with the gravity loading, demonstrated for a single column in Chapter 3. If all applied loads are presumed to be the critical buckling load, the term $S_c/S_{c,\mathrm{cr}}$ in Eq. (4.33) becomes unity irrespective of end-fixity factors, and thus the ratio of Q_n to Q_0 is determined by the recursive term θ_{i-1}/θ_n, which is related to the bracing stiffness ratio, α_b. As stipulated in the AISC specification [10], the brace stiffness shall be at least two times the ideal brace stiffness. Provided $\alpha = 2$ and $P = P_{cr}$, the variation of Q_n with the number of columns n is investigated in this section.

Sputo and Beery [12] indicated that there is a linear relationship between the brace force and the number of columns in a system, as shown in Eq. (4.36).

$$Q_n = n\bar{Q}_1 \tag{4.36}$$

where $\bar{Q}_1$ is the brace force for a single column. However, Blum et al. [13] pointed out that the assumption that the bracing force is linearly accumulated leads to conservative results because the column supports will participate in resisting the lateral force.

For a single column, with $\alpha_b = 2$ and $P = P_{cr}$, the induced brace force $\bar{Q}_1$ is $4Q_0$. The analytical results of $Q_n/\bar{Q}_1$ obtained from Eq. (4.34) and Eq. (4.35) are presented in Fig. 4.11, in which the results from Eq. (4.36) are also presented for comparison. The results indicate that Eq. (4.36) provides more conservative results than the analytical results. Since $Q_n/\bar{Q}_1$ is almost proportionate with the number of columns, a simple-to-use expression in Eq. (4.37) was obtained by linear fitting to predict the value of $Q_n/\bar{Q}_1$ associated with the number of columns. The fitting results agree well with the analytical results, as shown in Fig. 4.11.

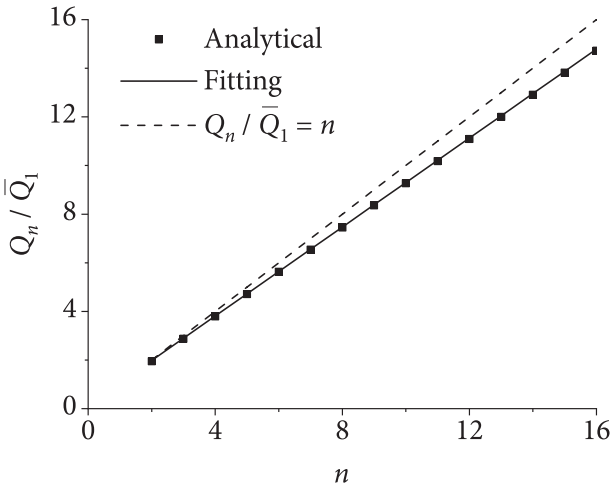

Figure 4.11: Maximum brace forces for n-column system anchored on one side

$$Q_n = (0.915n + 0.15)\bar{Q}_1 \quad n \geq 2 \tag{4.37}$$

With $\bar{Q}_1 = 4Q_0$, Eq. (4.37) becomes Eq. (4.38).

$$Q_n = (0.6 + 3.66n)Q_0 \quad n \geq 2 \tag{4.38}$$

Note that the influences of semi-rigid connections and initial imperfections on the brace forces are explicitly considered in the term Q_0 in Eq. (4.38).

If the number of columns n is even, it is theoretically proved that the maximum force in an n-column system anchored on both sides is the same as that in an $n/2$-column system anchored on one side. For such cases, the proposed equation in Eq. (4.38) can be extended to consider the case anchored on both sides by introducing a coefficient j.

$$Q_n = [(0.6 + 3.66n)Q_0] / j \quad n \geq 2 \tag{4.39}$$

where j is the number of anchors, $j = 1$ or 2. Note that if the braces are designed as tension only, two anchors shall be provided with j taken as 1.

The analytical results obtained from Eq. (4.26) indicate that the maximum brace force in a system anchored on both sides also exhibits an almost linear relationship with the number of columns, as shown in Fig. 4.12. Because of that, Eq. (4.39) also applies to a system with an odd number of columns.

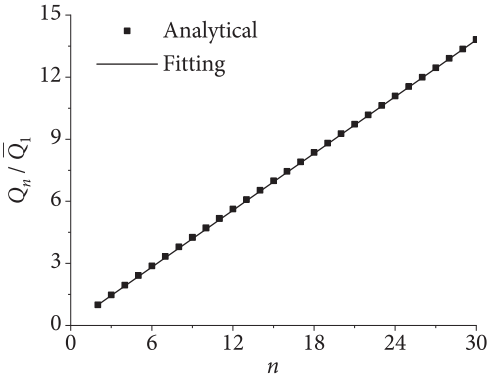

Figure 4.12: Maximum brace forces for n-column system anchored on both sides

4.6.3 Randomness of column initial imperfection

The derivation of brace forces for systems with uniform column lateral stiffness in Section 4.6.1 is based on the assumption that all the columns have the same initial imperfection in the same direction. This assumption is conservative because the magnitude and direction of column initial imperfections are random in reality, which has a favourable effect on brace force requirements. One way to investigate the effect of the randomness of column initial imperfections on the brace forces in multiple columns is to conduct stochastic analysis, as presented by Zhang et al. [14] and Zhao et al. [15] in which the probability density function of mid-height brace forces is established, but this is not considered in this study. The other prevailing practice is to assume that all the columns still have the same initial imperfection, but the magnitude of the initial imperfection for multiple columns, $\Delta_{0,\text{mul}}$, decreases with the number of columns:

$$\Delta_{0,\text{mul}} = \eta \Delta_0 \tag{4.40}$$

where η is a reduction factor of the initial imperfection for multiple columns, a function of number of columns n.

Although the Australian standard AS4100-2020 [27] considers the effect of nonuniform loading patterns on the brace force requirement, it neglects the effect of initial imperfection randomness as indicated in Eq. (2.12), which tends to be conservative. For the other current standards, the brace strength requirement for multiple columns is related to the accumulation of all the forces, ΣP, and the reduction factor, η. The brace strength requirements stipulated in different standards are tabulated in Table 4.1.

Table 4.1: Brace strength requirements in different standards

Standard	$\bar{Q}_1$	Δ_0	η
AISC 360-16 [10]	0.01 P_r	$L/500$	$1/\sqrt{n}$
EN 1993-1-1 (2005) [24]	0.01 P_r	$L/500$	$\sqrt{0.5\,(1+1/n)}$
AISI S100 [11]	0.01 P_r	$L/500$	$0.5\left(1+1/\sqrt{n}\right)/j$
CSA S16-19 [21]	0.008 P_r	$L/500$	$0.2+0.8/\sqrt{n}$
GB 50017-2017 [26]	$P_r/60$	-	$0.6+0.4/n$

P_r is the required column strength as stipulated in the corresponding standard. It is specified in GB50017-2017 that the number of columns should not exceed eight, $n \leq 8$. The variations of η with number of columns in different standards are presented in Fig. 4.13, indicating noteworthy discrepancies of η among different standards, in which EN 1993-1-1 is the most conservative, followed by AISI S100 [11], GB 50017-2017 [26], CSA S16-19 [21], and AISC 360-16 [10]. Replacing Δ_0 by $\Delta_{0,\text{mul}}$ enables Eq. (4.39) to account for the effect of column initial imperfection randomness on the maximum brace force of the parallel column system. Alternatively, the effect of the column initial imperfection randomness on the brace forces in parallel columns can be investigated by conducting stochastic analysis using the formulae proposed in Section 4.5, which is not within the scope of this study, though.

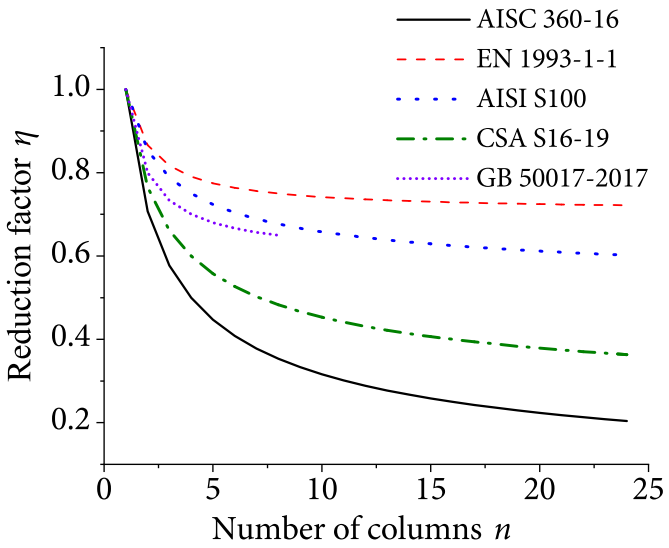

Figure 4.13: Comparison of the reduction factor of initial imperfection specified in different standards

4.7 Computational Procedure

The computational procedure of determining the ideal brace stiffness and brace forces in parallel semi-rigidly connected columns is summarized as follows.

1. Adopt the half-length column model in Fig. 4.6 to mimic the system as two equivalent frames. Calculate the elastic critical buckling load $P_{cr,i}$ of each half-length column in the equivalent frame using Eq. (3.12). If the inelastic stiffness reduction needs to be considered, check if the column is subjected to inelastic buckling using Eq. (2.26).

2. With obtained $P_{cr,i}$, the lateral stiffness $S_{c,i}$ of each half-length column can be calculated using Eq. (3.10). Note that the reduced modulus E_t in Eq. (2.26a) needs to be incorporated to replace E in Eq. (3.10) if the column behaves inelastically.

3. Calculate the ideal brace stiffness for the equivalent frame $S_{b,\text{id}}$ by solving Eq. (4.20) to find the maximum root. If the columns have the same lateral stiffness, Eq. (4.34) can alternatively be used to calculate the value of the scale factor $a_{\max}$ and subsequently attain the value of $S_{b,\text{id}}$ using Eq. (4.33).

4. Use Eq. (3.11a) to compute the value of curvature coefficient ψ_i.

5. Determine the value of bracing stiffness ratio α_b, and let $S_{b,i}$ equal $\alpha_b S_{b,\text{id}}$. With the obtained $P_{cr,i}$, ψ_i, $S_{c,i}$, and $S_{b,i}$, use Eq. (4.22) or Eq. (4.24) to calculate the brace forces in the equivalent unbraced frame. Note that the obtained brace forces need to be doubled for the whole system. For systems with uniform column lateral stiffness, Eq. (4.35) can be alternatively adopted to calculate the maximum brace force Q_n; and if $\alpha_b = 2$ and $P = P_{cr}$, Eq. (4.39) can be used to compute Q_n for convenience.

4.8 Examples of Multi-column Systems

4.8.1 Example 1: System with uniform column lateral stiffness

Effect of the end-fixity factor on brace force

The system consisting of five semi-rigidly connected columns rigidly anchored by one side with compression-tension braces shown in Fig. 4.14 was selected to investigate the influence of semi-rigid connections on brace forces and verify the validity of the formulae proposed in Section 4.6. The centre spacing of the columns is assumed to be 2400 mm, and each column has a length of 6000 mm. All columns were made of A992 steel (f_y = 345 MPa; E = 200 000 MPa). W360 × 60 (W12 × 40) was adopted as the column section with an in-plane moment of inertia $I = 1.83 \times 10^6$ mm^4 and cross-sectional area $A_c = 3060$ mm^2. The magnitude of the initial imperfection Δ_0 of all columns was taken as a thousandth full-length of the column ($L_c/1000$). Four different connections at column ends were considered: $r_e = 0$ (pinned), $r_e = 0.3$, $r_e = 0.6$ and $r_e = 1.0$ (fixed). As stipulated in the AISC [10], bracing ratio α_b is taken as 2.0 for all cases.

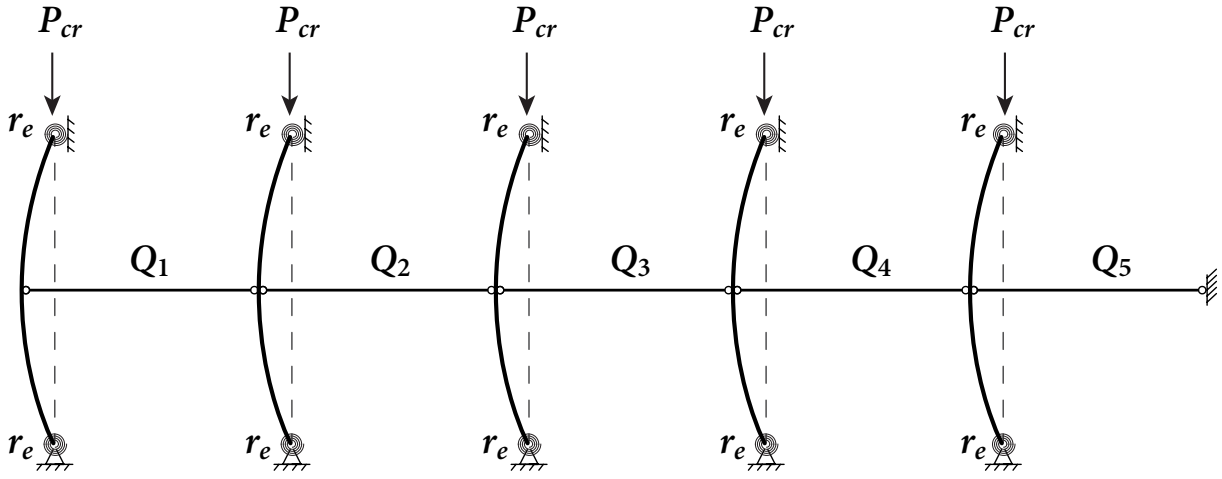

Figure 4.14: A system consisting of five parallel semi-rigidly connected columns anchored on one side

Analytical results

Take the case with $r_e = 0.6$ as an example and follow the computational procedure in Section 4.7 to calculate the brace forces.

1. Calculate the critical buckling load P_{cr} of the half-length column. By Employing the non-linear system solver *fsolve* in MATLAB to solve Eq. (3.12) with $K_0 = 1$ being the initial value, the exact value of effective length factor K is computed as $K = 0.8116$. The corresponding elastic critical buckling load P_{cr} is

$$P_{cr} = \frac{\pi^2 EI}{(KL)^2} = \frac{\pi^2 (200000)\left(1.83 \times 10^6\right)}{(0.8116 \times 3000)^2} = 609.3\,\text{kN}$$

   Since $P_{cr}/P_y > 0.5$, the inelasticity needs to be considered by adopting the stiffness reduction factor τ_b. Because the end-fixity factor is given, τ_b is attained as 0.982 from Eq. (2.27a). With $\tau_b = 0.982$, the inelastic critical buckling load is

$$P_{cr} = \frac{\pi^2 E \tau_b I}{(KL)^2} = 598.5\,\text{kN}$$

   Since it is confirmed that $P_{cr}/P_y > 0.5$, the column behaves inelastically, and the corresponding critical buckling load of the column is 598.5 kN.

2. By substituting $K = 0.8116$, $r_e = 0.6$ and $E = 0.982 \times 200\,000\,\text{MPa}$ into Eq. (3.10), the lateral stiffness of each half-length column is obtained as $S_c = -126.6\,\text{N/mm}$.

3. Since the system possesses uniform column lateral stiffness, Eq. (4.33) and Eq. (4.34) can be used to obtain the ideal brace stiffness: $a_{\max} = 12.34$, and $S_{b,\text{id}} = -12.34 \times (-126.6) = 1562.2\,\text{N/mm}$.

4. Using Eq. (3.11a), the value of the curvature coefficient was obtained as $\psi = 1.1707$.

5. With the obtained P_{cr}, ψ, S_c and $S_{b,\text{id}}$, solving Eq. (4.25) gives the solutions of Q_1 to Q_5 for the half-length column model, which shall be doubled for the whole system.

Following the above procedure, the analytical results for other cases are attained and tabulated in Table 4.2 and Table 4.3, in which Q_i are the brace forces for the whole system.

Table 4.2: Analytical results for a system with five parallel columns

r_e	0	0.3	0.6	1
ψ	1.3333	1.2606	1.1707	1.052
τ_b	1.0	1.0	0.982	0.873
P_{cr} (kN)	401.4	488.3	598.5	716.4
Q_0 (N)	1070.3	1231.0	1401.3	1507.2
S_c (N/mm)	-133.8	-124.7	-126.6	-153.6
$S_{b,\mathrm{id}}$(N/mm)	6605.7	6155.9	6248.7	7581.8

Table 4.3: Comparison of brace forces between analytical and FEM results for a five-column system anchored on one side

Method	r_e	Q_1 (N)	Q_2 (N)	Q_3 (N)	Q_4 (N)	Q_5 (N)
Analytical	0	4778.3	9363.0	13568.5	17224.3	20182.5
FEM	0	4769.6	9343.6	13537.6	17182.6	20132.0
Analytical	0.3	5495.8	10768.9	15605.8	19810.6	23212.9
FEM	0.3	5483.7	10741.8	15562.3	19751.4	23141.0
Analytical	0.6	6256.2	12258.9	17765.1	22551.7	26424.7
FEM	0.6	6242.8	12228.0	17714.5	22481.8	26338.9
Analytical	1	6728.6	13184.7	19106.7	24254.7	28420.3
FEM	1	6721.6	13166.1	19073.7	24206.6	28358.7

The results indicate that the brace force is not linearly accumulated to the anchored end, which confirms the observation by Blum et al. [13]. The analytical results achieve good agreements, with the FEM results for all the cases with the maximum discrepancy being 0.6%. The good agreements demonstrate the validity of the proposed formulae regarding brace forces and the curvature coefficient ψ. It can be seen from Table 4.2 that P_{cr} increases as r_e increases, although the stiffness reduction factor τ_b decreases as r_e increases. However, Q_0 increases slightly from $r_e = 0$ to $r_e = 0.6$ and decreases from $r_e = 0.6$ to $r_e = 1$. This is due to the consideration of the column curvature coefficient ψ, which decreases with the increase of r_e.

Effect of column axial load on the maximum brace force

For the system shown in Fig. 4.14, if all columns are assumed to be pin-connected, $r_e = 0$, the maximum brace forces, Q_n, with different applied loads obtained from the analytical expression in Eq. (4.35), fitting expression in Eq. (4.39), AISC 360-16 [10] and CSA S16-19 [21] are presented in Fig. 4.15. In the comparison, the initial imperfection reductions for multiple columns in Table 4.1 are not considered, i.e., $\eta = 1$.

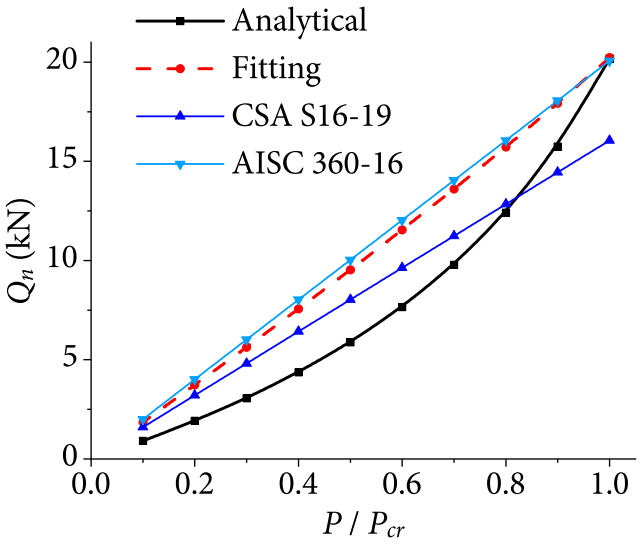

Figure 4.15: Effect of load ratio on the maximum brace force

When $P = P_{cr}$, the predictions obtained from the analytical, fitting, and AISC 360-16 expressions are practically the same, which is different from the observation on a single column, as discussed in Chapter 3. This indicates that the analytical result is noticeably greater than the prediction from AISC 360-16. In the case of a single column, the initial curvature coefficient is 1.333 when $P = P_{cr}$, which consequently leads to a 33.3% increase in the brace force. Such an increase is greater than the 25% increase considered in AISC 360-16 due to the compensation for neglecting the column flexibility and continuity in Winter's model. However, the theoretical value of the maximum brace force for multiple columns is lower than the results obtained from the summation of the brace force of each column, as shown in Fig. 4.11. Consequently, the prediction by AISC 360-16 happens to be close to the analytical result for multiple columns when $P = P_{cr}$. The fitting expression and AISC 360-16 yield similar results. As the applied load decreases, the brace force obtained from the fitting expression in Eq. (4.39) decreases faster than that obtained from AISC 360-16 because

Q_0 in Eq. (4.39) accounts for the effect of the column initial curvature, which decreases as the applied load decreases. Theoretically, the fitting expression and specification in AISC 360-16 [10] are applicable to cases with $P = P_{cr}$. For cases in which $P < P_{cr}$, the brace forces obtained from the fitting expression and AISC 360-16 are conservative compared to the analytical results due to neglecting the contribution of column lateral stiffness. Different from AISC 360-16, CSA S16-19 does not increase the results obtained from Winter's model, and thus the brace force predicted from CSA S16-19 can be unconservative when $P/P_{cr} > 0.8$.

Effect of the bending direction of columns' initial imperfections on brace forces

The above two cases of this example are based on the worst scenarios in that all the columns' initial imperfections bend toward the same direction, which neglects the randomness of column initial imperfections in reality. Basically, the randomness of column initial imperfections is associated with three parts: the shape, magnitude, and bending direction of the initial imperfection. In this subsection, the effect of the bending direction of columns' initial imperfections on the brace forces in multi-column systems are preliminarily investigated. All the columns are subjected to the critical buckling load with the fixed ends, $r_e = 1$. It is assumed that the initial imperfection magnitudes of all the columns are the same ($\Delta_{0,i} = L_c/1000$), whereas the initial imperfections of two columns have a different direction from others, as shown in Fig. 4.16.

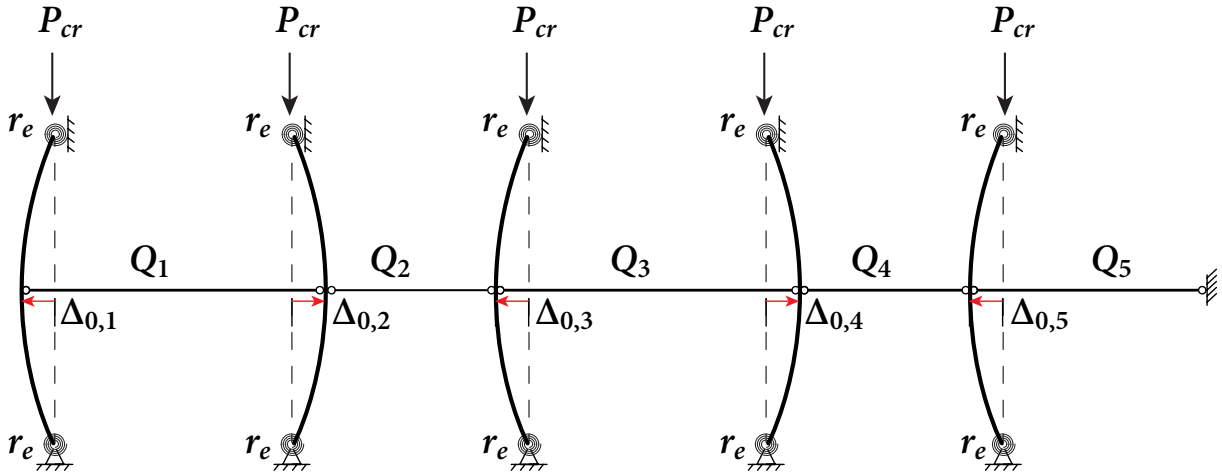

Figure 4.16: Columns arrangement associated with the pattern of $\{1,-1,1,-1,1\}$

The multiplier "1" is used to indicate the direction of the column initial imperfection bend towards the left in this case, so that the corresponding equivalent lateral force towards

the left, which will yield the tensile force in the brace adjacent to the anchor and vice versa. By doing so, the arrangement of the columns presented in Fig. 4.16 exemplifies the pattern of $\{1,-1,1,-1,1\}$.

By varying the locations of the two columns with the initial imperfection towards the right ("-1"), the results of the brace forces in the system are obtained, as tabulated in Table 4.4.

Table 4.4: Effects of the directions of columns' initial imperfections on the brace forces

No.	Pattern	$\Delta_{0,1}$ dir.	Q_1 (N)	$\Delta_{0,2}$ dir.	Q_2 (N)	$\Delta_{0,3}$ dir.	Q_3 (N)	$\Delta_{0,4}$ dir.	Q_4 (N)	$\Delta_{0,5}$ dir.	Q_5 (N)
1	$\{1,1,1,-1,-1\}$	$\leftarrow$	5115.4	$\leftarrow$	10023.5	$\leftarrow$	<u>14525.7</u>	$\rightarrow$	12410.7	$\rightarrow$	9793.1
2	$\{1,1,-1,1,-1\}$	$\leftarrow$	4635.6	$\leftarrow$	9083.4	$\rightarrow$	7134.6	$\leftarrow$	<u>10925.5</u>	$\rightarrow$	8245.2
3	$\{1,-1,1,1,-1\}$	$\leftarrow$	4218.5	$\rightarrow$	2237.5	$\leftarrow$	6194.6	$\leftarrow$	<u>9900.7</u>	$\rightarrow$	7177.0
4	$\{-1,1,1,1,-1\}$	$\rightarrow$	-2147.6	$\leftarrow$	1820.5	$\leftarrow$	5714.8	$\leftarrow$	<u>9377.6</u>	$\rightarrow$	6631.9
5	$\{1,1,-1,-1,1\}$	$\leftarrow$	4112.6	$\leftarrow$	<u>8058.5</u>	$\rightarrow$	5649.4	$\rightarrow$	3011.5	$\leftarrow$	6280.2
6	$\{1,-1,1,-1,1\}$	$\leftarrow$	3695.5	$\rightarrow$	1212.7	$\leftarrow$	4709.3	$\rightarrow$	1986.6	$\leftarrow$	<u>5212.1</u>
7	$\{-1,1,1,-1,1\}$	$\rightarrow$	-2670.6	$\leftarrow$	795.6	$\leftarrow$	4229.6	$\rightarrow$	1463.6	$\leftarrow$	<u>4667.0</u>
8	$\{1,-1,-1,1,1\}$	$\leftarrow$	3215.7	$\rightarrow$	272.6	$\rightarrow$	-2681.7	$\leftarrow$	501.4	$\leftarrow$	<u>3664.2</u>
9	$\{-1,1,-1,1,1\}$	$\rightarrow$	-3150.4	$\leftarrow$	-144.5	$\rightarrow$	<u>-3161.4</u>	$\leftarrow$	-21.6	$\leftarrow$	3119.0
10	$\{-1,-1,1,1,1\}$	$\rightarrow$	-3567.5	$\rightarrow$	<u>-6990.4</u>	$\leftarrow$	-4101.5	$\leftarrow$	-1046.5	$\leftarrow$	2050.9

In Table 4.4, the underlined values represent the maximum brace force in the relative pattern. It can be seen that the maximum tensile brace force decreases as the two columns of which the initial imperfections toward the right, namely Δ_0 direction being $\rightarrow$, become farther away from the anchor. This is because if a column with Δ_0 towards the right becomes farther away from the anchor, the corresponding applied axial load and initial imperfection will reduce the lateral displacement of the columns ($\leftarrow$) between this column and the anchor, and thus the applied axial loads on the in-between columns will induce smaller brace forces.

The results demonstrate that considering the different directions of columns' initial imperfections will decrease the maximum brace force in multi-column systems, as expected. More importantly, the results provide specific practical guidance to engineers if the columns

can be arranged on purpose to ensure that their initial imperfections toward different directions, which is easier to implement for cold-form steel channel columns. For instance, given that the braces are designed as capable of resisting both compressive and tensile forces in this example, pattern No. 9 is the optimum pattern because the maximum brace force of pattern No. 9 is less than those of other patterns. Accordingly, if the columns can be arranged according to pattern No. 9, it will reduce the maximum brace force by 88.9% from 28 420.3 N associated with the worst pattern (Table 4.3) to 3161.4 N.

In this example, if the braces in the system are to be designed as tension-only, pattern No. 6, in which the columns with different directions of initial imperfections are arranged alternately, can be seen as the optimum pattern because the maximum brace force of pattern No. 6 is the smallest among the patterns with brace forces in tension. Additionally, the arrangement of pattern No. 6 is symmetrical about the centre of the system, which applies to systems anchored on both sides.

4.8.2 Example 2: System with nonuniform column lateral stiffness

The influence of nonuniform column lateral stiffness on brace forces is investigated in this section. In practice, nonuniform column lateral stiffness may exist in a system due to differences in column sizes, end connections, or applied loads. In such cases, the stiffness interaction is likely different from the system with the uniform column lateral stiffness discussed previously. In the nonuniform column stiffness case, the ideal brace stiffness needs to be determined by Eq. (4.18), and the brace forces can be obtained by either Eq. (4.21) or Eq. (4.23).

This example investigates the bracing requirements for a rigidly anchored system which consists of nine parallel cold-formed steel columns representing the studs in a load-bearing wall, as shown in Fig. 4.17.

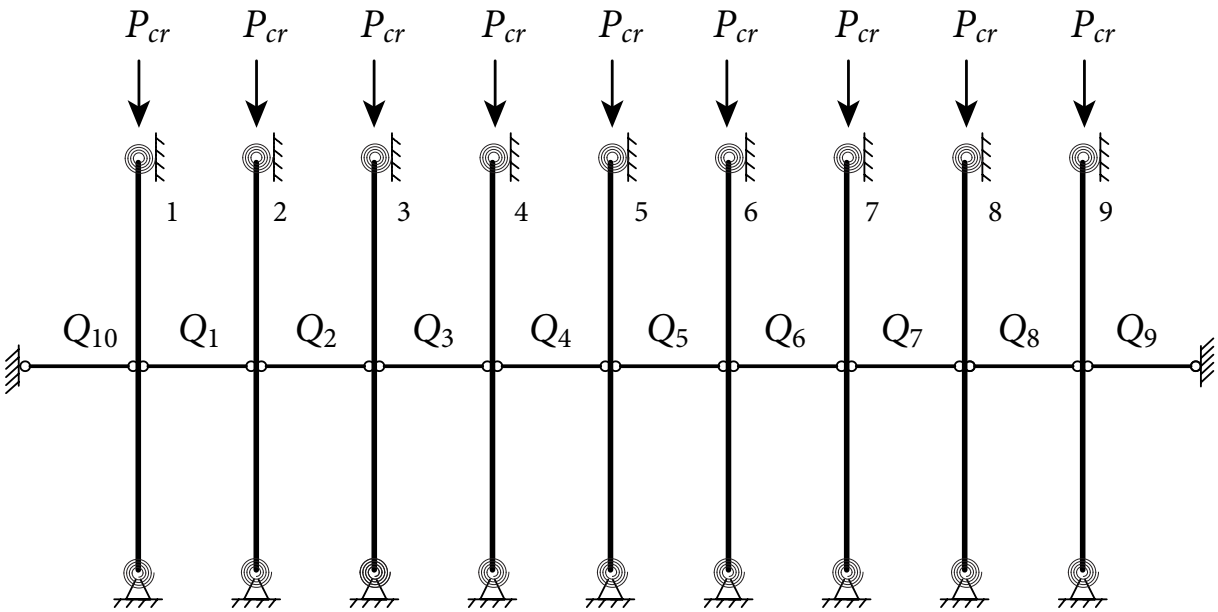

Figure 4.17: Diagram of a cold-formed load-bearing wall anchored on both sides

The column spacing and the height are 610 mm and 2400 mm, respectively. Only in-plane buckling is considered in this example. The 250S137-54 studs are adopted as the typical column section with a moment of inertia $I = 33\,299\,\text{mm}^4$ and cross-sectional area $A_c = 204\,\text{mm}^2$. The elastic modulus E and yield strength f_y of cold-formed steel are taken as 203 000 MPa and 345 MPa, respectively. The bracing stiffness ratio α_b is taken as 2.0 as per AISI S100-16 [11]. It is assumed that there is a distinctive column made of back-to-back 250S137-54 sections with $I_{c,v} = 120\,681\,\text{mm}^4$. All the columns have the same end-fixity factor, $r_e = 0.3$. Note that all the columns are subjected to their own critical buckling loads. Since the inelastic stiffness reduction factor τ_b has yet to be introduced in AISI S100-16 [11], the possible influence of inelastic behaviour on the stud lateral stiffness is not considered in this example. As described in Appendix A, finite element analyses were carried out to verify the results obtained from the proposed analytical method. Good agreements were achieved with a maximum discrepancy of 0.6% between the FEM and analytical results. Only analytical results are presented in this section for brevity.

Anchored on one side

Following the procedure presented in Section 4.7, the parameter values of the typical and distinctive columns are tabulated in Table 4.5.

Table 4.5: Calculation results regarding the ideal brace stiffness

	R (1×10^6 N/mm)	r_e	P_{cr} (kN)	S_c (N/mm)	ψ	Q_0 (N)
Typical column	7.24	0.3	56.36	-36.0	1.2606	142.1
Distinctive column	26.25	0.3	204.26	-130.4	1.2606	515.0

If all the braces shown in Fig. 4.17 are to be designed as tension-only, only one anchor needs to be considered. Assume that the initial imperfection Δ_0 causes the columns in the system to bend towards the left, then the brace connecting to the left anchor will fail in compression, and thus the left anchor and the adjacent brace should be removed in the analytical modelling. In that case, the analytical results of ideal brace stiffness and brace forces for different cases are tabulated in Table 4.6. The acronym "LDC" stands for the location of the distinctive column, which counts from left to right, and "None" means that there is no distinctive column in the system. If there is no distinctive column in the system, the ideal brace stiffness is $S_{b,\text{idt}} = 2638.1\,\text{N/mm}$. However, $S_{b,\text{idt}}$ equals $3465.9\,\text{N/mm}$ if the distinctive column is located in the middle (5th) of the system. This is because the lateral stiffness of the distinctive column is less than that of the typical columns when the columns are subjected to their critical buckling loads P_{cr} (Table 4.5), which is more detrimental to the stability of the system and requires larger brace stiffness, even though the distinctive column possesses a larger moment of inertia than the typical columns.

It is worth noting that the ideal brace stiffness increases as the LDC becomes farther away from the available anchor. Except for the brace adjacent to the rigid anchor (named exterior brace), the interior braces are in series with the adjacent column [1]. Therefore, if the distinctive column becomes farther away from the anchor, as the number of braces between the column and the anchor increases, the corresponding lateral stiffness provided by those braces decreases. Consequently, when the column becomes farther away from the anchor, it requires greater brace stiffness to maintain the system stability. In other words, the farther the column is from the anchor, the more impact it has on the stability of the system.

By comparing the systems with and without the distinctive column, perceptible brace force increments are found in the braces to the right of the distinctive column. However, the

forces in the braces to the left of the distinctive columns change slightly due to the removal of the left anchor in the analysis model to mimic the tension-only brace assumption.

Table 4.6: Analytical results of the ideal brace stiffness and brace forces for the system anchored on one side

LDC	$S_{b,\text{idt}}$ (N/mm)	Q_1 (N)	Q_2 (N)	Q_3 (N)	Q_4 (N)	Q_5 (N)	Q_6 (N)	Q_7 (N)	Q_8 (N)	Q_9 (N)
None	2638.1	638.2	1267.6	1879.8	2466.3	3019.2	3530.9	3994.4	4403.5	4752.5
1st	4183.8	2257.5	2860.9	3439.8	3989.1	4504.1	4980.3	5413.8	5800.6	6137.6
2nd	4059.7	619.5	2844.7	3433.4	3991.8	4514.8	4997.7	5436.4	5826.9	6165.7
3rd	3893.3	619.9	1234.0	3418.4	3989.6	4523.8	5016.3	5462.4	5858.0	6199.5
4th	3692.1	623.9	1241.7	1847.4	3977.4	4526.3	5031.2	5487.0	5889.3	6234.3
5th	3465.9	631.4	1256.2	1867.9	2460.3	4514.6	5034.6	5502.3	5912.9	6262.1
6th	3228.7	641.6	1276.0	1896.2	2495.3	3066.6	5013.0	5494.2	5914.2	6268.3
7th	2999.0	652.4	1297.0	1926.0	2532.0	3107.5	3645.8	5438.0	5867.3	6226.2
8th	2806.2	659.2	1309.9	1943.8	2552.8	3129.1	3665.2	4154.4	5734.1	6096.4
9th	2680.0	655.4	1301.9	1931.0	2534.2	3103.3	3630.8	4109.5	4533.1	5847.6

For all cases, the right-most brace has the maximum brace force Q_9. The variations of the required brace area and maximum brace force Q_9 with the LDC are presented in Fig. 4.18. It can be seen that Q_9 varies with the LDC and achieves the maximum value when the 6th column is distinctive.

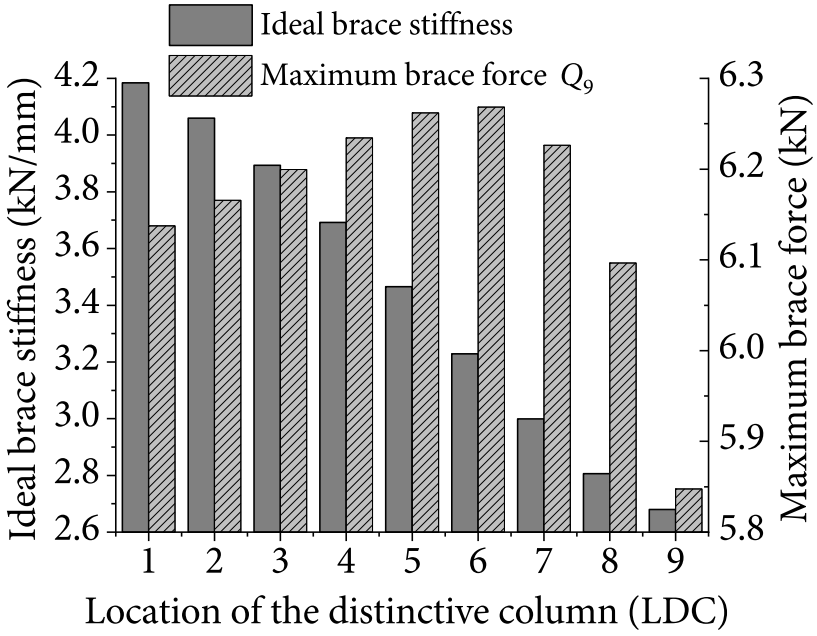

Figure 4.18: Influence of the distinctive column's location on the ideal brace stiffness and maximum brace force for the system anchored on one side

Intuitively, the brace force increases as the brace stiffness decreases. However, as the location of the distinctive column changes, the variation of the brace stiffness cannot reflect how the stiffness of the system to support the column varies. The effective lateral stiffness of the column, S_{ef}, the ratio of the lateral load applied on the column to the induced lateral displacement of the column, is introduced to describe the total stiffness of the system regarding the column. Eq. (4.18) can be used to attain the effective lateral stiffness, S_{ef}. For example, if the effective lateral stiffness of the first column is to be determined, with the equivalent lateral force applied on the column $Q_{0,1}$ set to be unit and other equivalent lateral forces zero, the displacement of the first column Δ_1 can be obtained by solving Eq. (4.18) with known $S_{b,i}$ and $S_{c,i}$. For the whole system, the effective lateral stiffness of the first column $S_{\text{ef},1}$ is $2/\Delta_1$. The effective lateral stiffnesses of columns when the distinctive column is located at different places are represented in Table 4.7. The underlined values in Table 4.7 represent the effective lateral stiffnesses of the distinctive column for different cases. On the one hand, although the brace stiffness decreases as the distinctive column becomes closer to the anchor, the effective lateral stiffness of the distinctive column increases, which has a favourable effect on the maximum brace force. On the other hand, the effective lateral stiffnesses of the typical columns decrease as the brace stiffness decreases (except for that

Table 4.7: Effective lateral stiffnesses of columns in the system anchored on one side

LDC	$S_{ef,1}$ (N/mm)	$S_{ef,2}$ (N/mm)	$S_{ef,3}$ (N/mm)	$S_{ef,4}$ (N/mm)	$S_{ef,5}$ (N/mm)	$S_{ef,6}$ (N/mm)	$S_{ef,7}$ (N/mm)	$S_{ef,8}$ (N/mm)	$S_{ef,9}$ (N/mm)
None	315.5	345.2	391.3	462.1	573.2	758.2	1098.1	1845.3	4296.3
1st	477.1	540.1	629.3	759.1	956.1	1275.6	1850.0	3086.7	7056.9
2nd	477.4	516.6	601.7	725.8	914.6	1221.4	1774.4	2967.8	6810.0
3rd	468.7	508.4	565.4	682.0	859.9	1149.8	1674.1	2809.7	6480.2
4th	451.8	491.1	548.1	630.4	795.3	1065.0	1554.8	2620.7	6083.7
5th	427.8	465.8	521.7	603.3	724.9	972.2	1423.7	2411.5	5641.4
6th	398.6	434.8	488.6	568.2	688.4	878.4	1290.1	2196.8	5182.4
7th	367.7	401.6	452.8	529.4	646.9	836.0	1167.6	1997.4	4749.6
8th	340.1	371.8	420.4	494.0	608.3	795.5	1131.4	1841.4	4401.7
9th	321.6	351.9	398.6	470.0	582.0	767.4	1106.2	1843.0	4199.9

$S_{ef,1}$ increases a little when the LDC changes from the 1st to the 2nd), which is unfavourable to the maximum brace force. Therefore, the variation of the maximum brace force with the LDC does not exhibit obvious regularity.

It is not considered in the foregoing study that the initial imperfection Δ_0 will induce the system to bend towards the right side of the system. However, the results for such a case can be obtained based on the mirror relation with those presented in this example. For instance, if the 9th column is distinctive and the system bends towards the right side due to the presence of Δ_0, the corresponding ideal brace stiffness and brace forces are the same as the results associated with LDC being the 1st column in Table 4.6. In this way, the ideal brace stiffness obtained with assuming that the system bends toward the right side governs because the ideal brace stiffness is larger than that with assuming the system bends towards the left side.

Anchored by both sides

If the system is designed as anchored on both sides with braces capable of resisting compressive forces, the analytical results of the brace forces for different cases are tabulated in

Table 4.8. Since the system is symmetric, it suffices to consider the LDC to be at the 5th to 9th. Comparing the results between the systems without and with the distinctive column in the system indicates that the farther the brace is away from the distinctive column, the less the brace force increases, similar to that in the cases the system is anchored on one side.

The variations of maximum brace force Q_9 and ideal brace stiffness $S_{b,\text{idt}}$ with the LDC are presented in Fig. 4.19. It can be seen that the ideal brace stiffness decreases as the LDC becomes farther away from the middle of the system. This indicates that for a system anchored on both sides, the closer the column is to the middle, the more impact it has on the stability of the system. The maximum brace force increases as the LDC changes from the middle (5th) to 8th but decreases as the LDC moves from 8th to 9th. The results for systems anchored by one side and by both sides indicate that the LDC significantly influences both ideal brace stiffness and brace forces for the system, even though the summations of gravity loads of the system for all cases are the same.

Table 4.8: Analytical results of ideal brace stiffness and brace forces for the system anchored on both sides

LDC	$S_{b,\text{idt}}$ (N/mm)	Q_{10} (N)	Q_1 (N)	Q_2 (N)	Q_3 (N)	Q_4 (N)	Q_5 (N)	Q_6 (N)	Q_7 (N)	Q_8 (N)	Q_9 (N)
None	735.1	-2419.5	-2016.9	-1515.6	-940.1	-318.6	318.6	940.1	1515.6	2016.9	2419.5
5	1154.0	-3108.1	-2727.0	-2260.9	-1724.3	-1133.9	1133.9	1724.3	2260.9	2727.0	3108.1
6	1123.6	-2931.8	-2553.8	-2093.9	-1567.0	-989.9	-381.1	1869.4	2430.5	2913.8	3303.8
7	1035.8	-2786.6	-2405.6	-1941.1	-1409.1	-828.2	-218.5	398.8	2585.7	3099.3	3505.2
8	905.7	-2684.5	-2293.6	-1811.7	-1257.8	-653.9	-24.0	606.8	1213.5	3237.6	3667.5
9	780.8	-2595.6	-2191.8	-1687.0	-1104.5	-471.0	184.1	830.7	1439.1	1981.2	3614.8

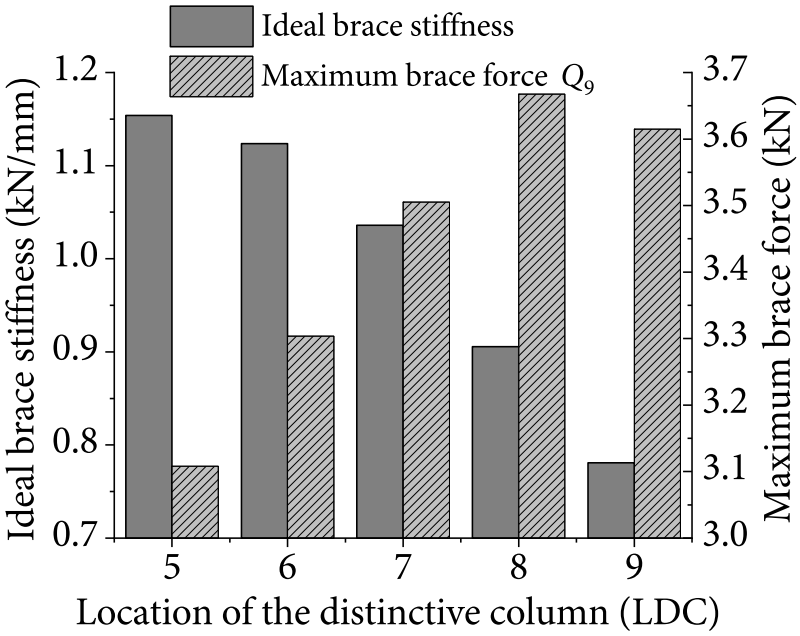

Figure 4.19: Influence of the distinctive column's location on the ideal brace stiffness and maximum brace force for the system anchored on both sides

As shown in Table 4.9, the effective lateral stiffness of the distinctive column increases, but the effective lateral stiffness of typical columns decreases as the distinctive column becomes farther away from the middle of the system. Similar to the system anchored by one side, the variation of the maximum brace force with the LDC has no obvious pattern for the system anchored by both sides.

Table 4.9: Effective lateral stiffnesses of columns in the system anchored on both sides

LDC	$S_{ef,1}$ N/mm	$S_{ef,2}$ N/mm	$S_{ef,3}$ N/mm	$S_{ef,4}$ N/mm	$S_{ef,5}$ N/mm	$S_{ef,6}$ N/mm	$S_{ef,7}$ N/mm	$S_{ef,8}$ N/mm	$S_{ef,9}$ N/mm
None	1288.2	614.3	418.4	342.9	322.2	342.9	418.4	614.3	1288.2
5th	2116.3	1021.9	687.0	542.2	476.8	542.2	687.0	1021.9	2116.3
6th	2086.8	1020.2	694.7	556.1	497.2	487.4	627.6	950.2	2008.6
7th	1923.0	943.6	647.3	523.9	476.0	477.3	528.4	817.3	1778.1
8th	1655.0	806.7	553.6	451.4	416.3	427.9	492.5	653.1	1470.4
9th	1387.1	666.1	454.8	372.2	347.8	366.2	438.6	623.4	1209.5

4.9 Discussion on the maximum brace force with nonuniform column lateral stiffness

The analytical results of the example with nonuniform column lateral stiffness indicate that the maximum brace force is influenced by the location of the distinctive column, i.e., different nonuniform lateral stiffness cases. This section discusses what if the effect of nonuniform column lateral stiffness is ignored in the design of braces.

In Section 4.6.2, an empirical formula in Eq. (4.39) is proposed to evaluate the maximum brace force of systems with uniform column lateral stiffness when the bracing stiffness ratio equals two. Eq. (4.39) can be reformulated as

$$Q_n = \left(\frac{0.6}{n} + 3.66\right) \sum Q_0 / j = \left(\frac{0.6}{n} + 3.66\right) \frac{\Delta_0 \psi}{L} \sum P_{cr} / j \quad n \geq 2 \tag{4.41}$$

That is to say, the maximum brace force Q_n in Eq. (4.39) is actually obtained by scaling the summation of critical buckling loads of columns, and such a hypothesis can also be found in current standards [10, 11, 21, 24]. If Eq. (4.41) is to be extended to calculate the maximum brace force of systems with nonuniform column lateral stiffness, it can be adapted as:

$$Q_n = \left(\frac{0.6}{n} + 3.66\right) \sum Q_{0,i} / j = \left(\frac{0.6}{n} + 3.66\right) \sum \frac{\Delta_{0,i} P_{cr,i} \psi_i}{L} / j \tag{4.42}$$

Eq. (4.42) implies that all the column axial loads contribute equally to the maximum brace force Q_n regardless of the magnitude and location of the loading.

Eq. (4.42) is used to compute the maximum brace force of the system in Example 2. If the tension-only braces are adopted so that the system shall be designed being anchored by one side, the maximum brace force obtained from Eq. (4.42) equals 6155.6 N, which is lower than the analytical results of the cases in each of which the 2nd to 7th column is distinctive, as tabulated in Table 4.6. If the system can be designed as anchored on both sides, the maximum brace force is 3077.8 N from (4.42), which is less than all the analytical results in Table 4.8. Therefore, the brace force can be underestimated by scaling the summation of applied column loads without considering the location of the distinctive column. For that reason, it is recommended to employ the proposed analytical method to assess the maximum brace force of systems with nonuniform column lateral stiffness.

4.10 Conclusions

By adopting the proposed half-length column model and formulating the stiffness interaction among columns and braces, analytical methods are proposed to assess the ideal brace stiffness and brace forces of a system consisting of parallel semi-rigidly connected columns. The proposed methods are comprehensively applicable to systems with different column sizes, end-fixity factors and applied loads. The methods perform well in all the presented examples and achieve good agreements with the finite element analysis results. The conclusions obtained from this chapter are summarized as follows:

1. Provided the system is composed of the same columns with the same connections, the method proposed by Ziemian and Ziemian [5] for determining the ideal brace stiffness of multi-column systems with pin ends can be extended to account for the effect of semi-rigid connections by incorporating the applicable equations developed in this chapter. For such cases, r_e = 0.392 can be taken as the optimum value for semi-rigid connections in elastic analysis, as it corresponds to the minimum ideal brace stiffness and provides a higher critical buckling compared to the columns with pin connections.

2. It is found that the influence of the difference of column lateral stiffness resulting from different column sizes, end-fixity factors or applied loads should be considered in the evaluation of the ideal brace stiffness for systems with nonidentical columns; in other words, the ideal brace stiffness obtained from a system with multiple identical columns is not applicable to a system with multiple nonidentical columns.

3. For systems with uniform column lateral stiffness, the analytical results indicate that assuming the brace forces as linearly accumulated leads to conservative results. The explicit solution for the maximum brace force for such systems is derived. According to the analytical results, a simple-to-use formula is proposed to evaluate the maximum brace force. The formula explicitly considers the effects of semi-rigid connections and initial imperfections on the maximum brace force and can incorporate the column initial imperfection randomness.

4. If the column retention lateral stiffness is considered, the brace force predicted by AISC

360-16 [10] is conservative when the applied load is lower than the theoretical critical buckling load. However, the prediction from CSA S16-19 [21] may be unconservative in some cases due to neglecting the effect of column initial curvature on brace force.

5. It was found that the maximum brace force in multi-column systems can be significantly reduced if the columns' initial imperfections can be arranged to bend toward different directions.

6. The presented examples investigate the effect of nonuniform column lateral stiffness on the bracing requirements for multi-column systems by introducing a distinctive column with a greater moment of inertia. The results indicate that the location of the distinctive column will affect the magnitudes of the ideal brace stiffness and brace forces. Therefore, it is recommended to employ the proposed analytical method to assess the bracing requirements for the system with nonuniform column lateral stiffness; otherwise, it may yield inaccurate results.

Chapter 5

Optimum Brace Stiffness

5.1 Introduction

Conventionally, the American standards, AISC 360-16 [10] and AISI S100-16 [11], adopt the bracing stiffness scale factor being 2.0 as the brace stiffness requirement, i.e., twice the ideal brace stiffness ($S_b = 2S_{b,\text{idt}}$), which has been incorporated in the previous numerical examples. Based on Winter's model, Blum et al. [13] indicated that for some cases where providing $2S_{b,\text{idt}}$ is practically infeasible, a lower bracing stiffness scale factor of 1.33 also could reduce the brace force from infinity to an acceptable value. However, since the column initial curvature is not considered in Winter's model to assess the brace forces, as presented in Chapter 3, the value 1.33 suggested by Blum et al. [13] may lead to a relatively high brace strength requirement. In that case, if the cross-sectional area of the brace is governed by the strength requirement, then adopting $S_b = 1.33S_{b,\text{idt}}$ finally leads to a greater stiffness scale factor, α_b. Nevertheless, the recommendation made by Blum et al. is still worth noting that an alternative value for α_b could be considered in practice.

Alternatively, the Canadian standard CSA S16-19 [21] specifies that the actual lateral displacement of multiple columns, including the displacement induced by the applied load, connection deformation, and the displacement due to the installation misalignment, etc., shall not exceed the initial imperfection of the column. The specifications in American and Canadian standards represent two different design philosophies regarding the brace stiffness requirement. The stiffness requirement in AISC 360-16 and AISI S100-16 ($S_b = 2S_{b,\text{idt}}$) is derived from the criterion that the displacement induced by the applied load equals the

initial imperfection of the column, $\Delta = \Delta_0$. However, this derivation not only neglects the adverse effect of column initial curvature, as discussed in Chapter 3; more importantly, since it is derived from a single column, whether it still applies to multiple columns is yet to be answered. Although the Canadian standard CSA S16-19 [21] explicitly stipulates the displacement limit, it does not provide a specific technique to evaluate the lateral displacement of multi-column systems induced by the applied axial loads.

A concept of optimum brace stiffness is introduced in this section to represent the minimum required brace stiffness that can satisfy both strength and stiffness requirements. The equations for evaluating the optimum brace stiffness of a single column and multiple columns are proposed with considering the effects of column initial curvature and nonuniform column lateral stiffness. By employing the proposed equations, the optimum brace stiffness for a single column and multiple columns following the design philosophies of AISC 360-16 [10] and CSA S16-19 [21] are compared.

Following AISC 360-16 [10], the brace stiffness S_b can be predetermined as twice the ideal brace stiffness $2S_{b,\text{idt}}$ to calculate the corresponding brace force Q_b induced by the axial load applied on the column. Next, the required brace stiffness is determined to satisfy the stiffness requirement, $S_b \geq 2S_{b,\text{idt}}$, and the strength requirement, $P_r \geq Q_b$. Assuming no buckling issues exist for the braces, the brace strength P_r is the yield strength, $A_b f_y$. Thus, the required brace stiffness per AISC 360-16 [10] is

$$S_{b,\text{AISC}} = \max \begin{cases} 2S_{b,\text{idt}} & \text{Stiffness requirement} \\ Q_b L_b / \left(f_y E_b\right) & \text{Strength requirement} \end{cases} \tag{5.1}$$

5.2 Design Philosophies in Current Standards

Fig. 5.1 illustrates the variations of the strength requirement with the selected brace stiffness scale factor, $\alpha_{b,\text{pre}}$. The case with $\alpha_{b,\text{pre}} = 1$ signifies that the brace stiffness is taken as the ideal brace stiffness. As $\alpha_{b,\text{pre}} = 1$ increases, the stiffness requirement increases, while the strength requirement decreases. Presupposing a brace stiffness scale factor such as $\alpha_{b,\text{pre}} = 2.0$ as per AISC 360-16 [10] could be either of the two cases shown in Fig. 5.1 and Fig. 5.2, wherein the shaded regions are the feasible domains for the brace stiffness scale factor.

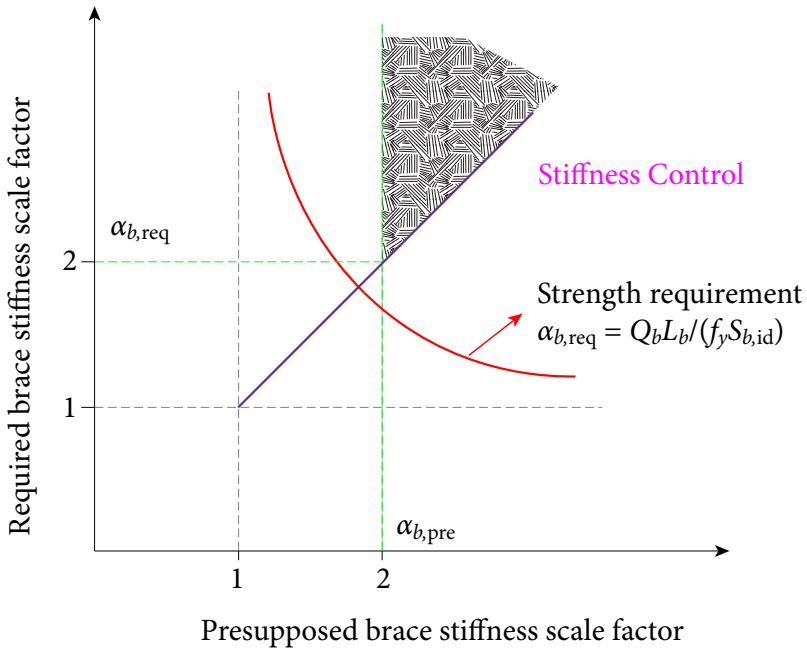

Figure 5.1: Required brace stiffness scale factor in stiffness-control cases

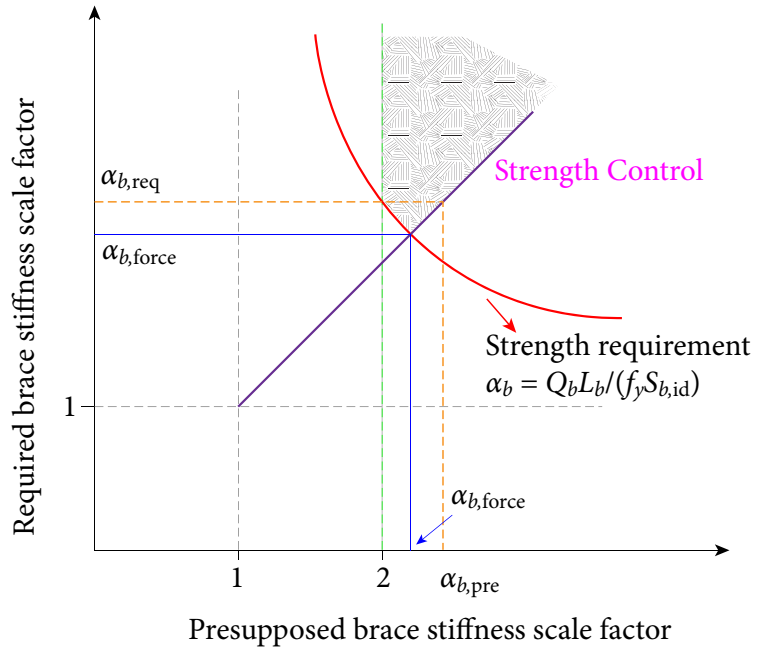

Figure 5.2: Required brace stiffness scale factor in strength-control cases

For the "stiffness control" case, as the design is governed by the stiffness requirement, the presupposed stiffness scale factor $\alpha_{b,\text{pre}}$ can be directly used to compute the corresponding required cross-sectional area of bracing $A_{b,\text{pre}}$. For the "strength control" case presented in Fig. 5.1, as the design is governed by the strength requirement, the required

cross-sectional area of bracing shall be computed according to the brace force; however, this area corresponds to a higher value of α_b than the presupposed value $\alpha_{b,\text{pre}}$, i.e., greater brace stiffness, which consequently reduce the brace force. That is to say, adopting such a design philosophy yields overestimated results for the "strength control" case — decreasing α_b to some extent can still satisfy the brace strength and stiffness requirements.

Different from the specifications in AISC 360-16 [10] and AISI S100-16 [11], CSA S16-19 [21] requires that the additional lateral displacement of the multi-column system shall not exceed the column initial imperfection. The design philosophy of the direct method in CSA S16-19 is as follows. First, calculate the brace force induced by the applied load by assuming $\Delta = \Delta_0$. Second, determine the cross-sectional area of bracing A_b according to the attained brace force. Third, check the stiffness requirement if the additional lateral displacement exceeds the column initial imperfection with the determined A_b. If the stiffness requirement is not satisfied, choose a larger A_b and repeat the foregoing steps. However, there are some issues with this procedure: 1) the iteration due to the selected A_b not satisfying the stiffness requirement can be tedious and may yield a quite conservative design; 2) the equation for assessing the brace force in CSA S16-19 does not consider the column initial curvature; 3) the method regarding the lateral displacement for multiple columns is not available in CSA S16-19. Hence, to address the aforementioned issues, the value of the brace stiffness scale factor that can equate the additional lateral displacement induced by the applied load to the column initial imperfection is investigated in this section.

5.3 Optimum Brace Stiffness for a Single Semi-rigidly Connected column

5.3.1 Brace stiffness scale factor satisfying the strength requirement

The brace stiffness scale factor, $\alpha_{b,\text{force}}$, is proposed to represent the minimum value of α_b that satisfies the strength requirement. With $\alpha_{b,\text{force}}$, the yield strength of the brace is the same as the brace force, as illustrated in Fig. 5.2 and expressed in Eq. (5.2).

$$\frac{Q_b}{f_y} = \frac{S_b L_b}{E_b} \tag{5.2}$$

For a single half-length column, Eq. (5.3) can be obtained by incorporating Eq. (3.19) into Eq. (5.2).

$$\frac{\alpha_{b,\text{force}} S_{b,\text{id}}}{\alpha_{b,\text{force}} S_{b,\text{id}} + S_c} \frac{\psi P \Delta_0}{f_y L} = \frac{\alpha_{b,\text{force}} S_{b,\text{id}} L_b}{E_b} \tag{5.3}$$

Rearranging Eq. (5.3) gives

$$\alpha_{b,\text{force}} = \frac{\psi P \Delta_0}{L f_y} \frac{E_b}{S_{b,\text{id}} L_b} + S_c / S_{c,\text{cr}} \tag{5.4}$$

Eq. (5.4) indicates that $\alpha_{b,\text{force}}$ is related to the end-fixity factor, applied load, steel yield strength, elastic modulus, and brace length. For the critical case where the column is subjected to the critical buckling load ($P = P_{cr}$) and the column ends are assumed to be ideally pin-connected ($r_e = 0$), Eq. (5.4) is simplified as

$$\alpha_{b,\text{force}} = 1.333 \frac{\Delta_0}{f_y} \frac{E_b}{L_b} + 1 \tag{5.5}$$

Thus, the brace stiffness scale factor obtained from Eq. (5.5) can be directly utilized to assess the minimum required cross-sectional area of bracing for a column with pinned-ends satisfying the strength requirement, which is economical. For other cases where the column is semi-rigidly connected ($r_e > 0$) and the beneficial effect of the applied load being lower than the critical buckling load ($P < P_{cr}$) can be considered, Eq. (5.4) can be used to compute the value of $\alpha_{b,\text{force}}$.

5.3.2 Brace stiffness scale factor satisfying the stiffness requirement

If the additional displacement is assumed to be entirely induced by the applied force (neglecting the displacement induced by the installation misalignment, the connection deformations, etc.), the stiffness requirement of CSA S16-19 is $\Delta < \Delta_0$. Thus, for a single column, the brace stiffness scale factor shall be no less than the limit $\alpha_{b,\text{disp}}$ in Eq. (5.6).

$$\alpha_{b,\text{disp}} = \frac{S_c}{S_{c,\text{cr}}} - \frac{P/L}{S_{c,\text{cr}}} \psi \tag{5.6}$$

Eq. (5.6) is obtained from Eq. (3.18) with $\Delta = \Delta_0$ considering the effect of column initial curvature. For a single column with pinned ends ($r_e = 0$) and subjected to the critical buckling load ($P = P_{cr}$), since $S_c = S_{c,\text{cr}} = -P_{cr}/L$, the value of $\alpha_{b,\text{disp}}$ is 2.333.

Here, the optimum brace stiffness, $S_{b,\text{op}}$, is proposed, which signifies the minimum required brace stiffness satisfying the strength requirement, $P_r = Q_b$, and stiffness requirement, $\Delta = \Delta_0$. Accordingly, let $\alpha_{b,\text{op}}$ be the optimum brace stiffness scale factor, and its value is governed by:

$$\alpha_{b,\text{op}} = \max\{\alpha_{b,\text{force}}, \alpha_{b,\text{disp}}\} \tag{5.7}$$

Thus, an analytical method is proposed in this section to evaluate the minimum required brace stiffness for a single semi-rigidly connected column by solving $\alpha_{b,\text{op}}$ in Eq. (5.7). Once the value of $\alpha_{b,\text{op}}$ is attained, the corresponding optimum brace stiffness is

$$S_{b,\text{op}} = \alpha_{b,\text{op}} S_{b,\text{ids}} \tag{5.8}$$

Accordingly, the optimum cross-sectional area for a horizontal bracing is

$$A_{b,\text{op}} = \frac{S_{b,\text{op}} L_b}{E_b} \tag{5.9}$$

Compared to the methods in current standards [10, 11, 21], the advantages of the proposed method are: 1) it considers the adverse effect of column initial curvature on the bracing requirements; 2) it can apply to columns with semi-rigid connections; 3) for strength-control cases, it may help to reduce the required cross-sectional area of bracing; 4) it avoids the possible iteration process.

5.3.3 Example of a Single Column

To illustrate the advantages of the proposed method, the required cross-sectional area of bracing for a single column shown in Fig. 5.3 are obtained by following the provisions in AISC 360-16 [10] with taking $\alpha_b = 2.0$ and obtained from the proposed method. This column is made of a W150×24 section, of which the moment of inertial (in-plane) is $I_y = 1.83\times10^6\,\text{mm}^4$. The elastic modulus and yield strength of the column and brace are $E = 200\,000\,\text{MPa}$ and $f_y = 345\,\text{MPa}$, respectively. Take $\Delta_0 = L/500 = 6\,\text{mm}$ as the column initial imperfection.

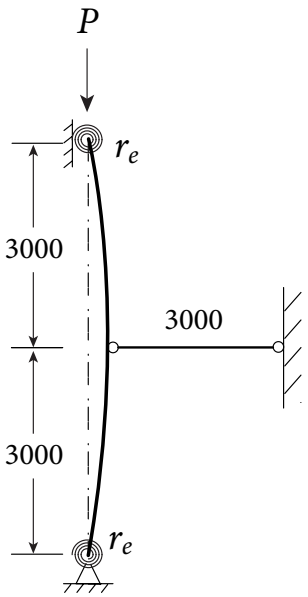

Figure 5.3: Diagram of Example 5.3.3

When $r_e = 0$, the critical buckling load of the column P_{cr} is

$$P_{cr} = \frac{\pi^2 E I_y}{L^2} = \frac{\pi^2 \times 2 \times 10^5 \times 1.83 \times 10^6}{3000^2} = 401\,363\,\text{N}$$

The corresponding ideal brace stiffness $S_{b,\text{id}}$ is

$$S_{b,\text{id}} = \frac{P_{cr}}{L} = \frac{401\,363\,\text{N}}{3000\,\text{mm}} = 133.8\,\text{N/mm}$$

Following AISC 360-16 [10], if the brace stiffness scale factor is taken as 2.0 then the required stiffness and cross-sectional area of the bracing associated with the stiffness requirement are

$$S_b = 2\alpha_b S_{b,\text{id}} = 2 \times 2 \times 133.8\,\text{N/mm} = 535.2\,\text{N/mm}$$

$$A_b = \frac{S_b L_b}{E_b} = \frac{535.2\,\text{N/mm} \times 3000\,\text{mm}}{2 \times 10^5\,\text{MPa}} = 8.03\,\text{mm}^2$$

The brace force with $\alpha_b = 2.0$ is

$$Q_b = \frac{4 P_{cr} \Delta_0 \psi}{L} = \frac{4 \times 401\,363\,\text{N} \times 1.333}{500} = 4281.2\,\text{N}$$

As mentioned in Chapter 3, the evaluation of the brace force in AISC 360-16 [10] neglects the effect of column initial curvature because it is based on Winter's model [7]. To better elucidate the difference between the method of AISC 360-16 and the proposed method, the effect of column initial curvature (ψ) is also considered when evaluating the brace strength

requirement in AISC 360-16. Thus, the required cross-sectional area of bracing associated with the strength requirement is

$$A_b = \frac{Q_b}{f_y} = \frac{4281.2\,\text{N}}{345\,\text{MPa}} = 12.41\,\text{mm}^2$$

Consequently, the required cross-sectional area of bracing obtained according to the AISC specification [10] is $A_{b,\text{AISC}} = 12.41\,\text{mm}^2$, which is governed by the strength requirement.

The optimum cross-sectional area of bracing with consideration of both stiffness and strength requirements can be obtained as follows. For the case with $r_e = 0$ and $P = P_{cr}$ of $\alpha_{b,\text{force}}$ can be obtained from Eq. (5.5):

$$\alpha_{b,\text{force}} = 1.333\frac{\Delta_0}{f_y}\frac{E_b}{L_b} + 1 = 1.333 \times \frac{1}{500} \times \frac{2 \times 10^5\,\text{MPa}}{345\,\text{MPa}} = 2.546$$

From Eq. (5.6), the value of $\alpha_{b,\text{disp}}$ is

$$\alpha_{b,\text{disp}} = \frac{S_c}{S_{c,\text{cr}}} - \frac{P/L}{S_{c,\text{cr}}}\psi = \frac{S_{c,\text{cr}}}{S_{c,\text{cr}}} - \frac{P_{cr}/L}{S_{c,\text{cr}}}\psi = 1 + 1.333 = 2.333$$

Thus, the optimum brace stiffness scale factor is

$$\alpha_{b,\text{op}} = \max\left\{\alpha_{b,\text{force}}, \alpha_{\text{b,disp}}\right\} = 2.546$$

With $\alpha_{b,\text{op}} = 2.546$, the corresponding optimum cross-sectional area of bracing can be directly attained:

$$A_{b,\text{op}} = \frac{\alpha_{b,\text{op}} S_{b,\text{ids}} L_b}{E_b} = \frac{2.546 \times 267.6\,\text{N/mm} \times 3000\,\text{mm}}{2 \times 10^5\,\text{MPa}} = 10.22\,\text{mm}^2$$

For this case, with the required cross-sectional area of bracing governed by the strength requirement, i.e., $\alpha_{b,\text{op}} = \alpha_{b,\text{force}}$, the evaluation of the brace force and corresponding required cross-sectional area of bracing are practically unnecessary because the obtained cross-sectional area of bracing satisfies the strength requirement as well as the stiffness requirement. Nevertheless, the calculation of A_b obtained from the brace force is presented for illustrative and verification purposes. The brace force with $\alpha_b = \alpha_{b,\text{force}}$ is

$$Q_b = 2 \times \frac{\alpha_{b,\text{op}} S_{b,\text{id}}}{\alpha_{b,\text{op}} S_{b,\text{id}} + S_{c,\text{cr}}} \frac{\psi P_{cr} \Delta_0}{L} = 2 \times \frac{2.546}{2.546 - 1} \times \frac{1.333 \times 401\,363\,\text{N}}{500} = 3525\,\text{N}$$

The corresponding required cross-sectional area of bracing is

$$A_{b,\text{force}} = \frac{Q_b}{f_y} = \frac{3525}{345\,\text{MPa}} = 10.22\,\text{mm}^2$$

For this case, therefore, adopting the optimum scale factor decreases the required cross-sectional area of bracing by 17.7% compared to that of AISC 360-16 [10].

Following the same procedure shown above, the required cross-sectional area of bracing for different magnitudes of applied loads obtained from AISC 360-16 [10] (with the consideration of column initial curvature, ψ) and the proposed method are tabulated in Table 5.1. Note that the variation of required brace stiffness is demonstrated in the required cross-sectional of bracing as the brace length and elastic modulus are the same for all cases. The reason for presenting the required cross-sectional area of the bracing instead of the required brace stiffness is to avoid the ambiguity led by the similarity between the terminologies, "required brace stiffness" and "stiffness requirement", in the following discussion.

Table 5.1: Minimum required brace cross-sectional areas for a pin-ended column with different load ratios obtained from AISC 360-16 and the proposed method

	AISC 360-16 [10]				Proposed method					Reduction
α_p	$\alpha_{b,\text{AISC}}$	Q_b (N)	Δ (mm)	$A_{b,\text{AISC}}$ (mm^2)	$\alpha_{b,\text{force}}$	Q_b (N)	$\alpha_{b,\text{disp}}$	Δ (mm)	$A_{b,\text{op}}$ (mm^2)	of A_b (%)
0.6	2.000	1569.9	1.92	8.03	1.326	1836.1	1.205	2.40	5.32	33.7%
0.7	2.000	2022.4	2.24	8.03	1.616	2237.7	1.473	2.40	6.49	19.2%
0.8	2.000	2585.5	2.56	8.03	1.915	2651.0	1.749	2.40	7.68	4.3%
0.9	2.390	3309.2	2.88	9.59	2.223	3078.9	2.035	2.40	8.92	7.0%
1	3.092	4281.2	3.20	12.41	2.546	3525.3	2.333	2.40	10.22	17.7%

Based on the design philosophy of AISC 360-16 [10], the brace stiffness requirement remains unchanged while the brace force decreases as the applied load decreases. Because of that, when the applied load ratio α_p decreases from 0.9 to 0.8, the governing criterion to determine the required cross-sectional area of bracing switches from strength to stiffness, and the required cross-sectional area of bracing remains the same when α_p decreases from 0.8 to 0.6. The optimum required cross-sectional area of bracing $A_{b,\text{op}}$ decreases as the applied load decreases. The optimum brace stiffness scale factor $\alpha_{b,\text{op}}$ is greater than 2.0 for cases in which the required cross-sectional area of bracing is controlled by the strength requirement and is less than 2.0 for cases in which the required cross-sectional area of

bracing is controlled by the stiffness requirement. It should be noted that the Q_b for AISC 360-16 [10] in Table 5.1 corresponds to the results obtained from $\alpha_b = 2.0$, and it is not the actual brace force when the required cross-sectional area of bracing, i.e., the required brace stiffness, is determined by the strength requirement, as illustrated in Fig. 5.2. Table 5.2 shows the results of $A_{b,\text{op}}$ and $A_{b,\text{AISC}}$ for this example with different end-fixity factors. Assume the column is subjected to its critical buckling load ($P = P_{cr}$).

Table 5.2: Minimum required brace cross-sectional areas for a single column subjected to P_{cr} with different r_e

	AISC 360-16 [10]				Proposed method					Reduction
r_e	$\alpha_{b,\text{AISC}}$	Q_b (N)	Δ (mm)	$A_{b,\text{AISC}}$ (mm^2)	$\alpha_{b,\text{force}}$	Q_b (N)	$\alpha_{b,\text{disp}}$	Δ (mm)	$A_{b,\text{op}}$ (mm^2)	of A_b (%)
0	3.092	4281.2	8.00	12.41	2.546	3525.3	2.333	6.0	10.22	17.7
0.1	3.331	4480.3	8.62	12.99	2.665	3585.4	2.436	6.0	10.39	20.0
0.2	3.576	4694.4	9.25	13.61	2.788	3659.8	2.542	6.0	10.61	22.0
0.3	3.816	4924.1	9.87	14.27	2.908	3752.5	2.646	6.0	10.88	23.8
0.4	4.030	5169.7	10.43	14.98	3.015	3867.7	2.738	6.0	11.21	25.2
0.5	4.193	5431.1	10.85	15.74	3.096	4010.9	2.808	6.0	11.63	26.2
0.6	4.279	5707.6	11.07	16.54	3.140	4187.6	2.845	6.0	12.14	26.6
0.7	4.272	5997.2	11.05	17.38	3.136	4402.5	2.842	6.0	12.76	26.6
0.8	4.171	6297.1	10.79	18.25	3.086	4658.3	2.799	6.0	13.50	26.0
0.9	4.000	6603.2	10.35	19.14	3.000	4952.5	2.725	6.0	14.36	25.0
1	3.793	6910.0	9.82	20.03	2.897	5276.7	2.636	6.0	15.29	23.6

It can be seen that $A_{b,\text{op}}$ and $A_{b,\text{AISC}}$ increase as the end-fixity factor increases and are controlled by the strength requirement for all cases. However, $\alpha_{b,\text{disp}}$ and $\alpha_{b,\text{force}}$ do not monotonically increase with r_e; they increase as r_e increases from 0 to 0.6 and decrease as r_e increases from 0.6 to 1. The reduction of A_b from the result obtained by following the philosophy of AISC 360-16 to that obtained by following the proposed method achieves the maximum value of 26.6% at $r_e = 0.6$.

5.4 Optimum Required Brace Stiffness for Multi-column Systems

This section discusses the calculation for the optimum brace stiffness scale factor $\alpha_{b,\text{op}}$ for multi-column systems. The criterion for $\alpha_{b,\text{op}}$ in Eq. (5.7) still holds true for the systems consisting of multiple columns, while the explicit expressions given in Eq. (5.4) and Eq. (5.6) cannot be used to obtain the values of $\alpha_{b,\text{force}}$ and $\alpha_{b,\text{disp}}$ because they only apply to cases of a single column.

5.4.1 $\alpha_{b,\text{force}}$ for multiple columns

For multi-column systems anchored on both sides with tension-only braces and multi-column systems anchored on one side with tension-compression braces, the value of $\alpha_{b,\text{force}}$ can be determined as follows. Incorporating Eq. (5.2) into Eq. (4.21) yields

$$\frac{Q_1}{\alpha_{b,\text{force}} S_{b,\text{id}}} = \frac{Q_{0,1} - Q_1}{S_{c,1}} - \frac{Q_{0,2} + Q_1 - Q_2}{S_{c,2}} \tag{5.10a}$$

$$\frac{Q_i}{\alpha_{b,\text{force}} S_{b,\text{id}}} = \frac{Q_{0,i} + Q_{i-1} - Q_i}{S_{c,i}} - \frac{Q_{0,i+1} + Q_i - Q_{i+1}}{S_{c,i+1}} \quad i = \{2, \ldots, n-1\} \tag{5.10b}$$

$$\frac{Q_n}{\alpha_{b,\text{force}} S_{b,\text{id}}/(1+c)} = \frac{Q_{0,n} + Q_{n-1} - Q_n}{S_{c,n}} \tag{5.10c}$$

$$Q_n = \frac{\alpha_{b,\text{force}} S_{b,\text{id}} L_b f_y}{E_b} \tag{5.10d}$$

The set of nonlinear equations shown in Eqs. (5.10) consists of $n+1$ equations and $n+1$ unknown variables, Q_1 to Q_n and $\alpha_{b,\text{force}}$. Because of the order-of-magnitude difference between $\alpha_{b,\text{force}}$ and Q_i, solving Eqs. (5.10) to attain the value of $\alpha_{b,\text{force}}$ will likely encounter an issue of non-convergence. To avoid this problem, eliminating $\alpha_{b,\text{force}}$ in Eqs. (5.10) yields:

$$\frac{Q_1}{Q_n}\frac{L_b f_y}{E_b} = \frac{Q_{0,1} - Q_1}{S_{c,1}} - \frac{Q_{0,2} + Q_1 - Q_2}{S_{c,2}} \tag{5.11a}$$

$$\frac{Q_i}{Q_n}\frac{L_b f_y}{E_b} = \frac{Q_{0,i} + Q_{i-1} - Q_i}{S_{c,i}} - \frac{Q_{0,i+1} + Q_i - Q_{i+1}}{S_{c,i+1}} \quad i = \{2, \ldots, n-1\} \tag{5.11b}$$

$$\frac{L_b f_y (1+c)}{E_b} = \frac{Q_{0,n} + Q_{n-1} - Q_n}{S_{c,n}} \tag{5.11c}$$

The accuracy of the numerical solution to a set of nonlinear equations highly depends on the selected initial values of variables and the numerical method. It is found that the

built-in solver *fsolve* in MATLAB is capable of obtaining the accurate solution to Eq. (5.11) when the initial values of Q_1 to Q_n are taken from the solution of Eq. (4.22) with $S_{b,i} = 2S_{b,\text{id}}$.

For a multi-column system with tension-compression braces and anchored on both sides, if the system is symmetric (e.g., the column lateral stiffness is uniform or the column lateral stiffness distribution is symmetric) then the magnitudes of Q_n and Q_{n+1} in Fig. 4.10 are identical. In addition, since the derivation for the brace force presented in Section 4.5 is based on that all the column initial imperfections toward the left, Q_n is in tension and positive. Therefore, for a symmetric system anchored on both sides, Q_n can be solved from Eq. (5.12), which is obtained by incorporating Eq. (5.2) into Eq. (4.23).

$$\frac{Q_1}{Q_n}\frac{L_b f_y}{E_b} = \frac{Q_{0,1} - Q_1 + Q_{n+1}}{S_{c,1}} - \frac{Q_{0,2} + Q_1 - Q_2}{S_{c,2}} \tag{5.12a}$$

$$\frac{Q_i}{S_{b,i}}\frac{L_b f_y}{E_b} = \frac{Q_{0,i} + Q_{i-1} - Q_i}{S_{c,i}} - \frac{Q_{0,i+1} + Q_i - Q_{i+1}}{S_{c,i+1}} \quad i = \{2, \ldots, n-1\} \tag{5.12b}$$

$$\frac{L_b f_y (1 + c_r)}{E_b} = \frac{Q_{0,n} + Q_{n-1} - Q_n}{S_{c,n}} \tag{5.12c}$$

$$\frac{Q_{n+1}}{Q_n}\frac{L_b f_y (1 + c_l)}{E_b} = -\frac{Q_{0,1} + Q_{n+1} - Q_1}{S_{c,1}} \tag{5.12d}$$

If a multi-column system is asymmetric (i.e., the column lateral stiffness distribution is asymmetric), either Q_n or Q_{n+1} could be the maximum brace force. For that case, it should be noted that in addition to solving Q_n from Eqs. (5.12), the value of Q_{n+1} also needs to be attained. As a matter of fact, the magnitude of Q_{n+1} can be obtained by solving Q_n using the established equations by reversing the order of the column indexes. Then, the maximum value of attained Q_n and Q_{n+1} is taken as the maximum brace force $Q_{\max}$. Once $Q_{\max}$ is obtained, $\alpha_{b,\text{force}}$ is

$$\alpha_{b,\text{force}} = \frac{Q_{\max} E_b}{S_{b,\text{id}} L_b f_y} \tag{5.13}$$

5.4.2 $\alpha_{b,\text{disp}}$ for multiple columns

For a multi-column system anchored on one side in analysis, because the column farthest from the anchor has the largest lateral displacement, as illustrated in Fig. 4.9, the criterion for brace stiffness requirement stipulated in current standards [10, 11] becomes $\Delta_1 = \Delta_0$.

Thus, substituting

$$\Delta_1 = \Delta_0 \tag{5.14a}$$

$$S_{b,i} = \alpha_{b,\text{disp}} S_{b,\text{id}} \tag{5.14b}$$

into Eqs. (4.16) gives:

$$\Delta_0 S_{c,1} = Q_{0,1} - (\Delta_0 - \Delta_2)\alpha_{b,\text{disp}} S_{b,\text{id}} \tag{5.15a}$$

$$\Delta_2 S_{c,2} = Q_{0,i} + (\Delta_0 - 2\Delta_2 + \Delta_3)\,\alpha_{b,\text{disp}} S_{b,\text{id}} \tag{5.15b}$$

$$\Delta_i S_{c,i} = Q_{0,i} + (\Delta_{i-1} - 2\Delta_i + \Delta_{i+1})\,\alpha_{b,\text{disp}} S_{b,\text{id}} \quad i = \{3, ..., n-1\} \tag{5.15c}$$

$$\Delta_n S_{c,n} = Q_{0,n} + (\Delta_{n-1} - 2\Delta_n)\,\alpha_{b,\text{disp}} S_{b,\text{id}}/(1+c) \tag{5.15d}$$

Eqs. (5.15) are a set of nonlinear equations consisting of n equations and n unknown variables, Δ_2 to Δ_n and $\alpha_{b,\text{disp}}$. To achieve accuracy, the initial value of $\alpha_{b,\text{disp}}$ can be taken as 2.0, and the initial values of Δ_2 to Δ_n can be taken as the results obtained from Eqs. (4.16) with $S_{b,i} = 2S_{b,\text{id}}$.

For the cases with uniform lateral stiffness of columns, Eqs. (5.15) becomes

$$\Delta_0 = Q_0/S_{c,\text{cr}} + (\Delta_0 - \Delta_2)\alpha_{b,\text{disp}} a_{\max} \tag{5.16a}$$

$$\Delta_2 = Q_0/S_{c,\text{cr}} - (\Delta_0 - 2\Delta_2 + \Delta_3)\,\alpha_{b,\text{disp}} a_{\max} \tag{5.16b}$$

$$\Delta_i = Q_0/S_{c,\text{cr}} - (\Delta_{i-1} - 2\Delta_i + \Delta_{i+1})\,\alpha_{b,\text{disp}} a_{\max} \quad i = \{3, ..., n-1\} \tag{5.16c}$$

$$\Delta_n = Q_0/S_{c,\text{cr}} - (\Delta_{n-1} - 2\Delta_n)\,\alpha_{b,\text{disp}} a_{\max}/(1+c) \tag{5.16d}$$

If the columns are subjected to the critical buckling load P_{cr} then the term, $Q_0/S_{c,\text{cr}}$, in Eq. (5.16) becomes

$$Q_0/S_{c,\text{cr}} = \frac{\psi P_{cr}\Delta_0}{L} \Big/ \frac{E_c I_c \beta_u}{12L^3} = \frac{\psi E_c I_c \pi^2 \Delta_0}{(KL)^2 L} \Big/ \frac{E_c I_c \beta_u}{12L^3} = \frac{12\psi\pi^2\Delta_0}{\beta_u K^2} \tag{5.17}$$

It can be seen from Eq. (5.17) that if the applied load equals P_{cr} then $Q_0/S_{c,\text{cr}}$ is only related to the end-fixity factor. The following is to prove that the magnitude of Δ_0 will not alter the solution of $\alpha_{b,\text{disp}}$ in Eqs. (5.18) for cases with uniform column lateral stiffness. Let $C_2 = 12\psi\pi^2/(\beta_u K^2)$, and Eqs. (5.16) can be written as:

$$\Delta_0 = C_2\Delta_0 + (\Delta_0 - \Delta_2)\alpha_{b,\text{disp}} a_{\max} \tag{5.18a}$$

$$\Delta_2 = C_2\Delta_0 - (\Delta_0 - 2\Delta_2 + \Delta_3)\,\alpha_{b,\text{disp}} a_{\max} \tag{5.18b}$$

$$\Delta_i = C_2\Delta_0 - (\Delta_{i-1} - 2\Delta_i + \Delta_{i+1})\,\alpha_{b,\text{disp}} a_{\max} \quad i = \{3, ..., n-1\} \tag{5.18c}$$

$$\Delta_n = C_2\Delta_0 - (\Delta_{n-1} - 2\Delta_n)\,\alpha_{b,\text{disp}} a_{\max}/(1+c) \tag{5.18d}$$

Let $\Delta'_0 = C_3\Delta_0$, then Eqs. (5.18) become

$$\Delta'_0 = C_2\Delta'_0 + (\Delta'_0 - C_3\Delta_2)\alpha_{b,\text{disp}}a_{\max} \tag{5.19a}$$

$$C_3\Delta_2 = C_2\Delta'_0 - \left(\Delta'_0 - 2C_3\Delta_2 + C_3\Delta_3\right)\alpha_{b,\text{disp}}a_{\max} \tag{5.19b}$$

$$C_3\Delta_i = C_2\Delta_0 - \left(C_3\Delta_{i-1} - 2C_3\Delta_i + C_3\Delta_{i+1}\right)\alpha_{b,\text{disp}}a_{\max} \quad i = \{3,...,n-1\} \tag{5.19c}$$

$$C_3\Delta_n = C_2\Delta'_0 - \left(C_3\Delta_{n-1} - 2C_3\Delta_n\right)\alpha_{b,\text{disp}}a_{\max}/(1+c) \tag{5.19d}$$

Let $\Delta'_i = C_3\Delta_i$ $(i = 2,3,...,n)$, then Eqs. (5.19) become

$$\Delta'_0 = C_2\Delta'_0 + (\Delta'_0 - \Delta'_2)\alpha_{b,\text{disp}}a_{\max} \tag{5.20a}$$

$$\Delta'_2 = C_2\Delta'_0 - \left(\Delta'_0 - 2\Delta'_2 + \Delta'_3\right)\alpha_{b,\text{disp}}a_{\max} \tag{5.20b}$$

$$\Delta'_i = C_2\Delta_0 - \left(\Delta'_{i-1} - 2\Delta'_i + \Delta'_{i+1}\right)\alpha_{b,\text{disp}}a_{\max} \quad i = \{3,...,n-1\} \tag{5.20c}$$

$$\Delta'_n = C_2\Delta'_0 - \left(\Delta'_{n-1} - 2\Delta'_n\right)\alpha_{b,\text{disp}}a_{\max}/(1+c) \tag{5.20d}$$

Because Eqs. (5.20) are equivalent to Eqs. (5.18), it indicates that the solution of $\alpha_{b,\text{disp}}$ is not related to the magnitude of Δ_0 but depends on the value of C_2 and the number of total equations, i.e., the end-fixity factor and the total number of columns in the system. Thus, the solution of $\alpha_{b,\text{disp}}$ in Eqs. (5.16) is constant with a given number of columns and column end-fixity factor. The effects of the number of columns and end-fixity factors on the values of $\alpha_{b,\text{disp}}$ for multi-column systems with uniform column lateral stiffness are presented in Fig. 5.4.

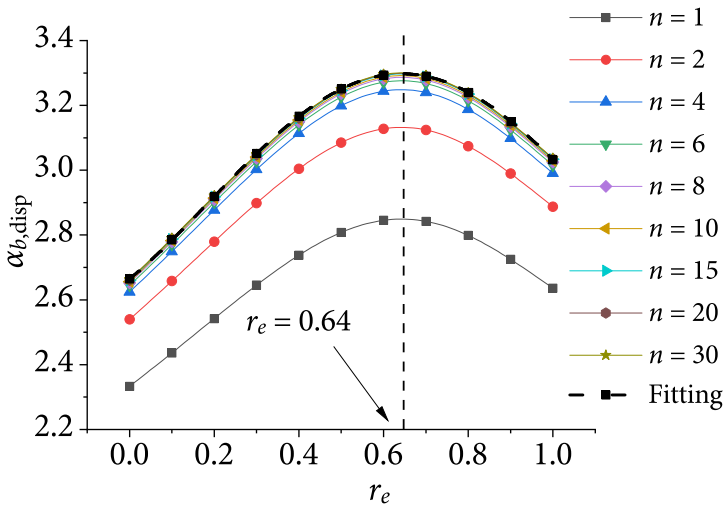

Figure 5.4: Variations of the brace stiffness scale factor $\alpha_{b,\text{disp}}$ with end-fixity factors r_e for multi-column systems with uniform lateral stiffness and different numbers of columns n

For comparison purposes, the variation of $\alpha_{b,\text{disp}}$ for a single column with r_e ($n = 1$) is also presented in Fig. 5.4. It can be seen that the variations of $\alpha_{b,\text{disp}}$ with r_e for multiple columns and a single column follow a similar trend that they all achieve the maximum value at $r_e = 0.64$. The results indicate that when r_e is given, then $\alpha_{b,\text{disp}}$ increases as the number of columns increases. However, the rate of increase of $\alpha_{b,\text{disp}}$ is considerably slower when the number of columns is more than five. Due to this characteristic, when the number of columns is more than five, 2.67 can be taken as the design value of the brace stiffness scale factor satisfying the stiffness requirement for multiple columns with pinned ends and uniform column lateral stiffness. Furthermore, an empirical formula in Eq. (5.21) is proposed to represent the upper bounds of $\alpha_{b,\text{disp}}$ for multiple columns with semi-rigid connections, as presented in Fig. 5.4, thus circumventing solving the nonlinear system in Eqs. (5.16).

$$\alpha_{b,\text{disp}} = 2.9 + 0.4 \sin(3.44 r_e - 0.636) \tag{5.21}$$

By neglecting the effect of column initial curvature ($\psi = 1$), the variations of $\alpha_{b,\text{disp}}$ with different end-fixity factors and numbers of columns are presented in Fig. 5.5 to solely observe the influence of the number of columns on the value of $\alpha_{b,\text{disp}}$.

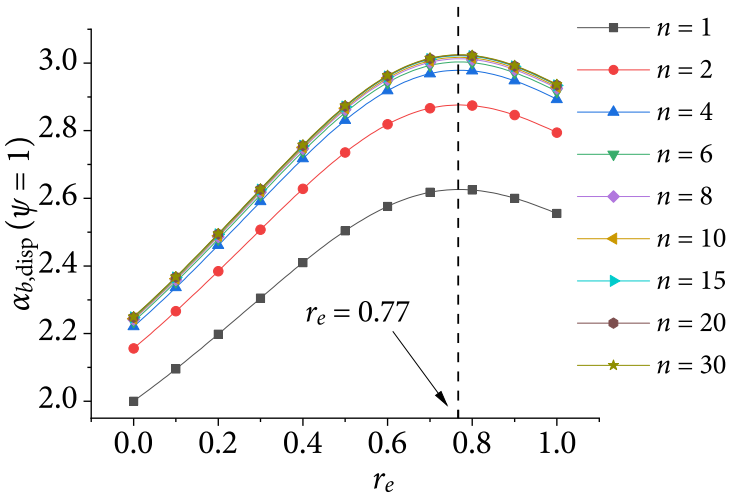

Figure 5.5: Variations of the brace stiffness scale factor $\alpha_{b,\text{disp}}$ with end-fixity factor r_e for multi-column systems with uniform lateral stiffness and different numbers of columns n without considering the effect of column initial curvature, ψ

It can be seen that even though the column initial curvature is not considered, the values

of $\alpha_{b,\text{disp}}$ increase as the number of columns increases. Additionally, $\alpha_{b,\text{disp}}$ achieves the maximum value for each case at $r_e = 0.77$ instead of $r_e = 0.64$. As expected, the values of $\alpha_{b,\text{disp}}$ neglecting the effect of column initial curvature are less than those considering the effect of column initial curvature, signifying that the initial curvature needs to be considered. In a nutshell, for multiple columns with uniform column lateral stiffness and subjected to the critical buckling load, the value of $\alpha_{b,\text{disp}}$ is affected by the end-fixity factor r_e, column initial curvature ψ, and the number of columns n.

The analytical results of $\alpha_{b,\text{disp}}$ are presented in Fig. 5.6 with $\Delta_n = \Delta_0$ to demonstrate the validity of the criterion in Eq. (5.14b). It can be seen that if the minimum displacement $\Delta_{\min}$ (Δ_n) is taken as Δ_0, the value of $\alpha_{b,\text{disp}}$ decreases and approaches unity as the number of columns increases. In that case, the maximum displacement of the system can be quite large since the magnitude of the brace stiffness is close to that of the ideal brace stiffness. Therefore, taking $\Delta_1 = \Delta_0$ as the criterion to determine the value of $\alpha_{b,\text{disp}}$ is imperative.

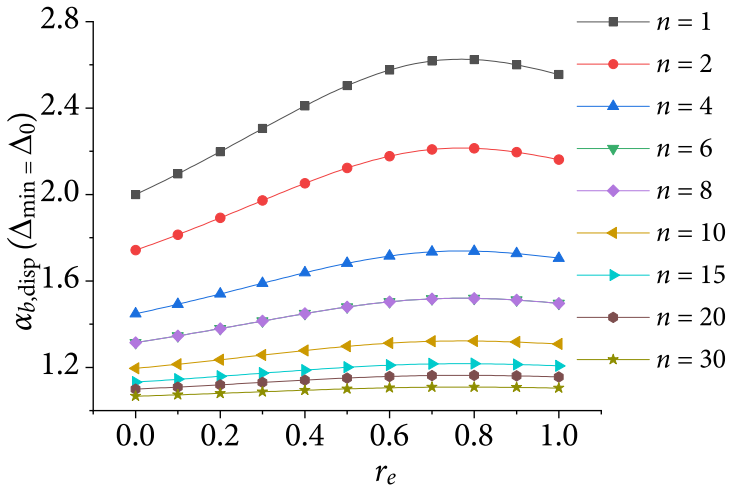

Figure 5.6: Variations of $\alpha_{b,\text{disp}}$ with r_e for multiple columns with uniform lateral stiffness when $\Delta_{\min} = \Delta_0$

It is worth noting that the criterion in Eq. (5.14b) does not hold true for a system anchored on both sides because which column has the maximum displacement is unknown, especially for cases with nonuniform column lateral stiffness. Since varying the value of α_b will not affect the location of the maximum displacement, the location of the maximum displacement can be found by obtaining the displacements from Eq. (4.18) with $S_{b,i} = 2S_{b,\text{id}}$. Finally, the value of $\alpha_{b,\text{disp}}$ can be obtained by Eq. (4.17) with $S_{b,i} = \alpha_{b,\text{disp}} S_{b,\text{id}}$ and setting

the corresponding maximum displacement as Δ_0. If the system is anchored on both sides in analysis and has uniform column lateral stiffness, Eq. (5.21) can still be used for reasons of conservation and simplicity.

5.4.3 Computational procedure

The computational procedure of calculating the optimum cross-sectional area of bracing for multi-column systems is summarized below.

1. Follow the computational procedure given in Section 4.7 to obtain the ideal brace stiffness $S_{b,\text{id}}$ and the brace forces with the brace stiffness being the twice ideal brace stiffness, i.e., $S_b = 2S_{b,\text{id}}$.

2. If the system is anchored on one side in the analysis, solve Eqs. (5.11) by employing the nonlinear solver *fsolve* in MATLAB to obtain the value of Q_n satisfying the criterion in Eq. (5.2), with the initial values being taken as the brace forces associated with $S_b = 2S_{b,\text{id}}$ obtained from the previous step. If the system is anchored on both sides in the analysis, solve Eqs. (5.12) twice with the actual and reversed order of column indexes to obtain the maximum value of Q_n.

3. With the obtained maximum brace force and given L_b, E_b, and f_y, compute the value of $\alpha_{b,\text{force}}$ by Eq. (5.13).

4. Calculate the lateral displacements, Δ_1 to Δ_n, associated with $S_b = 2S_{b,\text{id}}$ by solving Eqs. (4.16).

5. If the system is anchored on one side in the analysis, obtain the value of $\alpha_{b,\text{disp}}$ by solving Eqs. (5.15) by employing *fsolve* in MATLAB and adopting 2.0 as the initial guess of $\alpha_{b,\text{disp}}$ and the lateral displacements associated with $S_b = 2S_{b,\text{id}}$ as the initial values of Δ_2 to Δ_n. If the system is anchored by both sides, find the location of the maximum displacement from the previous step. Solve Eq. (4.17) with $S_{b,i} = \alpha_b S_{b,\text{id}}$ and setting the corresponding maximum displacement as Δ_0 to obtain the value of $\alpha_{b,\text{disp}}$. The initial guess of $\alpha_{b,\text{disp}}$ can be taken as 2.0, and the initial values of the other displacements, except for the maximum displacement, can be taken as the results of the previous step. In particular, if the system consists of columns with uniform lateral

stiffness, then Eq. (5.21) can be directly utilized to compute the value of $\alpha_{b,\text{disp}}$ for simplicity.

6. Take the maximum value of $\alpha_{b,\text{force}}$ and $\alpha_{b,\text{disp}}$ as the optimum brace stiffness scale factor, $\alpha_{b,\text{op}}$, and compute the optimum cross-sectional area of bracing for the system, as below:

$$A_{b,\text{op}} = \frac{2\alpha_{b,\text{op}} S_{b,\text{id}} L_b}{E_b} \tag{5.22}$$

5.4.4 Example with uniform lateral stiffness

The required cross-sectional areas of bracing for the example with five semi-rigidly connected columns presented in Section 4.8.1 are obtained using the proposed method, as tabulated in Table 5.3, in which the results obtained by following the design philosophy of AISC 360-16 [10] are provided from comparison. The computational procedure presented in Section 5.4.3 is followed without using the empirical equation in Eq. (5.21), which is applicable to this case, though.

The cross-sectional areas of bracing predicted following the design philosophy of AISC 360-16, $A_{b,\text{AISC}}$, are primarily controlled by the stiffness requirement except for cases when the end-fixity factor r_e ranges from 0.5 to 0.7. Consequently, the brace stiffness scale factors are 2.0 for most cases and approximate 2.0 for the other cases. Hence, as shown in Fig. 3.3, the variation of $A_{b,\text{AISC}}$ with r_e in this example follows a similar trend of the variation of $S_{b,\text{id}}$ with r_e: $A_{b,\text{AISC}}$ decreases as r_e increases from 0 to 0.4, achieving the minimum value at $r_e = 0.4$, and increases as r_e increases from 0.4 to 1.0. The strength requirement (Q_n) obtained by following AISC 360-16 increases as r_e increases.

The required cross-sectional areas of bracing obtained from the proposed method $A_{b,\text{op}}$ are all controlled by the stiffness requirements, i.e., $\alpha_{b,\text{op}} = \alpha_{b,\text{disp}}$, for all cases. The values of the brace stiffness scale factor associated with the strength requirement and stiffness requirement, $\alpha_{b,\text{force}}$ and $\alpha_{b,\text{disp}}$, increase as r_e increases from 0 to 0.6 and decrease as r_e increases from 0.6 to 1.0. Nevertheless, the brace force Q_n (strength requirement) corresponding to $\alpha_{b,\text{force}}$ monotonically increases as r_e increases. It is worth noting that $A_{b,\text{op}}$ increases as r_e increases, indicating the different variation from $\alpha_{b,\text{disp}}$. In this example, since the system is composed of five identical columns with uniform lateral stiffness, the

Table 5.3: Minimum required brace cross-sectional areas for a five-column system subjected to P_{cr} with different r_e

	AISC 360-16 [10]				Proposed method					Increase
r_e	$\alpha_{b,\text{AISC}}$	Q_n (N)	Δ (mm)	$A_{b,\text{AISC}}$ (mm^2)	$\alpha_{b,\text{force}}$	Q_n (N)	$\alpha_{b,\text{disp}}$	Δ (mm)	$A_{b,\text{op}}$ (mm^2)	of A_b (%)
0	2.000	20485.2	9.9	80.46	1.731	24019.5	2.637	6.0	106.09	31.9%
0.1	2.000	21438.0	10.6	78.16	1.789	24124.5	2.763	6.0	107.97	38.1%
0.2	2.000	22462.2	11.4	76.27	1.849	24329.7	2.892	6.0	110.28	44.6%
0.3	2.000	23561.1	12.2	74.98	1.908	24678.8	3.018	6.0	113.14	50.9%
0.4	2.000	24736.5	12.8	74.54	1.961	25210.8	3.130	6.0	116.67	56.5%
0.5	2.002	25987.5	13.4	75.33	2.002	25987.5	3.216	6.0	121.02	60.7%
0.6	2.043	27310.2	13.6	79.16	2.022	27032.9	3.261	6.0	126.37	59.6%
0.7	2.039	28696.0	13.6	83.18	2.020	28428.6	3.257	6.0	132.86	59.7%
0.8	2.000	30131.2	13.3	87.72	1.993	30161.8	3.205	6.0	140.55	60.2%
0.9	2.000	31595.8	12.8	95.92	1.953	32320.7	3.115	6.0	149.38	55.7%
1	2.000	33063.7	12.1	105.85	1.902	34736.4	3.006	6.0	159.09	50.3%

ideal brace stiffness for all cases is $S_{b,\text{idt}} = a_{\max} S_{b,\text{ids}}$, in which $S_{b,\text{ids}}$ is the ideal brace for a single column. In Chapter 4, it has been demonstrated that the ratio of the ideal brace stiffness for multi-column systems to that for a single column, $a_{\max}$, does not depend on the value of r_e if the system consists of uniform lateral stiffness. Thus, the variation of $A_{b,\text{op}}$ ($S_{b,\text{op}}$) in this example is related to the product of $\alpha_{b,\text{disp}}$ and $S_{b,\text{ids}}$.

Presented in Fig. 5.7 are the variations of $S_{b,\text{op}}$, $\alpha_{b,\text{disp}}$, and $S_{b,\text{ids}}$ with r_e, which are normalized by dividing by the values of $S_{b,\text{op}}$, $\alpha_{b,\text{op}}$, and $S_{b,\text{ids}}$ at $r_e = 0$, respectively. It can be seen that $S_{b,\text{ids}}$ decreases as r_e increases from 0 to 0.392 (investigated in Chapter 3) and increases as r_e increases from 0 to 0.392 to 1.0; particularly, the increasing rate of $S_{b,\text{ids}}$ becomes considerably large after $r_e = 0.64$, after which $\alpha_{b,\text{disp}}$ decreases with r_e. As a consequence, as the product of $\alpha_{b,\text{disp}}$ and $S_{b,\text{ids}}$, the optimum brace stiffness $S_{b,\text{op}}$ monotonically increases with r_e.

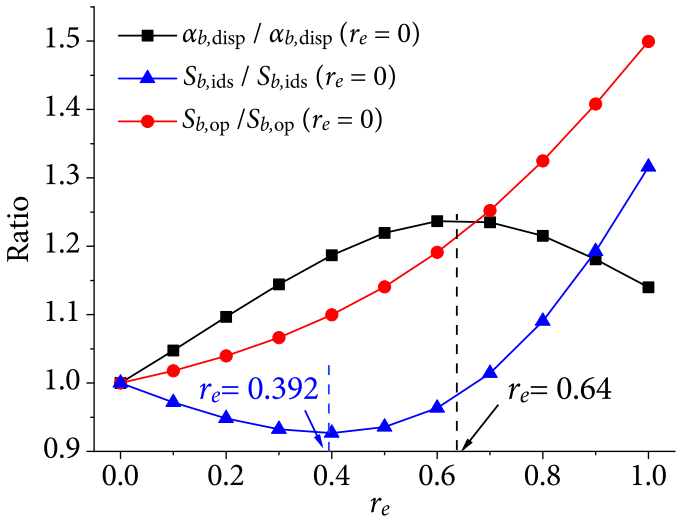

Figure 5.7: Normalized variations of $A_{b,\text{op}}$, $\alpha_{b,\text{disp}}$, and $S_{b,\text{ids}}$ with r_e

Overall, due to considering the effects of column initial curvature and accumulation of displacement for multi-column systems on the stiffness requirement, the predictions obtained from the proposed method are larger than those following the design philosophy of AISC 360-16 [10]. The maximum increase of A_b from the prediction of AISC 360-16 to the prediction of the proposed method is 60.7%, which is significant. Therefore, to some extent, the stiffness requirement $S_b = 2S_{b,\text{id}}$ in AISC 360-16 may be unconservative because its original assumption of $\Delta = \Delta_0$ cannot be satisfied, especially for the multi-column systems.

5.4.5 Example with nonuniform lateral stiffness

The effect of the nonuniform column lateral stiffness on the optimum required brace stiffness is investigated by analyzing the example presented in Section 4.8.2. Assume that the braces are tension-only and the columns are pin-connected at both ends. The analytical results for different locations of the distinctive column (LDC) are tabulated in Table 5.4. As specified in AISI S100-16 [11], anchors on both sides shall be provided for a tension-only braced system, while only one anchor should be considered in the analysis. In this example, assume the right anchor is available in the analysis.

Table 5.4: Optimum required cross-sectional areas of bracing for a nine-column system with different locations of a distinctive column

LDC	AISC 360-16 [10]				Proposed method					Increase
	$\alpha_{b,\text{AISC}}$	Q_b (N)	Δ (mm)	$A_{b,\text{AISC}}$ (mm^2)	$\alpha_{b,\text{force}}$	Q_b (N)	$\alpha_{b,\text{disp}}$	Δ (mm)	$A_{b,\text{op}}$ (mm^2)	of A_b (%)
None	2.0	4752.5	4.92	16.09	1.846	5125.3	3.039	2.4	24.45	51.9
1	2.0	6137.6	4.71	25.52	1.687	7426.9	2.955	2.4	37.70	47.7
2	2.0	6165.7	4.66	24.76	1.713	7316.7	2.936	2.4	36.35	46.8
3	2.0	6199.5	4.66	23.75	1.749	7166.2	2.938	2.4	34.89	46.9
4	2.0	6234.3	4.72	22.52	1.797	6981.1	2.961	2.4	33.34	48.0
5	2.0	6262.1	4.82	21.14	1.855	6764.2	3.002	2.4	31.73	50.1
6	2.0	6268.3	4.97	19.69	1.921	6523.8	3.057	2.4	30.10	52.9
7	2.0	6226.2	5.12	18.29	1.981	6251.4	3.115	2.4	28.50	55.8
8	2.0	6096.4	5.21	17.67	2.034	6005.6	3.152	2.4	26.97	52.6
9	2.0	5847.6	5.16	16.95	2.040	5751.6	3.132	2.4	25.60	51.0

Following the specifications of AISC 360-16 [10], the required cross-sectional areas of bracing are stiffness-controlled when the LDC ranges from the left-most to the 7th and strength-controlled when the LDC is at the 8th and the 9th. The actual brace stiffness scale factor ratios when the LDC is at 8th and 9th are slightly greater than 2.0, indicating that the required cross-sectional areas of bracing associated with the strength and stiffness requirements are very close to each other for these two cases. Thus, the magnitudes of $\alpha_{b,\text{force}}$ for these two cases are slightly lower than α_b. As discussed in Section 4.8.2, the ideal brace stiffness $S_{b,\text{id}}$ decreases as the distinctive column with lower lateral stiffness than the typical columns is closer to the anchor. Therefore, $A_{b,\text{AISC}}$ decreases as the LDC becomes closer to the anchor since the required cross-sectional area of bracing for most cases is controlled by the stiffness requirement.

However, all the optimum required brace cross-sectional areas obtained from the proposed method are controlled by the stiffness requirements and are greater than the required cross-sectional areas of bracing obtained by following AISC 360-16. The first reason is that the specifications in AISC 360-16 neglect the adverse impact of column initial curvature on

the additional lateral displacement, i.e., the stiffness requirement. The second reason is that taking brace stiffness as twice the ideal brace stiffness neglects the increase of $\alpha_{b,\text{disp}}$ as the number of columns increases; the criterion, $\alpha_b = 2.0$, is derived from a single column. As a consequence, if the cross-sectional area of bracing is governed by the stiffness requirement, following the specifications in AISC 360-16 yields underestimated results.

As the distinctive column becomes closer to the anchor (from the 1st to the 9th), the values of $\alpha_{b,\text{force}}$ and $\alpha_{b,\text{disp}}$ gradually increase except that $\alpha_{b,\text{disp}}$ decreases from 3.152 to 3.132 when the LDC moves from the 8th to the 9th column. However, the optimum cross-sectional area of bracing $A_{b,\text{op}}$ decreases as the LDC becomes closer to the anchor because in this example the optimum brace stiffness $S_{b,\text{op}}$ is a product of $\alpha_{b,\text{disp}}$ and the ideal brace stiffness $S_{b,\text{idt}}$, which decreases as the LDC becomes closer to the anchor.

It is worth noting that the analysis assuming the left anchor is available is also required for a system with tension-only braces. Since there is only one distinctive column in this example, the results shown in Table 5.4 also represent the predictions from the analysis in which the left anchor is available by reversing the order of column index the LDC. For example, if the LDC is at the 7th column, the optimum cross-sectional area of bracing is 28.5 mm^2 when the right anchor is available and 34.89 mm^2 when the left anchor is available, and thus the optimum cross-sectional area of bracing should be taken as 34.89 mm^2 for this scenario. Hence, $A_{b,\text{op}}$ achieves the minimum value when the LDC is at the centre of the system.

5.5 Conclusions

With the consideration of the effects of semi-rigid connections and column initial curvature, an analytical method is proposed in this chapter to evaluate the minimum required brace stiffness, which satisfies both strength and stiffness requirements. The expressions for determining the minimum brace stiffness scale factor associated with the strength requirement, $\alpha_{b,\text{force}}$, and the stiffness requirement, $\alpha_{b,\text{disp}}$, are proposed for a single column and multi-column systems. The following conclusions are drawn from this chapter:

1. For a single column, it is found that if the required brace stiffness is controlled by the strength requirement then the proposed method yields smaller results than following

AISC 360-16 [10] due to adopting $\alpha_{b,\text{force}}$ which is the minimum value of brace stiffness scale factor satisfying the strength requirement, which leads to more economical designs.

2. For multi-column systems with uniform lateral stiffness, the variations of $\alpha_{b,\text{disp}}$ (the value of the brace stiffness scale factor corresponding to $\Delta_{\max} = \Delta_0$) with the end-fixity factor r_e and number of columns n are investigated. It is found that the relationships between $\alpha_{b,\text{disp}}$ and r_e are in a similar trend regardless of the number of columns in the system. Once the number of columns n is given, $\alpha_{b,\text{disp}}$ increases as r_e increases from 0 to 0.64, achieves the maximum value at $r_e = 0.64$, and decreases as r_e increases from 0.64 to 1.0. If the value of r_e is predetermined, $\alpha_{b,\text{disp}}$ increases as n increases with a decreasing rate, while the rate of increase is considerably slow when n is greater than 5. Due to this characteristic, a simplified expression as a function of r_e is proposed to assess the maximum value of $\alpha_{b,\text{disp}}$ for multiple columns with semi-rigid connections, thus circumventing solving the nonlinear equations.

3. Due to neglecting the effect of column initial curvature and the displacement accumulation for multiple columns, for multiple columns the stiffness requirement in AISC 360-16 that the brace stiffness shall be taken as twice the ideal brace stiffness may not fulfill its original intention that the additional displacement is less than the initial imperfection. Consequently, if the required brace stiffness is controlled by the stiffness requirement (twice the ideal brace stiffness), the proposed method yields a larger cross-sectional area of bracing than following the specifications in AISC 360-16.

Chapter 6

Nonuniform Bracing of Multi-column Systems

The previous research [1,5,9] regarding assessing the bracing stiffness requirement assumed the stiffness of all the braces is identical, which is referred to as *uniform bracing* in this chapter. However, the uniform bracing pattern may not always be feasible or economical in practice. For example, solid blocking is often intermittently placed in a cold-formed steel wall framing to prevent the studs from twisting, as shown in Fig. 6.1. In such cases, the contribution of solid blocking to the stability of the wall studs is yet to be investigated.

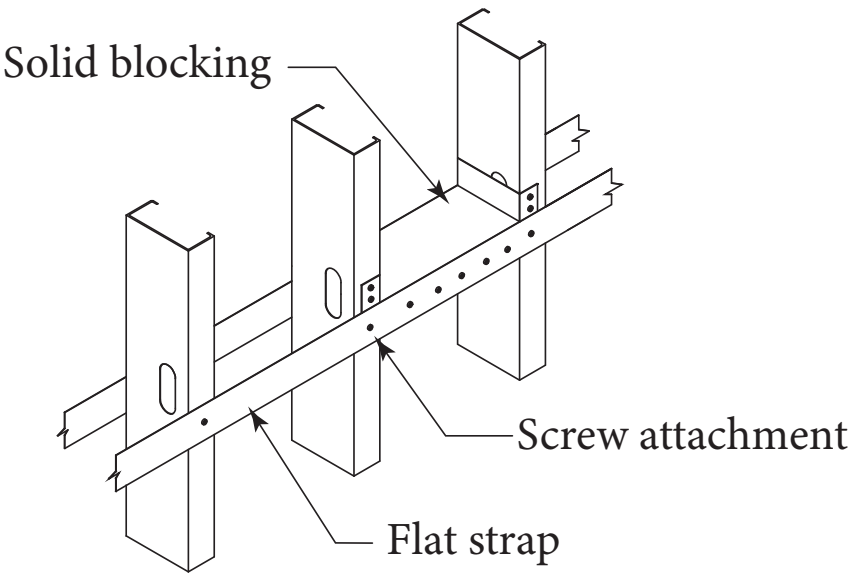

Figure 6.1: Flat strip bridging system [107]

For that reason, the following two issues are going to be investigated in this chapter.

1. How does nonuniform brace stiffness, such as the intermittent solid blocking brace, affect the requirements for tie bracing in a multi-column system?

2. In addition to the uniform bracing pattern, are there any alternative bracing patterns satisfying the bracing requirements and resulting in a more efficient or economical bracing design?

6.1 Effect of Solid Blocking on Bracing Requirements

In practice, the solid blocking is placed at intervals within a load-bearing wall to provide resistance to the rotational tendency of the studs within the wall [107]. Conventionally, the section of the solid blocking is predetermined in such a way that it is in accordance with the dimension of the studs, and the intervals are determined by design engineers. It is predictable that the presence of solid blocking could reduce the bracing requirement of tie bracing in the system, whereas this favourable effect induced by solid blocking has not been quantitatively investigated.

Illustrated in Fig. 6.2 is a multi-column system anchored by both sides or one side with the solid blocking placed at the column's mid-height.

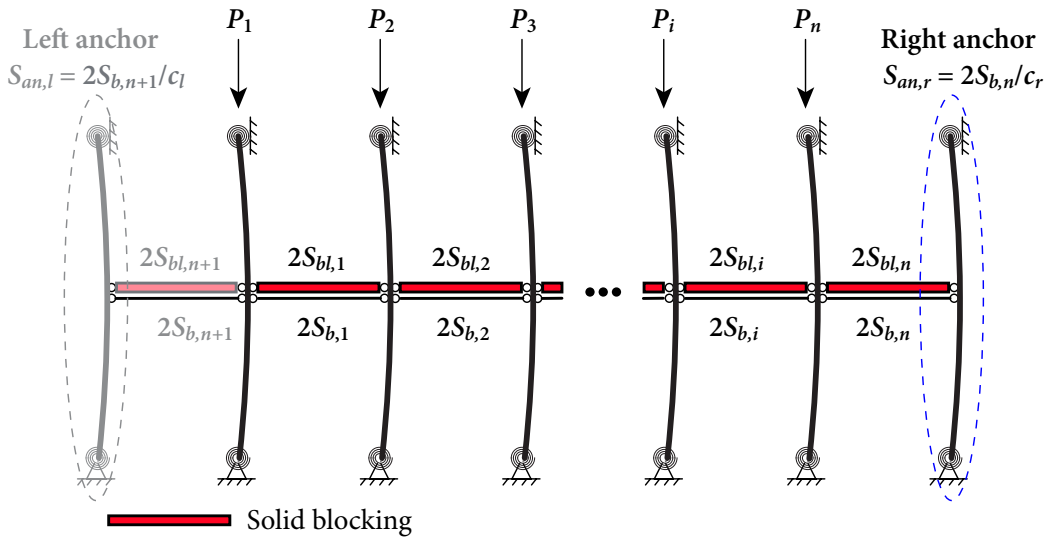

Figure 6.2: A multi-column system with solid blocking

Let $S_{bl,i}$ be the axial stiffness of solid blocking. Since the solid blocking is placed intermittently, $S_{bl,i} = 0$ if the solid blocking is not placed at the location of brace i. c_r and c_l are

the ratios of brace stiffness to the stiffness of the right anchor and left anchor, respectively.

The following two assumptions are made for simplicity.

1. The solid blocking is made of the same material as the tie bracing, and the length difference between the solid blocking and the brace is neglected. As such, the tie bracing and the solid blocking have the same mechanical properties (E and f_y) and length (L).

2. Like tie bracing, the stiffness of solid blocking in the half-length column model is assumed to be half of that in the whole system. In addition, the local buckling of solid blocking is not considered. Thus, the stiffness of solid blocking in the half-length column model is

$$S_{bl} = \frac{A_{bl} E_b}{2L_b} \tag{6.1}$$

where A_{bl} is the cross-sectional area of the solid blocking.

With the assumptions made above, the multi-column system with solid blocking can be simulated using the proposed half-length column model, as per Fig. 6.3.

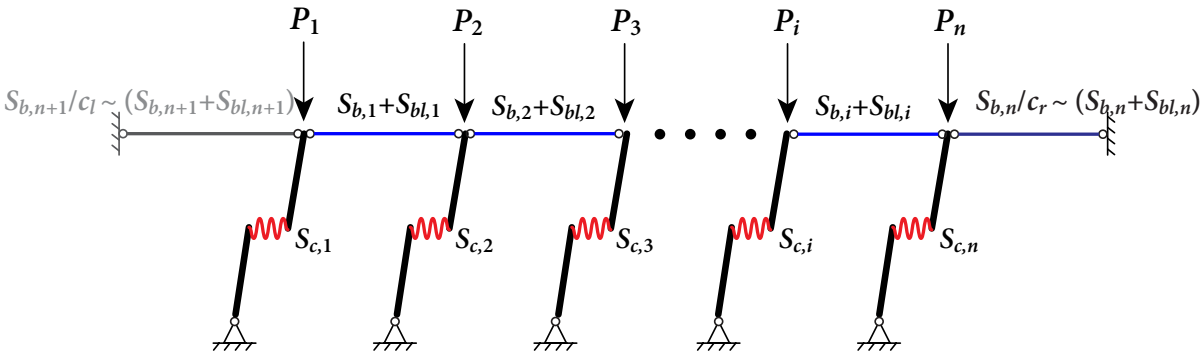

Figure 6.3: A multi-column system with uniform tie bracing and solid blocking simulated using the proposed model

As introduced in Chapter 4, the symbol "~" is used to represent the operation in series for simplicity. For example, the stiffness of the right-most brace is

$$\frac{S_{b,n+1}}{c_l} \sim \left(S_{b,n+1} + S_{bl,n+1}\right) = \left(\frac{c_l}{S_{b,n+1}} + \frac{1}{S_{b,n+1} + S_{bl,n+1}}\right)^{-1} \tag{6.2}$$

6.1.1 $\alpha_{b,\text{force}}$ for multi-column systems with solid blocking

In Chapter 4, the relationship between the multi-column system stiffness and displacements is derived and presented in Eq. (4.18). As per Fig. 6.3, substituting

$$S_{b,i} = S_{b,i} + S_{bl,i} (i < n) \tag{6.3a}$$

$$S_{b,n} = (S_{b,n}/c_r) \sim (S_{b,n} + S_{bl,n}) \tag{6.3b}$$

$$S_{b,n+1} = (S_{b,n+1}/c_l) \sim (S_{b,n+1} + S_{bl,n+1}) \tag{6.3c}$$

into the stiffness matrix in Eq. (4.18) yields the stiffness matrix for the multi-column system with uniform tie bracing and solid blocking:

$$\mathbf{K_{bl}} = \begin{bmatrix} \begin{pmatrix} S_{b,1} + S_{bl,1} + S_{c,1} + \\ \frac{S_{b,n+1}}{c_l} \sim (S_{b,n+1} + S_{bl,n+1}) \end{pmatrix} & -S_{b,1} - S_{bl,1} & & \\ -S_{b,1} - S_{bl,1} & \begin{pmatrix} S_{b,1} + S_{b,2} + S_{bl,1} + \\ S_{bl,2} + S_{c,2} \end{pmatrix} & \ddots & \\ & \ddots & \ddots & -S_{b,n-1} - S_{bl,n-1} \\ & & -S_{b,n-1} - S_{bl,n-1} & \begin{pmatrix} S_{b,n-1} + S_{bl,n-1} + S_{c,n} + \\ \frac{S_{b,n}}{c_r} \sim (S_{b,n} + S_{bl,n}) \end{pmatrix} \end{bmatrix} \tag{6.4}$$

Thus, the ideal brace stiffness of the tie bracing for multi-column systems considering solid blocking can be attained by finding the maximum root of the determinant of $\mathbf{K_{bl}}$ being zero with $S_{b,i} = S_{b,\text{id}}$.

Once the ideal brace stiffness of tie bracing is obtained, the bracing requirements can be assessed by following the proposed procedure in Chapter 5 by computing the brace stiffness scale factors, $\alpha_{b,\text{disp}}$ and $\alpha_{b,\text{force}}$. As discussed in Chapter 4, for multi-column systems anchored on one side, it is arguably that the brace adjacent to the anchor has the maximum brace force due to the accumulation of brace forces; thereby, it is reasonable to attain $\alpha_{b,\text{force}}$ by equating the force in brace n and the strength of brace n. However, when it comes to multi-column systems with solid blocking, the force in brace n may not be the largest because the solid blocking bears a part of the force. Consequently, the force in the brace without the solid blocking and closest to the anchor may be larger than the force in brace n. Therefore, the requisite of calculating $\alpha_{b,\text{force}}$ for multi-column systems with solid

blocking is to locate the brace possessing the maximum brace force $Q_{\max}$. With uniform tie bracing stiffness, the magnitude of the brace stiffness scale factor will not affect the order of brace forces' magnitudes. For that reason, the brace with $Q_{\max}$ can be located by solving Eqs. (6.5).

$$\mathbf{FQ} = \mathbf{D} \tag{6.5a}$$

$$\mathbf{F} = \begin{bmatrix} \frac{1}{2S_{b,\mathrm{id}}+S_{bl,1}} + \frac{1}{S_{c,1}} + \frac{1}{S_{c,2}} & -\frac{1}{S_{c,2}} & & & \\ -\frac{1}{S_{c,2}} & \frac{1}{2S_{b,\mathrm{id}}+S_{bl,2}} + \frac{1}{S_{c,2}} + \frac{1}{S_{c,3}} & -\frac{1}{S_{c,3}} & & \\ & -\frac{1}{S_{c,3}} & \ddots & \ddots & \\ & & \ddots & \frac{1}{2S_{b,\mathrm{id}}+S_{bl,n-1}} + \frac{1}{S_{c,n-1}} + \frac{1}{S_{c,n}} & -\frac{1}{S_{c,n}} \\ & & & -\frac{1}{S_{c,n}} & \frac{1}{(2S_{b,\mathrm{id}}/c_r)\sim(2S_{b,\mathrm{id}}+S_{bl,n})} + \frac{1}{S_{c,n}} \end{bmatrix} \tag{6.5b}$$

$$\mathbf{Q} = \begin{Bmatrix} Q_1 \\ Q_2 \\ \vdots \\ Q_{n-1} \\ Q_n \end{Bmatrix} \qquad \mathbf{D} = \begin{Bmatrix} \frac{Q_{0,1}}{S_{c,1}} - \frac{Q_{0,2}}{S_{c,2}} \\ \frac{Q_{0,2}}{S_{c,2}} - \frac{Q_{0,3}}{S_{c,3}} \\ \vdots \\ \frac{Q_{0,n-1}}{S_{c,n-1}} - \frac{Q_{0,n}}{S_{c,n}} \\ \frac{Q_{0,n}}{S_{c,n}} \end{Bmatrix} \tag{6.5c}$$

in which all the brace stiffness can be taken as twice the ideal brace stiffness $2S_{b,\mathrm{id}}$. Once the brace forces are attained from Eqs. (6.5), let k represent the index of the brace with the maximum internal force. Subsequently, letting the force in brace k equal the brace strength yields:

$$\frac{Q_k}{f_y}\frac{S_{b,k}}{S_{b,k}+S_{bl,k}} = \frac{S_{b,k}L_b}{E_b} \tag{6.6}$$

Subsequently, for multi-column systems anchored on one side, if the stiffness of solid blocking is considered, the nonlinear equations in Eqs. (5.11) regarding the brace forces become

$$\frac{Q_{0,1}-Q_1}{S_{c,1}} - \frac{Q_{0,2}+Q_1-Q_2}{S_{c,2}} = \frac{Q_1}{\alpha_{b,\mathrm{force}}S_{b,\mathrm{id}}+S_{bl,1}} \tag{6.7a}$$

$$\frac{Q_{0,i}+Q_{i-1}-Q_i}{S_{c,i}} - \frac{Q_{0,i+1}+Q_i-Q_{i+1}}{S_{c,i+1}} = \frac{Q_i}{\alpha_{b,\mathrm{force}}S_{b,\mathrm{id}}+S_{bl,i}} \qquad i=\{2,\ldots,n-1\} \tag{6.7b}$$

$$\frac{Q_{0,n}+Q_{n-1}-Q_n}{S_{c,n}} = \frac{Q_n}{\left(\alpha_{b,\mathrm{force}}S_{b,\mathrm{id}}\right)/c_r \sim \left(\alpha_{b,\mathrm{force}}S_{b,\mathrm{id}}+S_{bl,n}\right)} \tag{6.7c}$$

in which

$$\alpha_{b,\text{force}} = \left(\frac{Q_k E_b}{L_b f_y} - S_{bl,k}\right) \Big/ S_{b,\text{id}} \tag{6.8}$$

For multi-column systems anchored on both sides, substituting $S_{b,i} = 2S_{b,\text{id}} + S_{bl,i}$ into Eq. (4.24) gives

$$\mathbf{FQ} = \mathbf{D} \tag{6.9a}$$

$$\mathbf{F} = \begin{bmatrix} -\frac{c_l}{2S_{b,\text{id}}} - \frac{1}{2S_{b,\text{id}}+S_{bl,n+1}} + \frac{1}{S_{c,1}} & \frac{1}{S_{c,1}} & & & \\ -\frac{1}{S_{c,1}} & \frac{1}{2S_{b,\text{id}}+S_{bl,1}} + \frac{1}{S_{c,1}} + \frac{1}{S_{c,2}} & -\frac{1}{S_{c,2}} & & \\ & -\frac{1}{S_{c,2}} & \ddots & \ddots & \\ & & \ddots & \frac{1}{2S_{b,\text{id}}+S_{bl,n-1}} + \frac{1}{S_{c,n-1}} + \frac{1}{S_{c,n}} & -\frac{1}{S_{c,n}} \\ & & & -\frac{1}{S_{c,n}} & \frac{c_r}{2S_{b,\text{id}}} + \frac{1}{2S_{b,\text{id}}+S_{bl,n}} + \frac{1}{S_{c,n}} \end{bmatrix} \tag{6.9b}$$

$$\mathbf{Q} = \begin{Bmatrix} Q_{n+1} \\ Q_1 \\ \vdots \\ Q_{n-1} \\ Q_n \end{Bmatrix} \qquad \mathbf{D} = \begin{Bmatrix} \frac{Q_{0,1}}{S_{c,1}} \\ \frac{Q_{0,1}}{S_{c,1}} - \frac{Q_{0,2}}{S_{c,2}} \\ \vdots \\ \frac{Q_{0,n-1}}{S_{c,n-1}} - \frac{Q_{0,n}}{S_{c,n}} \\ \frac{Q_{0,n}}{S_{c,n}} \end{Bmatrix} \tag{6.9c}$$

Accordingly, the set of nonlinear equations regarding $\alpha_{b,\text{force}}$ for multi-column systems anchored on both sides considering the stiffness of solid blocking is

$$\frac{Q_{0,1} - Q_1 + Q_{n+1}}{S_{c,1}} - \frac{Q_{0,2} + Q_1 - Q_2}{S_{c,2}} = \frac{Q_1}{\alpha_{b,\text{force}} S_{b,\text{id}} + S_{bl,1}} \tag{6.10a}$$

$$\frac{Q_{0,i} + Q_{i-1} - Q_i}{S_{c,i}} - \frac{Q_{0,i+1} + Q_i - Q_{i+1}}{S_{c,i+1}} = \frac{Q_i}{\alpha_{b,\text{force}} S_{b,\text{id}} + S_{bl,i}} \qquad i = \{2, ..., n-1\} \tag{6.10b}$$

$$\frac{Q_{0,n} + Q_{n-1} - Q_n}{S_{c,n}} = \frac{Q_n}{\left(\alpha_{b,\text{force}} S_{b,\text{id}}\right)/c_r \sim \left(\alpha_{b,\text{force}} S_{b,\text{id}} + S_{bl,n}\right)} \tag{6.10c}$$

$$-\frac{Q_{0,1} + Q_{n+1} - Q_1}{S_{c,1}} = \frac{Q_{n+1}}{\left(\alpha_{b,\text{force}} S_{b,\text{id}}\right)/c_l \sim \left(\alpha_{b,\text{force}} S_{b,\text{id}} + S_{bl,n+1}\right)} \tag{6.10d}$$

in which

$$\alpha_{b,\text{force}} = \left(\frac{|Q_k| E_b}{L_b f_y} - S_{bl,k}\right) \Big/ S_{b,\text{id}} \tag{6.11}$$

Note that the brace forces can be negative if the system is anchored on both sides, indicating the braces are in compression, and thus the absolute value of Q_k should be

adopted in Eq. (6.11). As mentioned in Section 5.4, the built-in solver *fsolve* in MATLAB can be adopted to solve Eqs. (6.7) or Eqs. (6.10), with the initial values of Q_1 to Q_n being the solutions of Eqs. (6.5) or Eqs. (6.9). Once Q_k, i.e., the maximum brace force, is obtained, the brace stiffness scale factor associated with the strength requirement ($\alpha_{b,\text{force}}$) for multi-column systems considering the solid blocking can be computed via Eq. (6.11).

6.1.2 $\alpha_{b,\text{disp}}$ for multi-column systems with solid blocking

For multi-column systems anchored on one side in analysis, incorporating the stiffness of solid blocking into Eq. (5.15) yields:

$$\Delta_0 S_{c,1} = Q_{0,1} - (\Delta_0 - \Delta_2)\left(\alpha_{b,\text{disp}} S_{b,\text{id}} + S_{bl,1}\right) \tag{6.12a}$$

$$\Delta_2 S_{c,2} = Q_{0,i} + (\Delta_0 - 2\Delta_2 + \Delta_3)\left(\alpha_{b,\text{disp}} S_{b,\text{id}} + S_{bl,2}\right) \tag{6.12b}$$

$$\Delta_i S_{c,i} = Q_{0,i} + (\Delta_{i-1} - 2\Delta_i + \Delta_{i+1})\left(\alpha_{b,\text{disp}} S_{b,\text{id}} + S_{bl,i}\right) \qquad i = \{3, \ldots, n-1\} \tag{6.12c}$$

$$\Delta_n S_{c,n} = Q_{0,n} + (\Delta_{n-1} - \Delta_n)\left(\alpha_{b,\text{disp}} S_{b,\text{id}} + S_{bl,n-1}\right) - \Delta_n\left[\alpha_{b,\text{disp}} S_{b,\text{id}}/c_r \sim \left(\alpha_{b,\text{disp}} S_{b,\text{id}} + S_{bl,n}\right)\right] \tag{6.12d}$$

In this way, the brace stiffness scale factor satisfying the stiffness requirement ($\Delta_1 = \Delta_{\max} = \Delta_0$), $\alpha_{b,\text{disp}}$, considering the solid blocking stiffness can be obtained by solving Eqs. (6.12).

Once again, since the condition $\Delta_1 = \Delta_{\max}$ only applies to systems anchored on one side, an additional step is required for systems anchored on both sides: the location of the maximum displacement should be found by solving Eq. (4.18) with $S_{b,i} = 2S_{b,\text{id}} + S_{bl,i}$. Assume column k has the maximum displacement, then $\alpha_{b,\text{disp}}$ for multi-column systems anchored on both sides considering solid blocking can be attained by solving Eqs. (6.13).

$$\Delta_1 S_{c,1} = Q_{0,1} - (\Delta_1 - \Delta_2)\left(\alpha_{b,\text{disp}} S_{b,\text{id}} + S_{bl,1}\right) - \Delta_1\left[\alpha_{b,\text{disp}} S_{b,\text{id}}/c_l \sim \left(\alpha_{b,\text{disp}} S_{b,\text{id}} + S_{bl,n+1}\right)\right] \tag{6.13a}$$

$$\Delta_2 S_{c,2} = Q_{0,i} + (\Delta_1 - 2\Delta_2 + \Delta_3)\left(\alpha_{b,\text{disp}} S_{b,\text{id}} + S_{bl,2}\right) \tag{6.13b}$$

$$\Delta_i S_{c,i} = Q_{0,i} + (\Delta_{i-1} - 2\Delta_i + \Delta_{i+1})\left(\alpha_{b,\text{disp}} S_{b,\text{id}} + S_{bl,i}\right) \qquad i = \{3, \ldots, n-1\} \tag{6.13c}$$

$$\Delta_n S_{c,n} = Q_{0,n} + (\Delta_{n-1} - \Delta_n)\left(\alpha_{b,\text{disp}} S_{b,\text{id}} + S_{bl,n-1}\right) - \Delta_n\left[\alpha_{b,\text{disp}} S_{b,\text{id}}/c_r \sim \left(\alpha_{b,\text{disp}} S_{b,\text{id}} + S_{bl,n}\right)\right] \tag{6.13d}$$

in which

$$\Delta_k = \Delta_0 \tag{6.14}$$

6.1.3 Example with solid blocking

The system consisting of 23 cold-formed steel studs described in Section 4.4.1 is selected to investigate the effect of different solid blocking patterns on the bracing requirements. Assume the system is anchored on both sides. If the tie bracing in the system is capable of resisting both tension and compression forces, then the system can be simulated with anchored on both sides. However, if the braces are to be designed as tension-only, then only one side of the system is anchored in the analysis even though the system is actually anchored on both sides, which is to simulate that one of the anchors in compression will fail first. In accordance with the dimension of the stud section 250S137-54, the solid blocking is made of 250T125-54 with a cross-section area of 181.9 mm^2 (0.282 in^2).

In this example, since all the solid blocking patterns in the following analysis are assumed to be symmetrically placed about the centre of the system, plus all the tie bracing and column stiffness are uniform, removing either the left or right anchor will yield the same results. Based on this condition, assume the tie bracing adjacent to the left anchor will buckle first, and therefore the left anchor is removed in the analysis. The influences of the solid blocking associated with the location, interval, and flexible anchor on the bracing requirements for the multi-column system are investigated.

Effect of the location of solid blocking

In this case, for the purpose of investigating the effect of solid blocking's location on the ideal brace stiffness and bracing requirements, there is a pair of solid blocking symmetrically placed in the system, as shown in Fig. 6.4. It is assumed that the braces are capable of resisting both compression and tension forces and the system is rigidly anchored on both sides. Table 6.1 presents the analytical results regarding the ideal brace stiffness and required cross-sectional area of tie bracing for the system when the pair of solid blocking is placed at different locations. The results for the case without the solid blocking ("None") are also tabulated in Table 6.1 for comparison.

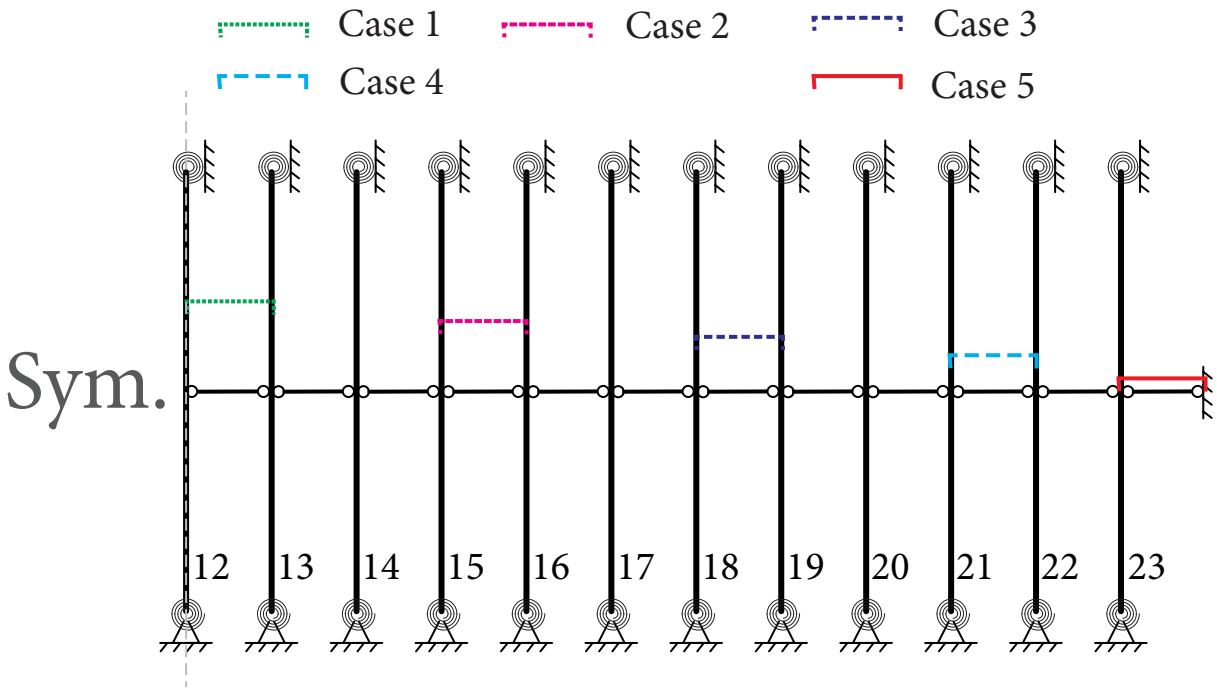

Figure 6.4: Different patterns of solid blocking with various locations

Table 6.1: Effect of the location of a pair of solid blocking on the bracing requirements for the 23-column system with braces being capable of resisting tension and compression forces

Case	$S_{b,\mathrm{id}}$ (N/mm)	$\alpha_{b,\mathrm{force}}$	$Q_{\max}$ (N)	$\alpha_{b,\mathrm{disp}}$	$\Delta_{\max}$ (mm)	$A_{b,\mathrm{op}}$ (mm^2)
None	2102.8	1.682	3667.1	3.047	2.4	38.50
1	2101.4	1.683	3666.0	3.036	2.4	38.34
2	2069.8	1.697	3640.5	3.019	2.4	37.55
3	1963.1	1.744	3548.5	3.060	2.4	36.10
4	1840.4	1.792	3419.8	3.125	2.4	34.56
5	1785.3	1.747	3234.1	3.103	2.4	33.30

In general, the optimum cross-sectional area of bracing $A_{b,\mathrm{op}}$ for all cases is controlled by the stiffness requirement as $\alpha_{b,\mathrm{disp}}$ is greater than $\alpha_{b,\mathrm{force}}$. As expected, the presence of solid blocking always reduces the ideal brace stiffness and requirements for tie bracing. It is worth noting that the ideal brace stiffness is greater as the solid blocking moves toward anchors. Although the brace stiffness scales factors, $\alpha_{b,\mathrm{disp}}$ and $\alpha_{b,\mathrm{force}}$, do not show monotonic variations with the change of the solid blocking location, the strength and stiffness requirements

of tie bracing (indicated by $Q_{\max}$ and $A_{b,\mathrm{op}}$, respectively) both decrease as the pair of solid blocking moves closer to the anchor. By comparing the results of the case without the solid blocking against those of Case 1, it can be seen that the pair of solid blocking located at the centre of the system reduces the ideal brace stiffness of tie bracing from 2102.8 N/mm to 2101.4 N/mm and reduces $\alpha_{b,\mathrm{disp}}$ from 3.047 to 3.036, resulting in an insignificant reduction of the required cross-sectional area of tie bracing from 38.50 mm^2 to 38.34 mm^2. While the solid blocking is placed adjacent to the anchor (Case 5), the resulting reduction for the ideal brace stiffness is 15% and for the required cross-sectional area of bracing is 13.5%. In all cases, the middle column has the maximum lateral displacement: $\Delta_{12} = \Delta_0 = 2.4$ mm in the calculation regarding $\alpha_{b,\mathrm{disp}}$. The maximum brace force $Q_{\max}$ occurs in the tie brace next to the anchor ($k = 23$) except for Case 5, where the maximum brace force is in the second tie brace from the right end ($k = 22$) as the solid blocking bears a part of the lateral force.

If the braces in the system are designed as tension-only, then only one anchor can be considered in the analysis [11]. In that case, the analytical results for all cases are shown in Table 6.2.

Table 6.2: Effect of the location of a pair of solid blocking on the bracing requirements for the 23-column system with tension-only braces

Case	$S_{b,\mathrm{id}}$ (N/mm)	$\alpha_{b,\mathrm{force}}$	$Q_{\max}$ (N)	$\alpha_{b,\mathrm{disp}}$	$\Delta_{\max}$ (mm)	$A_{b,\mathrm{op}}$ (mm^2)
None	8055.9	1.3420	11208.0	3.0479	2.4	147.564
1	7534.2	1.3760	10747.1	3.1068	2.4	140.675
2	7529.4	1.3757	10738.7	3.1085	2.4	140.662
3	7522.6	1.3737	10712.9	3.1109	2.4	140.643
4	7518.3	1.3696	10674.8	3.1123	2.4	140.626
5	7516.2	1.3587	10586.8	3.1128	2.4	140.611

Assume the system bends towards the left and the brace adjacent to the left anchor fails in compression. By doing so, the left anchor and its adjacent brace are removed from the analysis model, and consequently only one solid blocking is placed in Case 5. In all cases, the cross-section area of tie bracing is controlled by the stiffness requirement. As the pair of solid blocking moves far away from the middle of the system, the ideal brace stiffness of the

tie bracing $S_{b,\mathrm{id}}$ and the required cross-sectional area of tie bracing $A_{b,\mathrm{op}}$ decrease. However, compared to the cases anchored on both sides, the discrepancies of $A_{b,\mathrm{op}}$ due to different solid blocking locations are negligible. Even though Case 5 only has one solid blocking, the corresponding stiffness requirement ($A_{b,\mathrm{op}}$) is less than that of Case 4, while the strength requirement (Q_{max}) is greater than that of Case 4. Similar to the observations found in cases in which the analytical model is anchored on both sides, the strength requirement is governed by force in the second brace from the end ($k = 22$) in Case 5 and by force in the brace closest to the anchor ($k = 23$) in other cases. In general, considering the presence of a pair of solid blocking approximately decreases the optimum required cross-sectional area of tie bracing by 5% for the system anchored on one side (tension-only braces).

Overall, considering the solid blocking will decrease the ideal brace stiffness $S_{b,\mathrm{id}}$ and optimum required cross-sectional area of tie bracing $A_{b,\mathrm{op}}$ for a multi-column system, as expected. In addition, it is found that the solid blocking will have a larger impact on $S_{b,\mathrm{id}}$ and $A_{b,\mathrm{op}}$ if the solid blocking is placed farther away from the centre of the system. If the system can be simulated as anchored on both sides, the presence of solid blocking has a larger influence on $A_{b,\mathrm{op}}$ and the differences of $A_{b,\mathrm{op}}$ due to different solid blocking locations are more pronounced compared to the cases in which the system should be simulated as anchored on one side. This can be attributed to the following reason. For a multi-column system, the ideal brace stiffness and corresponding bracing stiffness requirement can be significantly reduced if one more anchor is added. Consequently, the ratio of solid blocking stiffness to required brace stiffness in cases with two anchors is considerably greater than that with one anchor. Therefore, the solid blocking will have a larger impact on the multi-column system's bracing requirements if the system can be simulated as anchored on both sides.

Effect of different solid blocking spacing

In practice, solid blocking is spaced intermittently with a solid blocking always being placed next to the anchor. Hence, four cases with different solid blocking spacing, as illustrated in Fig. 6.5, are analyzed in this subsection. If the system is anchored on both sides in the analysis and the braces are capable of resisting both tension and compression forces, the results are tabulated in Table 6.3.

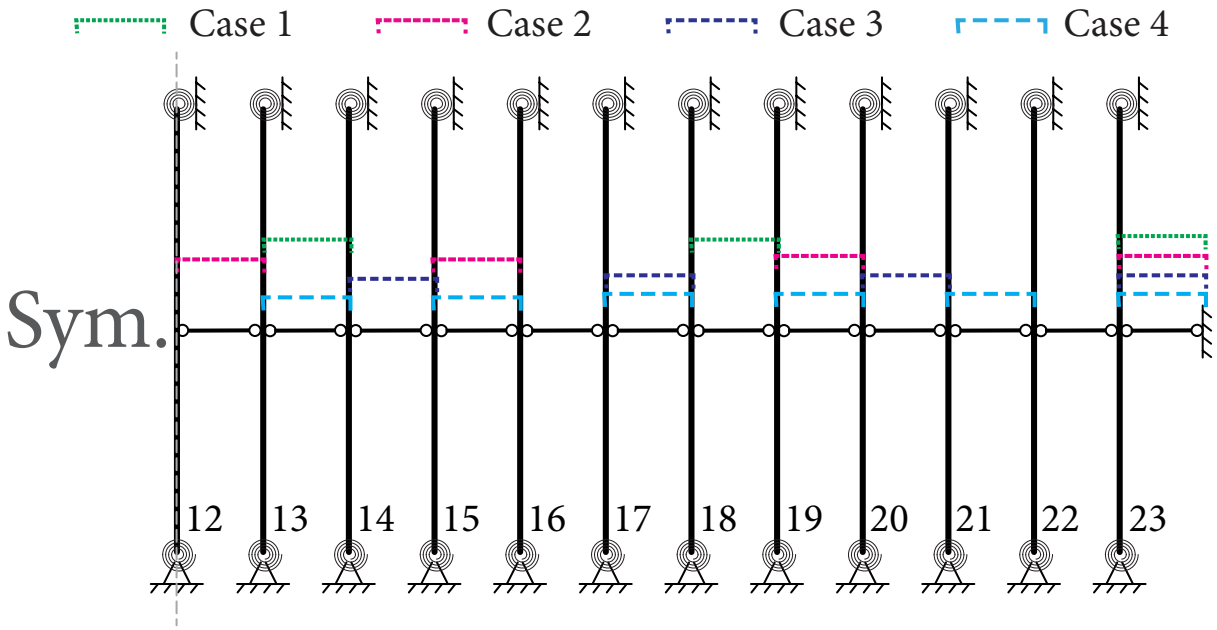

Figure 6.5: Different patterns and spacing of solid blocking

Table 6.3: Effect of the solid blocking spacing on the bracing requirements for the 23-column system with braces capable of resisting tension and compression forces

Case	$S_{b,\mathrm{id}}$ (N/mm)	$\alpha_{b,\mathrm{force}}$	$Q_{\max}$ (N)	$\alpha_{b,\mathrm{disp}}$	$\Delta_{\max}$ (mm)	$A_{b,\mathrm{op}}$ (mm^2)
None	2102.8	1.682	3667.1	3.047	2.4	38.50
1	1578.0	1.866	3052.1	3.122	2.4	29.61
2	1479.4	1.930	2960.6	3.140	2.4	27.92
3	1324.4	2.049	2813.6	3.189	2.4	25.39
4	1005.9	2.409	2511.6	3.261	2.4	19.71

Once again, the optimum required cross-sectional areas of tie bracing obtained from the proposed method are controlled by the stiffness requirement for all five cases. As the spacing of solid blocking reduces, the ideal brace stiffness of tie bracing $S_{b,\mathrm{id}}$ decreases. Because of that, the brace stiffness scale factors associated with the strength and stiffness requirements, $\alpha_{b,\mathrm{force}}$ and $\alpha_{b,\mathrm{disp}}$, increase as the solid blocking spacing decreases. Overall, the magnitude of required strength ($Q_{\max}$) and stiffness ($A_{b,\mathrm{op}}$) of tie bracing reduce as the solid blocking spacing decreases. This is because the presence of solid blocking always enhances the total stiffness of the multi-column system, and such enhancement increases as the spacing of

solid blocking decreases. In fact, the number of solid blocking is the same in Case 2 and Case 3, whereas the $S_{b,\text{id}}$ and $A_{b,\text{op}}$ for Case 3 are less than those for Case 2 because of closer solid blocking spacing near the anchor in Case 3. This confirms the conclusion drawn in the previous subsection that the farther the solid blocking is to the centre of the system (or closer to the anchor), the larger impact it has on the bracing requirements for multi-column systems. It can be observed that the contribution of solid blocking to bracing requirements can be significant. Even for Case 1 in which there are six solid blocking, considering the presence of solid blocking results in 23% reduction of the required cross-sectional area of tie bracing $A_{b,\text{op}}$ from 38.5 mm^2 to 29.61 mm^2. When the solid blocking spacing reduces to one column spacing as per Case 1, the corresponding reduction of $A_{b,\text{op}}$ is 49% from 38.5 mm^2 to 19.71 mm^2.

For comparison purposes, the results obtained by assuming only one anchor located at the right end of the system (tension-only braces) are presented in Table 6.4. It can be seen that the ideal brace stiffness and bracing requirements decrease as the number of solid blocking increases. The differences of $S_{b,\text{id}}$ and $A_{b,\text{op}}$ for Case 2 and Case 3 are almost unnoticeable compared to the results associated with two anchors.

Table 6.4: Effect of the solid blocking spacing on the bracing requirements for the 23-column system with tension-only braces

Case	$S_{b,\text{id}}$ (N/mm)	$\alpha_{b,\text{force}}$	$Q_{\max}$ (N)	$\alpha_{b,\text{disp}}$	$\Delta_{\max}$ (mm)	$A_{b,\text{op}}$ (mm^2)
None	8055.9	1.155	9644.8	3.048	2.4	147.56
1	6393.5	1.442	9559.5	3.273	2.4	125.75
2	5808.1	1.500	9030.7	3.372	2.4	117.71
3	5803.5	1.493	8983.9	3.374	2.4	117.69
4	4556.7	1.658	7834.6	3.650	2.4	99.94

Effect of flexible anchor

The effect of solid blocking on the optimum required cross-sectional area of tie bracing considering the flexible anchor is investigated in this subsection. Different flexible anchors are considered by varying the ratio of tie bracing stiffness to the anchor stiffness, c. If $c = 0$,

it means the system is rigidly anchored. Since the differences between cases anchored on one side and anchored on both sides have been investigated previously, only the cases with two anchors are considered in this subsection. The ratios of tie bracing stiffness to the right anchor and left anchor are presumed as the same, $c_r = c_l = c$. Assume the flexible anchor is an unloaded column with the same height and material as other studs. Thus, the moment of inertia of the end column on both sides are

$$I_{an} = \frac{A_{b,\text{op}} E_b}{c L_b} \frac{L_c^3}{48 E_c} \tag{6.15}$$

The results regarding the optimum cross-section area of tie bracing for the multi-column system with and without solid blocking (case 4) are obtained from the proposed method to illustrate the effects of solid blocking on the bracing requirements with different values of c, as tabulated in Table 6.5.

Table 6.5: Effect of ratios of tie bracing stiffness to anchor stiffness on the bracing requirements for the 23-column system with braces capable of resisting tension and compression forces

c	Solid blocking	$S_{b,\text{id}}$ (N/mm)	$\alpha_{b,\text{force}}$	$Q_{\max}$ (N)	$\alpha_{b,\text{disp}}$	$\Delta_{\max}$ (mm)	$A_{b,\text{op}}$ (mm^2)	I_{an} 10^6 mm^4	$\frac{A_{b,\text{op}}(\text{with } S_{bl})}{A_{b,\text{op}}(\text{without } S_{bl})}$ %
0	None	2102.8	1.682	3667.1	3.047	2.4	38.50	Infinity	
0	Case 4	1005.9	2.409	2511.6	3.261	2.4	19.71	Infinity	51.2
10	None	6026.2	1.258	7861.2	2.843	2.4	102.96	4.86	
10	Case 4	5106.3	1.291	6834.7	2.907	2.4	89.21	4.21	86.6
30	None	14248.2	1.110	16401.4	2.734	2.4	234.11	3.68	
30	Case 4	13529.3	1.109	15549.7	2.768	2.4	225.07	3.54	96.1
50	None	22510.0	1.070	24968.7	2.702	2.4	365.57	3.45	
50	Case 4	21912.3	1.067	24230.9	2.725	2.4	358.80	3.39	98.1

It can be seen that the ideal brace stiffness $S_{b,\text{id}}$ and required cross-sectional area $A_{b,\text{op}}$ of tie bracing increase as the ratio c increases because a larger value of c corresponds to a more flexible anchor, which needs stiffer braces. Accordingly, the required stiffness of the flexible anchor (I_{an}) decreases as the value of c increases. On the other hand, the brace

stiffness scale factor associated with strength and stiffness requirements decreases as the ratio c increases. When $c = 10$, considering the contribution of the solid blocking could still considerably reduce the required stiffness of tie bracing and anchor (represented as $A_{b,\text{op}}$ and I_{an}, respectively) by 13.4%. Nevertheless, the reduction of $A_{b,\text{op}}$ associated with the solid blocking decreases as the value of c increases, indicating that the influence of solid blocking dwindles as c increases. This can be attributed to the decreasing ratio of solid blocking stiffness to tie bracing stiffness.

6.2 Optimum Ideal Brace Stiffness

So far, the analyses presented in this thesis involving the ideal brace stiffness presuppose a uniform brace pattern in which the stiffness is the same for all tie braces. This section introduces the concept of nonuniform bracing patterns in that the stiffness of each brace in a system can vary independently to satisfy the ideal brace stiffness requirement. Thereby, the determination of the ideal brace stiffness of a system with nonuniform bracing involves not only one but n variables. In this way, there are numerous solutions to ideal brace stiffness that can satisfy Eq. (4.20). Hence, criteria for identifying the most appropriate bracing pattern are necessary. For example, the minimum steel consumption can be used as the objective for economical purposes. As such, a problem is proposed to determine the optimum bracing stiffness pattern for minimum bracing steel consumption and can be mathematically described as follows:

$$\text{minimize} \left\{ f = \sum A_{b,i} L_{b,i} = \sum \frac{S_{b,\text{id},i} L_{b,i}^2}{E_b} \right\} \tag{6.16a}$$

$$\text{Subjected to } \det[K] = 0 \tag{6.16b}$$

$$S_{b,\text{id},i} > 0 \tag{6.16c}$$

where the ideal brace stiffness $S_{b,\text{id},i}$ of each tie bracing is the variable to be determined by solving the optimization problem stated in Eqs. (6.16). The objective function in Eq. (6.16a) corresponds to the minimum steel consumption of braces, as calculated by the sum of each brace's volume.

Aiming to find the minimum of a constrained nonlinear multi-variable function, *fmincon* solver in the Optimization Toolbox in MATLAB can be used to address the problem shown in

Eqs. (6.16), in which Eq. (6.16a) is the objective function, Eq. (6.16b) is the nonlinear equality constraint, and Eq. (6.16c) represents the lower bound of the variables $S_{b,\mathrm{id},i}$. The default algorithm, *interior-point*, in *fmincon* solver is selected and is found to be feasible for finding the minimum value of the function in Eq. (6.16a). The ideal brace stiffness associated with the uniform bracing pattern is taken as the initial points of $S_{b,\mathrm{id},i}$.

6.2.1 Optimum nonuniform bracing for minimum stiffness

For systems with nonuniform column lateral stiffness, it is not likely to derive the general solutions to $S_{b,\mathrm{id},i}$, which vary on the different column section properties, applied axial loads, and boundary conditions. For a multi-column system with uniform column lateral stiffness, its ideal brace stiffness associated with the uniform bracing pattern can be expressed as $a_{\max}S_{b,\mathrm{ids}}$, in which $S_{b,\mathrm{ids}}$ is the ideal brace stiffness for the single column in the system and $a_{\max}$ is the ratio of the ideal brace stiffness for multiple columns to that of a single column. It has been shown in Chapter 4 that the value of $a_{\max}$ can be obtained by finding the maximum roots of Eq. (4.20) and only relates to the number of columns and the number of anchors; in other words, if the number of columns and the number of anchors are known, the solution of $a_{\max}$ is unique. Therefore, this section investigates solutions of ideal brace stiffness associated with nonuniform bracing patterns for systems with uniform column lateral stiffness.

If a system consists of multiple columns that have uniform lateral stiffness, and are evenly spaced and rigidly anchored, as the length of all braces is the same, the objective function in Eq. (6.16a) becomes

$$\text{minimize } \left\{\sum S_{b,\mathrm{id},i}\right\} \tag{6.17}$$

By doing so, the objective of the optimization problem is to find the minimum total brace stiffness $\Sigma S_{b,\mathrm{id},i}$, and the final solution is referred to as the optimum nonuniform bracing with minimum total stiffness. Following the procedure by Ziemian and Ziemian [5] on a multi-column system with uniform column lateral stiffness, by substituting the scale factor, $a_i = -S_{b,i}/S_{c,\mathrm{cr}}$, into Eq. (4.20), $S_{b,i}$ and $S_{c,\mathrm{cr}}$ are eliminated. $S_{c,\mathrm{cr}}$ is the lateral stiffness of the half-length column with the applied load being the critical buckling load, $P = P_{cr}$. In

consequence, the problem of finding the minimum total brace stiffness becomes

$$\text{minimize } \{f = \sum a_i\} \tag{6.18a}$$

$$\text{Subjected to } \det[K(a_i)] = 0 \tag{6.18b}$$

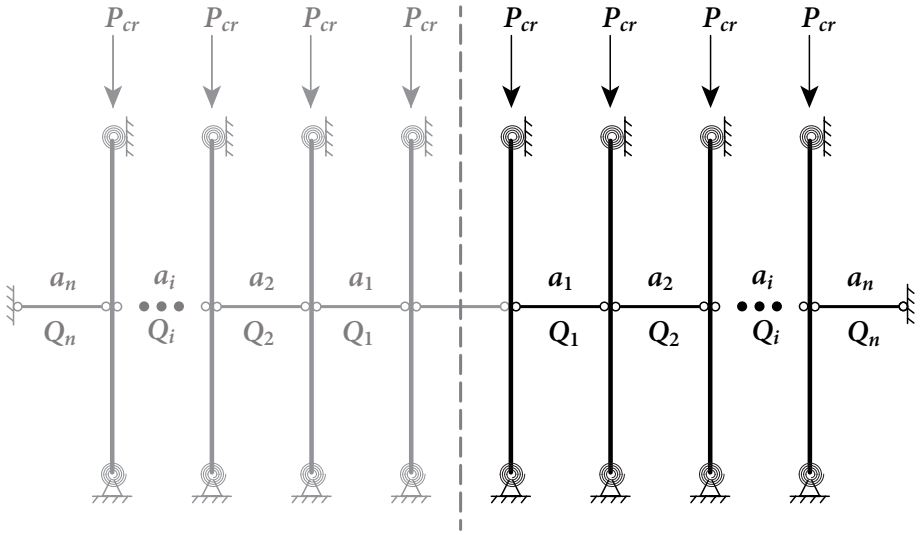

Figure 6.6: Optimum nonuniform bracing pattern for systems anchored on one side and systems anchored on both sides with an even number of columns

The ideal brace stiffnesses in such cases can be obtained by finding the maximum solution of a_i satisfying Eq. (6.18a). For systems anchored on one side in analysis, the maximum solutions of a_i for different numbers of columns n are tabulated in Table 6.6, in which $a_{\max}$ corresponds to the scale factor associated with the uniform bracing pattern and is obtained from Eq. (4.34). The locations of $S_{b,i}$ are shown in Fig. 6.6. Compared to the uniform bracing pattern, the optimum nonuniform bracing pattern possesses a lower total brace stiffness, and the reduction of total brace stiffness from uniform bracing pattern to optimum nonuniform bracing pattern increases as the number of columns increases. Particularly, the closer the brace is to the anchored side, the greater ideal brace stiffness is required.

Table 6.6: Optimum nonuniform bracing pattern for a system anchored on one side

n	Uniform bracing		Optimum nonuniform bracing								Reduction of the total stiffness
	$a_{\max}$	$na_{\max}$	a_1	a_2	a_3	a_4	a_5	a_6	a_7	Σa_i	$1-\Sigma a_i/(Na_{\max})$
2	2.62	5.24	2	3						5	4.5%
3	5.05	15.15	3	5	6					14	7.6%
4	8.29	33.16	4	7	9	10				30	9.5%
5	12.34	61.72	5	9	12	14	15			55	10.9%
6	17.20	103.21	6	11	15	18	20	21		91	11.8%
7	22.88	160.16	7	13	18	22	25	27	28	140	12.6%

The general expression of a_i for multi-column system anchored on one side in analysis is:

$$a_i = in - i(i-1)/2 \tag{6.19}$$

If a system with an even number of columns is anchored by both sides, it can be equivalently divided by two parts at the centre brace, as shown in Fig. 6.6. In that case, the ideal brace stiffnesses of each part are the same as those of a system consisting of $n/2$ columns and anchored on one side, and the ideal brace stiffnesses of the two parts have a mirror relationship. Theoretically, the stiffness of the middle brace can be arbitrarily determined since there is no brace force in it, as mentioned in Chapter 4. Consequently, the results in Table 6.6 also apply to the system that can be simulated as anchored on both sides and consists of an even number of columns, as per Fig. 6.6.

With the bracing scale factor α_b taken as 2.0, as per AISC 360-16 [10] and AISI S100-16 [11], the brace forces in the multi-column system in Fig. 6.6 associated with the optimum nonuniform bracing pattern are obtained from Eq. (4.22), as tabulated in Table 6.7. q_i represents the ratio of the force in ith brace Q_i to the equivalent lateral force, Q_0, induced by the initial imperfection Δ_0 and applied axial load P_i, as given in Eq. (4.10). Compared to the uniform bracing, adopting the optimum nonuniform bracing yields a smaller magnitude of the maximum brace force, as indicated by q_n in Table 6.7. The reduction of q_n increases as the number of columns increases, thus leading to a smaller strength requirement for brace n. However, it is worth noting that the forces in the braces far away from the anchor

associated with the optimum nonuniform bracing could be greater than those associated with the uniform bracing, e.g., q_1 and q_2 in the case with $n = 5$. This is because the brace stiffness in the optimum nonuniform bracing pattern decreases as the brace moves farther away from the anchor. As such, the stiffness requirements for the braces far away from the anchor decrease but the strength requirements increase. Consequently, the strength requirement for these braces may govern the design.

Table 6.7: Comparison of brace forces between uniform and optimum nonuniform bracing patterns for systems anchored on one side

n	Pattern	q_1	q_2	q_3	q_4	q_5	q_6	q_7	Reduction of q_n (%)
2	Uniform	4.32	7.81						
2	Optimum	4.36	7.64						2.17
3	Uniform	4.41	8.38	11.52					
3	Optimum	4.51	8.28	11.21					2.69
4	Uniform	4.45	8.62	12.28	15.19				
4	Optimum	4.60	8.62	12.02	14.76				2.83
5	Uniform	4.46	8.75	12.68	16.09	18.86			
5	Optimum	4.65	8.83	12.52	15.69	18.30			2.97
6	Uniform	4.48	8.82	12.91	16.62	19.86	22.51		
6	Optimum	4.68	8.98	12.86	16.32	19.32	21.84		2.98
7	Uniform	4.48	8.87	13.06	16.96	20.50	23.59	26.16	
7	Optimum	4.71	9.08	13.11	16.76	20.04	22.92	25.37	3.02

For systems with an odd number of columns anchored on both sides, as illustrated in Fig. 6.7, the results of a_i associated with the optimum bracing are shown in Table 6.8. Similar to the results in Table 6.6, the braces being rigidly anchored possess the maximum ideal stiffness in the optimum nonuniform bracing pattern. As the brace becomes far away from the anchor, its ideal stiffness decreases.

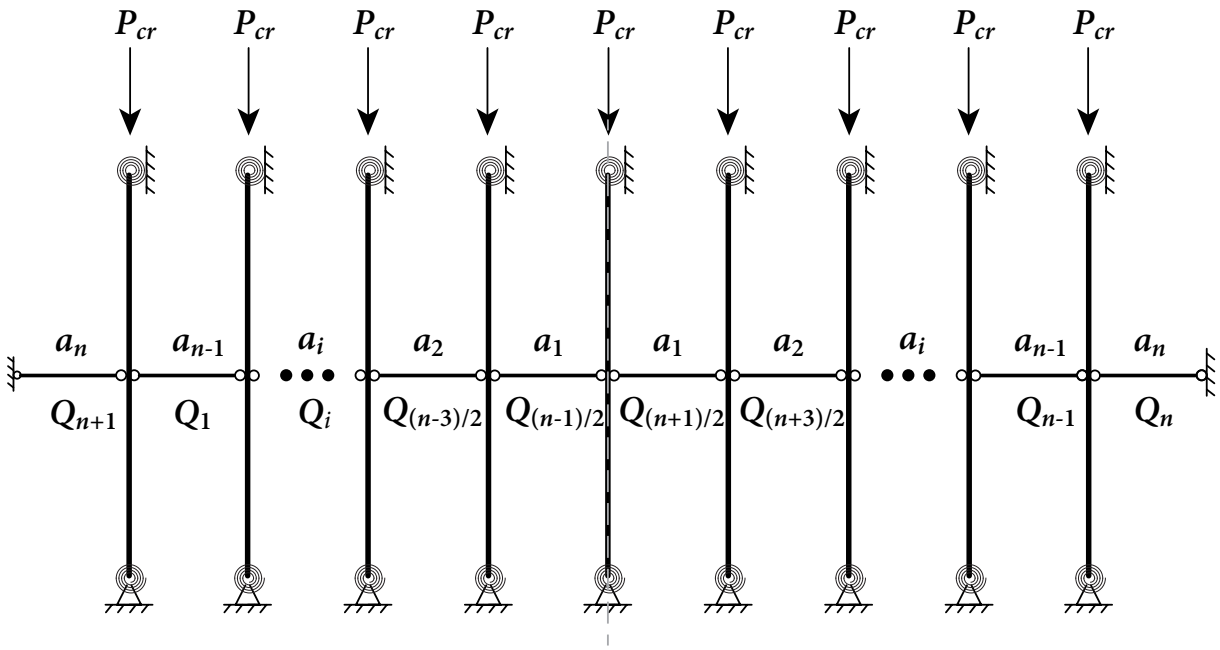

Figure 6.7: Optimum bracing nonuniform pattern for system anchored on one side or system anchored on both sides with an odd number of columns

Table 6.8: Optimum nonuniform bracing for systems anchored on both sides

n	Uniform bracing		Optimum nonuniform bracing								Total stiffness reduction
	$a_{\max}$	$(n+1)a_{\max}$	a_1	a_2	a_3	a_4	a_5	a_6	a_7	Σa_i	$1-\Sigma a_i/[(n+1)a_{\max}]$
3	1.71	6.83	1	2						6	12.1%
5	3.73	22.39	1.5	3.5	4.5					19	15.2%
7	6.57	52.55	2	5	7	8				44	16.3%
9	10.22	102.16	2.5	6.5	9.5	11.5	12.5			85	16.8%
11	14.67	176.09	3	8	12	15	17	18		146	17.1%
13	19.94	279.20	3.5	9.5	14.5	18.5	21.5	23.5	24.5	231	17.3%

The general expression of a_i for systems anchored on both sides in the analysis is:

$$a_i = \frac{1}{2}\left[\left(\frac{n+1}{2}\right)^2 - \left(\frac{n+1}{2} - i\right)\left(\frac{n+1}{2} + 1 - i\right)\right] \tag{6.20}$$

With $\alpha_b = 2$, the brace forces in the multi-column system in Fig. 6.7 associated with the optimum nonuniform bracing pattern are obtained from Eq. (4.24), as tabulated in Table 6.9. Similar to the observations from Table 6.7 for systems anchored on one side in the analysis,

adopting the optimum nonuniform bracing yields a smaller magnitude of the maximum brace force than adopting the uniform bracing. However, the reduction of q_n decreases as the number of columns increases, showing an opposite trend to that observed for systems anchored on one side in the analysis.

Table 6.9: Comparison of brace forces between uniform and optimum nonuniform bracing for systems anchored on both sides

n	Pattern	From $q_{(n+1)/2}$ to q_n							Reduction of q_n (%)
3	Uniform	2.19	5.92						
3	Optimum	2.29	5.71						3.51
5	Uniform	2.22	6.37	9.67					
5	Optimum	2.36	6.30	9.34					3.42
7	Uniform	2.24	6.54	10.34	13.36				
7	Optimum	2.39	6.58	10.11	12.92				3.29
9	Uniform	2.24	6.62	10.67	14.19	17.03			
9	Optimum	2.41	6.74	10.56	13.82	16.48			3.23
11	Uniform	2.25	6.66	10.84	14.66	17.98	20.68		
11	Optimum	2.42	6.85	10.85	14.40	17.47	20.02		3.19
13	Uniform	2.25	6.68	10.95	14.95	18.57	21.72	24.33	
13	Optimum	2.42	6.92	11.05	14.80	18.16	21.08	23.57	3.12

6.3 Conclusions

This chapter primarily investigates the effect of solid blocking on the bracing requirements, and the ideal brace stiffness associated with the nonuniform bracing pattern for multi-column systems. The following conclusions are drawn:

1. With the consideration of the presence of solid blocking, the formulae for evaluating the ideal brace stiffness of tie bracing, brace stiffness scale factor satisfying the strength and stiffness requirements, $\alpha_{b,\text{force}}$ and $\alpha_{b,\text{disp}}$, are proposed.

2. An example of a 23-column system is presented to investigate the effect of solid blocking on the bracing requirements. According to the predictions from the proposed method, it is verified that considering the solid blocking will always reduce the ideal brace stiffness and the bracing requirements for tie bracing in multi-column systems. The following are how the effects of the solid blocking on ideal brace stiffness and bracing requirements for tie bracing vary with different solid blocking locations and spacing, and rigidity of anchors. First, the ideal brace stiffness and bracing requirements decrease as the solid blocking is located closer to the anchor. Second, the solid blocking has a larger impact on the ideal brace stiffness and bracing requirements if the multi-column system is anchored on both sides instead of one side in the analysis. Third, the ideal brace stiffness and bracing requirements decrease as the spacing of solid blocking reduces. Fourth, the influence of solid blocking on the ideal brace stiffness and bracing requirements decreases as the ratio of tie bracing stiffness to anchor stiffness increases, i.e., as the anchor becomes more flexible.

3. An optimization problem is proposed to minimize the total bracing stiffness for nonuniform bracing. For systems with uniform column lateral stiffness, the solutions of ideal brace stiffnesses having the minimum total bracing stiffness, referred to as the optimum nonuniform bracing, are presented. It is found that the optimum nonuniform bracing has a pattern of stiffness that the brace stiffness increases as the brace is closer to the anchor. With the same brace stiffness scale factor ($\alpha_b = 2.0$), the maximum brace force in the multi-column system obtained by adopting the optimum nonuniform bracing pattern is less than that obtained by adopting the uniform bracing.

Chapter 7

Evaluating Column Deflection at Elevated Temperatures Considering Creep Effect

The foregoing research in this thesis regarding the bracing design for multi-column systems is limited to the analysis at the ambient temperature. Nowadays, as fire analysis has become an inseparable part of steel structural design, it is necessary to extend the proposed method to evaluate the fire resistance of braced multi-column systems. A numerical method is proposed in this chapter to evaluate the column's mid-height deflection at elevated temperatures considering the nonlinear stress-strain relationships and thermal creep effect. In particular, the proposed method aims to investigate the creep buckling behaviour of steel columns at elevated temperatures.

In practice, the steel members are required to be protected with insulation to acquire higher fire resistance. Steel columns, as primary load-bearing components in steel structures, often require two hours of fire resistance or more in practice [74]. Provided the creep effect is ignored, the heating rate will not affect the critical temperatures of steel members. However, for a steel structure subjected to a long fire exposed duration, creep strains develop as the increase of time, which consequently reduces stiffness and increases deformations of columns, leading to a premature failure of the structure. Therefore, the adverse effect of creep on steel columns at elevated temperatures has attracted researchers' attention in recent years.

Despite the fact that extensive studies [72, 73, 75, 82, 88, 97] have been carried out to assess the steel column's fire-structural response with the consideration of thermal creep

effects, it is hard to gauge the accuracy of the techniques of incorporating the creep effect adopted in these studies. For that reason, the creep buckling tests are the best resource to verify a proposed method that can accurately assess the creep effect on steel columns. The creep buckling tests [83] were carried out to solely observe the creep-induced deflection of steel columns at a constant load and elevated temperature levels, thus providing referential results to verify a proposed method that can accurately assess the creep effect on steel columns. In this section, a numerical method is proposed to predict the creep-induced lateral deflection of steel columns at elevated temperatures by tracing the variations of the cross-sectional stress and strain distributions. Verified against the creep buckling tests on steel columns at elevated temperature, the proposed method reveals the failure mechanism of column's creep buckling that the lateral deflection associated with the creep effect of an axially loaded steel column at elevated temperatures is initiated by the gradient of stress and strain distributions on the cross-section of the column.

7.1 Beam Deflection Analysis by Harmathy [108]

Harmathy [108] proposed a method to evaluate the deflection of a simply-supported beam subjected to a concentrated load at mid-span at elevated temperatures considering the creep effect. A brief summary of Harmathy's method [108] is presented below for the purpose of the development of the proposed method for predicting the mid-height lateral deflection of a steel column with consideration of the creep effect at elevated temperatures.

In Harmathy's model, the mid-span cross-section of a steel beam is divided into n strips, in which two strips are located in each flange, and the rest of $n-4$ strips are in the web, as shown in Fig. 7.1. The heating time is also divided into a series of time steps, and the stress and strain of each strip can be calculated through Eqs. (7.1).

$$\varepsilon_i^j = a^j Z_i^j + b^j \tag{7.1a}$$

$$\varepsilon_i^j = f\left(\sigma_i^j\right) \tag{7.1b}$$

$$\sum_{i=1}^{n} \sigma_i^j A_i^j = 0 \tag{7.1c}$$

$$\sum_{i=1}^{n} \sigma_i^j A_i^j (Z_i^j - H/2) = M \tag{7.1d}$$

where the subscript i and superscript j are employed to identify the strip and time step, respectively; σ and ε are the normal stress and strain, respectively. A is the cross-sectional area; Z is the distance from the centroid of a strip to the extreme fibre of the bottom flange; H is the overall depth of the beam; and M is the internal bending moment at mid-span. Eq. (7.1a) is based on Euler-Bernoulli's hypothesis, where a and b are parameters associated with the linear strain distribution of the cross-section.

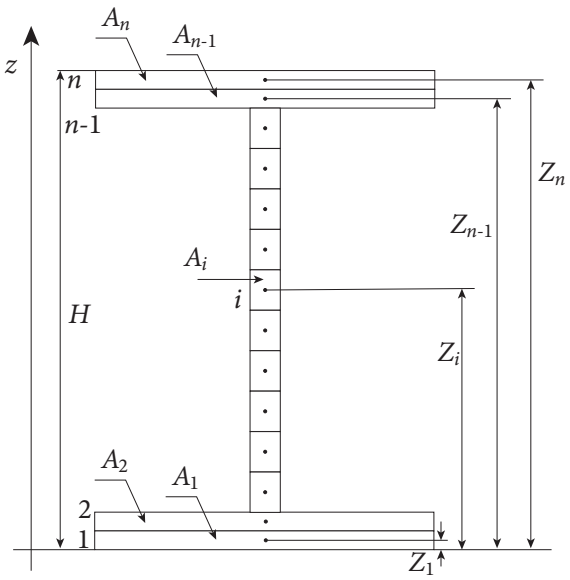

Figure 7.1: Beam mid-span cross-section model proposed by Harmathy [108]

At elevated temperatures, total strain ε consists of three components: the instantaneous mechanical strain ε_{st} induced by the stress, the thermal strain ε_{th} corresponding to thermal expansion, and creep strain ε_{cp}, as expressed in Eq. (7.2).

$$\varepsilon_i^j = (\varepsilon_{\text{st}})_i^j + (\varepsilon_{\text{th}})_i^j + \left(\varepsilon_{\text{cp}}\right)_i^j \tag{7.2a}$$

$$(\varepsilon_{\text{st}})_i^j = \frac{\sigma_i^j}{(E_T)_i^j} \tag{7.2b}$$

where E_T is the elastic modulus at elevated temperature.

Note that Harmathy assumes the relationships between the instantaneous strain and stress at elevated temperatures to be perfectly linear, as given in Eq. (7.2b). The thermal strain can be calculated based on the temperature and corresponding thermal expansion coefficient. Then the strain of each strip at the same time step can be calculated from Eq. (7.1a). As the creep strain rate is highly related to the stress and temperature, creep

strains at each time step vary with the changing stress distribution at elevated temperatures. The transcendental relationship in Eq. (7.1a) makes the equation difficult to be solved at the same step. Therefore, an iterative procedure is adopted such that the creep strain at time $t = j$ can be calculated through the stress and temperature distributions at the previous time step $t = j-1$, and the total creep strain is obtained from the accumulation of creep strains at previous time steps. This iterative approach is shown in Eqs. (7.3).

$$\left(\varepsilon_{\mathrm{cp}}\right)_i^j = \left(\varepsilon_{\mathrm{cp}}\right)_i^{j-1} + \left(\Delta\varepsilon_{\mathrm{cp}}\right)_i^j \tag{7.3a}$$

$$\left(\Delta\varepsilon_{\mathrm{cp}}\right)_i^j = f\left(T_i^{j-1}, \sigma_i^{j-1}\right) \tag{7.3b}$$

Considering that creep strains are not presented in the first step of calculating σ_i^0, ε_i^0, Eqs. (7.1) contain $2n+2$ variables ($n\sigma_i, n\varepsilon_i, a$ and b) and $2n+2$ equations, in which Eq. (7.1a) and Eq. (7.1b) consist of n equations, respectively. The general solutions of the coefficients, a and b, at each time j can be obtained by solving Eqs. (7.1). Once the strain distribution is obtained, the mid-span beam deflection Δ^j can be calculated as given in Eq. (7.4).

$$\Delta^j = \frac{L^2}{\pi^2}\frac{\varepsilon_1^j - \varepsilon_n^j}{Z_n - Z_1} \tag{7.4}$$

The derivation of Eq. (7.4) for calculating the beam deflection through strain difference on the cross-section is represented in the Appendix B.

7.2 Proposed Method of Evaluating Column Lateral Deflection at Elevated Temperatures Considering Creep Effect

The method established by Harmathy [108] accounts for the effects of the creep and cross-sectional temperature gradients by adopting the Euler-Bernoulli beam theory. However, the general solutions of coefficients a^j and b^j in Eq. (7.1a) are derived based on the assumption that the stress-strain relationships of steel are perfectly elastic at elevated temperatures and the yield strength reductions of steel at elevated temperatures are not considered. Apparently, neglecting inelastic deformations and yield stress reductions at elevated temperatures may lead to an underestimation of the deflection.

The assumption in Harmathy's method is adopted that the maximum deflection of a steel member can be derived according to the difference between the strains of the extreme fibre

of flanges at the location of the maximum moment. The method is extended to evaluate the mid-height deflection of steel columns at elevated temperatures. The sinusoidal function is taken as the deformed shape of the column at elevated temperatures. Different from the beam at elevated temperatures in which the bending moment at mid-span remains unchanged as there is no interaction of applied load and the deflection, the bending moment at mid-height of a column is induced by the interaction of axial load and lateral deflection, i.e., the second-order effect. Thus, the increased deflection associated with stiffness deterioration resulting from the elevated temperature will amplify the second-order effect. Therefore, the equilibrium conditions expressed in Eqs. (7.1a) need to be updated at each time step based on the deflection obtained from the previous step. Besides updating the equilibrium equations in each time step, nonlinear stress-strain relationships are incorporated to characterize the material behaviour of steel at elevated temperatures. The following is the proposed procedure to predict the lateral deflection of an unrestrained steel column subjected to elevated temperatures.

1. Specify the geometric parameters of the column section, column length L, elastic modulus E_0, and yield strength $f_{y,0}$ of steel at ambient temperature. Specify the creep model and stress-strain relationships of steel at elevated temperatures.

2. Input the axial load P applied on the column and the initial out-of-straightness of column Δ_0.

3. Divide the column mid-height cross-section into n strips and calculate the area of each strip A_i and the distance Z_i from the centroid of each strip to the bottom.

4. Input the corresponding heating curve of each strip. Let time step $j = 1$.

5. Calculate the elastic modulus E_T, yield strength f_{yT} of steel and the thermal strain ε_{th} of each strip based on the heating curve. Establish and solve the equilibrium equations expressed in Eqs. (7.5) to obtain the stress and strain distributions. If $j = 1$, let the creep strains $\left(\varepsilon_{\text{cp}}\right)_i^j = 0$ and $\Delta^{j-1} = \Delta^0 = 0$; if $j > 1$, the creep strains $\left(\varepsilon_{\text{cp}}\right)_i^j$ are calculated through the stress distributions of the previous time step based on the

specified creep model.

$$\varepsilon_i^j = a^j Z_i^j + b^j \tag{7.5a}$$

$$\varepsilon_i^j = (\varepsilon_{\text{st}})_i^j + (\varepsilon_{\text{th}})_i^j + \left(\varepsilon_{\text{cp}}\right)_i^j \tag{7.5b}$$

$$\sum_{i=1}^{n} \sigma_i^j A_i^j = P \tag{7.5c}$$

$$\sum_{i=1}^{n} \sigma_i^j A_i^j (Z_i^j - H/2) = P\left(\Delta^{j-1} + \Delta_0\right) \tag{7.5d}$$

6. Based on the strain distribution, calculate the column lateral deflection, Δ^j, using Eq. (7.4).

7. If the total lateral deflection of the column $\Delta^j + \Delta_0 \geq L/15$, stop; otherwise, let $j = j+1$ and go to Step 5.

Note that this study adopts $L/15$ as the failure criterion of creep buckling, and a discussion of the criterion is presented in the Appendix. The adopted stress-strain relationships and creep model of steel at elevated temperatures as well as the process of obtaining the creep strain are elaborated on in Section 7.3.

To satisfy the equilibrium conditions at each time step, a set of $2n+2$ equations which contains $2n+2$ unknown variables ($n\sigma_i$, $n\varepsilon_i$, a, and b) and known parameters (Z_i , $(\varepsilon_{\text{cp}})_i$, $(\varepsilon_{\text{th}})_i$, A_i , P , H , Δ, and Δ_0) as shown in Eqs. (7.5), can be solved by employing the nonlinear system solver *fsolve* provided in MATLAB. The initial values of the unknown variables can be taken as the results of the previous time step to guarantee the accuracy of the solution, except for the first time step in which the initial values are taken as zero. The finite difference type and termination tolerance in the nonlinear system solver was set as "central" and 1×10^{-10}, respectively. For an axially restrained steel column at elevated temperature, as the thermal expansion is restrained, the internal axial force will increase with the increase of the temperature, which can lead to premature failure of the column [88]. The foregoing procedure is also applicable to evaluate the fire response of axially restrained steel columns at elevated temperatures. In that case, the internal force P in Eqs. (7.5c) and (7.5d) need to be updated at each time step to account for internal force induced by thermal restraint.

7.3 Validation

The two types of tests adopted for the validation of the proposed method are the ISO 834 standard fire tests [109] and creep buckling tests of Q690 high-strength steel columns. In each standard fire test, the axial load applied on the steel column was maintained as constant, and the gas temperature was heated according to the ISO 834 standard curve [109] until the column failed. The creep buckling test on a steel column was conducted by applying a constant axial load and constant elevated temperature until failure. Lateral deflections at the column's mid-height were recorded in both types of tests. The comparison of results obtained from the proposed method and the standard fire tests aims to demonstrate the applicability of the proposed method of evaluating the column lateral deflection and critical temperature. The comparison made to the creep buckling tests aims to validate the accuracy of the proposed method in predicting creep-induced column lateral deflection upon the incorporation of the Fields-and-Fields creep model [67] and implementation of different creep strain evaluation procedures.

7.3.1 Material properties

Mechanical property reductions and stress-strain relationships

For steel structural fire analysis, reductions of yielding strength and elastic modulus at elevated temperatures are key factors affecting the fire behaviour of steel members. The experimental investigations on temperature-dependent material properties of high-strength steels [45, 65] show that the degradationof mechanical properties exhibits different variations with heating temperature among different steel grades [73], especially between mild steels and high-strength steels. The degradation of steel mechanical properties at elevated temperatures specified in current design standards is primarily obtained from the tension test results of mild steel. Maraveas et al. [110] found that adopting the specification in some existing standards may overestimate the mechanical properties of high-strength steels.

As shown in Fig. 7.2, there are obvious discrepancies between the reduction factors specified in Eurocode 3 [41] and the experimental results of Q690 steel. Therefore, the reduction factors of yield strength and elastic modulus of Q690 high-strength steel at elevated temper-

atures obtained from experimental results [45] were adopted for numerical simulations for better accuracy.

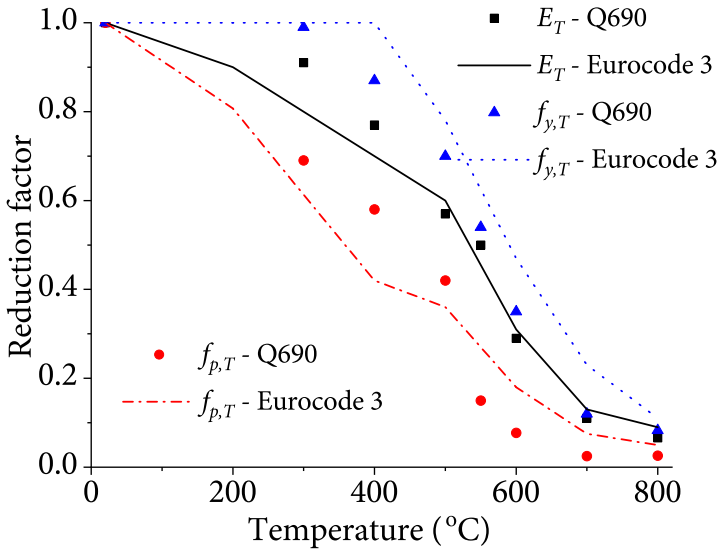

Figure 7.2: Comparison of reduction factors of mechanical properties at elevated temperatures between Eurocode 3 and Q690 steel

The format of a model proposed by Ramberg and Osgood [58] is adopted as the stress-strain relationships of Q690 steel at elevated temperatures, as expressed in

$$\varepsilon = \frac{\sigma}{E_T} + \alpha \left(\frac{\sigma}{f_{1.0}} \right)^n \tag{7.6}$$

Since Ramberg-Osgood model is differentiable, it avoids the non-convergence issue that may occur for piecewise models in the iterative computation. Note that Ramberg-Osgood equation [58] is modified by incorporating the $f_{1.0}$ (nominal yield strength corresponding to 1% residual strain at elevated temperature). By doing so, the fitting results have a better agreement with the experimental results of stress-strain curves at elevated temperatures, as shown in Fig. 7.3. The fitting results of the coefficients, a and n, at elevated temperatures are tabulated in Table 7.1.

Table 7.1: Fitting coefficients for Q690 steel in Ramberg-Osgood model

Temperature (°C)	E_T (MPa)	E_T/E	$f_{1.0}$ (MPa)	$f_{1.0}/f_y$	$\alpha(10^{-3})$	n
300	197000	0.93	747.7	0.94	6.21	40.43
400	165000	0.78	678.6	0.85	5.36	13.92
500	123000	0.58	549	0.69	5.04	19.52
550	106000	0.50	361	0.45	5.54	6.77
600	59000	0.28	205.5	0.26	5.68	6.81
700	21000	0.10	60	0.075	6.31	5.62
800	13000	0.06	41.9	0.053	6.85	7.47

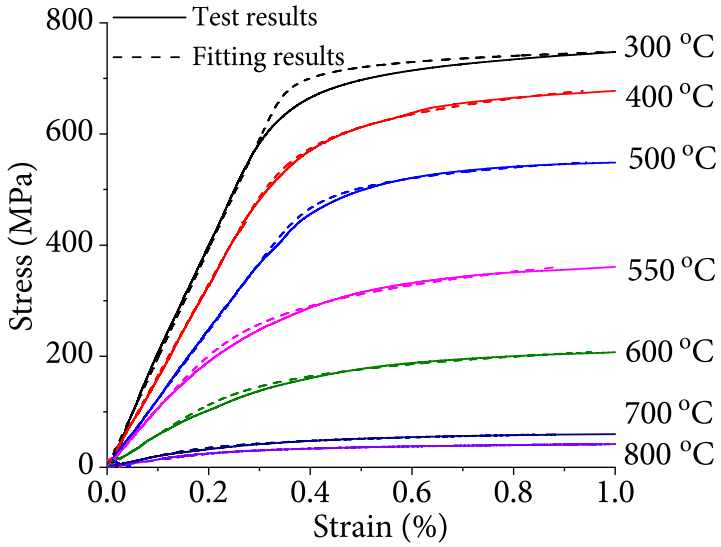

Figure 7.3: Fitting results of Q690 high-strength steel stress-strain curves at elevated temperatures

Creep model

The empirical equation in the form of power-law proposed by Fields and Fields [67] in Eq. (7.7) is employed to compute the creep strain of Q690 steel at elevated temperatures.

$$\varepsilon_{cp} = at^b\sigma^c \tag{7.7}$$

where ε_{cp} is the creep strain, %; t is time in minute; σ is stress in MPa; a, b and c are the coefficients that need to be determined from experimental results. For Q690 steel, the curve

fitting results of a, b and c are tabulated in Table 7.2 or expressed in Eqs. (7.8) based on the reported data [45]. The samples presented in Fig. 7.4 indicate that the Fields-and-Fields creep model with fitted coefficients agrees well with the test results. As the fitting process was carried out according to the steady creep test results at certain temperature levels, the predictions associated with the parameters in Table 7.2 are more accurate than Eqs. (7.8). Thereby, it is suggested Table 7.2 and Eqs. (7.8) be used for assessing the creep effect on steel members at constant temperature and heating temperature, respectively.

Table 7.2: Coefficients of Fields-and-Fields creep model for Q690 steel

Temperature (°C)	a	b	c
450	6.25×10^{-42}	1	14.47989
500	3.47×10^{-31}	0.999075	11.00699
550	3.08×10^{-22}	0.996882	8.36215
600	4.40×10^{-15}	0.991713	5.97602
700	3.69×10^{-6}	0.950795	2.7462
800	2.05×10^{-4}	0.723366	2.04585

$$a = 10^{-218.6676+0.5559T-3.5897\times10^{-4}\times T^2} \tag{7.8a}$$

$$b = \begin{cases} 175.17203 - 0.7863\times T + 0.00129T^2 - 7.51542\times10^{-7}T^3 & 450 \le T \le 600 \\ 77.68907 - 0.19475\times T + 1.25209\times10^{-4}T^2 & 600 < T \le 800 \end{cases} \tag{7.8b}$$

$$c = 1.0069 - 3.0446\times10^{-7}\times e^{T/58.3} \tag{7.8c}$$

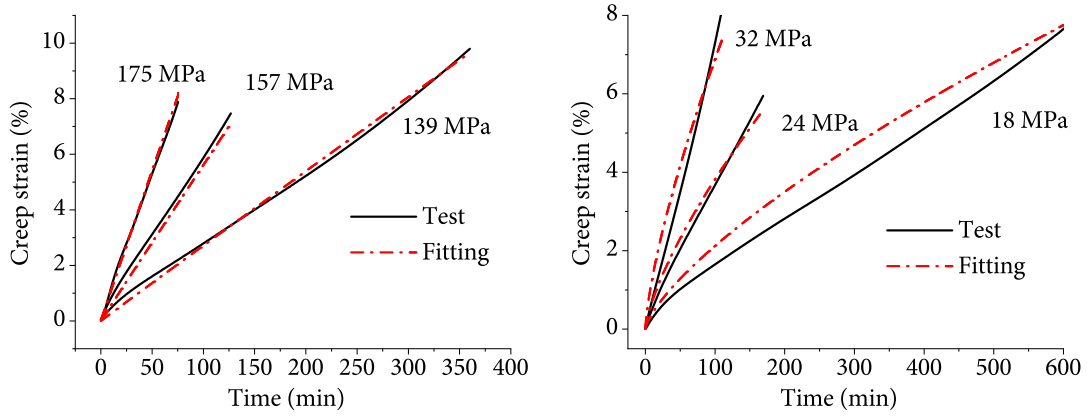

(a) $T = 600\,°C$ (b) $T = 800\,°C$

Figure 7.4: Comparison between tests and fitted results of creep strain curves of Q690 steel

As the stress level and creep strain rate is assumed to be constant in each time step for the iterative procedure, an equation for calculating the creep strain rate is necessary. Creep strain rate can be obtained in terms of either time-hardening or strain-hardening. In the case of time-hardening, the formulation of creep strain can be written as a function of time, as shown in Eq. (7.9). Since the time-hardening formulation is an explicit equation, the creep strain increment of each time step can be calculated based on the stress of the previous time step as expressed in Eq. (7.10). Then the creep strain can be formed as the sum of the creep strain increments during the time increment, Δt, as shown in Eq. (7.3a).

$$\dot{\varepsilon}_{\mathrm{cp}} = abt^{b-1}\sigma^{c} \tag{7.9}$$

$$\left(\Delta\varepsilon_{\mathrm{cp}}\right)^{j} = \Delta t \cdot (\dot{\varepsilon}_{cr})^{j} = \Delta t\left(abt^{b-1}\left(\sigma^{j-1}\right)^{c}\right) \tag{7.10}$$

In the format of strain-hardening, the creep strain rate formulation can be defined as a function of creep strain, as shown in Eq. (7.11). In the case that the strain-hardening formulation is adopted, the creep strain rate can be obtained by solving Eq. (7.12).

$$\dot{\varepsilon}_{\mathrm{cp}} = (a)^{\frac{1}{b}} b\left(\varepsilon_{\mathrm{cp}}\right)^{\frac{b-1}{b}} (\sigma)^{\frac{c}{b}} \tag{7.11}$$

$$\left(\varepsilon_{\mathrm{cp}}\right)^{j} - \left(\varepsilon_{\mathrm{cp}}\right)^{j-1} = \Delta t (a)^{\frac{1}{b}} b\left(\varepsilon_{\mathrm{cp}}\right)^{\frac{b-1}{b}} (\sigma)^{\frac{c}{b}} \tag{7.12}$$

7.3.2 ISO-834 standard fire tests on steel columns

Results obtained from fire tests on two unprotected Q690 high-strength steel columns [77] are selected to validate the proposed method. The two tested I-shape columns have a length of 2700 mm with a 16 mm thick end plate being welded at each end. The I-shape section is designated as 200 × 50 with a nominal section depth, H, and flange length, B, being 200 mm and 150 mm, respectively. The nominal thickness of the web and flanges are 14 mm. The column ends are hinge-supported about the column's weak axis, whereas the upper end of the column is not axially restrained. The two tested columns, designated as F-1 and F-2, were subjected to an axial load of 300 kN and 500 kN, respectively.

Franssen et al. [111] indicated that the mean temperature at the column's mid-height when the column collapsed could be taken as the failure temperature of the steel column. In this study, the average temperature curve obtained from measured ones at mid-height cross-section is adopted in the numerical simulations. The yield strength and elastic modulus of

steel at ambient temperature are taken as 821 MPa and 187 200 MPa, respectively, which are the measured values from the coupon tension tests. The initial deflections at the mid-height of steel columns at ambient temperatures and corresponding applied loads are taken as the measured values from the tests and shown in Table 7.3. Since the effect of residual stress on column capacity at elevated temperatures is considerably less than that at ambient temperature because the residual stress is released due to the thermal effect [87], the residual stress distribution is not considered in the subsequent validations.

Table 7.3: Parameters of Q690 steel columns in fire tests

Specimen No.	Cross-section	Load (kN)	Initial imperfection Δ_0 (mm)
F-1	200 × 150	300	1.37
F-2	200 × 150	500	1.43

Presented in Fig. 7.5 are comparisons of column mid-height lateral deflections obtained from the standard fire tests and the proposed method. To explore the creep effect on the predicted column lateral deflections in standard fire tests, three cases were simulated by the proposed method. They are a case without considering the creep effect, a case adopting the time-hardening formulation, and a case adopting the strain-hardening formulation. It can be seen from Fig. 7.5 that the lateral deflections obtained from the proposed method are similar to those of the tests. In the early loading phase, since the cross-sectional stress distribution at the mid-height of the column is in the elastic range, the lateral deflections of the steel column increase very slowly. At a later phase, the rate of lateral deflection accelerates due to the fact that the strain on a portion of the cross-section exceeds the elastic limit at elevated temperatures. Finally, the lateral deflection increases dramatically, which leads to failure as the full cross-section becomes plastic. As demonstrated in the figure, the proposed method provides reasonable predictions on the structural responses of steel columns at elevated temperatures.

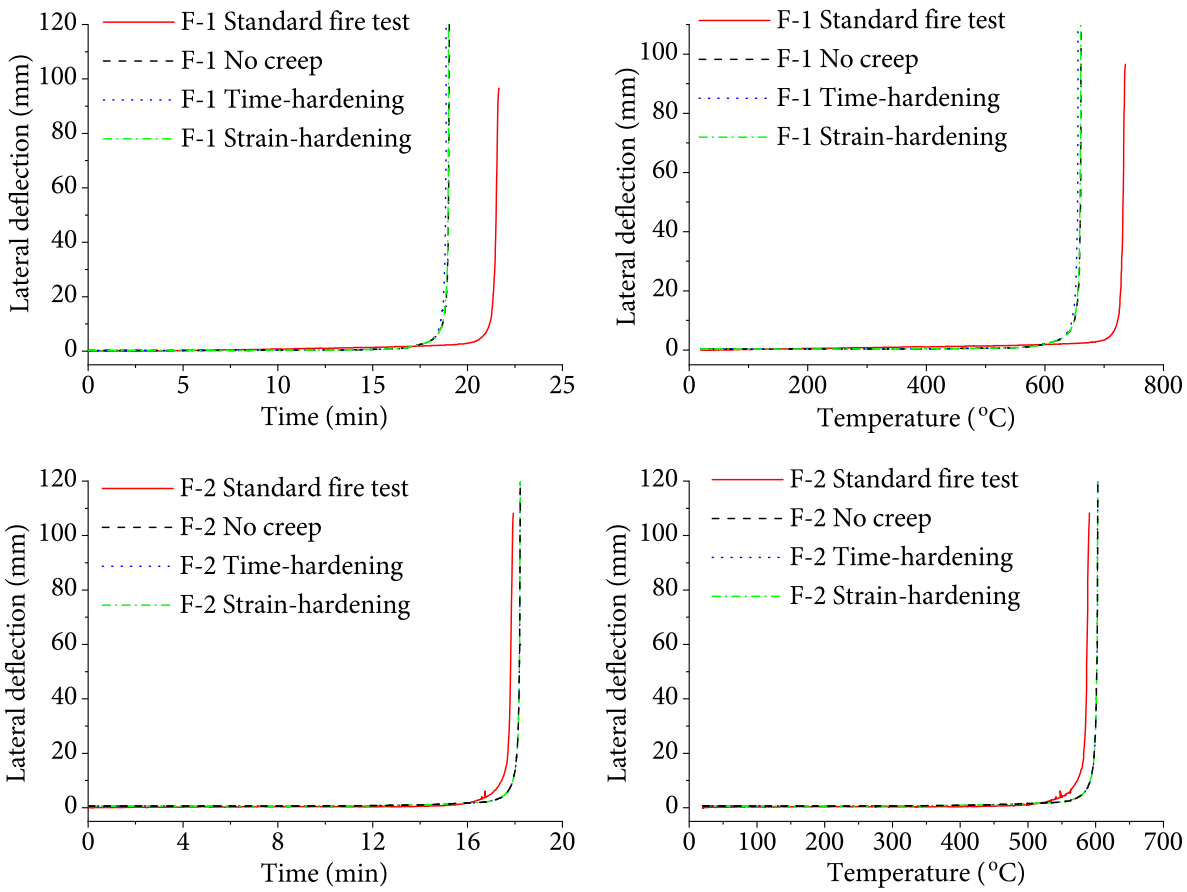

Figure 7.5: Comparison of column lateral deflections between standard fire tests and proposed method

The lateral deflection prediction of specimen F-1 shows a relatively larger discrepancy to the test results at the final phase compared to that of specimen F-2. Discrepancies between the test results and numerical predictions can be attributed to the following reasons. First, the fire behaviour of a steel column highly depends on the degradation of mechanical properties at elevated temperatures; however, the actual mechanical properties at elevated temperatures of the steel used in the tests might not be identical to the measured results by Wang et al. [45]. In addition, the steel mechanical properties at elevated temperatures adopted in the evaluation were computed by linear interpolation of the measured values at an increment of 100 °C, which was an approximation. Furthermore, non-uniform temperature distribution along the column length in the tests was not considered in the proposed method.

The comparison between the predictions with and without considering the creep effect indicates that the creep effect is negligible in standard fire tests. This is because the columns

are exposed to fire without insulation and experience relatively short fire duration. So, it is necessary to utilize the creep buckling tests to demonstrate if the proposed method can accurately assess the creep effect.

7.3.3 Creep buckling tests on steel columns at elevated temperatures

Unlike that in the standard fire test, the deformation of the column in the creep buckling test is mainly induced by the creep strain, as there is no transient degradation of mechanical properties in steel when it is subjected to a constant elevated temperature. Therefore, as an alternative failure mode, creep buckling is primarily attributed to the creep behaviour of the steel at elevated temperatures. Since the proposed method assumes that the creep strain rate is invariant in each time increment and calculated based on the stresses of the previous time step, the predicted deflections are sensitive to the creep model and the magnitude of the time step. Thus, it is necessary to validate the adopted creep model and proposed method against the results obtained from the creep buckling tests.

A set of creep buckling tests on high-strength Q690 steel columns at elevated temperatures carried out by the author [112] is utilized for the validation. The information of column specimens is tabulated in Table 7.4. All the columns have the same nominal length, dimensions and boundary conditions described in Section 7.3.2, except that specimens C-3 and C-4 have a different cross-section, 200×200: $H = 200\,\text{mm}$ and $B = 200\,\text{mm}$. Note that in practical cases columns are not likely to be exposed to a temperature higher than 800°C. The experiments aim to solely observe the column deflections due to the creep effect. By utilizing the experimental results, the proposed method is verified, and the failure mechanism of creep buckling phenomenon is explored in this chapter.

Table 7.4: Parameters of Q690 steel columns in creep buckling tests

Specimen No.	T (°C)	Cross-section	Load (kN)	Δ_0 (mm)
C-1	800	200×150	35	0.47
C-2	800	200×150	65	2.61
C-3	800	200×200	55	2.55
C-4	800	200×200	105	2.23

As shown in Fig. 7.6, a creep buckling test on steel columns at elevated temperatures consists of the heating phase, loading phase and creeping phase. In the heating phase, no axial load was applied to the column, and the furnace temperature was heated up to a target level. When the column temperature reached the target value, the axial load was applied to a predetermined magnitude, and this phase was referred to as the loading phase. In the creeping phase, both the axial load and temperature were maintained as invariant from their corresponding target values.

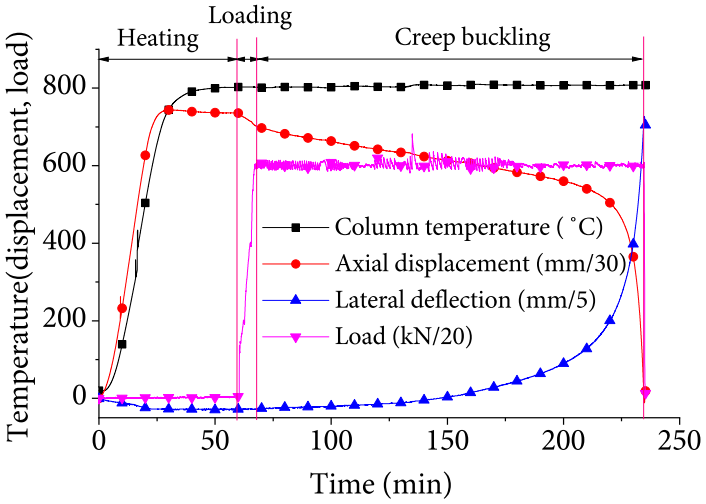

Figure 7.6: Creep buckling test on a steel column at the elevated temperature

The axial deformation of the column increased in the heating phase due to the thermal expansion and then remained almost constant because the column temperature increasing rate was slow when approaching the furnace temperature. It took a few minutes for the temperatures along the column height to reach the target temperature. In the loading phase, the axial deformation of the column decreased with increasing load magnitude, primarily resulting from the variation of instantaneous mechanical strain. In the creeping phase, the axial deformation of the column decreased gradually over time until the failure associated with creep buckling occurs. The lateral deflection of the column varied slightly in the heating and loading phases and accumulated at an increasing rate in the creeping phase. In the later period of the creep phase, the instantaneous inelastic deformation due to the increasing second-order effect accelerated the increase of the column lateral deflection. Finally, the creep buckling occurred when the lateral deflection became considerably large (approximate 120 mm), consequently the column failed to resist the applied axial load.

As the load was not applied to the column in the heating phase and the heating time was relatively short compared to the creeping phase, the creep effect in the heating phase is negligible. Therefore, the numerical simulations in this paper only account for the loading and creeping phases. It is noted that the measured lateral deflection shown in Fig. 7.6 is initially moved toward one direction in the heating phase but reverses its direction in the loading phase with a further increase in the creeping phase. The initial deflection in the heating phase likely resulted from the combination of column expansion and thermal effect on measurement devices. For that reason, the variation of the lateral deflection associated with the heating phase was neglected in the simulation, and the measured initial imperfection of the column at ambient temperature Δ_0 was taken as the initial lateral deflection at the beginning of the loading phase. In this way, the measured deflection was modified by adding the difference between Δ_0 and the measured value at the beginning of the loading phase. The temperature was set as 800 °C, and the recorded loading curve from each test was fed into the analysis. The analysis would continue with the associated predetermined target axial load if the column did not reach failure during the loading phase. The mechanical properties defined in the model were the same as illustrated in Section 7.3.2.

In this section, the time- and strain-hardening formulations are adopted respectively to carry out the analyses. In general, a smaller time increment size in numerical analysis yields higher accuracy in results but requires a longer computation time. In the following analyses, the time increment is 10 seconds, which is appropriate for acquiring relatively accurate results with reasonable computational time.

Presented in Fig. 7.7 are the creep-induced lateral deflections at the column's mid-height obtained from the test and predicted results. As the trivial deflection in the heating phase is neglected, the start point of the deflection curves in Fig. 7.7 corresponds to the initiation of the loading phase. For the purpose of comparison, the predictions without accounting for the creep effect are also presented in Fig. 7.7. If the creep effect is neglected, the column lateral deflection increases slightly as the applied load increases and remains unchanged when the applied load is invariant. By contrast, when the creep effect is considered, the lateral deflections of the steel columns increase slowly in the initiation of the creep phase and then grow with an increasing deformation rate until the occurrence of creep buckling. The predictions and test results are in good agreement, as shown in Fig. 7.7, which indicates

that the creep strain calculation in the proposed method is coherent with the deformation mechanism of the steel columns in the creep buckling tests.

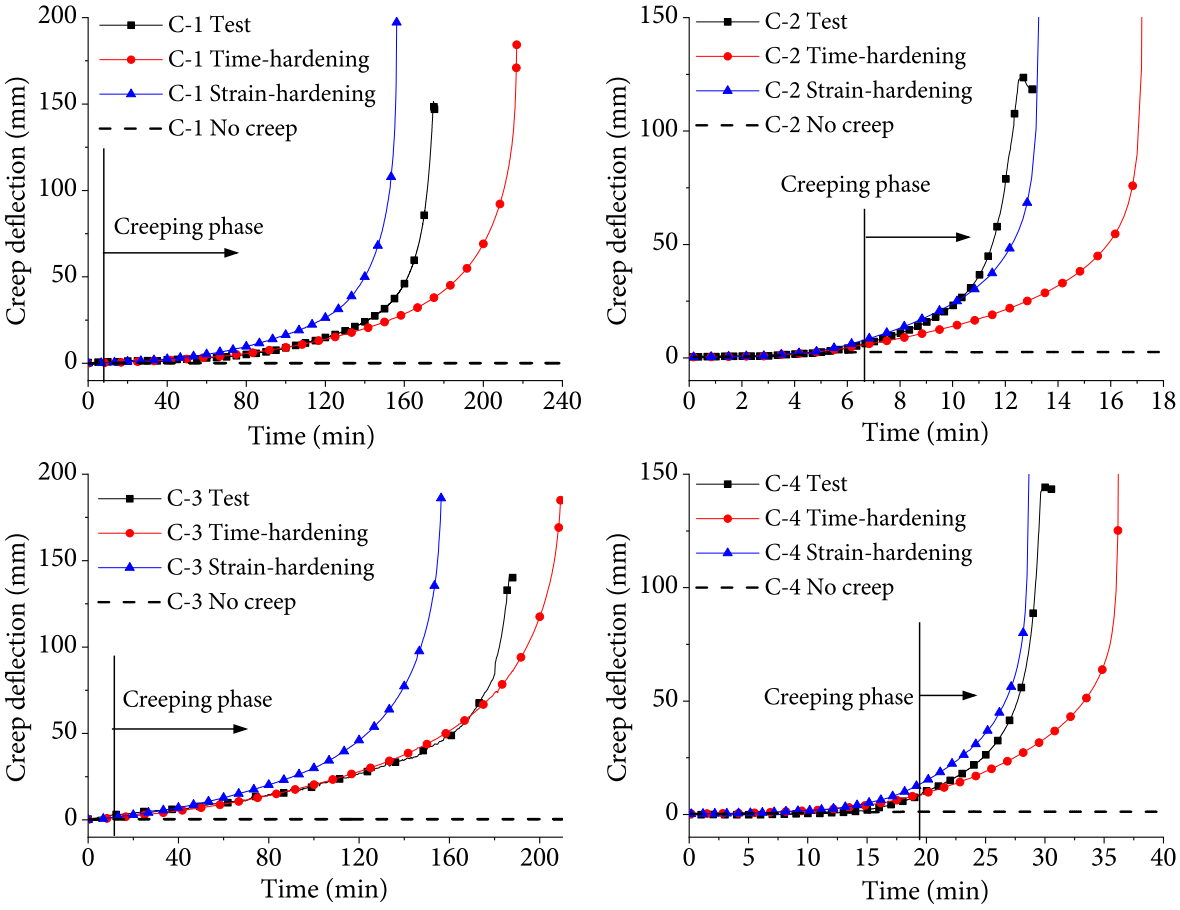

Figure 7.7: Comparisons of lateral deflections of steel columns subjected to creep buckling between test and predicted results

It is worth noting that compared to the predictions associated with using the time-hardening formulation, the predictions adopting the strain-hardening formulation yield shorter creep buckling time and a better agreement with test results. Since the time exponent coefficient b in Eq. (7.7) is smaller than unity at 800 °C, the creep strain rate decreases over time, which leads to unconservative results if the time-hardening formation is adopted for computing creep strain. The comparisons confirm the conclusion drawn by the previous studies [70, 108] that the analyses with the incorporation of the strain-hardening formulation yield more accurate results for cases with variable stress history.

7.4 Parametric Study

A parametric study is carried out to investigate the influences of some key factors on the creep buckling behaviour of steel columns at elevated temperatures. The analysis procedures illustrated in Section 7.2 are followed. The yielding strength and elastic modulus of steel are taken as 690 MPa and 200 000 MPa, respectively. The column length is 3000 mm. The parameters investigated in this study include load ratio α_p, temperature T, initial imperfection Δ_0 and slenderness ratio λ, with benchmark values of the parameters being 0.7, 600 °C, $L/1000$ and 62, respectively.

All the columns have an identical I-shape section with thicknesses of both flanges and web being 14 mm. The strain-hardening formulation in Eq. (7.12) is adopted to calculate the creep strain. As the creep buckling time of the column can be extremely long in some cases, the analysis will be terminated if the fire duration exceeds 10 hours.

7.4.1 Load ratio

The load ratio is one of the primary factors affecting the behaviour of steel columns at elevated temperatures. As illustrated in Section 7.3.3, the creep buckling time of the steel column decreases with a higher load ratio because the higher load will lead to higher stress on the cross-section and a larger creep strain rate. The load ratio α_p is taken as the ratio of the applied load and the column critical load at elevated temperature. The critical load of the column at elevated temperature, $N_{cr,T}$, is calculated based on the critical stress method [113] as expressed in Eqs. (7.13).

$$N_{cr,T} = \sigma_{cr,T} A_c \tag{7.13a}$$

$$\sigma_{cr,T} = \frac{1}{2}\left\{(1+\Delta_0)\,\sigma_{E,T} + f_{y,T} - \sqrt{\left[(1+\Delta_0)\,\sigma_{E,T} + f_{y,T}\right]^2 - 4 f_{y,T}\sigma_{E,T}}\right\} \tag{7.13b}$$

where $\sigma_{cr,T}$ is the critical stress at elevated temperature T; Δ_0 is the initial eccentricity, which is determined by the section type and slenderness ratio of the column; $\sigma_{E,T}$ is the Euler buckling stress of the column at elevated temperatures and equals $\pi^2 E_T I_c / L_c^2$.

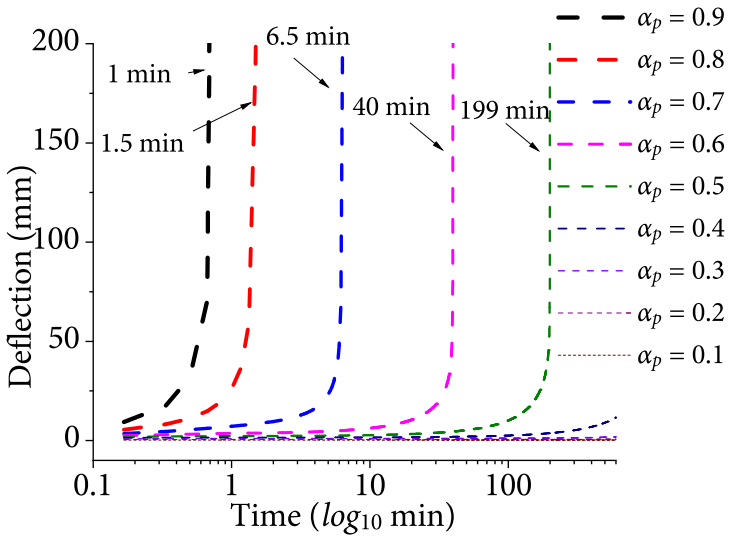

Figure 7.8: Influence of load ratio on creep buckling time of column when $\Delta_0 = L/1000$, $T = 600\,^{\circ}\mathrm{C}$ and $\lambda = 62$

With the increase of the load ratio, the creep buckling time reduces considerably; particularly, when the applied load approaches the column's critical load at the elevated temperature ($\alpha_p \geq 0.8$), the corresponding creep buckling time can be very short. This can be explained as follows. First, as the exponent of stress, i.e., coefficient c, in Eq. (7.7) approaches 6, the creep strain rate increases dramatically with the increase of stress. Second, when the applied load approaches the critical load, the instantaneous inelastic deformation of the column becomes dominant, and thus the column stiffness deteriorates rapidly. As a result, the larger creep strain rate and instantaneous inelastic deformation lead the column to fail in a very short time.

7.4.2 Temperature

With the same load ratio, the load applied on the column decreases with a higher temperature because the magnitude of the corresponding critical load is lower. Consequently, the reduced applied load will lead to lower stresses and lower creep strain rates. However, the creep strain rates increase with a higher temperature; thereby, there is a need to investigate the influence of temperature on the creep buckling behaviour of the column. The column deflection and corresponding creep buckling time at different temperatures are presented in Fig. 7.9.

It is noted is that the column failed within only one minute when the temperature is 700 °C or 800 °C. Besides the influence of the higher creep strain rate at a higher temperature, the other reason for creep buckling time being short is that the critical load obtained from the critical stress method neglects the adverse effect associated with the large plastic deformation at elevated temperatures. Therefore, when $\alpha_p = 0.7$ and $T = 700\,^{\circ}\text{C}$ (800 °C), the instantaneous plastic deformation in the column becomes dominant, which leads to the column failing immediately. For the temperature below 700 °C, the creep buckling time increases as temperature decreases.

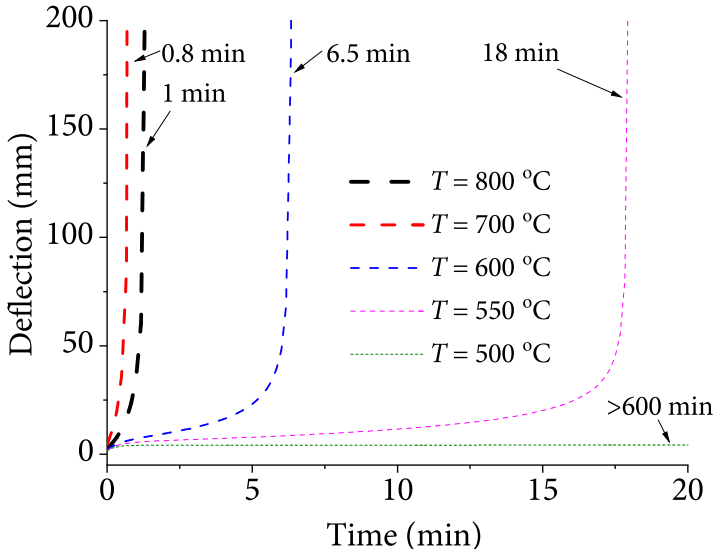

Figure 7.9: Influence of temperature on creep buckling time of column when $\lambda = 0.7, \Delta_0 = L/1000$ and $\lambda = 62$

7.4.3 Slenderness ratio

The influence of the column slenderness ratio on the creep buckling time of steel columns is illustrated in Fig. 7.10. For all cases, the length of the column is 3000 mm, and the slenderness ratio of the column varies by varying flange widths B. The slenderness ratios, 62, 70, 80 and 94, correspond to the cross-section 200 × 200, 200 × 180, 200 × 160 and 200 × 140, respectively. With a larger slenderness ratio, the column failure is more likely dominated by instability instead of yielding; thereby, a larger slenderness ratio results in a smaller critical load and thus the lower magnitude of the stress in the column. For cases with large stress, the creep strain rate can be quite large, which consequently accelerates the formation of the instantaneous plastic deformation. Consequently, the creep buckling time of steel columns

at elevated temperatures decreases for the column with a smaller slenderness ratio, as shown in Fig. 7.10.

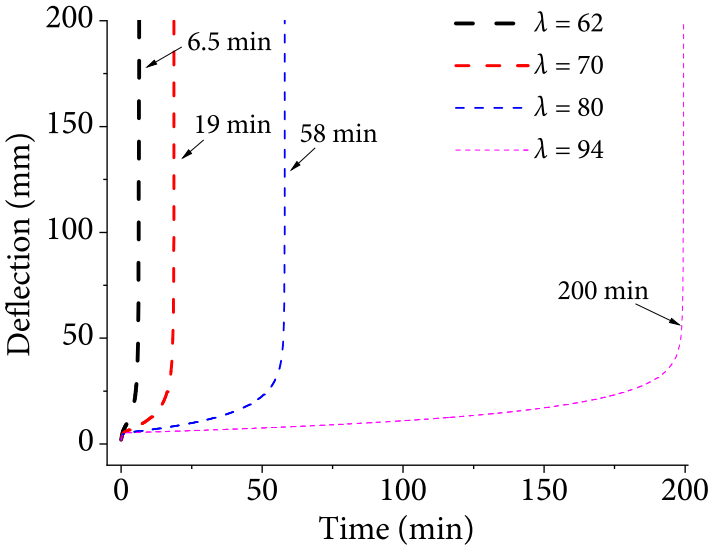

Figure 7.10: Influence of slenderness ratio on creep buckling time of column when $\alpha_p = 0.7, \Delta_0 = L/1000$ and $T = 600\,^{\circ}\mathrm{C}$

7.4.4 Initial imperfection

As shown in Fig. 7.11, the creep buckling time of the steel column increases as the magnitude of the initial imperfection reduces. Such phenomenon can be explained from the deformation mechanism of creep buckling as follows: 1) The initial imperfection influences the internal bending moment at column mid-height, which induces the stress gradient; the stress gradient in the current time step results in a larger strain gradient due to the creep effect and larger deflection in the next time step; and the larger deflection will consequently lead to further increase on stress gradient and creep strain rate. According to such interaction, the lateral deflection, stress gradient, creep strain rate and strain gradient increase interactively in each time increment until the occurrence of creep buckling. 2) A larger initial imperfection also leads to larger magnitudes of the stress at extreme fibres in column cross-section, which results in a higher creep strain rate in Fields-and-Fields creep model.

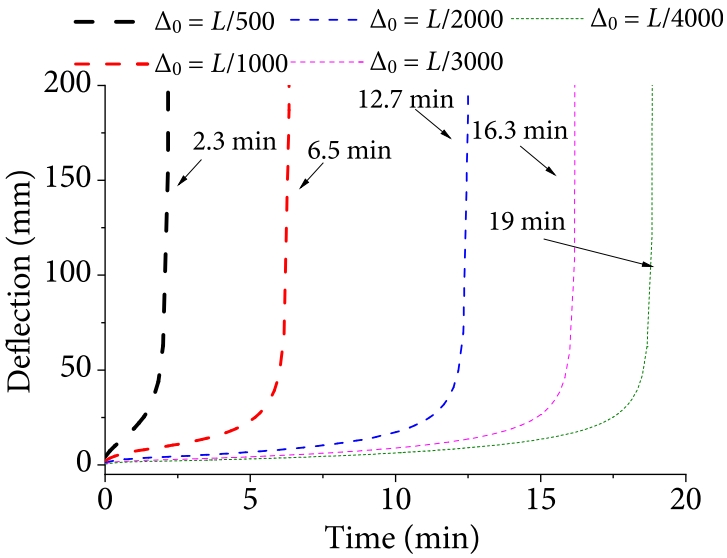

Figure 7.11: Influence of initial imperfection on column creep buckling time when $\alpha_p = 0.7$, $T = 600\,^{\circ}\mathrm{C}$ and $\lambda = 62$

The analysis results indicate that the creep buckling time of steel columns at elevated temperatures is highly influenced by the initial imperfections of steel columns. Theoretically, if a concentrically loaded column is assumed to be perfectly straight without initial imperfection and not subjected to any lateral disturbing force, the creep effect only influences the axial deformation of the column. In that case, the lateral deflection will not occur due to the lack of a stress gradient in the column cross-section, and thus the creep buckling of the column will not happen. Therefore, the initial imperfection can be regarded as the premise condition of column creep buckling.

The current standards [10, 26, 114] stipulate that the maximum acceptable initial imperfection of columns is $L/1000$. As presented in the parametric study, the creep buckling time may be considerably short with $\Delta_0 = L/1000$. Due to this observation, decreasing the maximum acceptable initial imperfection of steel columns can be an effective way to increase the creep buckling time at elevated temperatures.

7.5 Conclusions

A method to evaluate the creep buckling behaviour of steel columns at elevated temperatures is proposed. The proposed method has been validated against the results of the standard

fire tests and creep buckling tests of Q690 high-strength steel columns. The conclusions obtained from this study are summarized in the following:

1. The stress-strain relationships and creep strain variations of Q690 high-strength steel at elevated temperatures are simulated. The simulation results agree well with the test results and can be utilized in the fire design of Q690 high-strength steel structures.

2. The time-hardening and strain-hardening formulations are separately incorporated in the validation analyses against creep buckling tests. It is found that the strain-hardening model yields more accurate results for the cases with variable stress history.

3. The failure mechanism of creep buckling of steel columns is associated with the creep-induced lateral deflection, which is resulted from the cross-sectional strain gradient distribution and the nonuniform stress distribution triggered by the column initial imperfection. Therefore, the creep buckling will theoretically not occur, provided the initial imperfection is neglected because the stress is uniformly distributed on the cross-section.

4. When the applied load approaches the theoretical critical load of the column at elevated temperature ($\alpha_p \geq 0.8$), the creep buckling phenomenon can be easily observed; therefore, possible creep buckling of steel columns may occur in a certain fire scenario, which signifies the necessity of considering the creep effect in the fire design of steel columns.

5. Based on the outcome of the parametric study, it is concluded that the creep buckling time of the steel columns decreases with an increase in load ratio, temperature, and initial imperfection but a decrease in slenderness ratio of the columns.

As the proposed method demonstrates that the creep effect on the structural response of steel columns in fire is induced by the column initial imperfection, the adverse effect of creep can be explicitly considered in the evaluation of column critical temperature and critical load by incorporating a time-dependent factor to amplify the column initial imperfection. More importantly, the proposed numerical method's philosophy has been demonstrated to accurately consider the creep effect on column lateral deflection—the creep-induced deflection can be obtained by analyzing the cross-sectional strain gradient at the mid-height.

Following this philosophy, a simplified method is proposed in Chapter 8 to consider the creep effect on the lateral deflection of steel columns at elevated temperatures.

Chapter 8

Fire Resistance of Multi-column Systems

8.1 Introduction

Due to steel's high thermal conductivity and pronounced deterioration of mechanical properties, steel structures are vulnerable to fire hazards, and therefore fire safety assessment becomes an inseparable part of the design of steel structures. Given the complicated interaction of members and nonlinear behaviour of steel, unlike the case at ambient temperature, the development of an analytical method to evaluate the fire resistance of steel structure would be impractical. Hence, a simplified numerical method is proposed in this chapter to assess the fire resistance of multi-column systems by incorporating the effects of nonlinear stress-strain relationships, thermal expansions, creep, and partial yielding.

8.2 Effect of Thermal Expansion of Braces

The thermal expansion of beams was not considered in the previous research regarding the storey-based stability of multi-column systems at elevated temperatures [37, 98, 99], which is feasible for cases in which the beams are restrained by concrete slabs. However, for the braces in multi-column systems without the restraint from the concrete slabs, neglecting their thermal expansion may lead to unconservative design mainly due to the following two reasons. First, it has been shown in the Cardington fire tests that the columns are subjected to higher bending moments caused by additional deflection induced by the thermal expansion of connecting beams at elevated temperatures [115], as shown in Fig. 8.1,

which expedites the formation of plastic hinge in the column and subsequently cause the premature failure. Second, the thermal expansion of braces is restrained by the columns and anchors, and thus the additional forces will be induced in the braces, which may result in the brace yielding prematurely, as per Fig. 8.2. Hence, the additional lateral displacements of columns and forces in braces induced by the thermal expansion of braces for multi-column systems are investigated in this subsection.

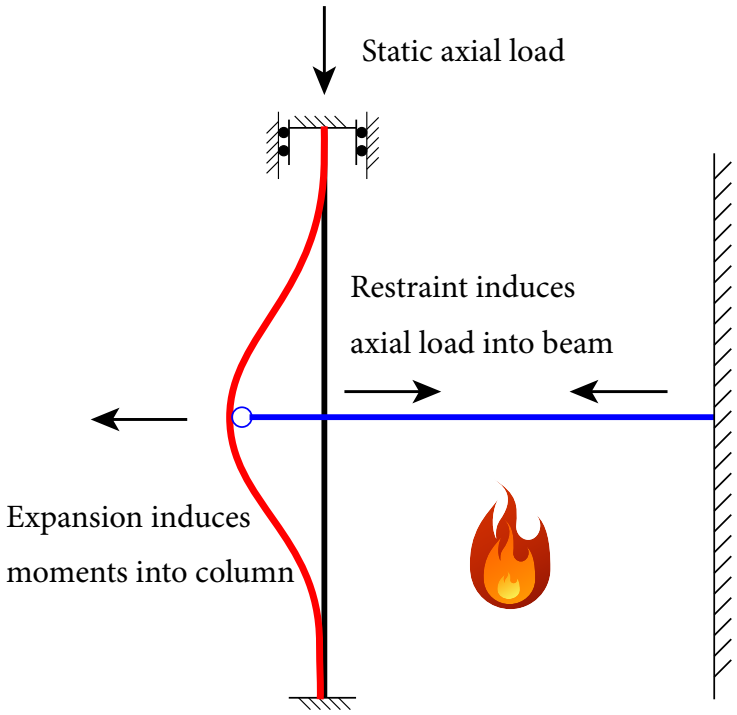

Figure 8.1: Structural behaviour of a braced column at elevated temperatures [115]

8.2.1 Thermal expansion of a single brace in a multi-column system

Fig. 8.2 illustrates the structural behaviour of a typical brace in the thermal expansion that it is restrained by the left and right subsystems.

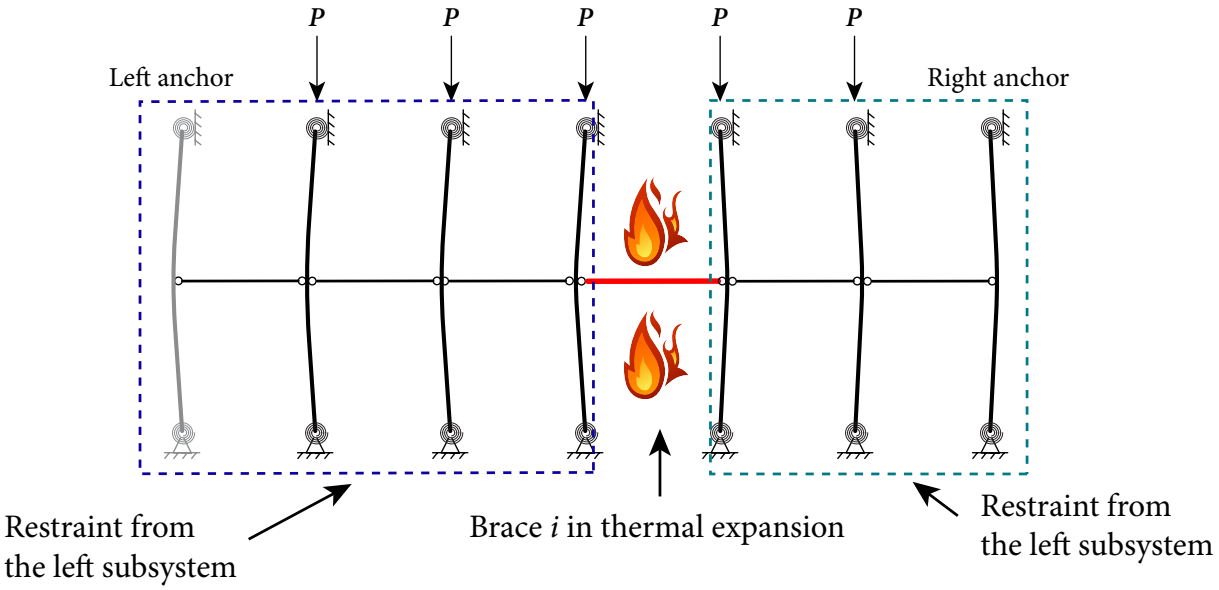

Figure 8.2: Thermal expansion of a brace in a multi-column system

If the restraints from the left and right subsystems are represented using two equivalent springs, the relationships among the deformations, additional force, and stiffness of brace i can be depicted as Fig. 8.3.

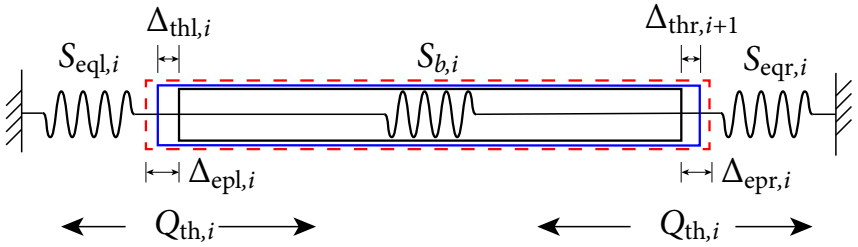

Figure 8.3: Diagram of a restrained brace in thermal expansion

In Fig. 8.3, $S_{\mathrm{eql},i}$ and $S_{\mathrm{eqr},i}$ are the equivalent lateral stiffness of the left and right subsystems, respectively, and they can be attained using the method described in Section 4.2. $\Delta_{\mathrm{epl},i}$ and $\Delta_{\mathrm{epr},i}$ are the deformations induced by free thermal expansion at the left and right ends of brace i, respectively; $\Delta_{\mathrm{thl},i}$ and $\Delta_{\mathrm{thr},i}$ are respectively the final deformations induced by the thermal expansion at the left and right ends of brace i subjected to the restraints from $S_{\mathrm{eql},i}$ and $S_{\mathrm{eqr},i}$; and $Q_{\mathrm{th},i}$ is the additional internal force induced by the thermal restraint. The difference between the total deformation in free thermal expansion $(\Delta_{\mathrm{epl},i}+\Delta_{\mathrm{epr},i})$ and the total final deformation in thermal restraint $(\Delta_{\mathrm{thl},i}+\Delta_{\mathrm{thr},i})$ is the compressive deformation

of the brace induced by the additional internal force $Q_{\mathrm{th},i}$. Thus,

$$\Delta_{\mathrm{epl},i} + \Delta_{\mathrm{epr},i} - (\Delta_{\mathrm{thl},i} + \Delta_{\mathrm{thr},i}) = \frac{Q_{\mathrm{th},i}}{S_{b,i}} \tag{8.1}$$

Let $\Delta_{\mathrm{ep},i}$ equal $(\Delta_{\mathrm{epl},i} + \Delta_{\mathrm{epr},i})$, representing the total change in the brace length if the brace expands freely. $\Delta_{\mathrm{ep},i}$ depends on the temperature change ΔT_i, brace length $L_{b,i}$, and thermal expansion coefficient $\alpha_{\mathrm{th},i}$:

$$\Delta_{\mathrm{ep},i} = L_{b,i} \int \alpha_{\mathrm{th},i} \, d T_i \tag{8.2}$$

Then, Eq. (8.1) can be written as:

$$\Delta_{\mathrm{ep},i} - (\Delta_{\mathrm{thl},i} + \Delta_{\mathrm{thr},i}) = \frac{Q_{\mathrm{th},i}}{S_{b,i}} \tag{8.3}$$

According to the equilibrium in Fig. 8.3, it yields

$$\Delta_{\mathrm{thl},i} = \frac{Q_{\mathrm{th},i}}{S_{\mathrm{eql},i}} \tag{8.4a}$$

$$\Delta_{\mathrm{thr},i} = \frac{Q_{\mathrm{th},i}}{S_{\mathrm{eqr},i}} \tag{8.4b}$$

From Eq. (8.3) and Eqs. (8.4a), the solutions of $Q_{\mathrm{th},i}$, $\Delta_{\mathrm{th}l,i}$, and $\Delta_{\mathrm{th}l,i}$ can be obtained:

$$\Delta_{\mathrm{thl},i} = \Delta_{\mathrm{ep},i} \frac{S_{\mathrm{eqr},i} S_{b,i}}{S_{\mathrm{eqr},i} S_{\mathrm{eql},i} + S_{b,i} \left(S_{\mathrm{eqr},i} + S_{\mathrm{eql},i} \right)} \qquad \text{for } S_{\mathrm{eql},i} > 0,\ S_{\mathrm{eqr},i} > 0 \tag{8.5a}$$

$$\Delta_{\mathrm{thr},i} = \Delta_{\mathrm{ep},i} \frac{S_{\mathrm{eql},i} S_{b,i}}{S_{\mathrm{eqr},i} S_{\mathrm{eql},i} + S_{b,i} \left(S_{\mathrm{eqr},i} + S_{\mathrm{eql},i} \right)} \qquad \text{for } S_{\mathrm{eql},i} > 0,\ S_{\mathrm{eqr},i} > 0 \tag{8.5b}$$

$$Q_{\mathrm{th},i} = \Delta_{\mathrm{thl},i} S_{\mathrm{eql},i} \qquad \text{for } S_{\mathrm{eql},i} > 0,\ S_{\mathrm{eqr},i} > 0 \tag{8.5c}$$

It should be noted that Eqs. (8.5) only hold true when $S_{\mathrm{eqr},i}$ and $S_{\mathrm{eql},i}$ are positive. If the equivalent stiffness of one subsystem becomes zero or negative, it means that this subsystem relies on the support from the remaining part of the system and cannot restrain the thermal expansion of the brace. In that case, the brace will expand freely towards the side with negative equivalent stiffness, and there is no additional force in the brace induced by the thermal restraint, as expressed in Eqs. (8.6).

$$\Delta_{\mathrm{thl},i} = \Delta_{\mathrm{ep},i},\ \Delta_{\mathrm{thr},i} = 0, \quad \text{if } S_{\mathrm{eql},i} \le 0 \tag{8.6a}$$

$$\Delta_{\mathrm{thr},i} = \Delta_{\mathrm{ep},i},\ \Delta_{\mathrm{thl},i} = 0, \quad \text{if } S_{\mathrm{eqr},i} \le 0 \tag{8.6b}$$

$$Q_{\mathrm{th},i} = 0 \qquad \text{if } S_{\mathrm{eqr},i} \le 0 \text{ or } S_{\mathrm{eql},i} \le 0 \tag{8.6c}$$

8.2.2 Thermal expansion of multiple braces in a multi-column system

The thermal-induced additional force and deformations of a single brace are formulated as Eqs. (8.5) and Eqs. (8.6). Nevertheless, in a multi-column system, it is not likely that only one brace is heated in fire scenarios. Then, the final additional force in a brace will be affected by the additional forces in other braces induced by the thermal expansions. By adopting the proposed half-length column model, the interplay of thermal-induced additional forces in a multi-column system anchored on the right side is depicted in Fig. 8.4. Note that the superposition principle is adopted that the internal forces induced by the initial imperfections and applied axial loads and those induced by thermal expansion are additive. Therefore, the internal forces induced by the initial imperfections and applied axial loads are not considered in Fig. 8.4 for clarity.

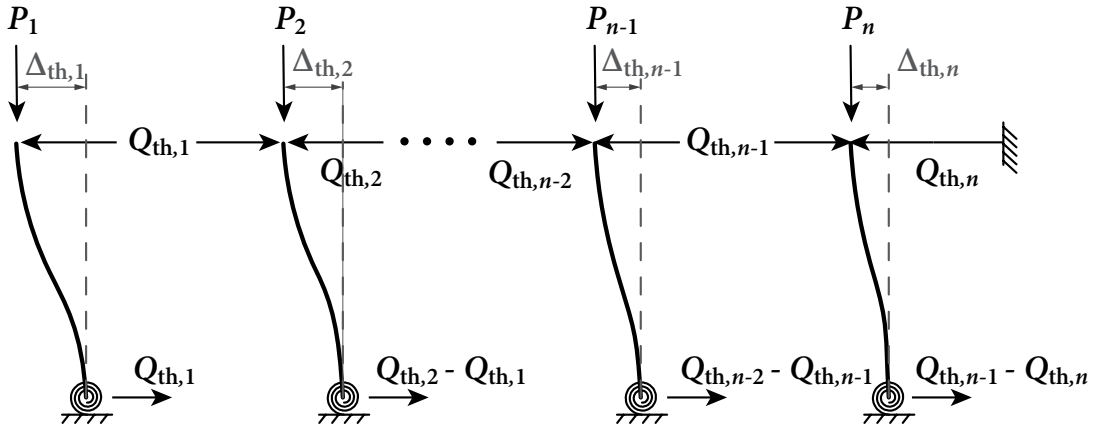

Figure 8.4: Thermal-induced additional forces in a multi-column system anchored on the right side simulated using the half-length column model

In Fig. 8.4, $\Delta_{th,i}$ is the lateral displacement of column i induced by the thermal expansion of braces. Thus, for brace i ($i = \{1,2,...,n-1\}$), the final length change is $\Delta_{th,i} - \Delta_{th,i+1}$, and the compressive deformation, i.e., the difference between the length change in free expansion and the final length change, is $\Delta_{ep,i} - \left(\Delta_{th,i} - \Delta_{th,i+1}\right)$. Similarly, the compressive deformation of brace n is $\Delta_{ep,n} - \Delta_{th,n}$. In addition, the compressive deformation of each brace equals the ratio of the internal force and the axial stiffness of the brace. In consequence, Eqs. (8.7) are attained based on the compatibility of each brace in a multi-column system anchored on the right side.

$$Q_{\text{th},i} = \left(\Delta_{\text{ep},i} - \Delta_{\text{th},i} + \Delta_{\text{th},i+1}\right) S_{b,i} \qquad i = \{1, \ldots, n-1\} \tag{8.7a}$$

$$Q_{\text{th},n} = \left(\Delta_{\text{ep},n} - \Delta_{\text{th},n}\right) S_{b,n} \tag{8.7b}$$

According to the equilibrium of each column in the system,

$$Q_{\text{th},1} = \Delta_{\text{th},1} S_{c,1} \tag{8.8a}$$

$$Q_{\text{th},i} - Q_{\text{th},i-1} = \Delta_{\text{th},i} S_{c,i} \qquad i = \{2, \ldots, n\} \tag{8.8b}$$

Eliminating $\Delta_{\text{th},i}$ in Eqs. (8.7) and Eqs. (8.8) yields

$$\frac{Q_{\text{th},1}}{S_{b,1}} = \Delta_{\text{ep},1} - \frac{Q_{\text{th},1}}{S_{c,1}} + \frac{Q_{\text{th},2} - Q_{\text{th},1}}{S_{c,2}} \tag{8.9a}$$

$$\frac{Q_{\text{th},i}}{S_{b,i}} = \Delta_{\text{ep},i} - \frac{Q_{\text{th},i} - Q_{\text{th},i-1}}{S_{c,i}} + \frac{Q_{\text{th},i+1} - Q_{\text{th},i}}{S_{c,i+1}} \qquad i = \{2, \ldots, n-1\} \tag{8.9b}$$

$$\frac{Q_{\text{th},n}}{S_{b,n}} = \Delta_{\text{ep},n} - \frac{Q_{\text{th},n} - Q_{\text{th},n-1}}{S_{c,n}} \tag{8.9c}$$

The set of linear equations in Eqs. (8.9) can be expressed as

$$\begin{bmatrix} \frac{1}{S_{b,1}} + \frac{1}{S_{c,1}} + \frac{1}{S_{c,2}} & -\frac{1}{S_{c,2}} & & & \\ -\frac{1}{S_{c,2}} & \frac{1}{S_{b,2}} + \frac{1}{S_{c,2}} + \frac{1}{S_{c,3}} & -\frac{1}{S_{c,3}} & & \\ & -\frac{1}{S_{c,3}} & \ddots & \ddots & \\ & & \ddots & \frac{1}{S_{b,n-1}} + \frac{1}{S_{c,n-1}} + \frac{1}{S_{c,n}} & -\frac{1}{S_{c,n}} \\ & & & -\frac{1}{S_{c,n}} & \frac{1}{S_{b,n}} + \frac{1}{S_{c,n}} \end{bmatrix} \begin{Bmatrix} Q_{\text{th},1} \\ Q_{\text{th},2} \\ \vdots \\ Q_{\text{th},n-1} \\ Q_{\text{th},n} \end{Bmatrix} = \begin{Bmatrix} \Delta_{\text{ep},1} \\ \Delta_{\text{ep},2} \\ \vdots \\ \Delta_{\text{ep},i} \\ \Delta_{\text{ep},n} \end{Bmatrix} \tag{8.10}$$

As such, the additional brace forces induced by the thermal expansion effect can be attained by solving the linear system in Eq. (8.10). Since the thermal-induced brace forces $Q_{\text{th},i}$ in the above derivation are compressive while the brace forces induced by the initial imperfections and applied axial loads in tension are assumed to be positive, the final brace force considering the thermal expansion effect is $Q_i - Q_{\text{th},i}$. It is found that the flexibility matrix in Eq. (8.10) is the same as that in Eq. (4.22), except that the thermal-induced brace forces $Q_{\text{th},i}$ obtained from Eq. (8.10) shall be positive, as explained previously.

Eliminating $Q_{\text{th},i}$ in Eqs. (8.7) and Eqs. (8.8) yields

$$\Delta_{\text{th},1} S_{c,1} = \left(\Delta_{\text{ep},1} - \Delta_{\text{th},1} + \Delta_{\text{th},2}\right) S_{b,1} \tag{8.11a}$$

$$\Delta_{\text{th},i} S_{c,i} = \left(\Delta_{\text{ep},i} - \Delta_{\text{th},i} + \Delta_{\text{th},i+1}\right) S_{b,i} - \left(\Delta_{\text{ep},i-1} - \Delta_{\text{th},i-1} + \Delta_{\text{th},i}\right) S_{b,i-1} \qquad i = \{2, \ldots, n-1\} \tag{8.11b}$$

$$\Delta_{\text{th},n} S_{c,n} = \left(\Delta_{\text{ep},n} - \Delta_{\text{th},n}\right) S_{b,n} - \left(\Delta_{\text{ep},n-1} - \Delta_{\text{th},n-1} + \Delta_{\text{th},n}\right) S_{b,n-1} \tag{8.11c}$$

The matrix format of Eqs. (8.11) is

$$\begin{bmatrix} S_{b,1}+S_{c,1} & -S_{b,1} & & \\ -S_{b,1} & S_{b,1}+S_{b,2}+S_{c,2} & \ddots & \\ & \ddots & \ddots & -S_{b,n-1} \\ & & -S_{b,n-1} & S_{b,n-1}+S_{b,n}+S_{c,n} \end{bmatrix} \begin{Bmatrix} \Delta_{\text{th},1} \\ \Delta_{\text{th},2} \\ \vdots \\ \Delta_{\text{th},n} \end{Bmatrix} = \begin{Bmatrix} \Delta_{\text{ep},1}S_{b,1} \\ \Delta_{\text{ep},2}S_{b,2}-\Delta_{\text{ep},1}S_{b,1} \\ \vdots \\ \Delta_{\text{ep},n}S_{b,n}-\Delta_{\text{ep},n-1}S_{b,n-1} \end{Bmatrix} \tag{8.12}$$

In this way, the column lateral displacements induced by the thermal expansion of braces in a multi-column system anchored on one side can be attained by solving Eqs. (8.12).

For multi-column systems anchored on both sides, the diagram of thermal-induced forces is shown in Fig. 8.5.

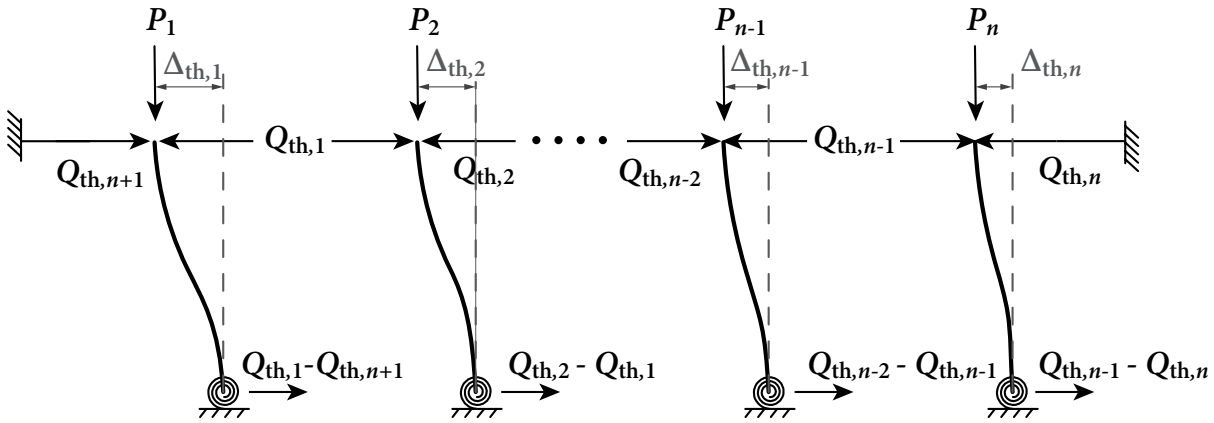

Figure 8.5: Thermal-induced additional forces in a multi-column system anchored on both sides simulated using the half-length column model

Following the above analytic process, the compatibility and equilibrium equations of the system in Fig. 8.5 are given in

$$Q_{\text{th},i} = \left(\Delta_{\text{ep},i} - \Delta_{\text{th},i} + \Delta_{\text{th},i+1}\right) S_{b,i} \qquad i = \{1, \ldots, n-1\} \tag{8.13a}$$

$$Q_{\text{th},n} = \left(\Delta_{\text{ep},i} - \Delta_{\text{th},i}\right) S_{b,n} \tag{8.13b}$$

$$Q_{\text{th},n+1} = \left(\Delta_{\text{ep},n+1} + \Delta_{\text{th},1}\right) S_{b,n+1} \tag{8.13c}$$

$$Q_{\text{th},1} - Q_{\text{th},n+1} = \Delta_{\text{th},1} S_{c,1} \tag{8.13d}$$

$$Q_{\text{th},i} - Q_{\text{th},i-1} = \Delta_{\text{th},i} S_{c,i} \qquad i = \{2, \ldots, n\} \tag{8.13e}$$

The linear equations for solving the brace forces and column lateral displacements induced by the thermal expansion of braces are shown in Eq. (8.14) and Eq. (8.15), respectively.

$$\begin{bmatrix} \frac{1}{S_{b,n+1}}+\frac{1}{S_{c,1}} & -\frac{1}{S_{c,1}} & & & \\ -\frac{1}{S_{c,1}} & \frac{1}{S_{b,1}}+\frac{1}{S_{c,1}}+\frac{1}{S_{c,2}} & -\frac{1}{S_{c,2}} & & \\ & -\frac{1}{S_{c,2}} & \ddots & \ddots & \\ & & \ddots & \frac{1}{S_{b,n-1}}+\frac{1}{S_{c,n-1}}+\frac{1}{S_{c,n}} & -\frac{1}{S_{c,n}} \\ & & & -\frac{1}{S_{c,n}} & \frac{1}{S_{b,n}}+\frac{1}{S_{c,n}} \end{bmatrix} \begin{Bmatrix} Q_{\text{th},n+1} \\ Q_{\text{th},1} \\ \vdots \\ Q_{\text{th},n-1} \\ Q_{\text{th},n} \end{Bmatrix} = \begin{Bmatrix} \Delta_{\text{ep},n+1} \\ \Delta_{\text{ep},1} \\ \vdots \\ \Delta_{\text{ep},n-1} \\ \Delta_{\text{ep},n} \end{Bmatrix} \tag{8.14}$$

$$\begin{bmatrix} S_{b,1}+S_{c,1}+S_{b,n+1} & -S_{b,1} & & & \\ -S_{b,1} & S_{b,1}+S_{b,2}+S_{c,2} & \ddots & & \\ & \ddots & \ddots & -S_{b,n-1} & \\ & & -S_{b,n-1} & S_{b,n-1}+S_{b,n}+S_{c,n} & \end{bmatrix} \begin{Bmatrix} \Delta_{\text{th},1} \\ \Delta_{\text{th},2} \\ \vdots \\ \Delta_{\text{th},n} \end{Bmatrix} = \begin{Bmatrix} \Delta_{\text{ep},1}S_{b,1}-\Delta_{\text{ep},n+1}S_{b,n+1} \\ \Delta_{\text{ep},2}S_{b,2}-\Delta_{\text{ep},1}S_{b,1} \\ \vdots \\ \Delta_{\text{ep},n}S_{b,n}-\Delta_{\text{ep},n-1}S_{b,n-1} \end{Bmatrix} \tag{8.15}$$

As shown above, with known elevated temperatures and corresponding thermal expansion coefficient values, the additional brace forces and column lateral displacements of multi-column systems induced by the thermal expansion of braces can be assessed using the expressions derived in this subsection.

8.3 Effect of Thermal Expansions of Columns

Columns will expand at different rates if subjected to different heating rates. As a result, an additional axial force may form in the column with a higher temperature induced by the restraint provided by adjacent beams and thereafter, the increased internal axial forces will lead the column to premature failure. The equations proposed by Xu and Zhuang [98] are adopted in this research to calculate the thermal-induced axial forces P_{th} in columns, while the elastic modulus in their equations is replaced by tangent modulus at elevated temperatures to signify the nonlinear behaviour of steel columns at elevated temperatures, as given in Eq. 8.16.

$$P_{\text{th}} = \frac{P + k_b L_c \int \alpha_{\text{th}} dT}{1 + k_b L_c (E_{c,0} - E_{c,\tan}) / (E_{c,0} E_{c,\tan} A_c)} - P \tag{8.16}$$

where $E_{c,0}$ is the elastic modulus of the column at ambient temperature, and k_b is the restraining stiffness of adjacent beams, as below:

$$k_b = \frac{12(r_1 + r_2 + r_1 r_2)}{4 - r_1 r_2} \frac{E_b I_b}{L_b^3} \tag{8.17}$$

in which r_1 and r_2 are the end-fixity factors at beam ends. For rigid frames, with $r_1 = r_2 = 1.0$, Eq. 8.17 can be simplified as

$$k_b = \frac{12 E_b I_b}{L_b^3} \tag{8.18}$$

For multi-column systems with intermediate bracing, since the end connections of braces are assumed to be pinned, the restraining stiffness k_b becomes zero with $r_1 = r_2 = 0$. It should be noted that since the additional axial force P_{th} is induced by the unequal thermal expansion of columns, the bounds of the integral term in Eq. 8.16 correspond to the temperature difference between the target column and the adjacent column.

8.4 Effect of Partial Yielding on Steel Columns

In their preliminary investigation of storey-based stability of steel frames at elevated temperatures, Xu and Zhuang [98] investigated the lateral stiffness of a steel column at elevated temperatures by incorporating the reduction factor of elastic modulus at elevated temperatures into Eqs. (2.20) derived by Xu [35]. Ma and Xu [99] adopted the tangent modulus instead of the elastic modulus of steel at elevated temperatures, which is more consistent with the realistic nonlinear stress-strain relationships of steel at elevated temperatures. The average stress on the column's cross-section was used to determine the tangent modulus for the reason of simplicity. However, as temperature increases, the stress gradient in the cross-section becomes more pronounced with an increasing internal moment. Subsequently, the portion of the cross-section with greater stress possesses a lower magnitude of tangent modulus. In that case, adopting the average cross-sectional stress may overestimate the column lateral stiffness at elevated temperatures if the exterior stress on the cross-section exceeds the proportional limit.

8.4.1 Comparison of column lateral stiffness at elevated temperatures with and without considering the partial yielding effect

To better illustrate the effect of partial yielding on the column lateral stiffness, the lateral displacement variations of a cantilever column (with a length of 1.18 m and an IPE 80 section) with heating temperature are investigated by Eqs. 2.20 with adopting tangent modulus of steel at elevated temperatures and by a finite element model (FEM) established via ABAQUS, respectively. The column is assumed to be subjected to an axial load of $P = 50\,\text{kN}$ and a lateral load of $Q = 2.5\,\text{kN}$ at its upper end. The steel yield strength and elastic modulus at ambient temperature are taken as 355 MPa and 210 GPa, respectively. The column is assumed to be initially perfectly straight and will bend about its strong axis. The retention factors of steel mechanical properties at elevated temperatures are taken as specified in EN 1993-1-2 [41].

If the partial yielding effect is not considered, the lateral stiffness of the column at elevated temperature, $S_{c,T}$, can be evaluated using the following equation [99]:

$$S_{c,T} = \frac{12 E_{c,\tan} I_{c,i}}{L_{c,i}^3} \beta_T \tag{8.19a}$$

where $E_{c,\tan}$ is the tangent modulus of the column at the elevated temperature depending on the temperature and stress levels; β_T is the modification factor at elevated temperature obtained from Eqs. (2.20) with $E_c = E_{c,\tan}$.

Since the partial yielding effect is not considered, the average stress on the cross-section $\sigma = P/A$ is used to evaluate the value of $E_{c,\tan}$. Thus, the lateral displacement of the column at elevated temperature induced by the applied load, Δ_T, can be obtained from:

$$\Delta_T = Q/S_{c,T} \tag{8.20}$$

In the finite element analysis (FEA), the 2-D BEAM element B23, which neglects the effect of shear deformations, is adopted to model the column. As B23 elements account for the effect of stress gradient on the deformation, the effect of partial yielding on the column lateral stiffness can be reflected in the numerical results from FEA. Because the creep effect is not considered in both methods, the heating rate will not affect the results; thereby, the temperature heating curve is arbitrarily set as 1 °C per step. In both methods,

the nonlinear stress-strain relationships of steel at elevated temperatures specified in EN 1993-1-2 [41] are adopted, as depicted in Fig. 8.6. For comparison purposes, the results with the elastic-perfectly plastic stress-strain relationships obtained from the FEM are also attained.

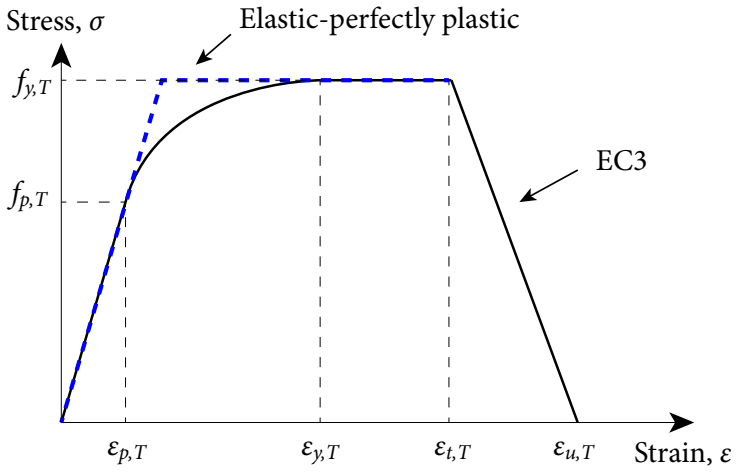

Figure 8.6: Nonlinear stress-strain curve in Eurocode 3 [41] and elastic-perfectly plastic stress-strain curve at the elevated temperature

Presented in Fig. 8.7 are the variations of column lateral displacement with heating temperature obtained from Eq. (8.20) and the FEA. The boundary lines in Fig. 8.7 denote when $\sigma_{ec,T}$ reaches the proportional limit $f_{p,T}$ and yield stress $f_{y,T}$ at the elevated temperature, respectively.

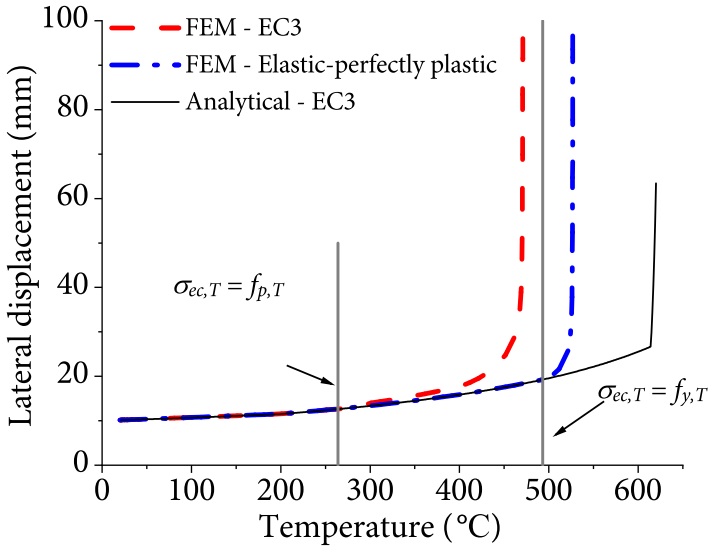

Figure 8.7: Comparison of lateral displacement variations with heating temperature between the FEA and analytical method

As the temperature increases, the stress gradient on the cross-section of the column increases due to the increasing lateral displacement and the accompanying increasing second-order effect. For the lateral displacement variation obtained from Eq. (8.20), the corresponding maximum exterior stress in compression on the cross-section is

$$\sigma_{ec,T} = \frac{P}{A_c} + \frac{QL_c + P\Delta_T}{S_x} \tag{8.21}$$

where S_x is the elastic section modulus about the strong axis.

When the maximum exterior stress is below the proportional limit ($\sigma_{ec,T} \leq f_{p,T}$), the tangent modulus distribution on the cross-section is uniform because the tangent modulus is the same as the elastic modulus. In that case, partial yielding has not occurred, and thus the predictions obtained from the analytical method and FEA are the same. Once the maximum exterior stress exceeds the proportional limit ($\sigma_{ec,T} > f_{p,T}$), the lateral displacement obtained from the FEA with EC3 model increases faster than those obtained from FEA with the elastic-perfectly plastic model and the analytical method with EC3 model. This is because when the stresses on a portion of the cross-section exceed the proportional limit $f_{p,T}$, the tangent modulus distribution on that portion is less than the elastic modulus, which leads to a reduction in the column lateral stiffness. However, such an effect is not considered in the analytical method and the FEA with the elastic-perfectly plastic model in which the tangent modulus is still the same as the elastic modulus when the stress exceeds the proportional limit, as presented in Fig. 8.7.

After the maximum exterior stress reaches the yield stress ($\sigma_{ec,T} = f_{y,T}$), the lateral displacement predicted from the FEA with the elastic-perfectly plastic model increases dramatically. This is because when $\sigma = f_{y,T}$ the tangent modulus in the elastic-perfectly plastic model is theoretically zero ($E_{c,\tan} = 0$), and consequently the stiffness of the portion with $\sigma = f_{y,T}$ diminishes. Although the tangent modulus is adopted in the analytical method, the average stress on the cross-section remains within the elastic state. Because of that, the lateral displacement calculated from the analytical method increases steadily as the temperature increases, even though the exterior stress reaches the yield stress ($\sigma_{ec,T} = f_{y,T}$), which results in an underestimation of the lateral displacement. Finally, the lateral displacement predicted by the analytical method reaches infinity, i.e., the lateral stiffness approaches zero, when the average stress reaches the yield stress ($P/A_c = f_{y,T}$).

8.4.2 Modification of column lateral stiffness to mimic the partial yielding effect

As discussed above, using the average stress to evaluate the column lateral stiffness neglects the adverse influence of the spread of plasticity, which leads to overestimated column lateral stiffness at elevated temperatures. Hence, the column lateral stiffness in the analytical expressions in Eq. (8.19) should be reduced gradually after the initial yield state is reached to consider the partial yielding effect, especially for fire analysis. In this section, the modified plastic-hinge approach proposed by King et al. [116] is adapted to modify the column lateral stiffness at elevated temperatures. The initial yield surface without considering the effect of residual stresses [117] is expressed in

$$\frac{P}{P_y} + \frac{fM}{M_p} = 1.0 \tag{8.22}$$

where f is the shape factor of the cross-section, the ratio of the plastic section modulus Z_x to the elastic section modulus S_x.

Based on the work by Duan and Chen [118], the full yield surface describing the cross-section strength without considering the adverse effect of residual stresses can be expressed as

$$\left(\frac{P}{P_y}\right)^{\xi} + \frac{M}{M_p} = 1.0 \tag{8.23}$$

where the exponent ξ depends on the shape of the member section and which axis the member bends about. For example, ξ equals 1.3 for wide-flange sections bending about the strong axis.

The initial yield surface and full yield surface are plotted in Fig. 8.8, wherein the partial yielding state is the region between the initial and full yield surfaces. The reduction coefficient ρ in Eq. (8.24) proposed by King et al. [116] is adopted to consider the gradual reduction from column's elastic lateral stiffness at the onset of yielding to the inelastic lateral stiffness associated with a full plastic hinge at the location with maximum bending moment.

$$0 \leq \rho = \frac{M - M_{yc}}{M_{pc} - M_{yc}} \leq 1 \tag{8.24}$$

where M_{yc} and M_{pc} are the bending moments at the initial yield and full yield, respectively, associated with the applied load P.

From Eq. (8.22) and Eq. (8.23), M_{yc} and M_{pc} are given in

$$M_{yc} = \left(1 - \frac{P}{P_y}\right) M_y \tag{8.25}$$

$$M_{pc} = \left[1 - \left(\frac{P}{P_y}\right)^{\xi}\right] M_p \tag{8.26}$$

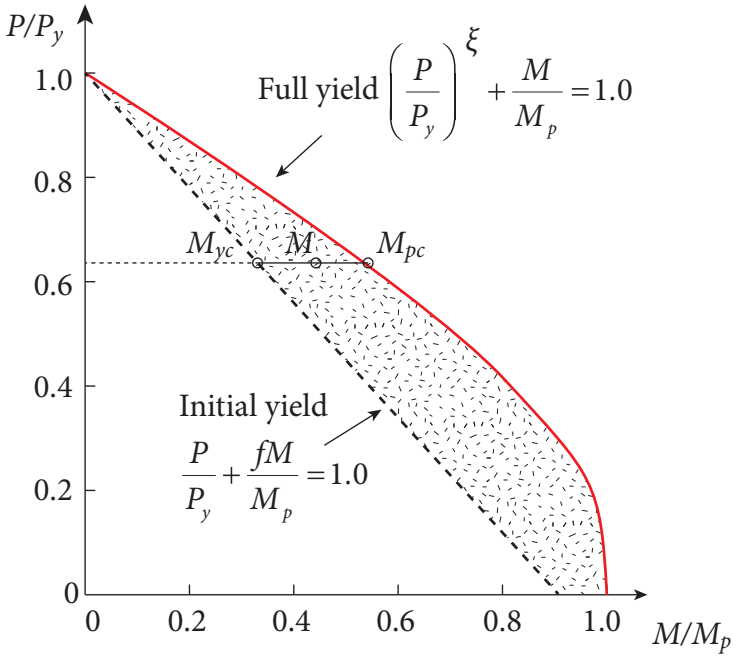

Figure 8.8: Cross-section strength surface (full yield) and initial yield surface neglecting the effect of residual stresses [116]

Alternatively, an initial surface that accounts for the effect of residual stresses can be adopted, as given in Eq. 8.27 and plotted in Fig. 8.9 [116].

$$\frac{P}{0.8P_y} + \frac{fM}{0.9M_p} = 1.0 \tag{8.27}$$

It was stated in [116] that Eq. (8.27) is more appropriate for use with the modified plastic-hinge method for wide-flange sections [116]. If Eq. (8.27) is adopted, then the term M_{pc} in Eq. (8.24) becomes

$$M_{yc} = \left(1 - \frac{P}{0.8P_y}\right) 0.9M_y \tag{8.28}$$

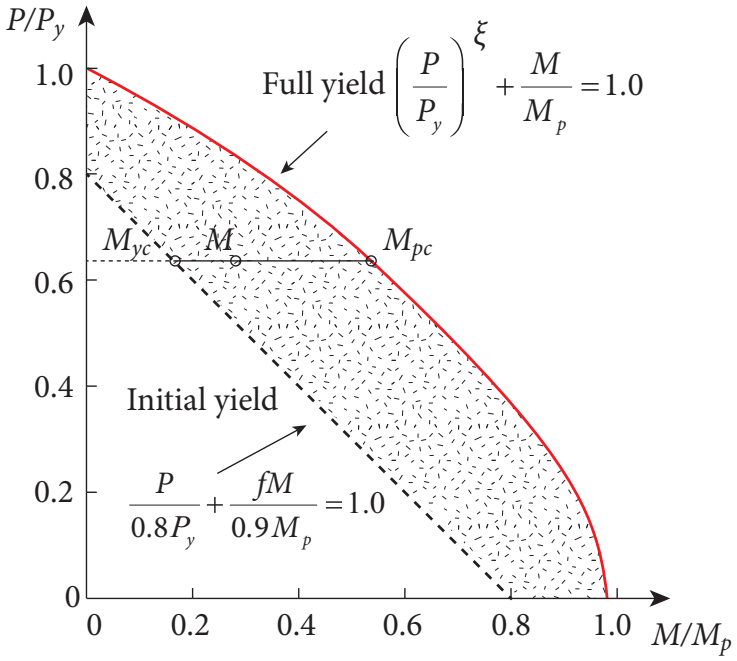

Figure 8.9: Full yield surface and initial yield surface considering the effect of residual stresses [116]

Using the simple incremental method, the column lateral stiffness considering the partial yielding effect at step j is

$$S^j_{c,\text{mod}} = S^j_{c,T}(1-\rho^j) \tag{8.29}$$

where ρ^j is computed based on the additional lateral displacement of the previous step $j-1$ and the moment criteria (M_{yc} and M_{pc}) at the current step j, as below:

$$0 \le \rho^j = \frac{M(\Delta^{j-1}) - M^j_{yc,T}}{M^j_{pc,T} - M^j_{yc,T}} \le 1.0 \tag{8.30a}$$

$$\Delta^{j-1} = \frac{Q}{S^{j-1}_{c,\text{mod}}} \tag{8.30b}$$

By adopting the modified column lateral stiffness in Eq. (8.29), the lateral displacement variations of the column presented in Section 8.4 with heating temperature are obtained and plotted in Fig. 8.10. As residual stresses were not considered in the FEA and analytical analysis, Eq. (8.25) is used to compute the reduction coefficient ρ.

Different from the case at the ambient temperature that $M_y = f_y S_x$, the elastic moment resistance $M_{y,T}$ at the elevated temperature should be taken as $f_{p,T} S_x$ if the nonlinear stress-strain relationships of steel are used. For comparison purposes, the variation of the column

lateral stiffness associated with $M_{y,T} = f_{y,T} S_x$ is also presented in Fig. 8.10. It can be seen that the results using the modified column lateral stiffness with $M_{y,T} = f_{p,T} S_x$ show better agreement with the FEA results than the analytical results without account for the partial yielding. Nonetheless, the results associated with $M_{y,T} = f_{y,T} S_x$ cannot consider the stiffness degradation induced by partial yielding after the exterior stress reaches the proportional limit $\sigma_{ec,T} = f_{p,T}$.

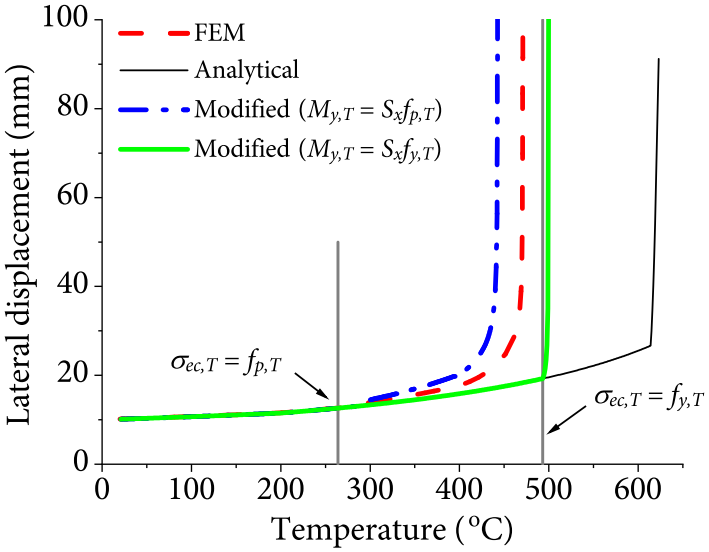

Figure 8.10: Comparison of lateral displacement between FEA and analytical methods with and without considering partial yielding

8.5 Effect of Thermal Creep on Column Lateral Stiffness

A numerical method was proposed in Chapter 7, to qualify the effect of thermal creep strain on the mid-height lateral deflection of steel columns. This method is mainly based on the assumptions that the deformed shape of the steel column is proportional to the column's mid-height deflection as temperature increases, and that the mid-height deflection depends on the strain gradient on the cross-section of the column's mid-height, as indicated in Eq. (8.31).

$$\Delta_T = \frac{L^2}{\pi^2} \frac{\varepsilon_{ec,T} - \varepsilon_{et,T}}{d} \tag{8.31}$$

where $\varepsilon_{ec,T}$ and $\varepsilon_{et,T}$ respectively represent the strains of the exterior edge in compression and in tension (after deducting the stress led by the axial force, P/A) at the elevated temperature T; d is the height of the cross-section. The term L^2/π^2 is associated with assuming

the column's deformed shape to be a sinusoidal curve.

Attaining precise values of $\varepsilon_{ec,T}$ and $\varepsilon_{et,T}$ is highly related to the accuracy of the cross-section stress and strain distributions. Illustrated in the left diagram of Fig. 8.11 is a typical cross-sectional normal stress distribution of a column subjected to axial load and bending moment. The stress gradient on the cross-section is nonlinear due to the nonlinear stress-strain relationships of steel at elevated temperatures, especially for the portion exceeding the proportional limit. Admittedly, if the nonlinear stress distribution is considered, obtaining the magnitudes of the exterior stresses and strains is rather complex, as illustrated in Chapter 7. Therefore, the cross-sectional stress gradient is assumed to be linear for simplicity, as illustrated in the right diagram in Fig. 8.11. Upon the plane section hypothesis, this assumption is feasible because of two reasons: 1) for the portion in which the stress distribution is below the proportional limit, the stress gradient is almost linear; 2) for the yielding portion in which the stress exceeds the proportional limit, assuming the stress gradient to be linear is conservative because it neglects the stress relaxation effect due to the reduced modulus.

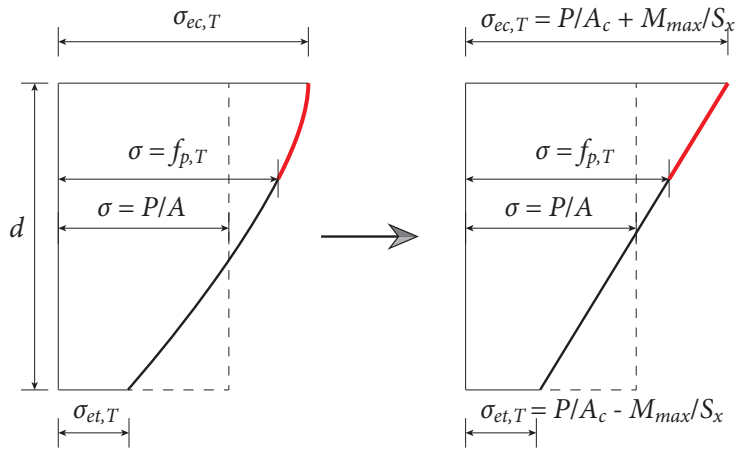

Figure 8.11: Cross-sectional normal stress distributions at elevated temperatures

By adopting the assumption of linear stress distribution, the exterior stresses are

$$\sigma_{ec,T} = \frac{P}{A_c} + \frac{M_{\max}}{S_x} \tag{8.32a}$$

$$\sigma_{et,T} = \frac{P}{A_c} - \frac{M_{\max}}{S_x} \tag{8.32b}$$

If the column bends about the weak axis, replace S_x in Eq. (8.32) with S_y.

If the cross-sectional temperature distribution is assumed to be uniform, then the strains in Eq. (8.31) consist of two parts: the instantaneous mechanical strain ε_{st} induced by the

stress and the thermal creep strain ε_{cp}:

$$\varepsilon = \varepsilon_{\text{st}} + \varepsilon_{\text{cp}} \tag{8.33}$$

In addition to the assumption that the deflection is related to the cross-sectional strain gradient in Eq. (8.31), the modified deflection Δ_{cp} considering the creep effect can be attained by

$$\Delta_{\text{cp}} = \frac{\varepsilon_{\text{st}}|_{\sigma=\sigma_{ec,T}} - \varepsilon_{\text{st}}|_{\sigma=\sigma_{et,T}} + \varepsilon_{\text{cpc}} - \varepsilon_{\text{cpt}}}{\varepsilon_{\text{st}}|_{\sigma=\sigma_{ec,T}} - \varepsilon_{\text{st}}|_{\sigma=\sigma_{et,T}}} \Delta_T = \alpha_{\text{cp}} \Delta_T \tag{8.34}$$

in which the exterior strains $\varepsilon_{ec,T}$ and $\varepsilon_{et,T}$ are determined according to the nonlinear stress-strain relationships of steel at elevated temperatures with known stress values. The exterior creep strains ε_{cpc} and ε_{cpt} can be determined using either the time-hardening formulation in (7.10) or the strain-hardening formulation in Eq. (7.12). Let α_{cp} correspond to the amplification factor of the lateral displacement considering the creep effect. Meanwhile, α_{cp} is the reduction factor of the column lateral stiffness:

$$S_{c,\text{cp}} = \frac{S_c}{\alpha_{\text{cp}}} \tag{8.35}$$

where $S_{c,\text{cp}}$ is the modified column lateral stiffness considering the thermal creep effects. Determining the bending moment at the mid-height of the column is the precondition of computing the exterior stresses as well as the exterior strains.

For semi-rigidly connected columns with known end-fixity factor r_e, the bending moment at the mid-height is

$$M_m = \Omega_1 LQ + \Omega_2 \frac{P\Delta_0}{L} \tag{8.36}$$

where Q is the lateral load applied on the mid-height of the column; for a column in a multiple-column system, the lateral load applied on the column is the difference between the internal forces in adjacent braces. Ω_1 and Ω_2 are coefficients related to the load factor (ϕ) and end-fixity factor (r_e):

$$\Omega_1 = \frac{3r_e\left(1-\cos\phi\right) + \phi\sin\phi\,(1-r_e)}{\phi(\phi\cos\phi\,(1-r_e) + 3r_e\sin\phi)} \tag{8.37a}$$

$$\Omega_2 = \pi^2 \frac{\phi\cos\phi\,(1-r_e) - 6\phi r_e/\pi + 3r_e\sin\phi}{(\pi^2-4\phi^2)(\phi\cos\phi\,(1-r_e) + 3r_e\sin\phi)} \tag{8.37b}$$

Since Eq. (8.36) is derived from the equilibrium illustrated in Fig. 3.2, it accounts for the effect of column initial curvature on the bending moment at the column mid-height.

8.6 Evaluating the Critical Temperature of Multi-column Systems

8.6.1 Problem formulation

This section proposes a numerical method for evaluating the critical temperature of multi-column systems. The calculation procedure is incremental because of considering the effects of partial yielding and creep. Based on Eq. (4.18), the force-displacement relationship without considering the thermal expansion effects for a multi-column system at time j can be written as

$$\mathbf{S}^j \mathbf{D}^j = \mathbf{Q}_\mathbf{0}^j \tag{8.38}$$

where the vector of the equivalent lateral forces $\mathbf{Q}_\mathbf{0}^j$ is $\left[Q_{0,1}^j, Q_{0,2}^j, ..., Q_{0,n}^j\right]^\mathrm{T}$, in which Q_0 is attained from Eq. (4.10), and the vector of the column mid-height deflections $\mathbf{D}^j$ is $\left[\Delta_1^j, \Delta_2^j, ..., \Delta_n^j\right]^\mathrm{T}$. The stiffness matrix for the multi-column system is

$$\mathbf{S}^j = \begin{bmatrix} S_{b,1}^j + S_{b,n+1}^j + S_{c,1}^j & -S_{b,1}^j & & & \\ -S_{b,1}^j & S_{b,1}^j + S_{b,2}^j + S_{c,2}^j & \ddots & & \\ & \ddots & \ddots & -S_{b,n-1}^j & \\ & & -S_{b,n-1}^j & S_{b,n-1}^j + S_{b,n}^j + S_{c,n}^j & \end{bmatrix} \tag{8.39}$$

At elevated temperatures, the adverse effects of material degradation, partial yielding, and creep on the stiffness of members shall be considered. On account of those factors, $S_{c,i}^j$ in Eq. (8.39) is

$$S_{c,i}^j = \frac{1-\rho_i^j}{\alpha_{\mathrm{cp},i}^j} S_{c,T,i}^j \tag{8.40}$$

where ρ_i^j and $\alpha_{\mathrm{cp},i}^j$ are attained from Eqs. (8.30a) and Eq. (8.34), respectively.

Since the possible buckling of braces is neglected in this study, the axial stiffness of braces associated with the tangent modulus can be attained based on the magnitude of the average cross-sectional stress. In that case, the modified secant modulus E_cp given in Eq. (8.41) proposed by Li et al. [119] can be adopted to account for the creep effect on the brace stiffness at elevated temperatures for simplicity.

$$E_\mathrm{cp} = \frac{E_\mathrm{tan}}{E_\mathrm{tan}\frac{\varepsilon_\mathrm{cp}}{\sigma} + 1} \tag{8.41}$$

Adopting the modified tangent modulus in Eq. (8.41), $S_{b,i}^{j}$ in Eq. (8.39) considering the creep effect at elevated temperatures is

$$S_{b,i}^{j} = \frac{E_{\mathrm{cp},i}^{j} A_{b,i}}{L_{b,i}} \tag{8.42}$$

With the above equations, the column displacements induced by the applied axial loads and initial imperfections at elevated temperatures can be attained from Eq. (8.38). Furthermore, the vector of column displacements caused by the thermal expansions of braces, $\mathbf{D_{th}}^{j}$, can be obtained from Eq. (8.12) or Eq. (8.15). As such, considering the effects of partial yielding, creep, and braces' thermal expansion, the total displacements of columns in the system at time j is

$$\mathbf{D_{total}}^{j} = \mathbf{D}^{j} + \mathbf{D_{th}}^{j} \tag{8.43}$$

Attaining $S_{b,i}^{j}$ requires knowing the value of the cross-sectional stress in the brace, which is determined by the internal force in the brace. Due to considering the creep effect, the relationships among the column displacements, column stiffness, brace stiffness, and brace forces become transcendental, and therefore, $S_{b,i}^{j}$ is determined based on the total brace forces at the previous step $j-1$, which can be obtained from

$$\mathbf{Q}_{\mathbf{total}}^{j-1} = \mathbf{Q}^{j-1} - \mathbf{Q}_{\mathbf{th}}^{j-1} \tag{8.44}$$

where $\mathbf{Q}_{\mathbf{th}}^{j-1}$ is the vector of thermal-induced brace forces at time $j-1$, which is attained from either Eqs. (8.10) or Eq. (8.14). $\mathbf{Q}^{j-1}$ is the vector of brace forces induced by the applied axial loads, which can be obtained by solving

$$\mathbf{F}^{j-1}\mathbf{Q}^{j-1} = \mathbf{D}_{\mathbf{dif}}^{j-1} \tag{8.45}$$

where $\mathbf{D}_{\mathbf{dif}}^{j-1}$ is the vector of the column lateral displacement differences induced by the axial loads, and $\mathbf{F}^{j-1}$ is the equivalent flexibility matrix of the multi-column system.

For the systems anchored on one side and on both sides, the expressions of $\mathbf{Q}^{j-1}$, $\mathbf{D}_{\mathbf{dif}}^{j-1}$,

and $\mathbf{F}^{j-1}$ are given in Eqs. (8.46) and Eqs. (8.47), respectively.

$$\mathbf{F}^{j-1} = \begin{bmatrix} \frac{1}{S_{b,1}^{j-1}} + \frac{1}{S_{c,1}^{j-1}} + \frac{1}{S_{c,2}^{j-1}} & -\frac{1}{S_{c,2}^{j-1}} & & & \\ -\frac{1}{S_{c,2}^{j-1}} & \frac{1}{S_{b,2}^{j-1}} + \frac{1}{S_{c,2}^{j-1}} + \frac{1}{S_{c,3}^{j-1}} & -\frac{1}{S_{c,3}^{j-1}} & & \\ & -\frac{1}{S_{c,3}^{j-1}} & \ddots & \ddots & \\ & & \ddots & \frac{1}{S_{b,n-1}^{j-1}} + \frac{1}{S_{c,n-1}^{j-1}} + \frac{1}{S_{c,n}^{j-1}} & -\frac{1}{S_{c,n}^{j-1}} \\ & & & -\frac{1}{S_{c,n}^{j-1}} & \frac{1}{S_{b,n}^{j-1}} + \frac{1}{S_{c,n}^{j-1}} \end{bmatrix} \tag{8.46a}$$

$$\mathbf{Q}^{j-1} = \begin{Bmatrix} Q_1^{j-1} \\ Q_2^{j-1} \\ \vdots \\ Q_{n-1}^{j-1} \\ Q_n^{j-1} \end{Bmatrix} \qquad \mathbf{D}_{\mathbf{dif}}^{j-1} = \begin{Bmatrix} \frac{Q_{0,1}}{S_{c,1}^{j-1}} - \frac{Q_{0,2}}{S_{c,2}^{j-1}} \\ \frac{Q_{0,2}}{S_{c,2}^{j-1}} - \frac{Q_{0,3}}{S_{c,3}^{j-1}} \\ \vdots \\ \frac{Q_{0,n-1}}{S_{c,n-1}^{j-1}} - \frac{Q_{0,n}}{S_{c,n}^{j-1}} \\ \frac{Q_{0,n}}{S_{c,n}^{j-1}} \end{Bmatrix} \tag{8.46b}$$

$$\mathbf{F}^{j-1} = \begin{bmatrix} -\frac{1}{S_{b,n+1}^{j-1}} + \frac{1}{S_{c,1}^{j-1}} & \frac{1}{S_{c,1}^{j-1}} & & & \\ -\frac{1}{S_{c,1}^{j-1}} & \frac{1}{S_{b,1}^{j-1}} + \frac{1}{S_{c,1}^{j-1}} + \frac{1}{S_{c,2}^{j-1}} & -\frac{1}{S_{c,2}^{j-1}} & & \\ & -\frac{1}{S_{c,2}^{j-1}} & \ddots & \ddots & \\ & & \ddots & \frac{1}{S_{b,n-1}^{j-1}} + \frac{1}{S_{c,n-1}^{j-1}} + \frac{1}{S_{c,n}^{j-1}} & -\frac{1}{S_{c,n}^{j-1}} \\ & & & -\frac{1}{S_{c,n}^{j-1}} & \frac{1}{S_{b,n}^{j-1}} + \frac{1}{S_{c,n}^{j-1}} \end{bmatrix} \tag{8.47a}$$

$$\mathbf{Q}^{j-1} = \begin{Bmatrix} Q_{n+1}^{j-1} \\ Q_1^{j-1} \\ \vdots \\ Q_{n-1}^{j-1} \\ Q_n^{j-1} \end{Bmatrix} \qquad \mathbf{D}_{\mathbf{dif}}^{j-1} = \begin{Bmatrix} \frac{Q_{0,1}}{S_{c,1}^{j-1}} \\ \frac{Q_{0,2}}{S_{c,1}^{j-1}} - \frac{Q_{0,3}}{S_{c,2}^{j-1}} \\ \vdots \\ \frac{Q_{0,n-1}}{S_{c,n-1}^{j-1}} - \frac{Q_{0,n}}{S_{c,n}^{j-1}} \\ \frac{Q_{0,n}}{S_{c,n}^{j-1}} \end{Bmatrix} \tag{8.47b}$$

It is worth noting that the equations proposed in this section for evaluating the structural responses of multi-column systems braced at columns' mid-height are also applicable for that of single-storey braced or unbraced frames with minor revisions.

8.6.2 Failure criteria and assumptions

The critical temperature of the multi-column system can be determined when satisfying any one of the following failure criteria at time j:

$$S^j_{\text{eq},1} \leq 0 \tag{8.48a}$$

$$P_i + P^j_{\text{th}} \geq P^j_{cr,T,i} \tag{8.48b}$$

$$P_i + P^j_{\text{th}} \geq P^j_{y,T,i} \tag{8.48c}$$

$$\sigma^j_{ec,T,i} \geq f^j_{y,T,i} \tag{8.48d}$$

$$\Delta^j_{\text{max}} \geq \Delta_{\text{limit}} \tag{8.48e}$$

$$Q^j_{\text{total},i} \geq f^j_{y,T,i} A_{b,i} \tag{8.48f}$$

The term $S^j_{\text{eq},1}$ in Eq. (8.48a) is the equivalent stiffness of the whole multi-column system, which is attained from Eq. (4.3) with known stiffness of columns and braces at time j. Eq. (8.48a) signifies the state when the system reaches its overall lateral instability. The criteria in Eqs. (8.48b) to (8.48d) indicate the failure of individual columns. In practice, the criterion in Eq. (8.48e) may be required to ensure that the maximum lateral displacement of the multi-column system will not exceed a certain value to damage the adjacent robust firewalls, thus preventing the fire from spreading to other buildings [71]. The criterion in Eq. (8.48f) denotes the yield strength failure of the brace.

The foregoing proposed equations of assessing the critical temperature of braced multi-column systems are established based on the following assumptions:

1. The temperature distributions throughout each column and brace are assumed to be uniform, and the maximum temperature in the member is used to attain the corresponding deteriorated mechanical properties for being conservative.

2. The other possible failure modes except those indicated in Eqs. (8.48) are neglected, such as buckling of braces, torsional buckling and local buckling of columns as well as connections' failure.

3. The axial deformations of columns are neglected, and as such the braces are assumed to be horizontal during the fire.

8.6.3 Computational procedure

An incremental procedure for predicting the critical temperature of a braced multi-column system is presented in this subsection.

1. Establish known and constant properties of the system, including the cross-sectional properties and lengths for each member ($L_{c,i}$, $A_{c,i}$, $I_{c,i}$, and $L_{b,i}$), the end connection stiffness for each column R_i, and the steel mechanical properties at ambient temperature f_y and E. Define the number of anchors in analysis. If flexible anchor(s) exists, specify the value of c_r (and c_l); if not, $c_r = c_l = 0$. Specify the gravity loads on each column, P_i.

2. According to the steel grade and type, designate the stress-strain relationships and retention factors of mechanical properties at elevated temperatures. Based on the heating curves, assign the temperatures of each member and end connections at each step.

3. Identify the maximum allowable lateral displacement of the system at elevated temperatures, Δ_{limit}, if required.

4. Calculate the resulting temperature-dependent mechanical properties of each member in the system, including the elastic modulus $E_{T,i}$, proportional limit $f_{p,T,i}$, and yield strength $f_{y,T,i}$. Based on the obtained column and end connection stiffnesses, calculate the value of end-fixity factor $r_{e,i}$.

5. Following the computation procedure given in Chapter 5, compute the required brace area $A_{b,i}$ and brace stiffness $S^1_{b,i}$ for the multi-column system. With obtained $S^1_{b,i}$, calculate the column displacements $\mathbf{D}^1$, and brace forces $\mathbf{Q}^1$ at ambient temperatures. Set the column displacements and brace forces induced by the thermal expansions, $\mathbf{D}^1_{\mathbf{th}}$ and $\mathbf{Q}^1_{\mathbf{th}}$, as zero. Knowing the magnitudes of brace forces, calculate the bending moment at the column mid-height M^1_i using Eq. (8.36) and Eq. (8.37). Set the time step $j = 2$.

6. Obtain the values of $S^j_{c,i}$ and $S^j_{b,i}$ using Eq. (8.40) and Eq. (8.42), respectively. Establish and solve the linear equations in Eq. (8.38) to obtain the values of column lateral

displacements $\mathbf{D}^j$. Establish and solve the linear equations in Eq. (8.45) to attain the values of brace forces $\mathbf{Q}^j$.

7. Calculate the thermal-induced brace forces $\mathbf{Q}_{\mathbf{th}}^j$ using either Eqs. (8.10) or Eq. (8.14). Calculate the column lateral displacements induced by the thermal expansion of braces $\mathbf{D}_{\mathbf{th}}^j$ using Eq. (8.12) or Eq. (8.15). Obtain the total column displacements and brace forces, $\mathbf{D}_{\mathbf{total}}^j$ and $\mathbf{Q}_{\mathbf{total}}$, from Eq. (8.43) and Eq. (8.44), respectively.

8. Attain the value of $S_{\text{eq},1}^j$ using Eq. 4.3 and the values of column cross-sectional maximum stress $\sigma_{ec,T,i}^j$.

9. Check if the failure criteria specified in Eqs. (8.48) have been exceeded. If any failure criterion has been exceeded, terminate the calculation procedure and output the temperature at the current step as the critical temperature; if not, set the time step as $j = j + 1$ and return to Step 6.

8.7 Validation

The foregoing proposed numerical method is validated using the results of a fire test on a two-bay steel frame (ZSR1), which was conducted by Rubert and Schaumann [60]. Due to the lack of experimental results regarding large-scale multi-column systems at elevated temperatures, this test data has been widely adopted by previous researchers [59, 71, 120]. The dimensions of the frame and the magnitudes of external loads are shown in Fig. 8.12. All the members in the frame are made of IPE 80 section bending about its strong axis. The moment of inertia, elastic section modulus, plastic section modulus, and cross-sectional area of IPE 80 section are $I_x = 8.01 \times 10^5\,\text{mm}^4$, $S_x = 2.00 \times 10^4\,\text{mm}^3$, $Z_x = 2.32 \times 10^4\,\text{mm}^3$, and $A_c = 764\,\text{mm}^2$, respectively. The decrease of the force in the left column and increase of the force in the right column due to the lateral force are considered when calculating the column lateral stiffness in the analysis. The yield strength and elastic modulus of steel at ambient temperature are 355 MPa and 210 GPa, respectively. The retention factors of steel mechanical properties and stress-strain relationships at elevated temperatures specified in Eurocode 3 [41] are adopted. The creep effect is not considered in the validation for the following reasons. First, the gas and members' heating curves were not provided by Rubert and

Schaumann [60], which are necessary for considering the creep effect. Second, the stress-strain relationship of steel stipulated in Eurocode 3 follows the same format of the stress-strain relationship proposed by Rubert and Schaumann, except that Eurocode 3 includes a decay phase. As stated by Rubert and Schaumann [60], this stress-strain relationship has implicitly considered the creep effects for heating rates within $2 \leq \dot{T} \leq 30\,\mathrm{K/min}$.

As illustrated in Fig. 8.12, only the left bay of the frame was uniformly heated without protection, while the right bay was protected and not heated. Because of that, Rubert and Schaumann [60] assumed that all the members exposed to fires possess uniform heating temperature distribution, and the temperature of protected members remained at room temperature (20 °C), as per Fig. 8.12. This assumption is adopted in the following numerical analysis. As the measured maximum angles of the member chord of the columns are approximately 1/600, the out-of-plumbness of all columns is taken as $L_c/600$ towards the right in the same direction as the lateral load. The column initial curvature is not considered in the analysis because the maximum initial mean deflection of the single column is less than $L_c/3000$, which is negligible. The initial yield surface given in Eq. (8.27) is adopted to account for the effect of residual stresses.

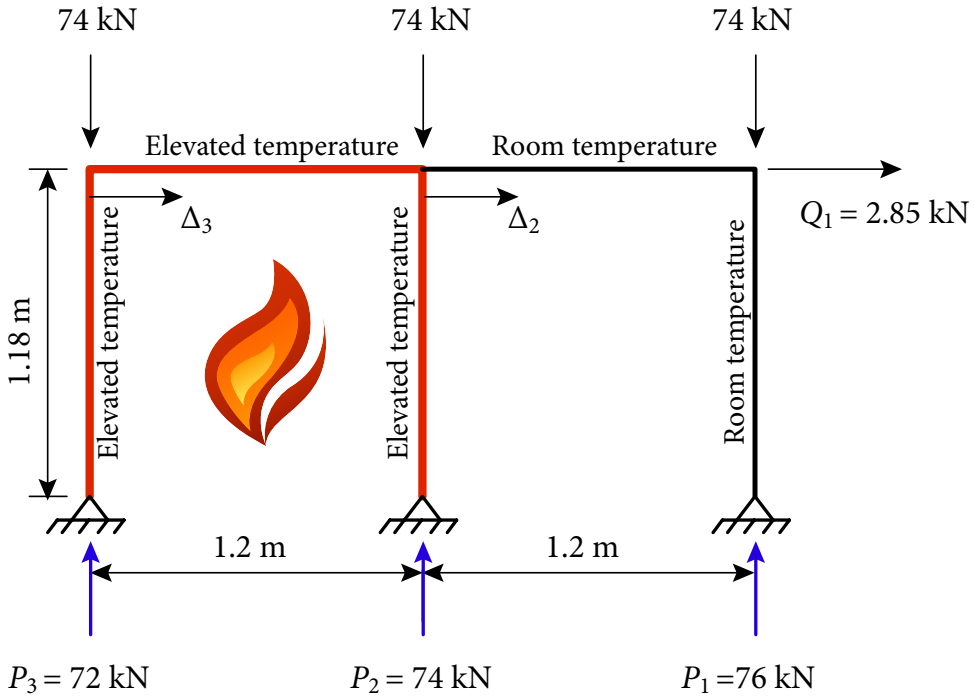

Figure 8.12: Unbraced frame in the fire test by Rubert and Schaumann

Not reported by Rubert and Schaumann, the thermal expansion coefficient is computed

using the expression given in [121], as below:

$$\alpha_{\text{th}} = (0.004T + 12)\,10^{-6}\,^{\circ}\text{C}^{-1} \tag{8.49}$$

The comparison of the variations of column lateral displacements between experimental results and numerical analysis results are plotted in Fig. 8.13. In the test, mainly due to the thermal expansion of the fire-exposed beam, the lateral displacement of the left column Δ_3 increased slower than that of the middle column Δ_2, which is also reflected in the numerical analysis results. The numerical results show good agreements with experimental results before the heating temperature reaches 250 °C, while the discrepancies increases afterwards. This may be explained that the fire behaviour of beam-column connections was neglected in the numerical analysis, which would lower the lateral stiffness of the frame and consequently lead to larger lateral displacements. As the temperature exceeded 265 °C, the reduction coefficient ρ for the middle column became greater than zero, indicating the inelastic behaviour in the middle column. Finally, with the increasing lateral displacements induced by the deteriorated stiffness of members, the assessed exterior stress in the middle column reached the yield strength at 549 °C, achieving a good agreement with the critical temperature obtained from the experimental result, 547 °C.

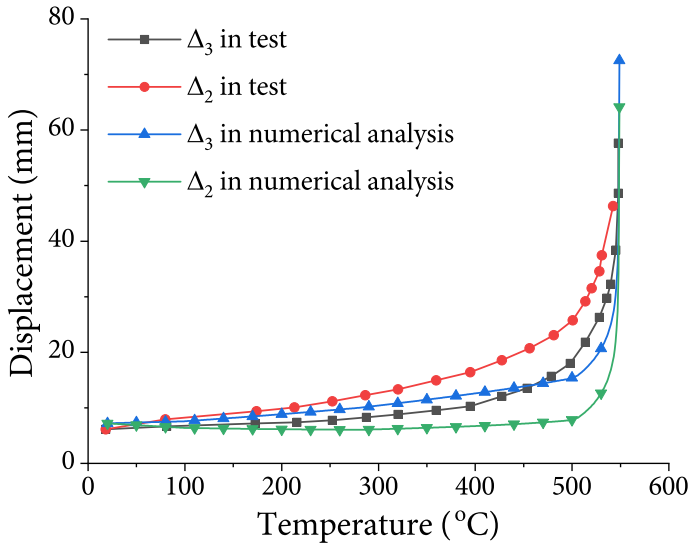

Figure 8.13: Comparison of structural responses of ZSR1 tested by Rubert and Schaumann between experimental results and numerical analysis results

For comparison, the predictions from the proposed numerical method without considering the thermal expansion of beams and without considering the partial yielding effect are

presented in Fig. 8.14 and Fig. 8.15, respectively.

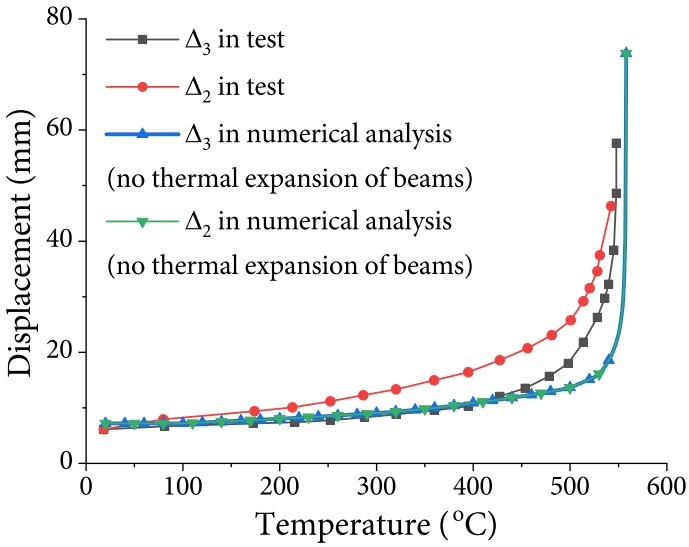

Figure 8.14: Comparison between experimental results and numerical analysis results without considering the thermal expansion of beams

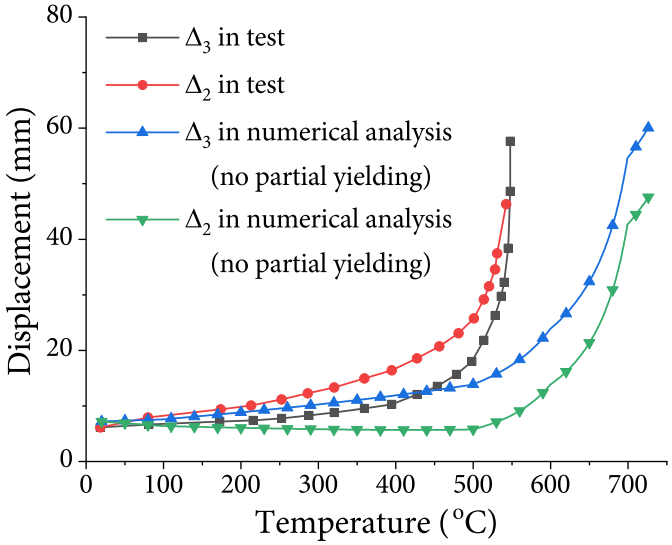

Figure 8.15: Comparison between experimental results and numerical analysis results without considering the partial yielding of columns

It can be seen that if the thermal expansion of the fire-exposed beam is neglected, the difference between the column lateral displacements is just the beam deformation induced by the internal axial load, which is negligible. As a consequence, without the contribution of the beam's thermal expansion, the lateral displacement of the middle column Δ_3 increases

slower, and consequently the inelastic behaviour in the middle column emerges when the column temperature surpasses 300 °C. At the end, the critical temperature obtained from the numerical analysis without considering the beam's thermal expansion is 557 °C. Provided that the partial yielding is neglected, the column lateral displacements increase slowly and steadily before 500 °C. Once the temperature exceeds 500 °C, there is an obvious acceleration in the column lateral displacements due to the more severe deterioration of the tangent modulus of columns $E_{c,\tan}$. In this case, the critical temperature is 582 °C based on the criterion that the exterior stress exceeds the yield strength. Therefore, the effects of the thermal expansion of beams and partial yielding shall not be neglected in assessing the critical temperature of multi-column systems at elevated temperatures; otherwise, it may lead to overestimated results.

8.8 Conclusions

Methods for investigating the effects of the thermal expansion of braces, partial yielding and thermal creep of columns on the fire behaviour of multi-column systems are proposed in this Chapter. Analytical expressions are derived to compute the additional internal forces in braces and lateral displacements of columns induced by the thermal expansions of braces in multi-column systems. These expressions are comprehensively applicable to cases with different applied axial loads, column sizes, and heating rates of members. It has been shown that the inelastic behaviour of steel columns' cross-section, i.e., the partial yielding effect, has a significant influence on the lateral stiffness of steel columns at elevated temperatures. Hence, the partial yielding effect on steel columns at elevated temperatures is considered by adopting the modified plastic-hinge method. It has been proved in Chapter 7 that the creep-induced deflection at elevated temperatures can be accurately assessed by computing the stress and strain gradients on the column's cross-section. In light of this discovery, a simplified method is proposed to consider the thermal creep effect on the lateral stiffness of steel columns at elevated temperatures, which can be adopted in assessing the fire behaviour of multi-column systems. Finally, a numerical method is proposed for evaluating the critical temperature of multi-column systems with the considerations of the foregoing discussed three factors. The proposed method is verified using fire test results of an unbraced frame, and good agreements have been achieved between numerical and experimental results.

Chapter 9

Summary and Conclusions

9.1 Introduction

Intermediate bracing has been commonly used in multi-column systems such as industrial buildings and cold-formed load-bearing walls to increase the system's strength and stability. The bracing must satisfy both the strength and stiffness requirements to ensure that the system can reach its full buckling strength. Due to adopting Winter's model [7], the previous research [5, 8, 9, 18–20, 22] and the provisions in current standards [10, 11, 24, 26] regarding the bracing requirements are based on the assumptions of uniform stiffness, which requires that 1) all the columns have the same size, are subjected to the identical axial load, and are connected with pinned-ends; 2) all the braces have the same stiffness. Such assumptions certainly restrict the applications of the design specifications in current standards. Therefore, this research project was initiated to investigate the bracing requirements for multi-column systems with nonuniform stiffness for both columns and braces by adapting the storey-based stability concept. In addition, the fire behaviour of multi-column systems is investigated as it has been an inseparable part of the design of steel structures. In particular, the detrimental effects of thermal expansion of braces, partial yielding of columns, and creep strains on the stability of multi-column systems at elevated temperatures are considered.

9.2 Bracing Requirements for a Single Semi-rigidly Connected Column

As the prerequisite of considering the effects of nonuniform stiffness and semi-rigid end connections of columns on the bracing requirements for multi-columns, a new half-length column model is proposed in lieu of Winter's model. The proposed model is capable of accounting for the effects of semi-rigid connections, column initial curvature, and column stiffness on the additional displacement of a single column braced at its mid-height. By adopting the proposed model, the bracing requirements for a single semi-rigidly connected column are analyzed. In particular, a coefficient is introduced to assess the effect of column initial curvature on the additional column lateral displacement induced by the axial load, which consequently increases the bracing requirement. It has been found that the column initial curvature coefficient increases as the applied load increases but decreases as the end-fixity factor increases. The design procedures in AISC 360-16 [10] and CSA S16-19 [21] are extended to assess the bracing requirements for a semi-rigidly connected column considering the effect of column initial curvature. Both the proposed half-length column model and corresponding derived analytical equations are demonstrated and validated via a numerical example and finite element analysis.

9.3 Bracing Requirements for Multi-column Systems

By extending the proposed half-length column model to multi-column systems, two analytical methods are proposed to evaluate the ideal brace stiffness of systems consisting of multiple semi-rigidly connected columns. The first analytical method adopts the equivalent spring concept to condense the whole multi-column system into an equivalent spring, and as such the equivalent spring's stiffness being zero or negative is an indicator of the system's lateral instability. The second analytical method relates the derivation of the stiffness matrix of the system by formulating the stiffness interaction among columns and braces in the system. In addition, the second method is capable of evaluating the brace forces in the system with known magnitudes of column initial imperfections. Overall, both methods are comprehensively applicable to multi-column systems with nonuniform stiffness, which may

result from different column sizes, end-fixity factors, applied axial loads, or brace sizes.

Provided the system possesses uniform column lateral stiffness, the expressions proposed by Ziemian and Ziemian [5] for determining the ideal brace stiffness of multi-column systems in which the column ends are pin-connected are extended to consider the effect of semi-rigid column end connections. Furthermore, the explicit solution to the maximum brace force of the multi-column system with uniform stiffness is derived with the considerations of column end rotational stiffness, applied axial load, column initial curvature, and column initial imperfection. Examples with a distinctive column are presented to investigate the nonuniform column stiffness on the bracing requirements for multi-column systems. It has been found that the location of the distinctive column would affect the ideal brace stiffness and braces forces of the system. In particular, if the distinctive column possesses smaller stiffness than the rest of typical columns, then the required ideal brace stiffness and brace strength are larger than those obtained by assuming the system is composed of identical columns. In such cases, the effect of nonuniform column stiffness has to be considered in evaluating the bracing requirements for multi-column systems for the reason of safety.

9.4 Optimum Brace Stiffness for Multi-column Systems

Following the design philosophies in AISC 360-16 [10] and CSA S16-19 [21] and adopting the established stiffness matrices in Chapter 4, the required brace stiffness can be assessed by computing the brace forces and displacements of the multi-column system with the presupposed brace stiffness. However, it may involve a procedure with tedious iteration, which may overestimate the bracing requirements due to the interactive relationship between the brace stiffness and brace force. Therefore, a method is proposed to evaluate the minimum required stiffness of tie bracing (referred to as the optimum brace stiffness, $S_{b,\text{op}}$) that satisfies both the bracing stiffness and strength requirement for multi-column systems. Compared to following the design philosophies of current standards [10, 21], the advantages of the proposed method for computing $S_{b,\text{op}}$ are as follows. First, if the required bracing is governed by the strength, the magnitude of $S_{b,\text{op}}$ is smaller than that obtained by following the design philosophies in standards [10, 21], which leads to a more economical result. Second, if the required brace stiffness is controlled by the stiffness requirement

($\Delta < \Delta_0$), adopting the proposed method avoids a tedious trial-and-errors procedure to determine the brace stiffness to satisfy the stiffness requirement. Third, due to considering the effect of column initial curvature, it has been found that the proposed method yields a higher stiffness requirement than that of twice the ideal brace stiffness, as stipulated in AISC 360-16 [10].

9.5 Nonuniform Bracing of Multi-column Systems

The research presented in Chapters 4 and 5 is based on the assumption that all braces in the multi-column system have identical axial stiffness. In Chapter 6, the effects of nonuniform bracing, including the presence of solid blocking and different tie bracing stiffnesses on the bracing requirements, are explored. The expressions proposed in Chapter 5 are extended to consider the stiffness of solid blocking. As expected, the presence of solid blocking always reduces the stiffness and strength requirements of tie bracing in multi-column systems. In particular, it has been found that the presence of solid blocking leads to a larger reduction of required tie bracing cross-sectional area if the solid blocking is placed closer to an end anchor, the solid blocking has smaller spacing, or the anchor has larger rigidity. An optimization problem is proposed to minimize the total bracing stiffness with nonuniform bracing, and the corresponding solution to brace stiffnesses is referred to as optimum nonuniform bracing. For multi-column systems with uniform column lateral stiffness, the optimum bracing has a pattern in which the brace stiffness increases as the brace is closer to the end anchor.

9.6 Effect of Thermal-creep on Lateral Deflection of Steel Columns

Chapter 7 proposes a numerical method for evaluating the creep-induced lateral deflection of steel columns at elevated temperatures. It is demonstrated and validated against the experimental results that the creep buckling behaviour of steel columns can be accurately assessed using the proposed method by observing the creep-induced lateral deflection of the column. More importantly, it has been found that the creep-induced lateral deflection

of steel columns results from the cross-sectional strain gradient and nonuniform stress distribution, which are triggered by the column initial imperfection. Thus, it is concluded that the creep buckling will theoretically not occur if the column initial imperfection is not considered because the strain and stress are uniformly distributed on the cross-section. Based on the outcome of the parametric study, it has been discovered that the creep buckling time of steel columns decreases with an increase of load ratio, temperature, and initial imperfection, but a decrease of slenderness ratio of columns. In addition, if the applied load approaches the theoretical critical buckling load of the column at elevated temperature ($\alpha_p \geq 0.8$), the creep buckling phenomenon may occur in a considerably short period, which signifies the necessity of considering the creep effect in evaluating the fire resistance of steel columns.

9.7 Fire Resistance of Multi-column Systems

Chapter 8 proposes methods for investigating a variety of effects that have not yet been considered in the storey-based stability analysis at elevated temperatures, including effects of thermal expansion of braces (beams), partial yielding of column, and thermal creep. For the purposes of considering the effects of thermal expansion of braces on the critical temperature of multi-column systems, analytical expressions are derived to attain displacements of columns and internal forces induced by the thermal expansion of braces in multi-column systems. The effect of partial yielding on the lateral stiffness of steel columns is considered by adopting the modified plastic-hinge method proposed by King et al. [116]. Because the creep-induced deflection at elevated temperatures can be accurately assessed via assessing the strain gradients on the column's cross-section, as proved in Chapter 7, a simplified method is proposed to consider the thermal creep effect on the lateral stiffness of steel columns at elevated temperatures. Finally, a numerical method is proposed for evaluating the critical temperature of multi-column systems with the considerations of the above factors. The proposed method is verified by the fire test results reported by [60], and good agreements have been achieved between numerical and experimental results.

9.8 Recommendations for Future Research

The following are some possible research areas related to the study presented in this thesis, which are mainly aimed at refining and addressing some assumptions of the proposed methods as well as extending the applicability of the proposed methods.

9.8.1 Randomness of columns' initial imperfections

It is important to realize that all the foregoing research presented in this thesis regarding computing the brace forces in multi-column systems assumes all the initial imperfections of columns have the same direction and magnitude, which is quite conservative due to neglecting the randomness of columns' initial imperfections in reality. The simple prevailing method to account for the randomness of columns' initial imperfections on brace forces is to incorporate a reduction factor into the expressions obtained by assuming identical column initial imperfections, as discussed in Chapter 4. However, it has been found that the location of the applied load would affect the brace forces in the system. Thereupon, stochastic analyses can be carried out to establish the probability density function of brace forces for multi-column systems to obtain corresponding reduction factors for different engineering applications with the proposed expressions in this thesis.

9.8.2 Initial imperfections of braces

The initial imperfections of braces are neglected in this research, which is feasible for a multi-column system with tension-only braces. However, if the braces are to be designed to be capable of resisting both tension and compression forces, the initial imperfections of braces would have a detrimental effect on the brace stiffness in compression and lead to additional lateral displacement and brace forces of the system, which subsequently requires larger bracing requirements. Hence, the investigation of the effects of initial imperfections of braces on the bracing requirements of multi-column systems could be carried out. A possible and viable way is to introduce the effects of the brace force and brace initial imperfection on the brace stiffness into the proposed expressions.

9.8.3 Longitudinal nonuniform column stiffness

The derivation of the relationship among the lateral deflection, applied axial load, and external lateral load in the proposed half-length column model assumes the column possesses the uniform flexural stiffness EI along the column length. At elevated temperatures, the longitudinal nonuniform column stiffness commonly exists due to the longitudinal nonuniform temperature distribution. As presented in Appendix C, the half-length column model is divided into two segments with different elastic modulus, and the corresponding lateral deflection induced by the applied axial and lateral loads are derived. By doing so, some equations presented in this thesis can be directly applied and further extended to evaluate the fire-structural responses of multi-column systems at elevated temperatures with considering the longitudinal nonuniform column stiffness.

9.8.4 Multiple bracing points along the column length

The scope of this research is limited to the multi-column systems with bracing at columns' mid-height, i.e., there is only one bracing point along the column length. Since bracing can be placed at multiple points along the column length in practice, it is necessary to extend the present research to assess the bracing requirements for multi-column systems braced at multiple points. This requires alternative derivations for relationships between column deflection and applied loads. Appendix D exemplifies how to derive the lateral deflection of a semi-rigidly connected column with two equally spaced braces.

9.8.5 Torsional buckling in storey-based stability analysis

The concept of storey-based stability signifies that the overloaded columns in a multi-column system can be laterally supported by other columns as long as the capacity of the whole system is not exceeded. However, the current research relating to the storey-based stability analysis focuses on the flexural buckling of columns. In practice, columns may fail in torsional buckling depending on their cross-sectional shapes, especially for columns made in cold-formed steel, which may govern the strength of the whole structural system. Consequently, torsional bracing may need to be placed in multi-column systems, and a column with lower torsional buckling resistance could be supported by other columns with

higher torsional buckling resistance. For that reason, the concept of storey-based stability could be extended to exploit the effect of such interplay among the torsional buckling of columns on the system's stability.

9.8.6 Experimental validation

The proposed methods in this thesis have been shown to be theoretically accurate by the validation in finite element analyses. Nevertheless, there is always a difference between theory and reality owing to many possible factors being neglected. In fact, the original plan of this research included the thermal-creep tests on steel columns to observe the creep effect on the lateral stiffness of steel columns at elevated temperatures; however, it was not able to conduct the tests due to the pandemic. Thus, as desired, further validation of the proposed methods regarding the bracing requirements of multi-column systems and the creep effect on the lateral stiffness of steel columns at elevated temperatures can be achieved via conducting experiments in a structural laboratory.

References

[1] Linbo Zhang, Terence Ma, and Lei Xu. Brace stiffness for parallel semi-rigid columns. *Journal of Constructional Steel Research*, 191:107146, 2022.

[2] Linbo Zhang and Lei Xu. Bracing requirements for multiple parallel nonidentical columns with initial curvature. *Engineering Structures*, 275:115279, 2023.

[3] Terence Ma, Linbo Zhang, and Lei Xu. Effects of beam axial deformations on storey-based critical gravity loads in tension-only semi-braced steel frames. *Engineering Structures*, 232:111862, 2021.

[4] Linbo Zhang and Lei Xu. A method of simulating creep buckling behaviour of steel columns at elevated temperatures. *Fire Technology*, 2022 (accepted).

[5] Ronald D. Ziemian and Constance W. Ziemian. Formulation and validation of minimum brace stiffness for systems of compression members. *Journal of Constructional Steel Research*, 129:263–275, 2017.

[6] Stephen Timoshenko. *Theory of Elastic Stability*. McGraw-Hill Book Company, Inc., 1936.

[7] George Winter. Lateral bracing of columns and beams. *Journal of the Structural Division*, 84(2):1561–1, 1958.

[8] G.S. Tong. Design approach of horizontal braces between columns. *Journal of Xi'an Institute of Metallurgy and Construction Engineering*, 20(3):110–140, 1986.

[9] Constance W. Ziemian and Ronald D. Ziemian. Threshold stiffness of lateral bracing in systems of parallel compression members. *Journal of Constructional Steel Research*, 186:106922, 2021.

[10] ANSI/AISC 360-16. *Specification for Structural Steel Buildings*, 2016.

[11] AISI S100-16. *North American Specification for the Design of Cold-Formed Steel Structural Members*, 2016.

[12] Thomas Sputo and Kevin Beery. Bracing demand in axially loaded cold-formed steel stud walls. *Journal of Architectural Engineering*, 14(3):85–89, 2008.

[13] H.B. Blum, V.Z. Meimand, and B.W. Schafer. Flexural bracing requirements in axially loaded cold-formed steel-framed walls. *Practice Periodical on Structural Design and Construction*, 20(4):04014043, 2015.

[14] Yaochun Zhang, Jinyou Zhao, and Wenyuan Zhang. Parametric studies on inter-column brace forces. *Advances in Structural Engineering*, 11(3):293–303, 2008.

[15] Jinyou Zhao, Yaochun Zhang, and YiYing Lin. Study on mid-height horizontal bracing forces considering random initial geometric imperfections. *Journal of Constructional Steel Research*, 92:55–66, 2014.

[16] Jinyou Zhao, Junming Wei, and Jun Wang. Design forces of horizontal braces unlocated at middle of columns considering random initial geometric imperfections. *Advances in Civil Engineering*, 2021, 2021.

[17] J. Dario Aristizabal-Ochoa. Stability and second-order non-linear analysis of 2d multi-column systems with semirigid connections: Effects of initial imperfections. *International Journal of Non-Linear Mechanics*, 47(5):537–560, 2012.

[18] N.S. Trahair and D. Nethercot. Bracing requirements in thin-walled structures. *Elsevier Applied Science Publishers, Developments in Thin-Walled Structures–2*, pages 93–130, 1984.

[19] Raymond H Plaut and Jae-Guen Yang. Lateral bracing forces in columns with two unequal spans. *Journal of Structural Engineering*, 119(10):2896–2912, 1993.

[20] Heungbae Gil and Joseph A. Yura. Bracing requirements of inelastic columns. *Journal of Constructional Steel Research*, 51(1):1–19, 1999.

[21] CSA S16:19. *National Standard of Canada: Design of Steel Structures*, 2019.

[22] Geng-Shu Tong and Shao-Fan Chen. Design forces of horizontal inter-column braces. *Journal of Constructional Steel Research*, 7(5):363–370, 1987.

[23] Studco. 4 nogging options you need to know about, 2017. https://archipro.co.nz/articles/misc/4-nogging-options-you-need-to-know-about-studco.

[24] EN 1993-1-1. *Eurocode 3 Design of Steel Structures-Part 1-1: General Rules and Rules for Buildings*, 2005.

[25] Shaofan Chen and Genshu Tong. Design for stability: correct use of braces. *Steel Structures, J. Singapore Struct. Steel Soc*, 5(1):15–23, 1994.

[26] GB50017-2017. *Standard for Design of Steel Structures*, 2017.

[27] Australian Standard. 4100–2020 steel structures. *Standards Australia, Sydney*, 2020.

[28] Joseph A. Yura. The effective length of columns in unbraced frames. *Engineering Journal*, 8(2):37–42, 1971.

[29] T.R. Higgins. Column stability under elastic support. *Engineering Journal*, 2(2):12, 1965.

[30] Adel Helmy Salem. Discussion of "buckling analysis of one-story frames". *Journal of the Structural Division*, 95(5):1017–1029, 1969.

[31] W.J. LeMessurier. A practical method of second order analysis, part 1—pin-jointed frames. *Engineering Journal*, 13(4), 1976.

[32] W.J. LeMessurier. Practical method of second order analysis, part 2—rigid frames. *Engineering Journal*, 14(2), 1977.

[33] L. Xu and Y. Liu. Story stability of semi-braced steel frames. *Journal of constructional steel research*, 58(4):467–491, 2002.

[34] G.R. Monforton and T.S. Wu. Matrix analysis of semi-rigidly connected frames. *Journal of the structural division*, 89(6):13–42, 1963.

[35] Lei Xu. The buckling loads of unbraced pr frames under non-proportional loading. *Journal of constructional steel research*, 58(4):443–465, 2002.

[36] Terence Ma and Lei Xu. Shear deformation effects on stability of unbraced steel frames in variable loading. *Journal of Constructional Steel Research*, 164:105811, 2020.

[37] Terence Ma. *The Storey-Based Stability of Steel Frames Subjected to Variable Gravity and Fire Loading*. PhD thesis, University of Waterloo, 2020.

[38] Tjalling J. Ypma. Historical development of the newton–raphson method. *SIAM review*, 37(4):531–551, 1995.

[39] Kevin LaMalva and Danny Hopkin. *International Handbook of Structural Fire Engineering*. Springer, 2021.

[40] Yaozhuang Li, Mengjie Wang, Guoqiang Li, and Binhui Jiang. Mechanical properties of hot-rolled structural steels at elevated temperatures: A review. *Fire Safety Journal*, 119:103237, 2021.

[41] EN 1993-1-2. *Eurocode 3 Design of Steel Structures-Part 1-2: General Rules - Structural Fire Design*, 2005.

[42] Ju Chen, Ben Young, and Brian Uy. Behavior of high strength structural steel at elevated temperatures. *Journal of structural engineering*, 132(12):1948–1954, 2006.

[43] Weiyong Wang, Bing Liu, and Venkatesh Kodur. Effect of temperature on strength and elastic modulus of high-strength steel. *Journal of materials in civil engineering*, 25(2):174–182, 2013.

[44] Amin Heidarpour, Niall S Tofts, Asghar H Korayem, Xiao-Ling Zhao, and Christopher R Hutchinson. Mechanical properties of very high strength steel at elevated temperatures. *Fire safety journal*, 64:27–35, 2014.

[45] Weiyong Wang, Kang Wang, Venkatesh Kodur, and Bin Wang. Mechanical properties of high-strength q690 steel at elevated temperature. *Journal of Materials in Civil Engineering*, 30(5):04018062, 2018.

[46] Weiyong Wang, Yanhong Zhang, Lei Xu, and Xiang Li. Mechanical properties of high-strength q960 steel at elevated temperature. *Fire Safety Journal*, 114:103010, 2020.

[47] Hélder D Craveiro, João Paulo C Rodrigues, Aldina Santiago, and Luís Laím. Review of the high temperature mechanical and thermal properties of the steels used in

cold formed steel structures–the case of the s280 gd+ z steel. *Thin-Walled Structures*, 98:154–168, 2016.

[48] BSI British Standard. Structural use of steelwork in building, part 8: Code of practice for fire resistant design. *British Standard Institution*, 1990.

[49] Ju Chen and Ben Young. Experimental investigation of cold-formed steel material at elevated temperatures. *Thin-Walled Structures*, 45(1):96–110, 2007.

[50] Nirosha Dolamune Kankanamge and Mahen Mahendran. Mechanical properties of cold-formed steels at elevated temperatures. *Thin-Walled Structures*, 49(1):26–44, 2011.

[51] Finian McCann, Leroy Gardner, and Sophie Kirk. Elevated temperature material properties of cold-formed steel hollow sections. *Thin-Walled Structures*, 90:84–94, 2015.

[52] Mohamed Imran, Mahen Mahendran, and Poologanathan Keerthan. Mechanical properties of cold-formed steel tubular sections at elevated temperatures. *Journal of Constructional Steel Research*, 143:131–147, 2018.

[53] Sivakumar Kesawan, Varathananthan Jatheeshan, and Mahen Mahendran. Elevated temperature mechanical properties of hollow flange channel sections. *Construction and Building Materials*, 87:86–99, 2015.

[54] Jyri Outinen, Jyrki Kesti, and Pentti Mäkeläinen. Fire design model for structural steel s355 based upon transient state tensile test results. *Journal of constructional steel research*, 42(3):161–169, 1997.

[55] Guobiao Lou, Chenghao Wang, Jian Jiang, Yaqiang Jiang, Liangwei Wang, and Guo-Qiang Li. Fire tests on full-scale steel portal frames against progressive collapse. *Journal of Constructional Steel Research*, 145:137–152, 2018.

[56] David C. Jeanes. Application of the computer in modeling fire endurance of structural steel floor systems. *Fire safety journal*, 9(1):119–135, 1985.

[57] L. Corradi, Carlo Poggi, and P. Setti. Interaction domains for steel beam-columns in fire conditions. *Journal of Constructional Steel Research*, 17(3):217–235, 1990.

[58] Walter Ramberg and William R. Osgood. Description of stress-strain curves by three parameters. Technical report, 1943.

[59] H.A. Saab and D.A. Nethercot. Modelling steel frame behaviour under fire conditions. *Engineering Structures*, 13(4):371–382, 1991.

[60] Achim Rubert and Peter Schaumann. Structural steel and plane frame assemblies under fire action. *Fire Safety Journal*, 10(3):173–184, 1986.

[61] K.W. Poh. Stress-strain-temperature relationship for structural steel. *Journal of materials in civil engineering*, 13(5):371–379, 2001.

[62] Thanuja Ranawaka and Mahen Mahendran. Experimental study of the mechanical properties of light gauge cold-formed steels at elevated temperatures. *Fire safety journal*, 44(2):219–229, 2009.

[63] G. Williams-Leir. Creep of structural steel in fire: analytical expressions. *Fire and Materials*, 7(2):73–78, 1983.

[64] Maria Cowan and Kapil Khandelwal. Modeling of high temperature creep in astm a992 structural steels. *Engineering Structures*, 80:426–434, 2014.

[65] Weiyong Wang, Shouhai Yan, and Venkatesh Kodur. Temperature induced creep in low-alloy structural q345 steel. *Journal of Materials in Civil Engineering*, 28(6):06016003, 2016.

[66] T.Z. Harmathy. A comprehensive creep model. 1967.

[67] B.A. Fields and R.J. Fields. Elevated temperature deformation of structural steel. *National Institute of Standards and Technology*, 1988.

[68] Neno Torić, Alen Harapin, and Ivica Boko. Experimental verification of a newly developed implicit creep model for steel structures exposed to fire. *Engineering Structures*, 57:116–124, 2013.

[69] Neno Torić, Ivana Uzelac Glavinić, and Ian W Burgess. Development of a rheological model for creep strain evolution in steel and aluminium at high temperature. *Fire and materials*, 42(8):879–888, 2018.

[70] Elie G. Hantouche, Karim K. Al Khatib, and Mohammed A. Morovat. Modeling creep of steel under transient temperature conditions of fire. *Fire Safety Journal*, 100:67–75, 2018.

[71] Hosam M. Ali, Paul E. Senseny, and Ronald L. Alpert. Lateral displacement and collapse of single-story steel frames in uncontrolled fires. *Engineering Structures*, 26(5):593–607, 2004.

[72] Mohammed Ali Morovat, Ahmad H. El Ghor, and Elie G. Hantouche. Time-dependent response of flush endplate connections to fire temperatures. *Journal of Structural Engineering*, 144(4):04018023, 2018.

[73] Venkatesh Kodur, Mahmud Dwaikat, and Rustin Fike. High-temperature properties of steel for fire resistance modeling of structures. *Journal of Materials in Civil Engineering*, 22(5):423–434, 2010.

[74] Morgan J. Hurley, Daniel T. Gottuk, John R. Hall Jr., Kazunori Harada, Erica D. Kuligowski, Milosh Puchovsky, John M. Watts Jr., CHRISTOPHER J. WIECZOREK, et al. *SFPE handbook of fire protection engineering*. Springer, 2015.

[75] Zhan-Fei Huang, Kang-Hai Tan, and Seng-Kiong Ting. Heating rate and boundary restraint effects on fire resistance of steel columns with creep. *Engineering Structures*, 28(6):805–817, 2006.

[76] Guo-Qiang Li and Chao Zhang. Creep effect on buckling of axially restrained steel columns in real fires. *Journal of Constructional Steel Research*, 71:182–188, 2012.

[77] Weiyong Wang and Guoqiang Li. Experimental study on the fire resistance of high strength q690 steel columns. *Journal of architectural structure*, 40(08):155–162, 2019.

[78] Joseph Marin. Creep deflections in columns. *Journal of applied physics*, 18(1):103–109, 1947.

[79] Joseph Kempner and Sharad A. Patel. Creep buckling of columns. Technical report, 1954.

[80] V.O. Shestopal and P.C. Goss. The estimation of column creep buckling durability from the initial stages of creep. *Acta mechanica*, 52(3):269–275, 1984.

[81] M.N. Kirsanov. Singular points of the creep deformation and buckling of a column. *International journal of engineering science*, 35(3):221–227, 1997.

[82] Mohammed Ali Morovat, Michael D. Engelhardt, Eric M. Taleff, and Todd Helwig. Importance of time-dependent material behavior in predicting strength of steel columns exposed to fire. In *Applied Mechanics and Materials*, volume 82, pages 350–355. Trans Tech Publ, 2011.

[83] Weiyong Wang, Hongyang Zhou, and Lei Xu. Creep buckling of high strength q460 steel columns at elevated temperatures. *Journal of Constructional Steel Research*, 157:414–425, 2019.

[84] Xing Chen. *Prohabilistic creep buckling*. PhD thesis, University of Waterloo, 1984.

[85] Y.C. Wang and J.M. Davies. Fire tests of non-sway loaded and rotationally restrained steel column assemblies. *Journal of Constructional Steel Research*, 59(3):359–383, 2003.

[86] Guo-Qiang Li and Shi-Xiong Guo. Experiment on restrained steel beams subjected to heating and cooling. *Journal of Constructional Steel Research*, 64(3):268–274, 2008.

[87] Kuo-Chen Yang, Hung-Hsin Lee, and Olen Chan. Experimental study of fire-resistant steel h-columns at elevated temperature. *Journal of Constructional Steel Research*, 62(6):544–553, 2006.

[88] Weiyong Wang, Linbo Zhang, Yong Ge, and Lei Xu. Behaviour of restrained high strength steel columns at elevated temperature. *Journal of Constructional Steel Research*, 148:251–264, 2018.

[89] Chien-Ming Wang, Yang Xiang, and Sritawat Kitipornchai. Buckling of restrained columns with shear deformation and axial shortening. *Journal of engineering mechanics*, 117(9):1973–1989, 1991.

[90] T.T. Lie and Martin Chabot. Evaluation of the fire resistance of compression members using mathematical models. *Fire safety journal*, 20(2):135–149, 1993.

[91] Jianguo Cai and Jian Feng. Thermal buckling of rotationally restrained steel columns. *Journal of Constructional Steel Research*, 66(6):835–841, 2010.

[92] Anil Agarwal, Lisa Choe, and Amit H. Varma. Fire design of steel columns: Effects of thermal gradients. *Journal of Constructional Steel Research*, 93:107–118, 2014.

[93] Binhui Jiang, Guo-Qiang Li, and B.A. Izzuddin. Dynamic performance of axially and rotationally restrained steel columns under fire. *Journal of Constructional Steel Research*, 122:308–315, 2016.

[94] Lei Xu and Yi Zhuang. Storey stability of unbraced steel frames subjected to non-uniform elevated temperature distribution. *Engineering structures*, 62:164–173, 2014.

[95] Y.C. Wang and D.B. Moore. Steel frames in fire: analysis. *Engineering Structures*, 17(6):462–472, 1995.

[96] Mohamed Mahmoud El-Heweity. Behavior of portal frames of steel hollow sections exposed to fire. *Alexandria Engineering Journal*, 51(2):95–107, 2012.

[97] Ruirui Sun, Zhaohui Huang, and Ian W. Burgess. Progressive collapse analysis of steel structures under fire conditions. *Engineering structures*, 34:400–413, 2012.

[98] Lei Xu and Yi Zhuang. Storey-based stability of unbraced steel frames at elevated temperature. *Journal of Constructional Steel Research*, 78:79–87, 2012.

[99] Terence Ma and Lei Xu. Stability-based fire resistance duration of unbraced steel frames. *Journal of Structural Fire Engineering*, 2019.

[100] Ronald D. Ziemian and William McGuire. Mastan2 v3.5, 2018.

[101] Wai-Fah Chen, Yoshiaki Goto, and JY Richard Liew. *Stability design of semi-rigid frames*. John Wiley & Sons, 1995.

[102] ME Kartal, HB Basaga, A Bayraktar, and M Muvafik. Effects of semi-rigid connection on structural responses. *Electronic journal of structural Engineering*, 10:22–35, 2010.

[103] Wai-Fah Chen. *Semi-rigid connections handbook*. J. Ross Publishing, 2011.

[104] David C. Weggel, David M. Boyajian, and S. Chen. Modelling structures as systems of springs. *World Transactions on Engineering and Technology Education*, 6(1):169, 2007.

[105] The Mathworks, Inc., Natick, Massachusetts. *MATLAB (R2021b)*, 2021.

[106] Riaz A. Usmani. Inversion of a tridiagonal jacobi matrix. *Linear Algebra and its Applications*, 212(213):413–414, 1994.

[107] EIT Paul Lackey, Nabil A. Rahman, and Gary Bennett. Mechanical and bridging anchorage of load bearing cold-formed steel studs. 2012.

[108] T.Z. Harmathy. Creep deflection of metal beams in transient heating processes, with particular reference to fire. *Canadian Journal of Civil Engineering*, 3(2):219–228, 1976.

[109] ISO. ISO 834: Fire resistance tests - elements of building construction. Technical report, International Standard Office, Geneva, 1975.

[110] Chrysanthos Maraveas, Zacharias C. Fasoulakis, and Konstantinos Daniel Tsavdaridis. Mechanical properties of high and very high steel at elevated temperatures and after cooling down. *Fire Science Reviews*, 6(1):1–13, 2017.

[111] Jean-Marc Franssen, D. Talamona, J. Kruppa, and L.G. Cajot. Stability of steel columns in case of fire: experimental evaluation. *Journal of structural engineering*, 124(2):158–163, 1998.

[112] Linbo Zhang. Fire resistance study on high strength Q690 steel columns considering creep and residual stress. Master's thesis, Chongqing University, 2018.

[113] G.Q. Li, L.H. Han, G.B. Lou, and S.C. Jiang. *Fire resistance design of steel structure and composite steel and concrete structure*. Chinese Architecture and Building Press, Beijing, China, 2006.

[114] CEN EN. 1090-2: 2018 execution of steel structures and aluminium structures-part 2: Technical requirements for steel structures. *Brussels, Belgium: European Committee for Standardization (CEN)*, 2018.

[115] Colin G Bailey. The influence of the thermal expansion of beams on the structural behaviour of columns in steel-framed structures during a fire. *Engineering Structures*, 22(7):755–768, 2000.

[116] W.S. King, D.W. White, and W.F. Chen. Second-order inelastic analysis methods for steel-frame design. *Journal of Structural Engineering*, 118(2):408–428, 1992.

[117] Lei Xu, Yuxin Liu, and Donald E. Grierson. Nonlinear analysis of steel frameworks through direct modification of member stiffness properties. *Advances in Engineering Software*, 36(5):312–324, 2005.

[118] Lian Duan and Wai-Fah Chen. Design interaction equation for steel beam-columns. *Journal of Structural Engineering*, 115(5):1225–1243, 1989.

[119] Guo-Qiang Li, Xin-Xin Wang, Chao Zhang, and Wen-Yu Cai. Creep effect on critical strength of high-strength steel columns exposed to fire. *Engineering Structures*, 220:110971, 2020.

[120] Jin-Cheng Zhao. Application of the direct iteration method for non-linear analysis of steel frames in fire. *Fire safety journal*, 35(3):241–255, 2000.

[121] Jean Marc Franssen, Venkatesh Kodur, and Raul Zaharia. *Designing steel structures for fire safety*. CRc Press, 2009.

[122] J.L. Zeng, K.H. Tan, and Z.F. Huang. Primary creep buckling of steel columns in fire. *Journal of Constructional Steel Research*, 59(8):951–970, 2003.

[123] *BS 476: Part 20: 1987, Fire Tests on Building Materials and Structures*. British Standards Institution, 1987.

APPENDICES

Appendix A

General Features of Finite Element Modelling

From Chapter 3 to Chapter 6, given that the proposed methods are purely theoretical, finite element analyses are used just to verify the analytical results. In order to avoid repetition of description regarding the modelling and make it easy for readers, the general features of the finite element are presented in this section.

The finite element analysis (FEA) software ABAQUS is used to establish the models for a single braced column and multiple braced columns, in which the columns and braces are modelled using B23 elements, neglecting the effect of shear deformations. The sensitivity analysis was performed to investigate the effect of the number of elements modelling the members on the numerical results. It was found that the variation of the results was almost unnoticeable when the number of elements used for each member exceeded 20. Therefore, 20 elements were used to model each column and each brace in the FEM. The tie bracing is pin-connected at the mid-height between each column. The semi-rigid connections are simulated by a rotational spring at each end of the columns. The rotational stiffness R of the spring defined in ABAQUS is calculated by

$$R = \frac{3E_c I_c}{L_c (1/r_e - 1)} \tag{A.1}$$

Since braces are assumed to be elastic and perfectly straight, the cross-sectional area of bracing A_b is computed by

$$A_b = S_b L_b / E \tag{A.2}$$

The discrepancies between the analytical and FEA results are quite insignificant (within 0.7%), mainly resulting from the assumption that there is no rotation at the columns' mid-height. Consequently, the FEA results are not presented in some examples for the sake of brevity.

A.1 Ideal Brace Stiffness

Unlike the proposed analytical methods in which the ideal brace stiffness can be set as an unknown variable and directly obtained, employing the established finite element model to attain the ideal brace stiffness requires a series of iterations. The ideal brace stiffness is the minimum stiffness for the bracing, ensuring that the full buckling strength of the system can be achieved. In other words, once the brace stiffness exceeds the ideal brace stiffness, increasing the brace stiffness will not increase the buckling strength of the system. Therefore, buckling analyses are performed in ABAQUS using the *Subspace* eigensolver to obtain the first buckling mode and corresponding buckling load with presupposed brace stiffness. Subsequently, the ideal brace stiffness can be found by varying the brace stiffness and repeating the analysis until the critical buckling mode just changed from sway buckling mode to non-sway buckling mode or the other way around [5]. The corresponding brace stiffness at which this conversion occurs is determined as the ideal brace stiffness.

A.2 Brace Forces and Displacements

Once the ideal brace stiffness is obtained, the brace stiffness can be determined by amplifying the ideal brace stiffness with a proper scale factor. Subsequently, with the determined brace stiffness, static analysis in ABAQUS can be used to capture the columns' lateral displacements and brace forces.

In order to introduce the columns' initial imperfections into the static analysis, the buckling analysis should be conducted first. It should be noted that different from the buckling analysis carried out to attain the ideal brace stiffness, there is no horizontal displacement restraint applied on the ends, and all the columns are pin-connected at both ends. This is to ensure that all the columns have the same magnitude of lateral deflection in the buck-

ling analysis and that the column buckling shape is in a half-sine wave. By doing so, the column's initial shape in a half-sine wave with the same magnitudes can be introduced in the subsequent static analysis. In the static analysis, the NLgeom option shall be turned on to consider the effect of nonlinear geometry. All the loads applied on the columns in the finite element model are the same as the loads in the theoretical analyses.

Appendix B

Derivation of Column Lateral Deflection at the Mid-height

From the Euler-Bernoulli beam theory, the relationship between the radius of curvature of the centroidal axis ρ and strain ε is shown in Figure B.1 and can be expressed as Eqs. (B.1).

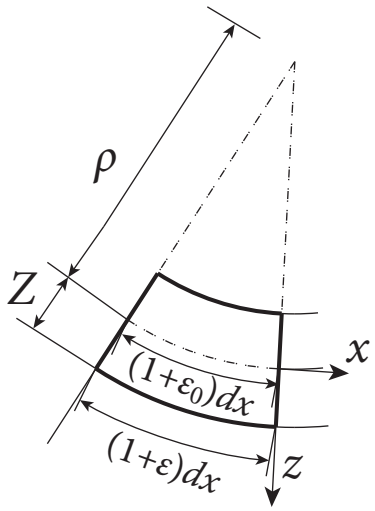

Figure B.1: Relationship between the radius of curvature of the centroidal axis and strain

$$\frac{\rho + Z}{\rho} = \frac{(1+\varepsilon)\,dx}{(1+\varepsilon_0)\,dx} \tag{B.1a}$$

$$\rho = Z\frac{(1+\varepsilon_0)}{(\varepsilon-\varepsilon_0)} \tag{B.1b}$$

If the strains are considered small compared to unity, Eq. (B.1b) becomes Eq. (B.2).

$$\rho = \frac{Z}{(\varepsilon-\varepsilon_0)} \tag{B.2}$$

Meanwhile, the general curvature equation is given as

$$\frac{1}{\rho} = \frac{\partial^2 y/\partial x^2}{\left[1+\left(\partial y/\partial x\right)^2\right]^{1.5}} \tag{B.3}$$

Utilizing small deflection theory [122], if

$$f'(x) = \frac{\pi}{L}\Delta \cos\frac{\pi x}{L} \leq 0.2 \tag{B.4}$$

Eq. (B.3) can be simplified as

$$\frac{1}{\rho} = \frac{\partial^2 y}{\partial x^2} \tag{B.5}$$

At the mid-height of column ($x = L/2$), Eq. (B.4) is equivalent to Eq.(B.6).

$$\Delta \leq 0.0637L \approx \frac{1}{15}L \tag{B.6}$$

Therefore, within the small deflection range ($\Delta \leq L/15$), the following calculation procedure is applicable. The failure of a steel column at elevated temperature is said to occur when the deflection rate exceeds 0.003 L/mm [123], where L is the column length. Unlike the steel columns in a fire, the mid-height lateral deflection of the column subjected to creep buckling exhibits a relatively lower deformation rate until failure. Therefore, the criterion of deflection rate is not suitable for the failure associated with creep buckling. Therefore, $L/15$ is selected as the failure criterion of the column's creep buckling in this paper. When subjected to elevated temperature, the deformed shape curve of the column can be written as Eq. (B.7).

$$f_T(x) = \Delta_T \sin\left(\frac{\pi x}{L}\right) \tag{B.7}$$

where Δ_T is the corresponding maximum displacement at elevated temperature. The second derivative of $f_T(x)$ can be written as

$$f_T''(x) = -\Delta_T \frac{\pi^2}{L^2}\sin\left(\frac{\pi x}{L}\right) \tag{B.8}$$

For column lateral deflection at mid-span where $x = L/2$, by substituting Eq. (B.5) into Eq. (B.8), the mid-height deflection can be obtained as expressed in Eq. (B.9b).

$$-\Delta_T \frac{\pi^2}{L^2} = \frac{1}{\rho} \tag{B.9a}$$

$$\Delta_T = \frac{L^2}{\pi^2}\frac{\varepsilon_1 - \varepsilon_n}{Z_n - Z_1} \tag{B.9b}$$

Appendix C

Derivation for the Lateral Deflection of the Half-length Column Model with two segments

If the proposed half-length column model consists of two segments with different moment of inertia or elastic modulus (EI), as per Fig. C.1, its lateral deflection induced by the axial and lateral loads considering the initial curvature and imperfection is derived as follows.

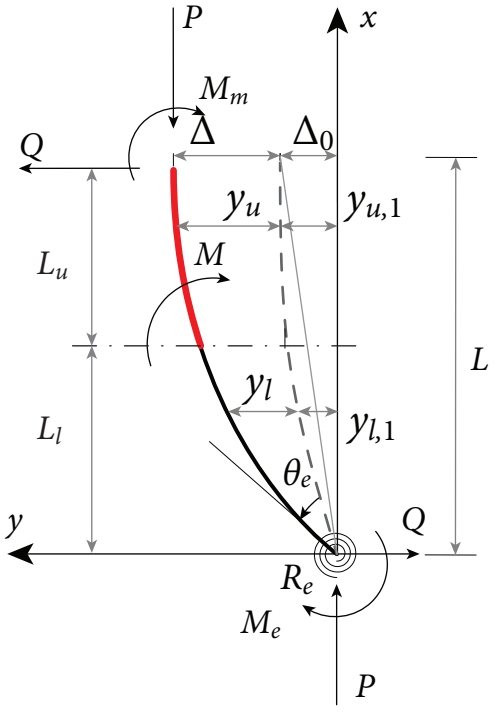

Figure C.1: Half of the deformed axially loaded column with two segments

The relationship between the bending moment and rotational stiffness at the lower end of the half-length column is:

$$M_e = R_e \theta_e \tag{C.1}$$

Thus, based on the equilibrium of the half-length column:

$$M_m + R_e \theta_e = QL + P(\Delta + \Delta_0) \tag{C.2}$$

The governing differential equations associated with the flexural deformation of the half-length column shown in Fig. C.1 can be written as:

$$-(EI)_l \frac{d^2 y_l}{dx^2} = P(y_l + y_{l,1}) - \theta_e R_e + Qx \tag{C.3a}$$

$$-(EI)_u \frac{d^2 y_u}{dx^2} = P(y_u + y_{u,1}) - \theta_e R_e + Qx \tag{C.3b}$$

By solving the differential equation, the deformation and rotation of the column can be obtained from Eqs. (C.4).

$$y_l(x) = C_1 \cos\left(\frac{\phi_l x}{L}\right) + C_2 \sin\left(\frac{\phi_l x}{L}\right) + \frac{\theta_e R_e}{P} - \Delta_0 \frac{4\phi_l^2}{4\phi_l^2 - \pi^2} \frac{\sin(\pi x/2L)}{P} - \frac{Q}{P} x \tag{C.4a}$$

$$y_l'(x) = -C_1 \frac{\phi_l}{L} \sin\left(\frac{\phi_l x}{L}\right) + C_2 \frac{\phi_l}{L} \cos\left(\frac{\phi_l x}{L}\right) - \Delta_0 \frac{4\phi_l^2}{4\phi_l^2 - \pi^2} \frac{\pi}{2L} \frac{\cos(\pi x/2L)}{P} - \frac{Q}{P} \tag{C.4b}$$

$$y_u(x) = C_3 \cos\left(\frac{\phi_u x}{L}\right) + C_4 \sin\left(\frac{\phi_u x}{L}\right) + \frac{\theta_e R_e}{P} - \Delta_0 \frac{4\phi_u^2}{4\phi_u^2 - \pi^2} \frac{\sin(\pi x/2L)}{P} - \frac{Q}{P} x \tag{C.4c}$$

$$y_u'(x) = -C_3 \frac{\phi_u}{L} \sin\left(\frac{\phi_u x}{L}\right) + C_4 \frac{\phi_u}{L} \cos\left(\frac{\phi_u x}{L}\right) - \Delta_0 \frac{4\phi_u^2}{4\phi_u^2 - \pi^2} \frac{\pi}{2L} \frac{\cos(\pi x/2L)}{P} - \frac{Q}{P} \tag{C.4d}$$

where ϕ_u and ϕ_l are the axial load coefficients, defined as

$$\phi_u = \sqrt{\frac{PL^2}{(EI)_u}} = \frac{\phi}{\sqrt{u_u}} \tag{C.5a}$$

$$\phi_l = \sqrt{\frac{PL^2}{(EI)_l}} = \frac{\phi}{\sqrt{u_l}} \tag{C.5b}$$

in which u_u and u_l are the retention factors for the flexural stiffness of the upper and lower segments, respectively.

C_1, C_2, C_3, and C_4 are coefficients to be determined by the boundary conditions, namely:

$$y_l(0) = 0 \tag{C.6a}$$

$$y_u(L) = \Delta \tag{C.6b}$$

$$y_l(L_l) = y_u(L_l) \tag{C.6c}$$

$$y_l'(0) = \theta_e \tag{C.6d}$$

$$y_u'(L) = 0 \tag{C.6e}$$

$$y_l'(L_l) = y_u'(L_l) \tag{C.6f}$$

By substituting the boundary conditions and Eq. (C.2) into Eqs. (C.4), the system of seven equations is obtained and then solved for Δ, C_1, C_2, C_3, C_4, M_m, and θ_e. The lateral displacement of the column Δ is therefore obtained:

$$\Delta = \frac{Q + \frac{P\Delta_0}{L}\psi_2}{\frac{12E_cI_c}{L^3}\beta_2} \tag{C.7}$$

where β_2 and ψ_2 are the lateral stiffness modification factor and column initial curvature coefficient for a half-column with two segments, as given in:

$$\beta_2 = \frac{\phi^2\left[\phi^2\phi_u\tau_l(1-r_l)A_1 + 3\phi_l\phi_u r_l A_2\right]}{12(\phi^2(1-r_l)\tau_l A_3 + 3r_l A_4)} \tag{C.8}$$

$$\psi_2 = \frac{2\phi^2\phi_u\tau_l(1-r_l)A_5 + 6\phi_u\phi_l r_l\left[A_6 - \pi\phi_l\left(4\phi_u^2-\pi^2\right)\left(\phi_l + A_1\right) - 2\phi_u^2\left(4\phi_l^2-\pi^2\right)A_2\right]}{\left(4\phi_l^2-\pi^2\right)\left(4\phi_u^2-\pi^2\right)\left[(1-r_l)\tau_l\phi^2 A_3 + 2r_l A_4\right]} \tag{C.9}$$

where

$$A_1 = \phi_u S_l C_u \sin\phi_u - \phi_l C_l S_u \sin\phi_u - \phi_u S_l S_u \cos\phi_u - \phi_l C_l C_u \cos\phi_u \tag{C.10a}$$

$$A_2 = \phi_u C_l S_u \cos\phi_u - \phi_u C_l C_u \sin\phi_u - \phi_l S_l S_u \sin\phi_u - \phi_l S_l C_u \cos\phi_u \tag{C.10b}$$

$$A_3 = \left(\cos\phi_u + \phi_u \sin\phi_u\right)\left(\phi_l C_l S_u - \phi_u C_u S_l\right) - \left(\sin\phi_u - \phi_u\cos\phi_u\right)\left(\phi_l C_l C_u + \phi_u S_l S_u\right) \tag{C.10c}$$

$$A_4 = \left(S_l S_u \cos\phi_u - C_u S_l \sin\phi_u\right)\left(\phi_l^2 + \phi_u^2\right) + \phi_l\phi_u(2C_l C_u\cos\phi_u + 2C_l S_u \sin\phi_u - 2 - A_2) \tag{C.10d}$$

$$A_5 = \pi^2\left(\phi_l^2 - \phi_u^2\right)\left(\pi S_l \cos\frac{\pi L_l}{2L} - 2\sin\frac{\pi L_l}{2L} C_l\phi_l\right) - 2\phi_u^2\left(4\phi_l^2-\pi^2\right)A_1 \tag{C.10e}$$

$$A_6 = \pi^2\left(\phi_u^2 - \phi_l^2\right)\left[\pi\cos\frac{\pi L_l}{2L}\left(C_l - C_u\cos\phi_u - S_u\sin\phi_u\right) + 2\sin\frac{\pi L_l}{2L}\left(\phi_l S_l + \phi_u C_u\sin\phi_u - \phi_u S_u\cos\phi_u\right)\right] \tag{C.10f}$$

$$S_l = \sin\left(\frac{L_l\phi_l}{L}\right); \quad S_u = \sin\left(\frac{L_l\phi_u}{L}\right); \quad C_l = \cos\left(\frac{L_l\phi_l}{L}\right); \quad C_u = \cos\left(\frac{L_l\phi_u}{L}\right) \tag{C.10g}$$

Since the internal bending moment at the mid-height M_m is of significant to assess the onset of column's yielding at elevated temperatures, the attained solution of M_m considering the partial yielding effect is presented herein.

$$M_m = \frac{QL^3 A_7 + \frac{P\Delta_0}{L} A_8}{EI\left[\phi^4 \phi_u \tau_l \left(1 - r_l\right) A_1 + 3\phi^2 \phi_u \phi_l r_l A_2\right]} \tag{C.11}$$

where

$$A_7 = -\tau_l \phi^2 \left(1 - r_l\right)\left(\phi_u S_l S_u + \phi_l C_l C_u\right) - 3r_l\left(\phi_l \phi_u \sin\phi_u + \phi_l^2 S_l C_u - \phi_l \phi_u C_l S_u\right) \tag{C.12a}$$

$$A_8 = \frac{2L^3 \phi_u \pi \sin\phi_u \left[\begin{array}{l} \phi^2 \tau_l \pi \left(\phi_u^2 - \phi_l^2\right)\left(1 - r_l\right)\left(2\phi_l \sin\alpha_l C_l - \pi \cos\alpha_l S_l\right) \\ +3r_l \phi_l \left(\phi_l^2\left(\pi^2 - 4\phi_u^2\right) - \pi\left(2\phi_l \sin\alpha_l S_l + \pi\cos\alpha_l C_l\right)\left(\phi_l^2 - \phi_u^2\right)\right) \end{array}\right]}{\left(4\phi_u^2 - \pi^2\right)\left(4\phi_l^2 - \pi^2\right)} \tag{C.12b}$$

Appendix D

Derivation for the Mid-height Deflection of a Semi-rigidly Connected Column with Two-point Bracing

In this section, the relationship among the lateral load Q, axial load P, and the mid-height deflection Δ for a semi-rigidly connected column braced at two points is derived, which will be served as the basis for extending the foregoing research to investigate the requirements of multi-point bracing.

For the column with two equally spaced braces, i.e, the brace is located at the one third and two thirds of the column's full-length, the equilibrium of the half-length column is illustrated in Fig. D.1. The relationship between the bending moment and rotational stiffness at the lower end of the half-length column is:

$$M_e = R_e \theta_e \tag{D.1}$$

Thus, based on the equilibrium of the half-length column:

$$M_m + R_e \theta_e = \frac{2}{3} QL + P(\Delta + \Delta_0) \tag{D.2}$$

The governing differential equations associated with the flexural deformation of the half-length column shown in Fig. D.1 can be written as:

$$-EI\frac{d^2 y_1}{dx^2} = P(y_1 + y_{1,0}) - \theta_e R_e + Qx, \quad 0 \le x \le \frac{2}{3}L \tag{D.3a}$$

$$-EI\frac{d^2 y_2}{dx^2} = P(y_2 + y_{2,0}) - \theta_e R_e, \qquad \frac{2}{3}L \le x \le L \tag{D.3b}$$

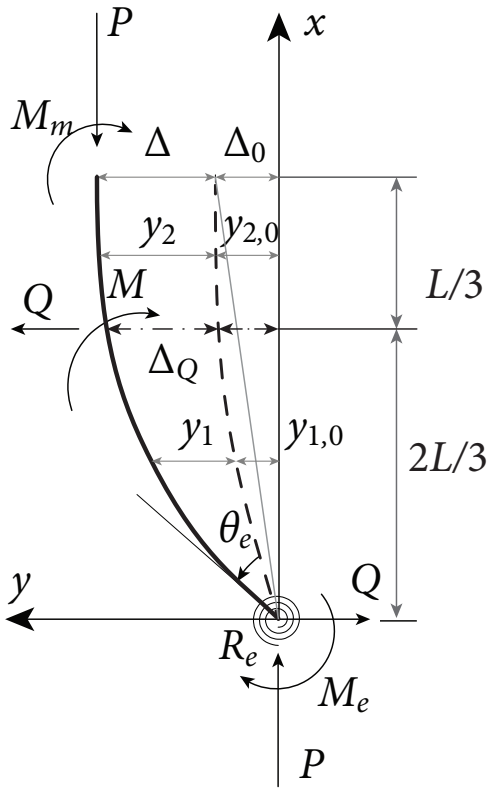

Figure D.1: Half of the deformed axially loaded column with two equally-spaced braces

By solving the differential equation, the deformation and rotation of the column can be obtained from Eqs. (D.4).

$$y_1(x) = C_1 \cos\left(\frac{\phi x}{L}\right) + C_2 \sin\left(\frac{\phi x}{L}\right) + \frac{\theta_e R_e}{P} - \Delta_0 \frac{4\phi^2}{4\phi^2 - \pi^2} \frac{\sin\left(\frac{\pi x}{2L}\right)}{P} - \frac{Q}{P}x, \quad 0 \le x \le \frac{2}{3}L \tag{D.4a}$$

$$y_2(x) = C_3 \cos\left(\frac{\phi x}{L}\right) + C_4 \sin\left(\frac{\phi x}{L}\right) + \frac{\theta_e R_e}{P} - \Delta_0 \frac{4\phi^2}{4\phi^2 - \pi^2} \frac{\sin\left(\frac{\pi x}{2L}\right)}{P}, \quad \frac{2}{3}L \le x \le L \tag{D.4b}$$

C_1, C_2, C_3, and C_4 are coefficients to be determined by the boundary conditions, namely:

$$y_1(0) = 0 \tag{D.5a}$$

$$y_2(L) = \Delta \tag{D.5b}$$

$$y_1(2L/3) = y_2(2L/3) \tag{D.5c}$$

$$y_1'(0) = \theta_e \tag{D.5d}$$

$$y_2'(L) = 0 \tag{D.5e}$$

$$y_1'(2L/3) = y_2'(2L/3) \tag{D.5f}$$

By substituting the boundary conditions and Eq. (D.2) into Eqs. (D.4), the system of eight equations is obtained and then solved for Δ, C_1, C_2, C_3, C_4, M_m, and θ_e. The lateral dis-

placement of the column Δ is therefore obtained:

$$\Delta = \frac{Q + \frac{P\Delta_0}{L}\psi_{\text{ef,2b}}}{S_{\text{ef,2b}}} \tag{D.6}$$

where $S_{\text{ef,2b}}$ is the effective lateral stiffness of the half-length column subjected to the axial applied load P and lateral load Q considering the initial curvature, as below:

$$S_{\text{ef,2b}} = \frac{3EI}{L^3}\beta_{\text{ef,2b}} = \frac{3EI}{L^3}\frac{A_{\text{2b}}}{\beta_{\text{ef,2b,DEN}}} \tag{D.7a}$$

$$A_{\text{2b}} = \phi^3\left[3r_e\sin\phi + \phi\cos\phi\,(1-r_e)\right] \tag{D.7b}$$

$$\beta_{\text{ef,2b,DEN}} = \left[\begin{array}{l} 3\phi\sin\left(\frac{2\phi}{3}\right) - 2\phi^2\cos\left(\frac{2\phi}{3}\right)(1-r_e) - 6\phi r_e\sin\left(\frac{\phi}{3}\right) - \\ 9r_e\left(\cos\phi + \phi\sin\left(\frac{2\phi}{3}\right) + \cos\left(\frac{2\phi}{3}\right) - \cos\left(\frac{\phi}{3}\right) - 1\right) \end{array}\right] \tag{D.7c}$$

The expression of $\psi_{\text{ef,2b}}$ is

$$\psi_{\text{ef,2b}} = \frac{6\phi^2\left[2\phi^2\cos\phi\,(1-r_e) + 3\pi r_e\left(\cos\phi - 1\right) + 6\phi r_e\sin\phi\right]}{\left(\pi^2 - 4\phi^2\right)\beta_{\text{ef,2b,DEN}}} \tag{D.8}$$

Thus, the deflections at column's mid-height for multi-column systems braced at the one third and two thirds of the full length can be analyzed by adopting Eq. (D.6).

Knowing the expressions of C_1, C_2, θ_e, the solution to Δ_Q can be attained from Eq. (D.4) with $x = 2L/3$:

$$\Delta_Q = \frac{Q + \frac{P\Delta_0}{L}\psi_{\text{2b}}}{S_{\text{2b}}} \tag{D.9}$$

where

$$S_{\text{2b}} = \frac{3EI}{L^3}\frac{2A_{\text{2b}}}{\beta_{\text{2b,DEN}}} \tag{D.10a}$$

$$\beta_{\text{2b,DEN}} = \left[\begin{array}{l} 3\phi\left(\sin\phi + \sin\left(\frac{\phi}{3}\right)\right) - 2\left(\cos\phi + \cos\left(\frac{\phi}{3}\right)\right)(1-r_e) \\ -27r_e\left(\cos\phi - \cos\left(\frac{\phi}{3}\right)\right) - 9\phi r_e\left(\sin\phi + 3\sin\left(\frac{\phi}{3}\right)\right) \end{array}\right] \tag{D.10b}$$

and

$$\psi_{\text{2b}} = \frac{24\phi^4\sin\frac{\pi}{3}\cos\phi\,(1-r_e) + 36\phi^2 r_e\left(2\phi\sin\frac{\pi}{3}\sin\phi + \pi\cos\phi - \pi\cos\frac{\pi}{3}\right)}{\left(\pi^2 - 4\phi^2\right)\beta_{2b,DEN}} \tag{D.11}$$